UNIVERSITA'
DEGLI STUDI
DI PADOVA

UNIVERSITA' DEGLI STUDI DI PADOVA

CISAS "G. Colombo" Centro Interdipartimentale di Studi e Attività Spaziali

SCUOLA DI DOTTORATO DI RICERCA
IN SCIENZE TECNOLOGIE E MISURE SPAZIALI
INDIRIZZO DI ASTRONAUTICA E SCIENZE DA SATELLITE
CICLO XXV

Numerical and Experimental Investigation of Hybrid Rocket Motors Transient Behavior

-

Caratterizzazione numerica e sperimentale del comportamento transitorio nei propulsori ibridi

Direttore della Scuola: Ch.mo Prof. GIAMPIERO NALETTO

Coordinatore d'indirizzo: Ch.mo Prof. GIAMPIERO NALETTO

Supervisore: Ch.mo Prof. DANIELE PAVARIN

Co-supervisore: Dott. Ing. ALBERTO BETTELLA

Dottorando: FRANCESCO BARATO

31 January 2013

To whom it may concern:

Topics discussed in Chap.3, Chap.4, Chap.5 and Chap.6 are to be considered innovative. The aforementioned chapters are related to numerical codes completely developed and validated during PhD.

A chi vi possa essere interessato:

Gli argomenti discussi nei Cap.3, Cap.4, Cap.5 e Cap.6 devono essere considerati innovativi. I suddetti capitoli sono pertinenti a codici numerici interamente sviluppati e validati nel corso del Dottorato di Ricerca.

To Giacomo

1984-2010

Abstract

As the space business is shifting from pure performances to affordability a renewed interest is growing about hybrid rocket propulsion. Hybrid rocket motors are attractive for their inherent advantages like simplicity, reliability, safety and reduced costs. Moreover hybrid motors are easy to throttle and thus they are ideal candidate when soft-landing or energy management capabilities are required.
This thesis is mainly involved with a theoretical/numerical study of hybrid transient behavior. The study of transient behavior is a very important aspect in the development of affordable, efficient, stable hybrid motors, particularly when throttling and controllability is concerned. Moreover transient behavior is important also for motors that work at a fixed operating point, not only in the prediction of ignition and shutdown phases but particularly in the analysis of instabilities. The prediction and reduction of instabilities are one of the main challenge in hybrid propulsion (as in general in all rocket motors).

The aim of this doctoral thesis is to investigate and simulate hybrid rocket transient behavior through the development of a numerical code. The numerical code is composed by several independent parts coupled together, each one referring to a different subsystem of the hybrid rocket motor.

Due to budget and time constraints it has not been possible to perform a dedicated experimental activity for this thesis. However the numerical results have been compared with experimental data obtained from literature, from CISAS partners (like NAMMO), and from other CISAS experimental activities performed both before and during this doctoral period.
Each subsystem of the hybrid propulsion unit and its related codes are described in a different chapter.

In the first chapter hybrid boundary layer steady combustion is introduced together with a discussion about the effect of steady hybrid regression physics on the shift of motor operating parameters with time.

In the second chapter typical necessary or intentional transient events occurring during the operation of a hybrid rocket (ignition, throttling and shutdown) are classified and described.

With chapter 3 begins the description of the several sub-models defining hybrid rocket transient behavior. In this chapter the attention is focused on the numerical modeling of the solid grain thermal behavior. The main object of this work is to determine the response of the solid fuel to variations of the heat flux on the surface. A 1D numerical model of transient grain thermal response has been developed with this goal. The model is based on the work performed by Karabeyoglu and solves the temperature profile in the direction normal to the surface. In the first paragraph a model suited for classical polymeric fuels is developed. In the second paragraph the grain model is coupled with the boundary layer response in order to investigate typical hybrid low frequency instabilities. In the third paragraph a version of the original grain model suited for liquefying propellants is developed. In fact recently a new class of fast burning fuels has been discovered at Stanford University. These fuels form a liquid layer on the melting surface during combustion, hence the term 'liquefying fuels'. Entrainment of droplets from the liquid-gas interface creates the desired high regression rate by increasing the rate of fuel mass transfer. Several researchers included people at CISAS have experimental confirmed that paraffin-based fuels burn at surface regression rates 3 to 4 times that of conventional hybrid fuels. Others following studies showed with the use of visualization experiments the presences of waves on the liquid surfaces and droplets entrained by the gas flow, confirming original theoretical predictions. The third paragraph is divided in three parts. In the first part the model developed to predict the regression rate and the thermal profile inside a paraffin fuel is presented. The second part deals with the phenomenology of supercritical entrainment. Finally the third part discusses the problem of the closure of the equations to take into account the space-time variability of the entrainment phenomenon.

In chapter 4 the attention is focused on the gas dynamic inside the hybrid combustion chamber. For this purpose two time-varying numerical models are developed. The aim of these unsteady codes is to determine the transient behavior of the main parameters of the hybrid rocket motor. The combustion chamber model represents the core of the hybrid rocket motor simulation. In fact the combustion chamber model gives directly the main parameter of a propulsion system, that is, motor thrust. The sub-models presented in the previous and the next chapters define the input parameters for the combustion chamber

model. In fact the grain model of chapter 3 determine the fuel mass flow while the tank and feed lines model of chapter 5 gives the oxidizer mass flow. In the first part of this chapter a global 0D time-varying numerical model of the combustion chamber is developed. The code is then coupled with the grain model described in the previous chapter to account for the transient fuel production. It follows a brief discussion about the main hybrid rocket motor characteristic times and their relative values. In the second part a 1D time-varying numerical model of the combustion chamber is developed. The unsteady 1D code is able to simulate all the features of the 0D code. It should add the acoustic response of the system and the spatial variation of the fluid-dynamic unknowns along the flow direction, increasing the accuracy of the results at the expense of an higher computational effort.

Chapter 5 end the description of the several sub-models of the hybrid rocket propulsion system. Together with chapter 3 and 4 it composes the code describing hybrid rocket transient behavior. In this chapter the attention is focused on the numerical modeling of the oxidizer path. This includes the sub-systems ahead of the combustion chamber like the pressurization system, the main tank and the feed lines. Moreover it considers also the injector elements and some aspects of droplets vaporization and atomization in the combustion chamber.

This work is complementary to the one described in chapter 3, defining the input parameters for the core of the code, that is the chamber gas-dynamic model shown in chapter 4. The main object of this work is to determine how the feed system affects the performance parameters of the hybrid motor with time. For this purpose the prediction of several unknowns like the oxidizer mass flow, tank pressure and the amount of residual gases is obtained through the modeling of the principal subsystem behavior. Moreover the full transient coupling between the feed system and the combustion chamber is also investigated.

This chapter is divided in three parts. The topic of the first paragraph regards the main tank and the pressurization system. After a brief description of the main alternatives the discussion goes on with the numerical modeling of the typical solutions adopted for hybrid rockets (i.e. pressure-regulated, blowdown and self-press). First of all a numerical model of a pressure fed tank is developed. The code is able to predict several parameters like masses, densities, temperatures and pressures of the gas in the ullage volume and in the pressurant tank, the pressurant mass flow and the filling level of the tank. The model takes into account several aspects like heat losses, liquid oxidizer evaporation, eventual gas phase combustion of the pressurant gas, the use of by-pass and digital valves.

Later a numerical model of a self pressurized tank is developed. The code is able to determine the oxidizer mass, temperature, pressure, density and the vapor/liquid volume/mass fractions during the discharge. The numerical results are compared with experimental hot tests performed at CISAS.
The second paragraph takes into account the full transient coupling between the feed system and the combustion chamber. The main challenge is to determine the instantaneous liquid mass flow and the relation between the liquid oxidizer and the gaseous oxidizer that takes part in the hybrid motor combustion processes (i.e. droplets vaporization). In this way it is possible to simulate feed system coupled instabilities.
The third paragraph deals with the prediction of the mass flow through the injector elements. In particular the behavior of self-pressurized systems is investigated. In this case the chamber pressure is below the vapor pressure of the liquid inside the tank. Consequently cavitation and flashing occur inside the injector elements. This kind of two-phase flow with vaporization involves several important modeling issues. Different models are compared with cold-flow tests performed at CISAS in order to check the accuracy of their predictions.

In chapter 6 some advanced techniques developed to increase the regression rate and combustion efficiency of hybrid rockets are investigated with a particular focus on their influence on the transient behavior of the motor, particularly regarding combustion instabilities. The two methods studied in this thesis are the use of a diaphragm in the midst of the grain and the use of a swirling oxidizer injection. The reason for this choice is related to the fact that both solutions have been tested (among others) at CISAS and look very promising with respect to the overcoming of historical hybrid weaknesses. Even if working in very different ways both methods induce a strong increase of the turbulence level and mixing of the reactants in the combustion chamber, promoting a more complete combustion and an higher heat flux on the grain surface. Beside improving significantly hybrid performances this two techniques can affect the stability behavior of an hybrid motor directly (i.e. modifying the flowfield in the chamber) and indirectly (e.g. reducing the chamber length due to increased regression rate).

In the final chapter a summary of the activities carried out and the results achieved is given.

Sommario

Man mano che le attività spaziali stanno passando da una fase di ricerca delle prestazioni pure ad una fase di maggior accessibilità, sta crescendo un rinnovato interesse nei confronti della propulsione ibrida.
I motori a razzo ibridi sono interessanti per i loro vantaggi intrinseci, come la semplicità, l'affidabilità, la sicurezza e la riduzione dei costi. Inoltre è facile modulare la spinta dei motori ibridi e quindi essi rappresentano un candidato ideale per le applicazioni che richiedono un atterraggio morbido o la gestione dell'energia. Questa tesi riguarda principalmente uno studio teorico/numerico del comportamento transitorio dei motori ibridi. Lo studio del comportamento transitorio è un aspetto molto importante nello sviluppo di motori ibridi stabili, efficienti, in particolare quando sono richiesti throttling e controllabilità. Inoltre il comportamento transitorio è importante anche per motori che operano ad un punto di funzionamento fisso, non solo nella previsione delle fasi di accensione e spegnimento ma soprattutto nell'analisi delle instabilità. La previsione e la riduzione delle instabilità rappresentano una delle principali sfide della propulsione ibrida (come in generale in tutti i propulsori a razzo).

Lo scopo di questa tesi di dottorato è quello di indagare e simulare il comportamento transitorio di un propulsore ibrido attraverso lo sviluppo di un codice numerico. Il codice numerico è composto da più parti distinte accoppiate tra loro, ciascuna facente riferimento a un sottosistema differente del motore a razzo ibrido.

A causa di vincoli di bilancio e di tempo non è stato possibile effettuare una attività sperimentale dedicata per questa tesi. Tuttavia, i risultati numerici sono stati confrontati con i dati sperimentali ottenuti dalla letteratura, dai partner del CISAS (come Nammo), e da altre attività sperimentali del CISAS effettuate sia prima che durante questo periodo di dottorato. Ogni sottosistema del propulsore ibrido e i suoi relativi codici sono descritti in un capitolo diverso.

Nel primo capitolo viene introdotta la fisica stazionaria della combustione ibrida seguita

da una discussione sull'effetto che essa ha sulla variazione temporale dei parametri operativi del motore.

Nel secondo capitolo vengono classificati e descritti i tipici eventi transitori che avvengono durante il funzionamento di un motore ibrido (accensione, throttling, spegnimento).

Nel terzo capitolo inizia la descrizione dei vari modelli che definiscono il comportamento transitorio dei motori ibridi. In questo capitolo l'attenzione è focalizzata nella modellazione numerica del comportamento termico del grano solido. L'obiettivo principale è quello di determinare la risposta del combustibile solido alle variazioni di flusso termico sulla superficie. A tal fine è stato sviluppato un modello numerico monodimensionale della risposta termica transitoria del grano. Il modello è basato sul lavoro di Karabeyoglu e risolve il profilo termico nella direzione normale alla superficie. Nel primo paragrafo viene sviluppato il modello base per combustibili polimerici. Nel secondo paragrafo il modello è accoppiato con la risposta dello strato limite allo scopo di simulare le tipiche instabilità a bassa frequenza dell'ibrido. Nel terzo paragrafo il modello base viene esteso per simulare combustibili che formano uno strato fuso sulla superficie del grano. Difatti recentemente è stata scoperta da ricercatori dell'università di Stanford una nuova classe di combustibili ad elevata velocità di regressione. Questi combustibili formano uno strato di liquido sulla superficie fusa durante la combustione. Grazie all'entrainment di goccioline di combustibile la velocità di regressione è aumentata considerevolmente a causa del nuovo meccanismo di trasporto di massa. Diversi ricercatori hanno confermato una velocità di regressione pari a 3-4 volte quella dei combustibili ibridi tradizionali. Studi successivi hanno mostrato tramite esperimenti visivi la presenza di onde sulla superficie liquida e di goccioline trasportate dalla corrente, confermando le previsioni iniziali. Il terzo paragrafo è diviso in tre parti. Nella prima parte è presentato il modello sviluppato per predire il profilo di temperatura e il regression rate in un combustibile a base di paraffina. Nella seconda parte viene discussa la fenomenologia dell'entrainment supercritico. Nella terza parte viene discusso il problema della chiusura delle equazioni per tener conto della variabilità spaziale e temporale del fenomeno dell'entrainment.

Nel quarto capitolo l'attenzione è concentrata sulla gasdinamica della camera di combustione. A tal fine sono stati sviluppati due modelli numerici transitori. L'obiettivo di questi codici è di determinare il comportamento transitorio dei principali parametri del motore ibrido. Il modello della camera di combustione rappresenta il cuore della simulazione del motore ibrido. Difatti questo modello fornisce direttamente il parametro principale di un

sistema propulsivo, cioè la spinta. I modelli dei capitoli precedente e successivo definiscono i parametri di ingresso per il modello della camera di combustione. Infatti il modello del grano del capitolo 3 determina la portata di combustibile mentre il modello del serbatoio e delle linee di alimentazione del capitolo 5 fornisce la portata di ossidante. Nella prima parte di questo capitolo viene sviluppato un modello non-stazionario globale della camera di combustione. Il codice viene poi accoppiato con il modello del grano descritto nel capitolo precedente per tener conto della produzione transitoria di combustibile. Segue una breve discussione sui tempi caratteristici di un motore ibrido e la loro relativa grandezza. Nella seconda parte viene sviluppato un codice monodimensionale non-stazionario della camera di combustione. Il codice transiente monodimensionale è in grado di simulare tutti gli aspetti già trattati dal codice zero-dimensionale. Esso aggiunge la risposta acustica del sistema e la variazione spaziale delle grandezze fluidodinamiche nella direzione del flusso, incrementando l'accuratezza a scapito di un maggiore costo computazionale.

Il quinto capitolo termina la descrizione dei vari modelli del sistema propulsivo ibrido. Insieme ai capitoli 3 e 4 compone il codice che descrive il comportamento transitorio dei motore ibridi. In questo capitolo l'attenzione è concentrata sula modellazione numerica del percorso dell'ossidante. Ciò include tutto ciò che si trova a monte della camera di combustione, come il sistema di pressurizzazione, il serbatoio principale, le linee di adduzione. Inoltre considera anche la piastra di iniezione e alcuni aspetti dell'atomizzazione ed evaporazione del liquido nella camera di combustione.
Questa parte è complementare con quella descritta nel capitolo 3 e definisce i parametri d'ingresso per il cuore del codice, cioè la gasdinamica della camera di combustione del capitolo 4. Il principale obiettivo di questo lavoro è determinare come il sistema di alimentazione influenza i principali parametri prestazionali del motore nel tempo. Per questo motivo varie incognite come la portata di ossidante, la pressione nel serbatoio e la quantità di gas residuo vengono determinate attraverso la modellazione del comportamento dei vari sottosistemi. Inoltre viene indagato anche l'accoppiamento non-stazionario tra il sistema di iniezione e la camera di combustione.
Questo capitolo è diviso in tre parti. Il primo paragrafo riguarda il sistema di pressurizzazione. Dopo una breve descrizione delle principali alternative la discussione continua con la modellazione numerica delle principali soluzioni adottate nei motori ibridi (pressure-regulated, blowdown e autopressurizzato). Prima di tutto viene sviluppato un modello numerico di un sistema pressure-fed. Il codice è in grado di predire svariati parametri tra cui le

masse, temperature, densità e pressioni del gas nel serbatoio principale e in quello del pressurizzante, la portata di pressurizzante e il livello di riempimento del serbatoio. Il modello considera vari aspetti tra cui gli scambi termici, l'evaporazione del liquido, la combustione finale in fase gassosa, l'uso di by-pass e valvole digitali. Successivamente viene sviluppato un modello numerico di un sistema autopressurizzato. Il codice è in grado di predire la temperatura, densità, pressione dell'ossidante assieme al titolo della miscela. I risultati numerici vengono comparati con i test sperimentali condotti dal CISAS. Il secondo paragrafo considera l'accoppiamento non-stazionario tra il sistema di iniezione e la camera di combustione. La principale difficoltà deriva dalla determinazione della portata istantanea di liquido e della relazione che lega la portata di liquido a quella di gas che partecipa alla combustione. In questo modo è possibile simulare le instabilità dovute a tale accoppiamento. Il terzo paragrafo riguarda la determinazione della portata di massa attraverso la piastra di iniezione. In particolare viene investigato il comportamento di sistemi autopressurizzanti. In questo caso la pressione in camera di combustione è al di sotto della pressione di vapore dell'ossidante nel serbatoio. Per questo motivo nell'iniettore si sviluppano importanti fenomeni di cavitazione. Questo tipo di flussi bifasici coinvolgono diversi aspetti di modellazione. Tre modelli differenti sono comparati con test sperimentali effettuati dal CISAS con l'obiettivo di determinare l'accuratezza delle previsioni numeriche.

Nel sesto capitolo vengono analizzate alcune tecniche avanzate per aumentare la velocità di regressione e l'efficienza dei motori ibridi con una particolare attenzione al loro effetto sul comportamento transitorio del motore, soprattutto sulle instabilità. I due metodi studiati in questa tesi sono l'uso di un diaframma in mezzo al grano e l'utilizzo di un'iniezione swirl. La ragione di questa scelta è legata al fatto che entrambe le tecniche sono state testate (tra gli altri) dal CISAS e risultano essere molto promettenti a riguardo del superamento degli storici punti deboli dei motori ibridi. Anche se funzionanti con principi molto diversi entrambi i metodi inducono un elevato incremento della turbolenza e del miscelamento di reagenti nella camera di combustione, promuovendo il completamento della combustione e un più elevato flusso termico a parete. Oltre ad incrementare notevolmente le prestazioni dei motori ibridi queste due tecniche possono influenzare anche il comportamento transitorio di un motore sia direttamente (modificando il campo fluido all'interno della camera di combustione), sia indirettamente (ad esempio riducendo la lunghezza della camera per via di una maggiore velocità di regressione).

Nell'ultimo capitolo vengono riassunte le attività svolte ed i risultati ottenuti.

Contents

List of Figures

Nomenclature

ρ	= density
t	= time, transparency
V	= volume
D	= port diameter
L	= length, latent heat
p	= pressure
A	= area, Arrhenius constant
η	= motor efficiency
R	= gas constant
T	= temperature
e	= energy
h	= enthalpy, liquid layer thickness
O/F	= oxidizer to fuel ratio
c	= specific heat, constant
κ	= thermal diffusivity
λ	= thermal conductivity
E_a	= activation energy
G_0	= oxidizer mass flux
C_f	= friction coefficient
B	= blowing parameter
ϵ	= emissivity
Q_{comb}	= heat of combustion
x	= grain, chamber coordinate

b = empirical constant for the absorption coefficient

y = distance from the surface (gas side)

$\dot{m}$ = mass flow

$\dot{r}$ = regression rate

σ = Boltzmann constant

δ = thermal boundary layer

μ = viscosity

τ_1, τ_2 = boundary layer diffusion times

f = frequency

Cd = discharge coefficient

K = droplet, entrainment equation constants

α, β, γ = entrainment constants

a_t = thickness parameter

X_r = roughness group

Fr = roughness parameter

P = pressure

Re = Reynolds number

Q = heat flux

d_{vm} = volume median diameter

d_h = hydraulic diameter

subscripts

0 = initial, without blowing

bf = beneath flame

$break$ = break up

c = combustion chamber

$conv$ = convective

d = droplet

ent = entrainment

f = fuel, flame

g = gas

inj = injection

l = liquid

m = melting

op = operative (design point)

ox = gaseous oxidizer

p = port, pipe

pr = products

rad = radiative

ref = reference

s = surface, solid

t = throat

u = universal

v = vapor

vap = vaporization

w = wall

Introduction

Three main types of chemical rocket exist: **liquid, solid** and **hybrids**. The subdivision is related to the phase which the propellant is stored. In a liquid rocket the liquid oxidizer and the fuel are stored in the respective tanks and injected in the combustion chamber. In a solid rocket the fuel and oxidizer are mixed together in a solid matrix that is stored directly in the combustion chamber. However in a more general term is possible to consider like a liquid rocket also system were the propellant is stored in a gaseous or gelled form and is injected in the combustion chamber afterward.

In an hybrid rocket one component is stored as a liquid (or a gas or a gel) in a tank and the other is a solid placed inside the combustion chamber. Usually the liquid is the oxidizer and the solid is the fuel, the so called classical configuration. However also reverse hybrid could exist were the liquid is the fuel and the solid is the oxidizer. The most part of the work up to now (and almost surely in the future) regards the classical scheme mainly because liquid oxidizers have higher energetic content than solid ones. Exceptions are cryogenic solids oxidizers like solid oxygen, the solidified version of liquid oxygen. However solid cryogenic storage is even more complex than its liquid counterpart. Moreover an almost infinite combination of solid fuels exists for hybrid propulsion while generally the choice of oxidizer is much limited (both in solid and liquid phase) and in this case the manufacturing of the grain requires a binder. No particular advantages seem to come from the reverse approach.

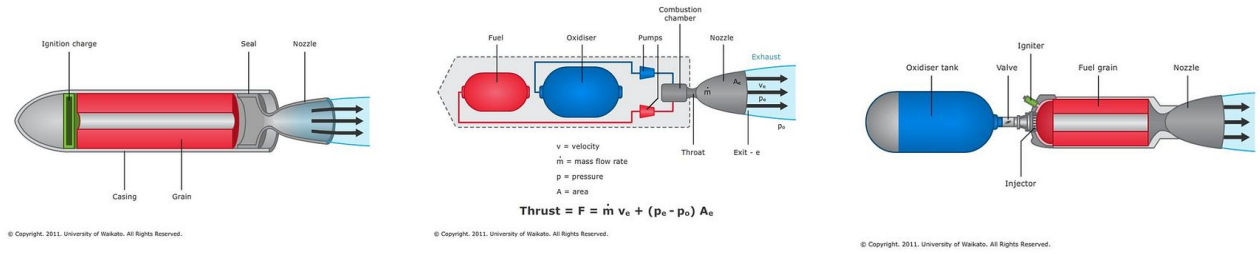

Figure 1: *Solid (left), liquid (center), and hybrid (right) rocket schematics.*

Solid and liquid engine have monopolized the military and commercial market up to know leaving hybrids only a limited room in research program (and more recently in amateur/academic activities). The reason for that is related to the peculiar characteristics of the three propulsion systems coupled with the requirements of the cold war era.
Solid rocket are very simple, ready to launch and could reach the highest value of impulse density making them ideal for volume constrained applications such as military weapons, sounding rockets and boosters. Liquids can reach the highest specific impulse; they can be stopped and started multiple times in flight making them ideal for launchers and spacecraft. Hybrids have long been considered an intermediate case between the two, so not showing a clear advantage respect to both extremes in a performances oriented environment.
Moreover the greatest advancement of rocket propulsion have been done in the 50-60. In that period almost everything has been designed and tested. After an initial assessment only the most promising technology have been chosen for extensive further work. Some hybrid issues were still not solved at that time (and partially today). Hybrids maturity, as other propulsion technologies still suffer nowadays for being excluded from that choice. In fact after the golden age of space investments have been decreased and this prevents today hybrids to make a considerable step toward maturity.
Anyway the space business has been slowly changing in the last decades (and it is expected to change even more in the future, hopefully). Today more attention is paid toward safety, reliability, cost, and environmental friendliness. This in turn has paved the way for a renewed interest for hybrid propulsion favored by its inherent characteristics.
First of all is necessary to highlight that hybrid rocket combustion is much different from solid or liquid rocket combustion. In a solid rocket the fuel and the oxidizer are intimately pre-mixed in the grain at a specific O/F ratio. The propellant burns with a thin flame next to the surface (few μm). The amount of propellant depends on the linear regression of the grain surface that generally in turns depends on chamber pressure. In a liquid rocket the oxidizer and the fuel are injected in the combustion chamber. The average O/F ratio is dependent simply on the ratio between the two mass flows. In a hybrid rocket the oxidizer is usually injected at the head end of the combustion chamber mixing later with the pyrolized fuels in a macroscopic turbulent diffusion flame. The regression of the fuel is dependent of the convective heat exchange from the flame to the surface.
In a liquid rocket the total mass flow and O/F ratio can be perfectly (at least nominally) controlled. In a solid rocket the O/F ratio is fixed by the grain composition and the pro-

pellant mass flow being dependent only on chamber pressure can be defined with a proper design of the fuel grain. For both propulsion systems the motor O/F ratio and propellant mass flow are independent variables.

On the contrary only the oxidizer mass flow can be directly controlled in a hybrid rocket, while the fuel mass flow is dependent on the complex physic of its coupled fluid dynamic/-combustion. The regression rate in a hybrid has a time and space variability. The motor O/F ratio and total mass flow are not independent variables. This complex coupling between motor parameters, the difficult prediction/scaling and the space variability of hybrid regression makes hybrid physics and design more complex/difficult to deal with. This added complexity has always hampered the realization of a competitive hybrid rocket unit.

Moreover in a liquid rocket motor the oxidizer and fuel are intimately mixed in the vicinity of the injector to form a combustible mixture. As already said in a solid rocket the two components are already mixed in a single solid phase. In both case, therefore a uniform mixture is achieved in the combustion chamber. In a hybrid motor the oxidizer and the fuel enter the chamber from different sides, mixing slowly in the diffusion flame. This characteristic is also responsible for the usually lower performances of hybrid rockets. However due to its peculiar characteristics hybrid propulsion presents several advantages compared to solids and liquids. Here a general list:

- **SAFETY.** The fuel is inert and can be manufactured, transported, and handled safely as standard commercial products. The system is non-explosive because an intimate mixture of oxidizer and fuel is not possible. NASA classifies hybrid LOX-HTPB combination as 0 TNT equivalent. In case of an abort procedure the motor can be stopped turning off the liquid flow. Unlike solid rockets, fuel grain cracks are not catastrophic because burning occurs only when the fuels encounter the oxidizer flow. Hybrid combustion is diffusion controlled so its usually not pressure sensitive as in liquids and solids. This in turn makes hybrid less prone to catastrophic failures due to thermoacoustic instabilities or other parameters shifting outside nominal conditions. Hybrid failures are usually benign in nature.

- **RELIABILITY.** An hybrid rocket requires roughly only half of the components of a liquid engine. Respect to solids the grain is much more insensitive to defects. Being diffusion controlled hybrid combustion is more tolerant than in both solids and liquids.

- **MASS FLOW CONTROL.** The engine can be throttled by modulating only the

liquid flow rate. This is simpler than for liquid propulsion when two liquids have to be modulated simultaneously. This doesnt require only double plumbing but also synchronization between the two flows. The engine can be started and stopped several time if a suitable ignition system is used.

- **PROPELLANT VERSATILITY.** The selection of propellants is (nominally) much greater than with either solids or liquids even if the great part of the attention has been focused on a narrower band of combinations. Liquid oxidizers are more energetic than solid oxidizers used in solid propulsion. Metals particles can be added easily in a solid matrix to improve performances unlike liquids, where the formation of slurries implies several drawbacks like sedimentation, feeding-pressurization and atomization issues.

- **TEMPERATURE SENSITIVITY.** Because the temperature effect of the burning rate is small (as in liquids), ambient launch temperature variations have little effect on operating chamber pressure. Thus, the concern in solid rockets in designing for a maximum expected operating pressure ($MEOP$) is greatly reduced (this claim is partially negated in the case of self-pressurized oxidizer).

- **PROPELLANT SPECIFIC IMPULSE AND DENSITY.** The theoretical specific impulse of hybrid rockets is higher than solids and can be comparable with liquid rockets except for those using cryogenic fuels. With the addition of metals in the fuel grain the specific impulse of hybrid can be even higher of liquid rockets of the same class. In fact the highest possible experimental I_{sp} has been achieved with a tribrid configuration. The density impulse is lower than solids but nominally higher than liquids, particularly for metal loaded fuels.

- **LOW COST.** Considering the components composing the inert mass fraction of a rocket propulsion system the cost of an hybrid should stay between the more complex and expensive liquids and the simpler and cheaper solids. However the total hybrid operational costs should take advantage of its safety characteristics and inert propellant. Manufacture of the fuel can be done in a commercial facility that does not require the large areas and many buildings of solid-propellant manufacture. Furthermore, the system can tolerate large design margins, resulting in lower fabrication costs. Transport and handling costs are greatly reduced.

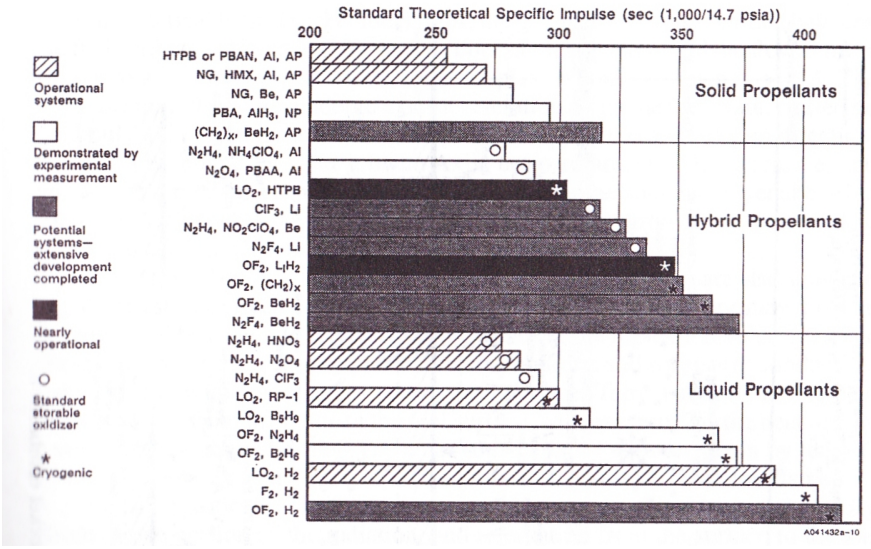

Figure 2: *Theoretical I_{sp} for solid,liquid, and hybrid rocket propellants [42].*

- **ENVIRONMENTAL FRIENDLINES.** Several green propellant combinations are possible for hybrid propulsion; many of them have been commonly used.

Unfortunately hybrid rocket have also some distinct disadvantages, such as:

- **LOW REGRESSION RATE.** As it would be explained later hybrids are generally characterized by low regression rates. This in turn requires a large burning area to achieve the required thrust. This large area could be obtained with a very long combustion chamber resulting in a too long motor. Moreover the resulting web thickness is small concurring to a very poor volume loading (fuel volume/total volume).

  The problem is increased with scale-up for several reasons. First of all the port area is proportional to the thrust while the web thickness is proportional to the product of the burning time with the average regression rate. Usually with scale up burning time increases much slower than thrust resulting in a much higher ratio between internal diameter and web thickness. Moreover hybrid regression rate decreases with scaling, exacerbating the issue.

  A better alternative is the use of a multiport grain. However multiport design implies several other problems, like high residuals, deviation of regression rate for different ports, port shape change with time, structural issues (e.g. need for web support), generally higher O/F shift than single port design and even much stronger if merging of ports is allowed, increased complexity and manufacturing costs. Several ways to increase the regression rate have been proposed and tested, almost no one has reached

operational status but some of them present an interesting potential for the future particularly up to medium scales.

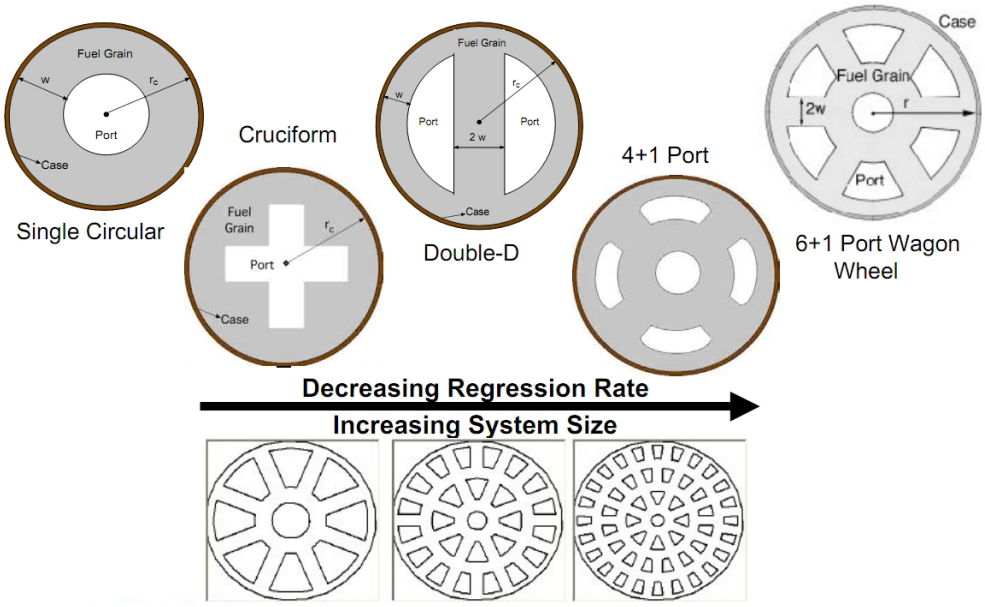

Figure 3: *Examples of multiport grain configurations.*

- **PACKAGING ISSUES.** In a liquid rocket the large part of the system is composed by the storage propellant tanks. This aspect is increased particularly for low thrust to total impulse ratios (e.g. spacecrafts). Tanks can be easily packaged choosing different configurations in terms of tanks number, shape and positions. Solid rockets are composed mainly by the combustion chamber that encloses the solid grain (plus the nozzle). Several geometrical solutions are available for solid motors allowing to fulfill multiple different mission constraints (e.g. different L/D ratios), moreover the propulsion engineer can tailor the regression rate and the grain shape for the specific needs.

  In a hybrid rocket the liquid oxidizer can be easily packaged as in a liquid rocket. The hybrid combustion chamber geometry is dictated by the solid fuel envelope. Due to the complex dependency of the hybrid regression on several parameters (like oxidizer flux) its not possible to play easily with geometries as in solid propulsion where the mass flow is readily related with the burning area. On the contrary in a hybrid motor the fuel mass flow changes even with a constant burning area. Thats why a constant burning area (e.g. star shaped) grain produces a neutral burning in a solid while its strongly regressive in a hybrid configuration [60] (inducing also a significant O/F shift for a constant oxidizer flow). For this reason a star shaped grain is not an attractive

option for hybrids to increase the burning area and the volume loading as it is for solids.

Usually hybrid combustion chambers tend to be slender. Often it is stated that this is related to the low regression rate and should not be a problem for low-thrust long duration applications. However this is not completely correct. Considering a classical design (single or multiport) even with a complete freedom on the regression rate its difficult to design a performing system exceeding a certain ratio between the initial and final oxidizer flux (amount of O/F shift, max flux limited by flooding or exit Mach number, lower flux limited by chuffing etc.). This in turn fixes the ratio between the internal and external port diameter and consequently the required regression rate and L/D ratio (for a given motor O/F). Very 'fat' hybrid motors are not likely possible for low thrust-long burning time. An exception could be other alternative configurations like the vortex pancake which however bring its own problematic.

Another important aspect compared to liquids is that its not possible to design a propulsion unit that can be used on different spacecraft with different total impulse requirements because again, the combustion chamber contains the solid fuel. On the contrary a liquid motor is (nearly) only related to thrust so it can be combined with different tanks to deliver different total impulses.

- **COMBUSTION EFFICIENCY.** As previously said hybrid combustion tends to be more rough and less complete than for solids and liquids producing a larger I_{sp} penalty respect to theoretical values.

  Several techniques have been proposed, two of them are described in chapter 6.

- **O/F shift.** The general impossibility to maintain the motor O/F ratio fixed at the optimal value lead to a decrease in the average specific impulse. Careful design can reduce these losses to less than 1%.

- **SLOWER TRANSIENTS.** Ignition transients are generally slower for hybrids. The response to throttling is slower too. The combustion chamber of a hybrid is much bigger than an equivalent liquid because it has to contain the solid fuels, moreover the chamber volume changes with time reaching its maximum value at the end of burn when the grain is consumed. Also the thermal lag in the solid fuel change with time and reach is maximum toward the end. This prevents hybrids to be used when very accurate, repeatable, fast response is necessary like in the case of hypergolic liquid

mono-bipropellant operating in multi-pulse mode, but should be no major issue in the general case.

The fact that generally hybrid theoretical figures (I_{sp}, ρI_{sp}) are intermediate between solids and liquids make them less attractive when only few performance parameters have to be maximized for a specific task. This was one of the reasons for the discard of hybrids in the main choice outlined before. The other fundamental aspect was the performance penalty caused mainly by the low regression rate and related negative attributes.

Finally, as already mentioned the complex coupling of motor parameters make hybrid less attractive from an ideal design point of view. Other hybrid concepts have been conceived and (to a less extent) developed/tested to overcome conventional hybrid issues but usually the added complexity or drawbacks of these solutions make them not sufficiently (or even less) attractive.

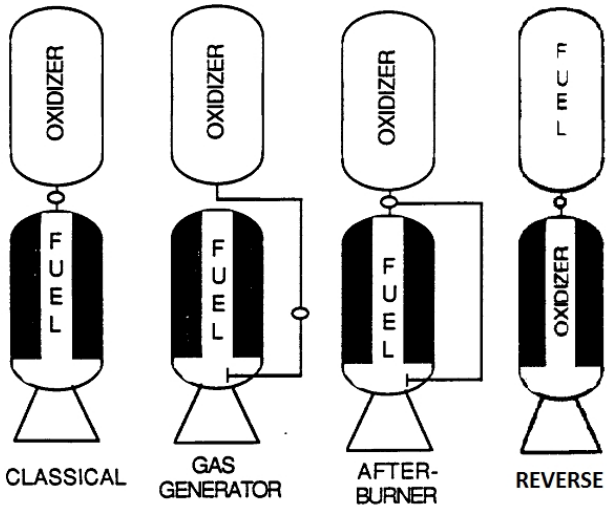

Figure 4: *Some alternative hybrid schematics.*

One aspect to underline is that all the claimed advantages of hybrid propulsion are often not possible for the same propulsion unit because of the propellant choice or system configuration (this can be partially attributed also to the other two propulsion types to a less extent) and because they tend to be counteracting. Typical examples are the LEX sounding rocket or the *Firebolt* presented later. Moreover some of the solutions proposed to solve specific hybrid issues negate other hybrid advantages. A typical example is the use of small amount of oxidizer in the fuel grain to increase the regression rate. Even if this solution is safer than a conventional solid propellant grain it loses the fundamental attribute

of complete grain inertness.

Its also important to remark that the comparison between hybrids and liquids is often ill-posed; for example the ablative cooling of hybrid rockets is claimed simpler than regenerative cooling for liquid rockets. This comparison is a bit unfair because ablative cooled liquid rocket exist and also an hybrid rocket could be regenerative cooled (even if its less attractive for hybrids than liquids). Similar examples can be done for other aspects like the pressurization system.

However its worth noting that some hybrid characteristics like safety and simplicity could lead indirectly to a performance advantage. For example a safe and simple propulsion system has more chances to exploit the advantages of air launch. Moreover a simpler, safer, cheaper system can be tested much more times in a smaller timeframe. This in turn allows the possibility to continuously upgrade, optimize and improve the system with new state of art technology, for example in materials science. This fact is particular significant during period of low investments like the current one.

An analysis of the technology used nowadays on launchers and spacecrafts shows that state of art for space system is often far from being the real state of art of the same technology. The reason for that is the following. The tremendously high costs of space (and the impossibility of repairing the failures) impose the need for a very high reliability. High reliability drives up costs that in turn increase the demand for high reliability. This phenomenon is called the space spiral [68]. The required high reliability in a period of limited budgets induces a very conservative approach, a typical example being the fact that a common Pc has more capability than the computer used on the ISS. Any improvement is introduced to operational level very slowly. This behavior has prevented the real birth of a large private autonomous space business limiting the great part of the activities to a relative small number of governmental funded projects.

Figure 5: *The Space Spiral, how it is now (left) and how it should be (right) [68].*

Without the actual governmental support the space business would collapse (unlike the

aviation segment for example). A dramatic reduction of the cost of space is deemed necessary to reverse the space spiral. A decrease of space costs coupled with less fragile and more flexible systems permits a lower demand of reliability that in turn requires less cost allowing an increased number of missions. More missions could guarantee a real sustainable business. It is hoped that hybrid propulsion could be one element (but for sure not the only one!) that could help to reverse the space spiral. This could be possible only if hybrids could afford a significant cost reduction, not being simply on the level of current liquids-solids. Thats why its not possible to consider an hybrid as a sort of mixture between solid and liquid components otherwise the challenge is loss in advance. At the same time the exponential form of Tsiolkovsky equation allows only limited losses of performances. A larger penalty translates indirectly on high costs because of large size increase (these aspects have been highlighted by Grosse [43]). To achieve this ambitious object classical hybrid issues have to be fixed preserving its inherent advantages like safety and simplicity, guarantying high reliability and very low costs [54].

Hybrid History

The early history of hybrid rocket development dates back to the '30s, the decade when the bases of modern experimental rocketry have been set [61]. The first often claimed hybrid rocket (unless sometimes referred as a liquid) is the GIRD 09 developed by a Soviet group of scientist (such as Korolev, the father of Soyuz family) and launched (only partially successful) in 1933. It used liquid oxygen fed by its own pressure with gelled gasoline supported on a metal mesh.

Afterwards other experiments were made by a few researchers using carbon as a fuel. They found a very low regression rate caused by the very high heat of ablation of carbon (in fact carbon based material are often used as ablative protections). Further work was done during the '40-'50 at the Pacific rocket society, General Electric and Jet Propulsion laboratory. These preliminary activities demonstrated the basic characteristics of hybrid rockets like low regression rate, insensitivity to crack, regression rate dependency on oxidizer flow and consequently the possibility to modulate the thrust varying the oxidizer flow.
Remarking aspects are the first use of rubber-based fuels, the first catalytic decomposed H2O2 hybrid rocket and the first (unsatisfactory) attempts of the reverse approach.
The following decade (the '60) has been probably the most prolific ever for rocket propulsion

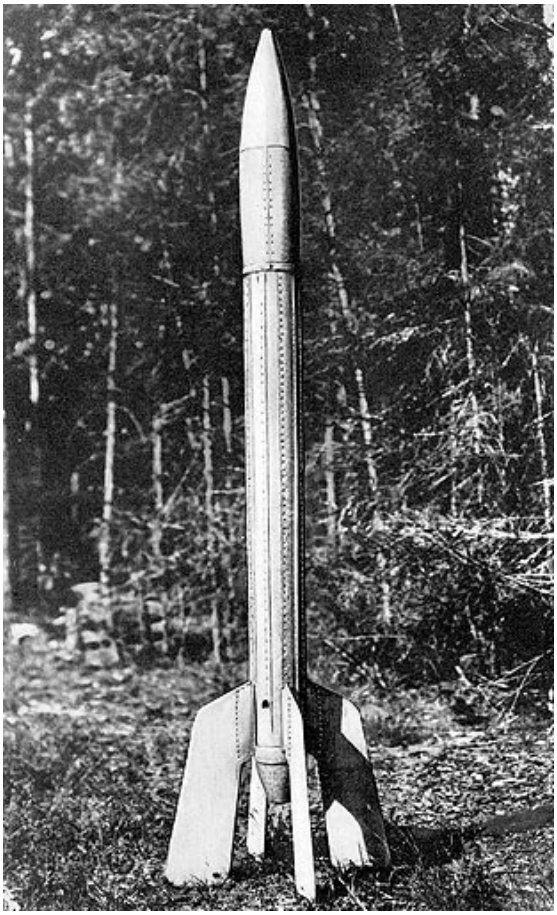

Figure 6: *GIRD 09 combustion chamber (left) and complete rocket (right).*

with a huge amount of investments on research and operational programs thanks to the space race initiated by the Sputnik launch in 1957 and culminated with the Moon landing in 1969. A great boost in hybrid rocket activity occurred as well even if on a smaller scale respect to solids and liquids and without operational developments. However the work done in that period has produced a great step in hybrid propulsion, defining the major part of the actual knowledge. A lot of experimental work was done in the United States, particularly at UTC. A wide variety of fuels and oxidizers were tested in different conditions defining the basis of hybrid rocket motor behavior.

The main finding was that hybrid regression rate data correlate well with the expression:

$$\dot{r} = aG_0^n L^m \tag{1}$$

Where G_0 is the oxidizer flux, L is the length, a, n and m are coefficient determined empirically. Using the previous equation engine design studies were conducted and equations were developed to determine stoichiometric length and to predict thrust and O/F shift with time.

A significant accomplishment during that period was the development of a regression rate model by Marxman and coworkers. The key of the model was to relate the regression rate with the convective heat flux from the turbulent diffusion flame to the fuel surface. This successful treatment was favored by several advancements made in that period in the analytical description of combustion and in the study of the flow above blowing surfaces (this last work was pushed by the need of ablative shield for the reentry warhead of ballistic missiles). The result of the model was an equation for the regression rate having the same structure of the experimental developed correlations, confirming the understanding of the basic hybrid physic. In particular the model was able to describe the blocking effect, which is the reduction of the heat flux on a blowing surface. This effect was responsible for the low sensitivity of hybrid regression rate to the termochemical parameters of the propellant combination.

Several aspects of the theory were investigated with the use of schlieren photographs of a slab burner [15].

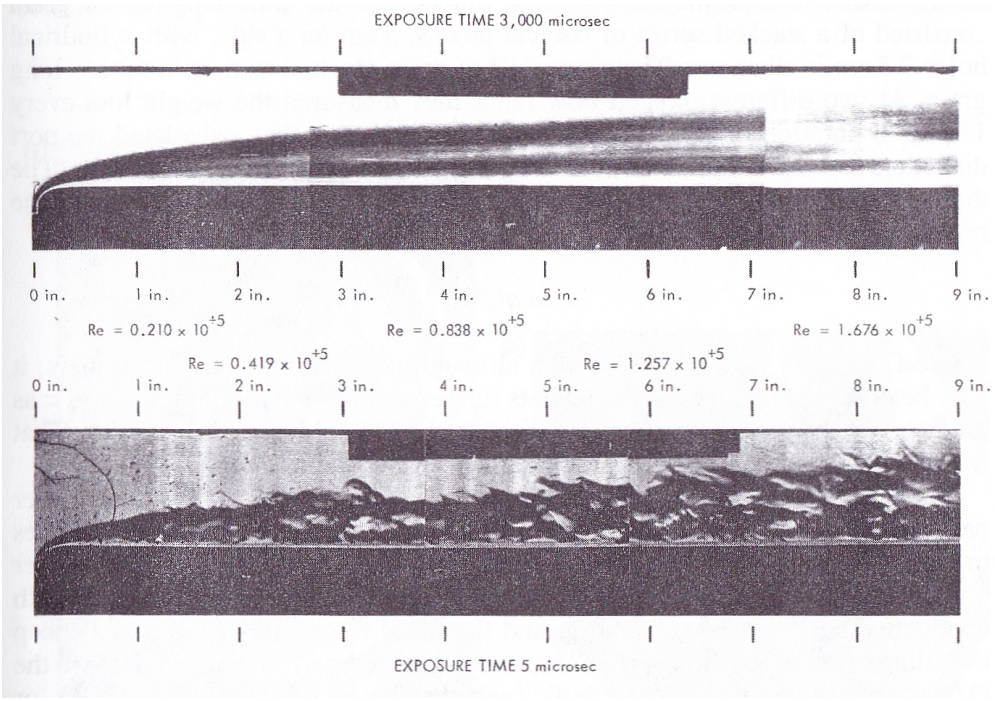

Figure 7: *Hybrid combustion boundary layer Schlieren photographs.*

In 1967 there was the first attempt to scale up hybrid technology with the test of a large motor (180 kN) using the multiport configuration. This solution was conceived to compensate for the low regression rate. The wagon-wheel grain design paved the way to the larger works made two decades later.

In the mid 1960s NASA sponsored a series of study about high-energy combination for space

engines. One concept was based on the reaction of lithium with fluorine, elements at the opposite ends of Mendeleev periodic table. A large eleven port motor (1.07 m diameter) was tested using 70% FLOX (70% fluorine 30% oxygen) as oxidizer and a mixture of lithium and lithium hydride incorporated on a HTPB binder. The ignition was hypergolic and the combustion was smooth. Probably the high reactivity of the propellants helped the vaporization and burning of the incoming oxidizer. This throttleable system exhibited high performances with an I_{sp} efficiency of 93% corresponding to a delivered vacuum impulse of 380s at an area ratio of 40.

Another approach called tribrid was conceived. The name indicates that three propellants were used, one of which in the solid phase. The motor should have burned liquid hydrogen, liquid oxygen and beryllium powder placed in a solid matrix (HTPB) The principle was to burn the beryllium with the oxygen to produce a large amount of heat used to accelerate a low molecular weight fluid (the hydrogen). This solution should have provided the highest possible I_{sp} for a chemical rocket (more than 500s). Both programs were cancelled because of the very dangerous characteristics of the propellants used (Fluorine ad Beryllium respectively) . The same destiny was shared with almost all the exotic propellants tested in that period (e.g. boranes).

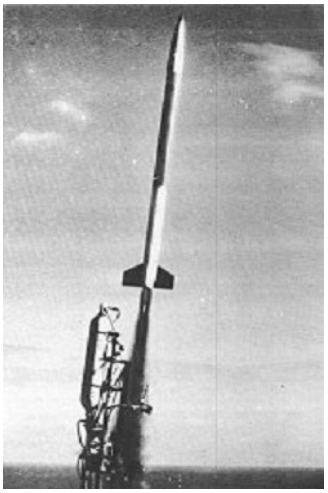

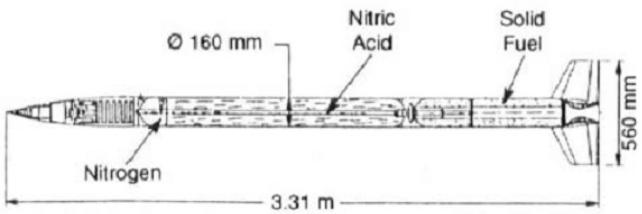

Figure 8: *LEX sounding rocket.*

At the same time in Europe two important activities were performed, culminating with successful ground and flight tests of hybrid sounding rockets. One was done in France by ONERA that developed the Lithergol experimental (LEX) [27]. The oxidizer was nitric acid while the fuel was based on amine consisting of metatoluene diamine/nylon. The ignition was hypergolic. To increase the regression rate and efficiency a diaphragm was placed in the

midst of the grain. An automatic system was developed to fill the oxidizer tank immediately before launch. The rocket was launched a few times reaching more than 100 km with 10 kg of payload and an initial weight of 70 kg, a record at that time and still an impressive figure. A larger version (LEX 04) was ground tested successfully 12 times afterwards.
A similar design and propellant combination was used in Sweden by Volvo Flygmotor. They developed fuels called Tagaform (PB plus an aromatic amine) and Sagaform. After the successful flight test of small rockets two large sounding rockets called SR-1 and SR-2 were planned but never launched. Both programs were abandoned in the '70.
Its worth to remark that the LEX sounding rocket was one of the high performing hybrid ever developed, achieving a very high combustion efficiency and propellant mass fraction and competing with solid rockets. However the use of a toxic propellant combination with the consequent handling complications and the lack of synergy with other (military) programs were probably the reason of the discard of the hybrid solution in favor of solid rockets.
A peculiar series of programs about hybrid target drones covered three decades from the '60s to the '80s. In the mid-1960's UTC and Beech Aircraft began to work on the Sandpiper under an USAF contract following a requirement for a unit capable to be launched from an altitude of 12 km, accelerate to 30 km at Mach values between 2 and 4 and fly for 300 s. The system required a propulsion unit able to guarantee a short boost - long sustain thrust profile with a throttle ratio of 8:1. Hybrid propulsion was considered an optimal candidate for this objective. The Sandpiper used the storable liquid oxidizer MON-25 (25% NO, 75% N2O4) and was pressure-fed with a Nitrogen tank. The solid fuel was composed by PMMA loaded with Mg. The system flew six times.
Later another program followed called High Altitude Supersonic Target (HAST). In contrast to the Sandpiper the propellant changed to IRFNA (inhibited red fuming nitric acid) and PB/PMMA and the oxidizer was pressurized by a ram air turbine that provided also electrical power. The grain configuration was changed from a single cylindrical port to a cruciform using four liquid injectors. Unlike the Sandpiper, which was expendable, the HAST was recoverable by use of an onboard drogue chute and retrieved in midair by helicopter. The thrust range on command was controlled by a throttle valve providing a 10:1 range. This work later became the Firebolt target missile system produced by Teledyne Ryan Aircraft (with CSD as the motor manufacturer). 40 units have been delivered.
These drones were the only hybrid flight programs built to military specifications. However, no follow-on contract for Firebolt production was awarded, presumably because it was signif-

icantly more expensive than the simpler expendable liquid fueled AQM-37. Its worth noting (and an ironic paradox) that both LEX and Firebolt were discarded not for their (excellent) performances but for reason of cost/complexity. This is in contrast with the common view that hybrid rocket motors are cheap but poor performing!

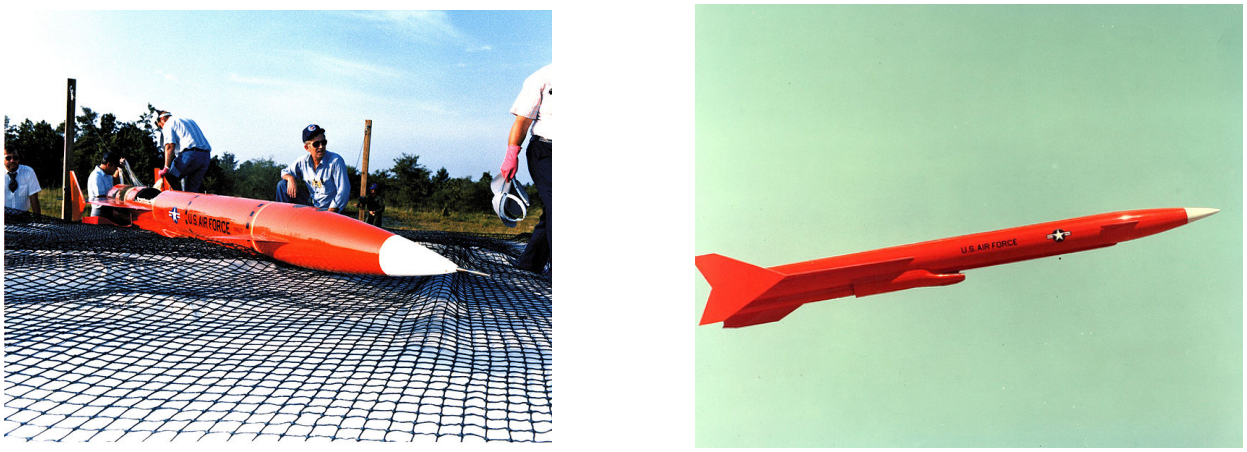

Figure 9: *Teledyne Ryan AQM-81 Firebolt Drone.*

After a decade of stagnation there was a revival of the interest for hybrid propulsion in the '80s. The growth of the commercial satellite market and the increased international competition prompted the search for a low-cost access to space. Two private ventures selected the hybrid approach as a way to reduce development and launch costs. The company STARSTRUCK was created to develop a large sounding rocket named Dolphin. The selected propellant combination was LOX/PB. A sea launch of this vehicle was attempted on 1984. Unfortunately a thrust vector LOX valve froze in the closed position causing a pitch over and a subsequent command termination. The company was subsequently reorganized in 1985 and renamed AMROC (American Rocket Company). With private funding AMROC began to develop a low-cost launcher called AQUILA [44]. The Aquila was composed by 4 LOX-HTPB common core boosters, a small solid upper stage and a final hybrid stage (N2O-HTPB) for accurate orbit insertion. The basic philosophy was to use high design margins to reduce development and production costs and to increase the reliability of the system. The inert characteristics of hybrid propellants were perfectly suited for this kind of approach.

AMROC fired the largest hybrid motors ever tested to that time. They relied on a multiport configuration to achieve the necessary burning area and had to face several stability issues. That work laid the foundation of our modern know-how on large hybrid systems. As an intermediate step the sea launch of a large sounding rocket called SET-1 was planned on 1989. Again a similar fate affected the new attempt. A LOX valve froze in a partially open

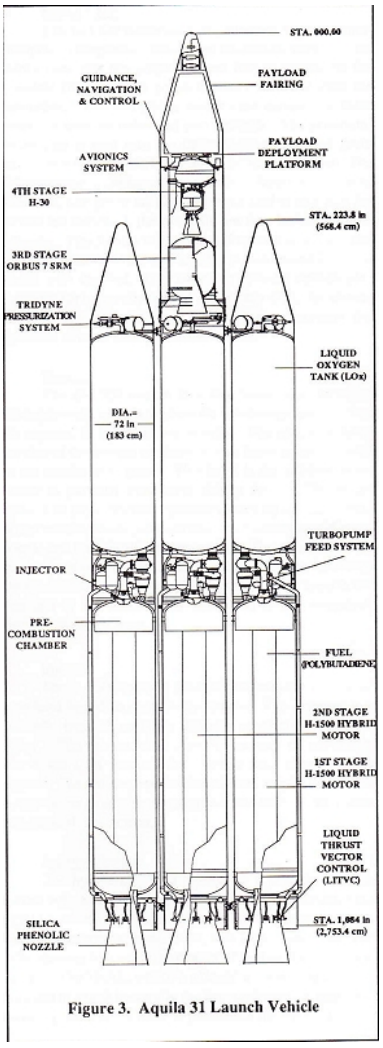

Figure 10: *Aquila Launch Vehicle.*

position resulting in insufficient thrust for lift-off.

The failures of both Dolphin and SET-1 were a negative setback; however they demonstrated an important hybrid feature. The damage made by the two accidents was very limited proving definitely the safety and nonexplosive characteristics of hybrid systems also at large scales. This attribute of hybrid propulsion gained more attention after the disaster of the Shuttle Challenger on 1986 when NASA became interested in a possible replacement of the Shuttle solid rocket boosters (SSRM). Hybrids were seen has an interesting option because of their larger grain manufacturing tolerances, their benign failure modes and their possibility to stop the motor in flight. Several design study were made to assess the use of hybrids for large boosters.

Meanwhile AMROC continued its work testing a 250000 lbf (1.1MN) hybrid motor at the beginning of the '90s. A new sounding rocket called HyFlyer using this motor was conceived. Because AMROC had insufficient founding to pursue the program on their own a new group

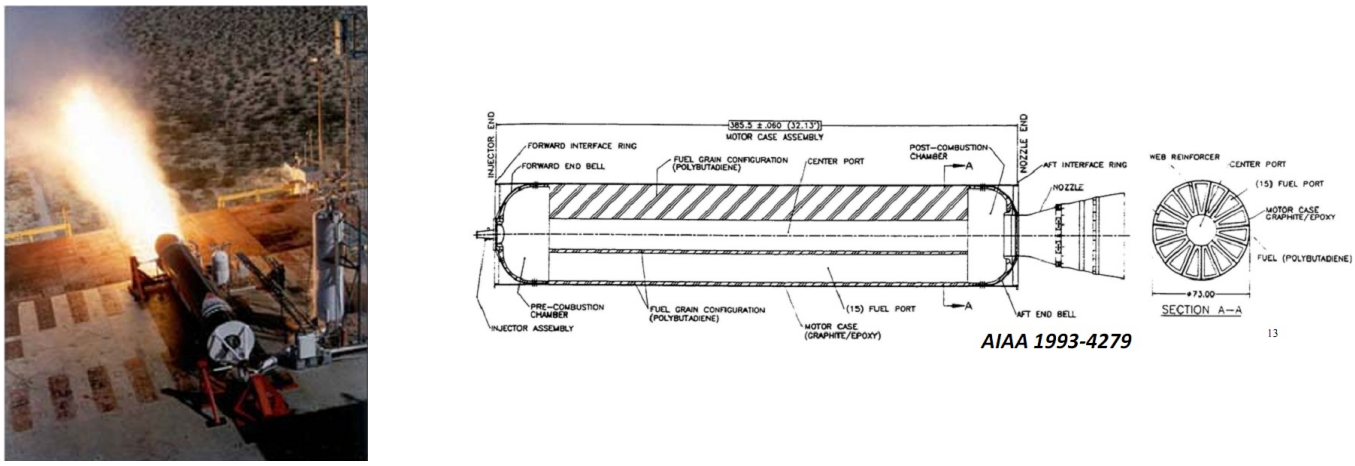

Figure 11: *Large scale test firing of AMROC Motors [49].*

was formed with support from NASA. The project was renamed Hybrid Technology Option Project (HyTOP) and included the companies AMROC, Martin Marietta and CSD. AMROC lost its sponsor and failed in 1995. The work continued within the Hybrid Propulsion Demonstration Program (HPDP) with a new member (Thiokol) replacing AMROC in the consortium [5]. New tests were done on a configuration slightly different from the previous ones. Some improvements were made but the basic limits remained. The multiport design chosen to overcome the low regression rate suffers of several drawbacks (as previously cited) resulting in a poor volume loading and fuel utilization.

Moreover the instabilities related to the difficult LOX vaporization and the flow unbalance between different ports were never completely understood slowing the development and leading to a more complex injector pre-chamber design. Often it was necessary to add an external heat sources to help LOX vaporization, like the injection of a pyrophoric fuid (e.g.TEA) or the use of small hybrids gas generators [62].

In the frame of the HDPD program Environmental Aeroscience Corp (eAc) designed, manufactured and tested the Hyperion sounding rocket using N_2O and HTPB as propellants. Four flights took place between 1996-1997 reaching a maximum of 36.5 km. These flights demonstrated a safe nonpyrophoric / nonpyrotechnic ignition, inexpensive component manufacturing, simple launch operations and a quick launch turnaround time. They represent also the first time a self-pressurized oxidizer was successfully employed in flight.

During the '90s hybrid research began to gain more attention also in the academic word and between small companies following the shifting from the performance dominated cold war era to a new period of increased attention for safety, cost and environmental friendliness. New (or sometime forgotten) ideas were conceived and tested in order to improve the low

regression rate of hybrids because it was seen (properly) as a major show-stopper for hybrid propulsion.

One of the most successful solutions proposed was the swirl or vortex injection (as it would be explained later there isn't a unanimous definition). In this configuration the oxidizer is injected tangentially to the chamber walls in order to create a rotating flowfield. This strong swirling flow inside the combustion chamber enhances the mixing of reactants, improving the efficiency. Moreover the higher local mass flux due to the tangential component of the velocity, the stronger generated turbulence, the flame position nearer to the fuel surface due to centrifugal forces all concur to a large increase of the heat transfer to the grain wall, leading to a noticeable improvement of the regression rate.

Yuasa [29][50] experimented swirl injection wherein the oxidizer entered the combustion chamber at the head end as in a conventional hybrid. He obtained regression rate values several times higher than with a classical axial injection. In the US Knuth [46] at Orbital technologies Corporaton (ORBITEC) experimented the (double) vortex hybrid wherein the swirl oxidizer was located at the aft end (opposite to Yuasa) of the fuel grain just upstream of the converging portion of the nozzle. Knuth discovered that this arrangement generated a pair of coaxial, co-rotating, bidirectional vortices in the combustion chamber. Following visualization experiments, numerical and analytical work confirmed this behavior. This configuration achieved a very high combustion efficiency and an impressive regression rate (even 7 times the classical values).

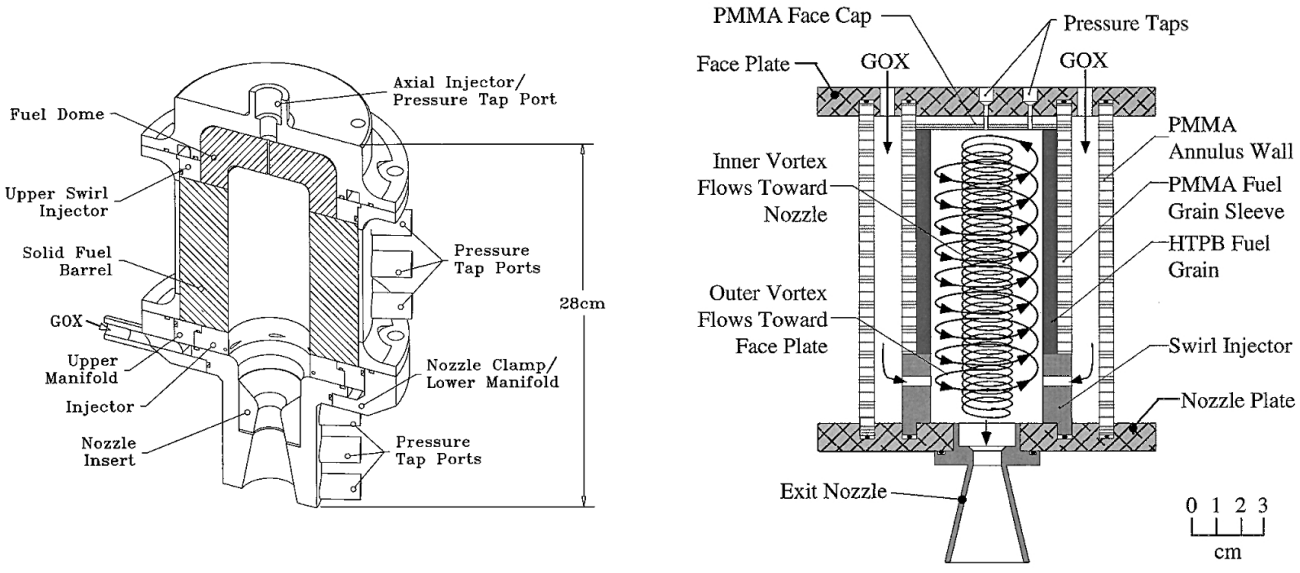

Figure 12: *ORBITEC Vortex Rocket Engine.*

At the end of the decade the vortex flow pancake (VFP) concept was developed at Surrey

[48]. In this case the swirling oxidizer flow is generated between two fuel disks that end burn in opposite directions during combustion. A very smooth combustion and high efficiency were obtained.

More recently NAMMO Raufoss applied the head end vortex injection on a H_2O_2-HTPB hybrid motor [69][70]. The great advantage of this solution regards the possibility to catalytic decompose the H_2O_2 prior to chamber injection. In fact most of the work with vortex injection has been done with the oxidizer in the gaseous phase (mainly GOX). However in a real motor the oxidizer needs to be stored in the liquid phase for performance reasons. Liquid vortex injection has received less attention and the few works are not as impressive as for gaseous injection. An alternative is to gasify the oxidizer prior to chamber injection but this usually adds complexity. An exception is the case of H_2O_2 that can be decomposed easily using a catalyst pack. In this way the fool potential of gaseous vortex injection can be exploited on an operational motor.

NAMMO configuration resulted in a motor that is stable, throttleable, achieving a good efficiency and a regression rate several times higher than a classical hybrid. Moreover the hot products of H_2O_2 decomposition are able to ignite the solid fuel. In this way the motor can be started and stopped several times without a separate ignition device.

Meanwhile several research groups began investigating the regression rate and combustion characteristics of hybrid motors that employed cryogenic solid fuels in the frame of a preparatory program about the combustion of high energy density matter (HEDM). A large number of cryogenic (here the term cryogenic is used in a extended meaning) solid fuels (pentane, methane, ethylene, RP-1 etc.) were tested at Air Force Philips Laboratory in the '90s and by ORBITEC in the early 2000s. ORBITEC tested also a reverse cryogenic hybrid using solid oxygen for the grain. The experiments revealed an unexpected large regression rate, even an order of magnitude higher than HTPB. These results could not be explained by a lower vaporization enthalpy because the blocking effect reduces the sensitivity of the regression rate to the thermochemical parameters and it is responsible for the relative narrow range usually encountered. Later Karabeyoglu at Stanford University developed a theory explaining the anomalous high regression rate of cryogenic fuels [6]. He postulated that an additional mechanism was present in the case of fuels forming a melt layer of low viscosity and surface tension (e.g. pentane or SOX). It has been shown that this melt layer could become unstable under the influence of shear stress of the gas flow in the port resulting in the formation of liquid droplets that are subsequently entrained by the main flow. After-

wards he determined that a class of storable fuels like paraffin waxes (alkanes with carbon number between 25 and 60) could present the same behavior [20]. Experiments at Stanford and NASA Ames confirmed the initial predictions [21]. Regression rate 4 times higher than HTPB were obtained.

Moreover the experiments showed also that the regression rate of paraffin wax is almost independent from the motor scale. This has the twofold advantage of making lab-scale testing more meaningful and to avoid the regression rate decay that classical fuels encounter when the motor is scaled up. Karabeyoglu later founded the small company SPG (Space Propulsion Group) which is developing paraffin-based hybrid motors under a contract for the Air Force. SPG is also collaborating with Stanford university and NASA Ames to the development of the Peregrine sounding rocket which is aimed to be a reusable and throttleable $paraffin\text{-}N_2O$ demonstrator able to lift 5 kg above 100 km [65][66][67]. In recent years paraffin has begun to be used by several researchers, academics and amateur worldwide (included CISAS).

After the HDPD experience Lockheed Martin started a new program in 1999 called HYSR [47]. The object of this work was the development and flight test of a large hybrid sounding rocket, advancing readiness level of this kind propulsion and shows its positive attributes. The three-year technology demonstration program was a collaborative effort between NASA and Lockheed Martin and had a total budget under $6 million. The oxidizer was Lox while the fuel was HTPB loaded with Aluminum. The motor had an initial thrust of 267kN for 33 s of burning time.

In the frame of this project Lockheed Martin developed and patented two hybrid based subsystems. One is the use of small hybrid rockets fed by gaseous oxygen (GOX) to ignite the main motor and to maintain combustion stability for the entire burn. The second relates with the pressurization technique. For simplicity a pressure-fed solution was selected in order to meet the budget and time constraints. However to limit the volume and the weight of the pressurization system, a special upgrade was conceived.

In LM patent the helium is stored at cryogenic temperature and moderate pressure. In this way the pressurant tank can be smaller and lighter. The helium is then mixed with the exhausts of a small GOX fed hybrid heater. Afterwards the hot helium mixture (94% He) flows through a minimal surface area heat exchanger to heat up the helium in the tank to minimize the helium residuals. Finally the pressurant enters the LOX tank trough a stainless steel diffuser, which disperses the flow into the ullage. The use of a warm pressurant reduces

the amount needed decreasing further the total weight and volume of the pressurization system. The HYSR was finally launched from Wallops on December 2002 reaching an altitude of 42 km.

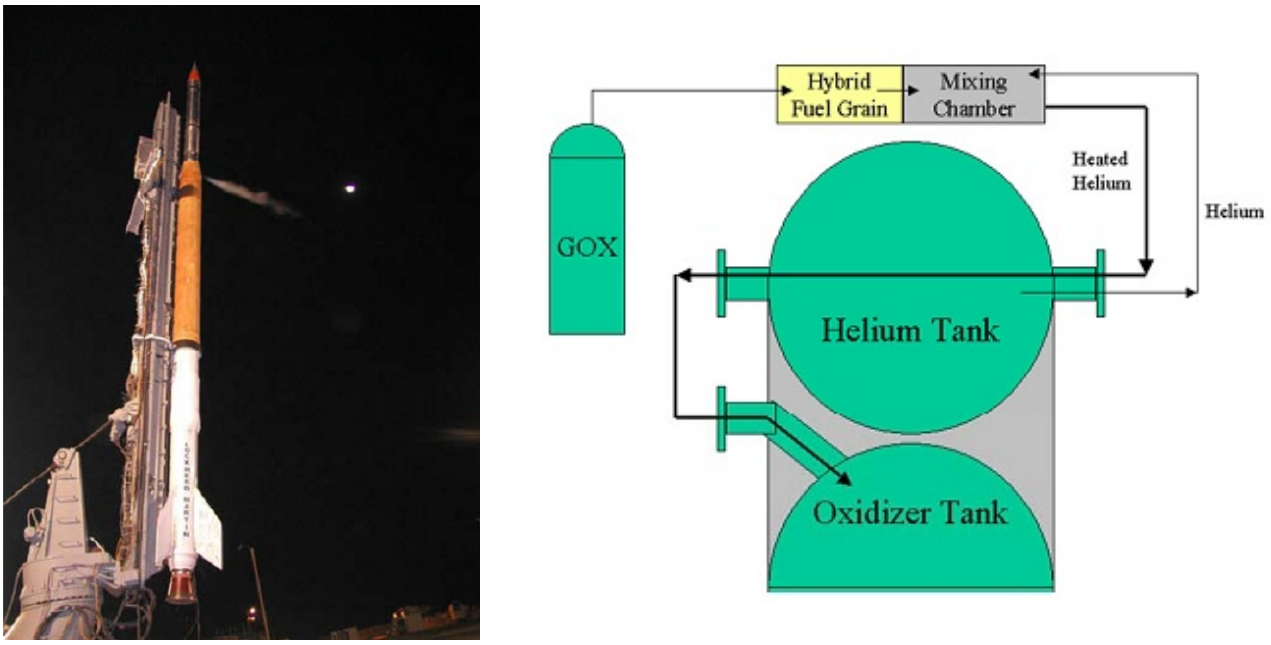

Figure 13: *HYSR Sounding rocket (left) and LM patented heated helium pressurization system (right).*

Based on the previous experience Lockheed Martin participated to the DARPA Falcon small launch vehicle (SLV) program aimed to develop and demonstrate an affordable and responsive space lift capability. LM claimed to have made several important improvements to the conventional design of large hybrids. The first aspect is the use of a pump-fed pressurization driven by a gas generator where an amount of LOX is vaporized mixing with the exhaust of GOX fed hybrid motor. The second fundamental achievement is a notable increase in the mechanical properties respect to the basic HTPB. This added strength allows a more complete consumption of the fuel without the need for leaving an overly thick residual or the use of web stiffener, reducing the inert weight and lowering the risk of potential fuel failure modes. As a consequence of this it was possible to shift to a multi-row configuration in order to increase the volume loading. Thanks to its high strength the internal rows can be consumed until the port merge. LM tested successfully a 3 rows - 43 ports upper stage motor in 2005 [64].

Doubtless the most famous hybrid success has been the victory of the Ansari X prize obtained by Burt Rutan's company Scaled Composites with its SpaceShipOne (SS1). The Ansari X Prize was a contest for the first commercial company to flight twice above 100km. Scaled

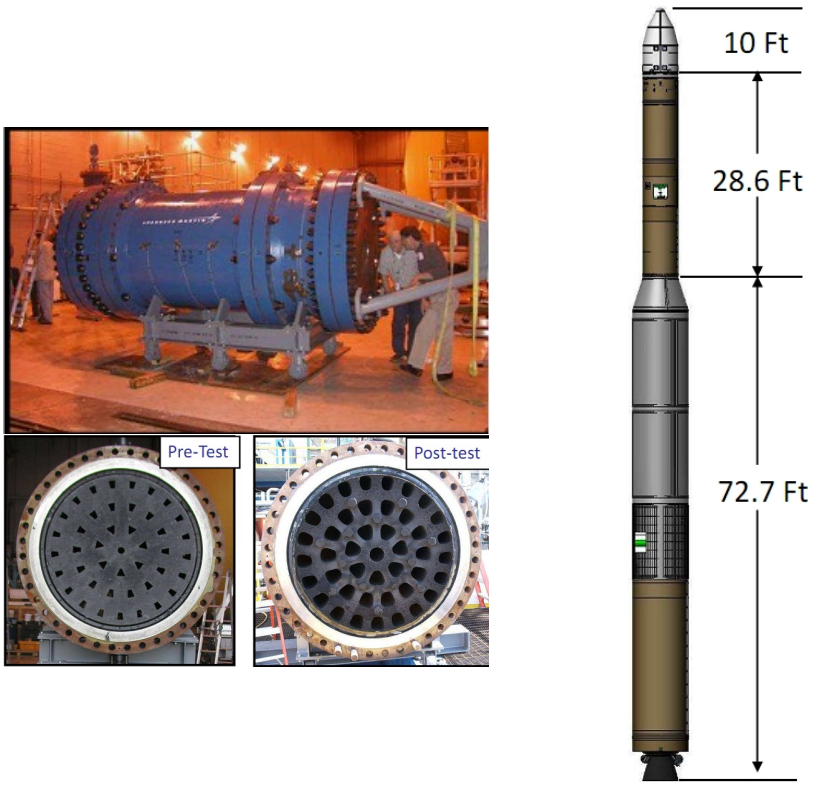

Figure 14: *Lockheed Martin DARPA Falcon hybrid rocket [52].*

composite built a two stage airplane to win the prize. The first stage was an air-breathing plane called WhiteKnight and was used as a carrier for the second stage plane, the already cited SS1 powered by an $N_2O/HTPB$ hybrid rocket motor. Two companies competed for the hybrid motor. eAc developed a single port hybrid motor loaded with aluminum while Spacedev (which had acquired AMROC intellectual property in 1999) presented a 4 port grain design. Finally SpaceDev was chosen to build the hybrid grains for the flight vehicles while eAc's design for some of the oxidizer system plumbing and valves was also adopted in the flight vehicle. The motor has a thrust of 74 kN for 87 s of burning time. Scaled Composites developed multiple unique and innovative solutions for its hybrid system.

SS1 is completely built around the hybrid motor and oxidizer tank, the latter bonded to the inside of the airframe. The N_2O valves were placed inside the oxidizer tank. This eliminates leak paths and allows the hybrid motor case to bolt directly to the oxidizer tank in a cantilever configuration. The use of N_2O high vapor pressure eliminates the need of a pressurization system. The motor was made in a single piece of graphite-epoxy composite materials (CTN: Case Throat Nozzle). Also the tank is made as a composite fibers overwrap with an internal liner. The case had burn through sensors built into the motor (fiber optic wire), so that if unusual burning is detected the motor could be shut-off.

SS1 flew successfully in 2004 reaching more than 100 km and winning the X prize. Thanks to SS1 accomplishment hybrid propulsion has begun to be known outside a restricted niche of propulsion engineers. The choice of hybrid propulsion by Scaled Composites confirmed its positive attributes like safety, good performance, system cost, quick turnaround, thrust termination. SS1 experience could indicate a path for the successful implementation of hybrid propulsion, that is extensive use of composite materials, self-pressurization, and integrated design [63].

Figure 15: *SpaceShipOne.*

Today Scaled Composite together with Sierra Nevada Corporation (SNC, which acquired SpaceDev) is developing the hybrid motor for the successor of SS1, the SpaceShipTwo. This larger vehicle is able to accommodate six passengers and two pilots and would be used by Virgin Galactic for suborbital space tourism.

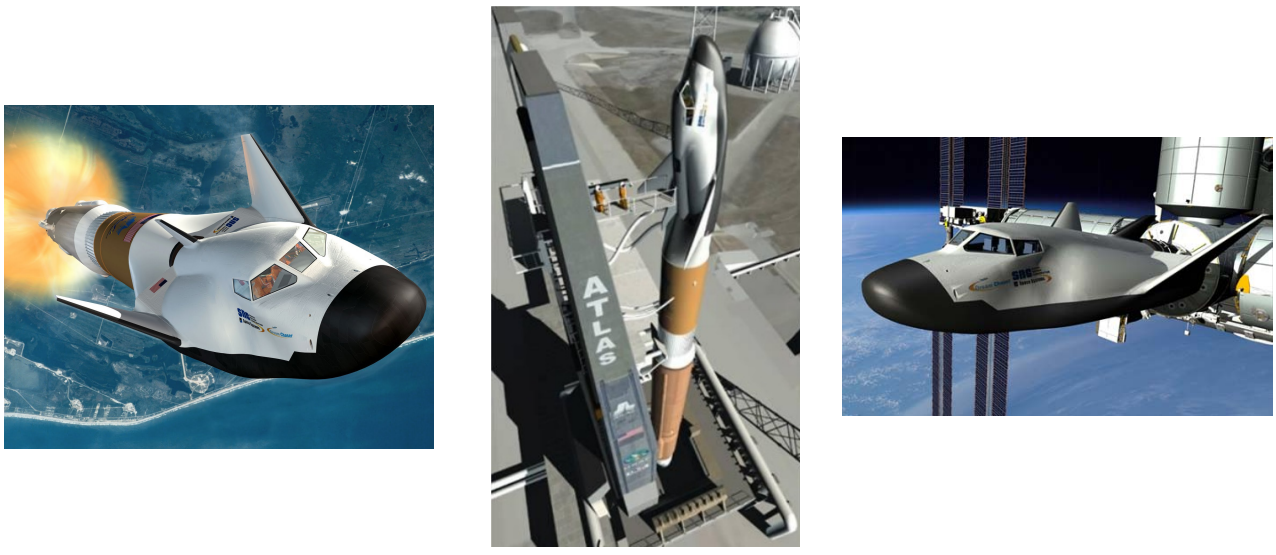

Figure 16: *Dreamchaser.*

SNC is also developing the Dreamchaser [51] under NASA Commercial Crew Development Program (CCDev). The Dreamchaser is a reusable composite spacecraft designed to

carry from two to seven people and/or cargo to orbital destinations such as the International Space Station (ISS). The vehicle would launch vertically on an Atlas V and land horizontally on conventional runways. Its lifting body design guarantee a soft-reentry from space (1.5 g versus several g for conventional capsules). On-orbit propulsion of the Dream Chaser is provided by twin hybrid rocket engines developed from SS1. The motors allow the vehicle to be used also as a Launch Escape System in a emergency situation, eliminating the need of a separate system (as it has been in previous manned capsules). Several milestones have been already achieved. If the program would be completed successfully the Dreamchaser could be the first hybrid propelled orbital spacecraft.

Finally two other events are considered worthy to be cited. The first is the launch of Atea-1 sounding rocket developed by the New-Zealand company RocketLab in 2009. The rocket was composed by a first N_2O hybrid booster and a second inert dart. The rocket had an empty weight of nearly 20 kg with a lift-off weight of 60 and was designed to reach more than 100 km of altitude. Unfortunately the second stage was not recovered so actual performances have been not verified. However it represents a demonstration that with a proper use of composite material a hybrid rocket could reach very good values of propellant mass fraction. The second event is the test of the largest hybrid rocket ever fired outside the United States occurred in 2012 in the frame of the Bloodhound project. This project aim to break the land speed record with a pencil-shaped car, powered by a combination of a jet engine (EJ200 from Eurofighter Typhoon combat aircraft) with a hybrid rocket and designed to reach 1,000 miles per hour (1,609 km/h). The pump-fed hybrid rocket motor burns 86% H2O2 with HTPB and it has a design average thrust of 111 kN (25,000lbf) for 20 seconds. The pump is driven by an F1 Cosworth V8 motor.

Chapter 1

Steady Hybrid Combustion

Before going into hybrid rocket transient behavior it is necessary to introduce the physics of steady hybrid combustion. The fundamental theory of hybrid combustion and fuel regression has been proposed by Marxman and coworkers at the beginning of the '60s and it will be described briefly in the following. In a typical hybrid rocket the oxidizer enters the combustion chamber from the head end and flows over the solid surface. After motor ignition a macroscopic diffusion flame develops above the grain. This flame heats up the grain surface until the solid fuel decomposes. The vaporized fuel mixes with the incoming oxidizer sustaining the combustion.

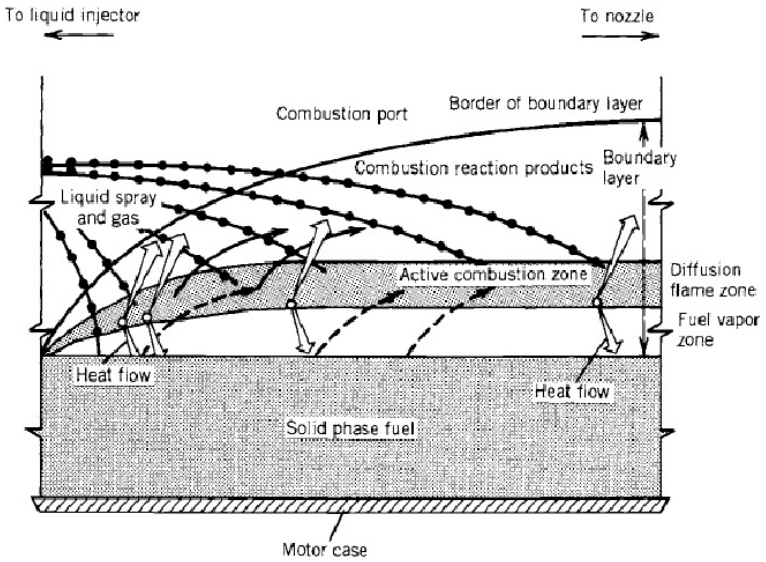

Figure 1.1: *Hybrid boundary layer [85].*

These phenomena take place inside the boundary layer. The boundary layer is defined as the region that is affected by the presence of the wall. It is possible to define multiple boundary layers, each one related to a specific variable. For example there is a thermal

boundary layer defined as the zone where the temperature changes from the value of the incoming flow to the wall temperature. There is a species boundary layer defined as the zone where the chemical concentration changes from the value of the incoming flow to the value at the wall. There is a momentum boundary layer as the region where the velocity is affected by friction and the fluid has to slow down to fulfill the no slip condition at the wall. In the boundary layer large gradients of the fluid variables occur. Let's consider the general conservation equation for a fluid quantity in the eulerian form (fixed reference frame):

$$\frac{\partial \Phi}{\partial t} + \bar{v} \cdot \nabla \Phi = D_\Phi \nabla^2 \Phi + S_\Phi \tag{1.1}$$

The first term is the time variation of Φ, the second term is the convective transport of Φ, the third term is the diffusion of Φ and the last term represents a source (or sink) for the variable Φ. The diffusion of Φ is proportional to the gradient of Φ. It is possible to state that the boundary layer is the region where the diffusive term cannot be neglected. Outside the boundary layer the fluid flow can be approximated as inviscid (dominated only by convection). The fact that all the fluid unknowns follow a similar equation suggests a similar behavior for all of them. In fact this is the basis for the so called Reynolds analogy. This analogy states that under specific conditions also the solutions to the equations should be similar that is they follow the same profile. These profiles can be related each other by adimensional parameters defined as the ratio between the diffusive transport of Φ_1 and the diffusive transport of Φ_2. Some parameters of interest for next discussions are the following:

Prandtl $Pr = \frac{\nu}{\kappa} = \frac{\mu c_p}{\lambda}$

Lewis $Le = \frac{\kappa}{D} = \frac{\lambda}{\rho c_p D}$

Schmidt $Sc = \frac{\nu}{D} = \frac{\mu}{\rho D} = LePr$

These numbers also represent the ratio between the thicknesses of the several boundary layers. For example when $Pr > 1$ the thermal boundary layer is thinner than the momentum boundary layer. When all the previous numbers are equal to one all boundary layers have the same thickness.

The important implication of the Reynolds analogy is that only one profile need to be known while the other can be scaled from the first accordingly with the respective boundary values

and the adimensional parameter cited before. If the profiles of the different variables are similar the same happens for the derivatives of those profiles. This fact has a fundamental outcome. In fact the heat flux is proportional to the thermal gradient ($\dot{Q} = -\lambda\frac{\partial T}{\partial y}$) so it can be inferred from the shear stress (that is proportional to the velocity gradient $\tau = \mu\frac{\partial v}{\partial y}$). This technique has been (and is still) widely used to solve heat transfer problems using the larger amount of analytical and semi-empirical data about the solution of the momentum equation. As it will be shown next the Reynolds analogy has been used also by Marxman in its treatment of the regression rate determination.

As previously announced inside the boundary layer the oxidizer diffuses from the external flow and mixes together with the fuel blowing from the surface. A specific concentration profile is formed through the balance of diffusion and convection. The flame is established inside the boundary layer at a position where the right species concentration occurs. For typical hybrid rocket motor operating conditions the rate at which chemical reactions occur is much faster than the time required by the reagents to reach the flame. The ratio between the fluid dynamic time scale τ_c and the chemical reaction time scale τ_k is called the *Damkohler number* $Da = \frac{\tau_c}{\tau_k}$. Following the previous consideration $Da >> 1$ for hybrids so the combustion is defined as diffusion controlled. In this case it is possible to neglect the chemical reaction rate and consider the combustion at the flame as occurring at an infinite fast rate.

It is possible to demonstrate that in a laminar boundary layer when the reaction rate approach an infinite value the flame thickness goes to zero and the flame occurs where the concentration corresponds to stoichiometric conditions. Mathematically it is possible to approximate the flame as a line where the reagents concentration goes to zero. This is the so called flame-sheet approximation.

In a turbulent boundary layer the physics is more complex because of the local time and spatial fluctuations. In fact experimental observations made by Marxman allowed to estimate that the fame thickness is on the order of 10% the boundary layer thickness. However the flame-sheet hypothesis is considered a first acceptable approximation in order to be able to handle the problem.

Based on this model it is possible to divide the boundary layer in two regions separated by the flame-sheet. In the upper part the oxidizer diffuses through the combustion products from the outer edge of the boundary layer to the flame position. The lower part extends from the flame to the wall surface and is composed by the vaporized fuel and the remaining

combustion products.

The point of departure of Marxman regression rate theory is a heat balance at the grain surface. For simplicity the initial development regarded a slab configuration. At steady state the heat flux to the wall surface should be equal to the heat required to vaporize the fuel plus the heat that is transported inside the grain through conduction:

$$\dot{Q}_w = \dot{r}\rho_f L_v + \dot{Q}_{in} \tag{1.2}$$

Solving the heat equation (see chapter) it is easy to demonstrate that the heat of conduction is equal to the energy required to heat up the fuel from the initial (ambient) temperature to the surface temperature. In this way it is possible to define simply an effective heat of vaporization:

$$\dot{Q}_w = \dot{r}\rho_f h_v \qquad\qquad h_v = c\,(T_s - T_0) + L_v \tag{1.3}$$

The wall heat flux is composed by a radiative term and a convective term. Usually the radiative term is small compared to convection and it is neglected in the basic theory of hybrid combustion. However a correction for the radiative part was introduced later. One of the key elements of Marxman theory is to find a way to determine the convective wall heat flux. First of all Marxman set the Prandtl and Lewis numbers equal to one in order to simplify the calculation. This hypothesis is made frequently for turbulent flows of gas mixtures and implies (as already stated) that all the boundary layers have the same size and their profiles are linearly related each other. Moreover he considered the fluid as incompressible. This is for sure a strong (and incorrect) hypothesis but it is acceptable for an initial treatment to make the calculation easier.

Remembering that $dh = c_p dT$ and $Pr = \mu c_p/\lambda = 1$ the wall heat flux becomes:

$$\dot{Q}_w = -\frac{\lambda}{c_p}\left(\frac{\partial h}{\partial y}\right) = -\mu\left(\frac{\partial h}{\partial y}\right) \tag{1.4}$$

Then he applied the Reynolds analogy in the region between the fuel surface and the flame. In this way it could relate linearly the enthalpy gradient to the velocity gradient. The proportional constant between the two gradients is given by the ratio of the difference of the corresponding variables at the two region boundaries (the flame and at the wall):

$$\frac{\dot{Q}}{h_c - h_w} = \frac{\tau}{u_c - u_w} \qquad u_w = 0 \tag{1.5}$$

so $\dot{Q}_w = \tau_w \frac{h_c - h_w}{u_c}$

Using the definition of the friction coefficient $\tau_w = 1/2\rho_e u_e^2 C_f$ where in this case e means the outer edge of the boundary layer:

$$\dot{Q}_w = \frac{1}{2}\rho_e u_e C_f \frac{u_e}{u_c}(h_c - h_w) \tag{1.6}$$

So with the use of eq.1.3:

$$\dot{r}\rho_f h_v = \frac{1}{2}\rho_e u_e C_f \frac{u_e}{u_c}(h_c - h_w) \tag{1.7}$$

Hereafter $\Delta h = h_c - h_w$ The enthalpy ratio could be generalized considering also heterogeneous chemical reactions occurring at the wall, like O_2 attack at the surface. In fact some experiments found a non-negligible presence of oxidizer in the region below the flame. Now the unknowns are the friction coefficient and the ratio u_e/u_c.

Before proceeding further it is important to highlight some aspects. Marxman model of hybrid combustion is based on the flow over a blowing flat plate. The presence of blowing alters the velocity profile and the shear stress respect to the case without blowing. The vertical flow from the surface enlarges the boundary layer increasing its thickness, reducing at the same time the velocity gradients and consequently the shear stress and heat flux. To describe the flow over a blowing surface it is necessary to introduce the blowing parameter B:

$$B = \frac{\dot{m}_f}{1/2\rho_e u_e C_f} \tag{1.8}$$

The blowing parameter represents the adimensional form of the vertical flow and so it is also a parameter that guarantees similitude. Different flows with the same blowing number present similar velocity profiles.

The blowing number is determined by the ratio of the vertical and horizontal flow. In the general case the blowing number can assume any value. Let's consider for example a perforated flat plate where two gas flows are injected, one parallel to the plate and the other through the holes on the plates. In this case it is possible to achieve any value of B simply changing the amount of the vertical or the horizontal flow. However in a hybrid rocket motor only the oxidizer flow can be selected while the regression rate is dependent on hybrid combustion physic so the blowing number B is not a free parameter but it's univocally determined by the complex hybrid boundary layer fluid dynamic. Comparing eq.1.7 to the definition of the blowing parameter we get:

$$\dot{r}\rho_f = \frac{1}{2}\rho_e u_e C_f B \qquad\qquad B = \frac{u_e}{u_c}\frac{\Delta h}{h_v} \tag{1.9}$$

This result means that for steady hybrid rocket operation the blowing parameter is determined only by the thermo-chemical properties of the propellant combination used. In fact, with a treatment that is omitted here for the sake of brevity, Marxman was able to obtain the ratio u_c/u_e and the position of the flame:

$$\Phi_c = \frac{u_c}{u_e} = \frac{O/F\,\Delta h/h_v}{K_{oxe} + (O/F + K_{oxe})\,\Delta h/h_v} \tag{1.10}$$

$$\eta_c = \frac{y_c}{\delta} = \left(\frac{\sqrt{1 + 2B\Phi_c\,(1 + B/2)} - 1}{B}\right)^{1/n} \tag{1.11}$$

The velocity ratio at the flame is dependent only on the enthalpy ratio $\Delta h/h_v$ and the O/F at the flame position. As a first approximation the O/F ratio at the flame is considered equal to the stoichiometric value, however the oxidizer moves almost parallel to the flame while the fuel is transported also by the vertical flow normal to the wall caused by vaporization (because the gas density is much lower than the solid density, so the gas has to move vertically). Moreover several other approximations are present in the model. Experimental measurements have confirmed that the flame is on the fuel rich side, burning at the slightly lower O/F ratio and hence accordingly to 1.11 at the lower position (smaller value of y_c).

Now that the blowing parameter has been determined the only quantity to determine is the friction coefficient. The friction coefficient with blowing could be related to its value without blowing:

$$C_f = \frac{C_f}{C_{f_0}} C_{f_0} \tag{1.12}$$

The value of C_f in the absence of blowing (C_{f_0}) is calculated through the empirical formula for a turbulent incompressible flow over a flat plate given by Schlichting:

$$\frac{C_{f_0}}{2} = 0.03 Re_x^{-0.2} \tag{1.13}$$

The ratio Cf/C_{f_0} represents the reduction of the friction coefficient caused by wall blowing. Its value should be 1 for $B = 0$ and continuously decreasing as $B \to \infty$. Marxman was also able to derive the following analytical expression:

$$\frac{C_f}{C_{f_0}} = \left[\frac{ln\,(1+B)}{B}\right]^{0.8} \left[\frac{1+13B/10+4B^2/11}{(1+B)\,(1+B/2)^2}\right]^{0.2} \tag{1.14}$$

that fulfills the condition $C_f/C_{f_0} = 1$ for $B = 0$ and $C_f/C_{f_0} \to 0$ for $B \to \infty$. Eq.1.14 can be approximated in a large interval with the following fit:

$$C_f/C_{f_0} = 1.2B^{-0.77} \qquad (5 \leq B \leq 100) \tag{1.15}$$

Afterward Altman [17] showed that in the range typical of hybrid motor the following fit is more accurate:

$$C_f/C_{f_0} = B^{-0.68} \qquad (5 \leq B \leq 20) \tag{1.16}$$

It is important to highlight that both fits provide the correct asymptotic value for $B \to \infty$ but gives unphysical results for $B \to 0$ ($C_f/C_{f_0} \to \infty$ instead of $C_f/C_{f_0} \to 1$) so they have to be used with caution. Substituting 1.12, 1.13 and 1.16 in eq. 1.9 and remembering that $Re_x = \frac{\rho_e u_e x}{\mu_e}$ we finally get:

$$\rho_f \dot{r} = 0.03 \left(\frac{\mu_e}{x}\right)^{0.2} (\rho_e u_e)^{0.8} B^{0.32} \tag{1.17}$$

The product $\rho_e u_e$ is then approximated with the average local mass flux G:

$$\rho_f \dot{r} = 0.03 \left(\frac{\mu_e}{x}\right)^{0.2} G^{0.8} B^{0.32} \tag{1.18}$$

It is possible to rearrange the equation combining all the terms that are considered approximately constant:

$$\dot{r} = a' G^{0.8} x^{-0.2} \tag{1.19}$$

The first important achievement of Marxman theory is that it leads to an equation that has the same functional form of the empirical fits obtained from experimental data. This confirms the validity of the basic physical model underneath Marxman formulation. Usually the regression rates derived from experimental testing are spatial and temporal averaged obtained from the weight of the fuel mass before and after the test (with rare exceptions like ultrasound or X-ray measurements). Following reference [53] it is possible to derive the correct averaged form of equation 1.19:

$$\dot{r} = a''\,(O/F)\,G_{tot}^{0.8} L^{-0.2} \qquad \text{or} \qquad \dot{r} = a'''\,(O/F)\,G_0^{0.8} L^{-0.2} \tag{1.20}$$

That corresponds qualitatively to the general expression found from experiments:

$$\dot{r} = aG_0^n L^m \tag{1.21}$$

The values of a, n and m obtained from experimental testing are different (generally lower) from the prediction of Marxman theory. This could be expected, taking into account the large number of approximations (sometimes with effects far from being considered negligible) that has been done in order to be able to handle the problem.
However Marxman theory represented a fundamental breakthrough for hybrid propulsion because for the first time it permitted to understand the key elements of hybrid combustion with a mathematical description.
Often the length dependency in eq. 1.21 is not explicitly considered because the experiments are done on a single scale and so the term L^m is implicitly included in the a coefficient. Also the O/F correction given in 1.20 is usually forgotten.
Unfortunately this practice has a negative outcome; in fact if the author does not indicate clearly the scale of its tests (and the O/F ratio) the regression rate data become less meaningful. As announced on the introduction the difficulties to scale the regression rate to different sizes and configurations have always been a great impediment on hybrid rocket development (as opposite to solids).
Coming back to equation 1.18 it is possible to highlight several aspects. First of all the regression rate is dependent on the local mass flux. This is a consequence of the convective heat transfer; in fact this is a result common to a wide range of other heat transfer problems. Another aspect is that the regression rate varies along the port. In fact the mass flux increases along x because of the fuel addition enhancing the heat transfer and consequently the regression rate down the port. At the same time the boundary layer grows and so the flame distance from the surface, leading to a relaxation of the temperature gradients and consequently a decrease of the regression rate along x. This effect is represented by the x term. These two opposite effects tend to counterbalance each other resulting in a relative slow variation along x. The final behavior is a regression rate that as an initial decrease reaching a minimum at a certain axial distance from the leading edge. Then the regression rate begins to increase again if the grain is long enough (as shown in figure 1.2). The first part is dominated by the flame departing from the surface while the second part (where the flame distance variation is slower) is dictated by the increase in the local mass flux [22][42].

Equation 1.18 is singular for $x \to 0$ because relation 1.13 is not valid close to the leading

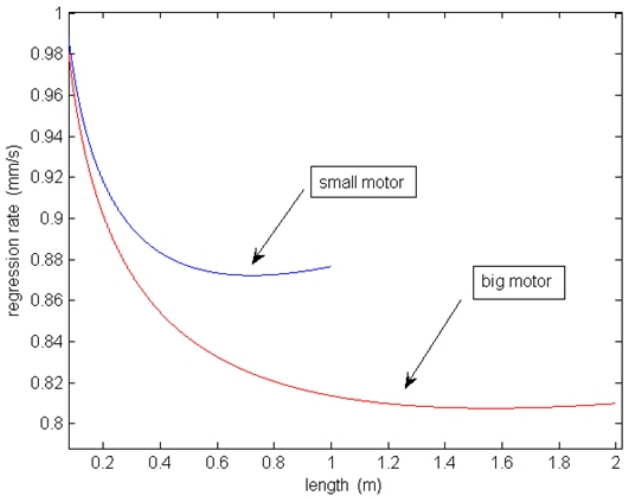

Figure 1.2: *Variation of regression rate along the axial direction.*

edge of the boundary layer. The regression rate at that point has a finite value that is related to the complex (and configuration dependent) flame-holding at the beginning of the grain. Another phenomenon contributes to smooth the change in port diameter along the axial direction. In fact considering again eq.1.19 it is possible to note that if the port diameter is locally larger the mass flux at that point is reduced. This in turn decreases locally the regression rate. The self-compensating mechanism of hybrid regression rate tends to flatten grain consumption and to counterbalance for local non-uniformities. This is a positive behavior in contrast with solid rocket where a unexpected variation of the burning area could lead to catastrophic failure caused by the coupling between burning area $\rightarrow$ mass flow $\rightarrow$ chamber pressure $\rightarrow$ regression rate. The relative smooth behavior of hybrid consumption allows the use of spatially averaged expression as 1.21 for preliminary calculations. However for demanding applications the residuals given by the non uniformity of grain burning cannot be neglected and can cause a performance penalty [45][43].

Another important aspect to underline from equation 1.21 is that, as anticipated, hybrid regression rate is scale dependent. Marxman theory predict a scaling coefficient equal to -0.2, while experimental data gives generally slightly lower values. Anyway the important consequence is that regression rate decreases for larger motor. Unfortunately this is the opposite of the desired behavior because, as previously said, larger motors require larger regression rates (i.e. web thickness) to achieve the same volume loading as small motors. The low regression rate of hybrid rockets and its reduction with increasing size has been for long (and partilly still is) the Achille's heel of hybrid propulsion.

Concerning the variation with size again it should be remarked that lab-scale testing could be meaningless without taking into account scaling issues because the data cannot be reported to different sizes. Even the comparison of different formulations could be misleading if the scaling law for them is different. A typical example deals with paraffin wax. This fuel has an higher regression rate than classical polymers and a fairly flat behavior with scaling, so its advantage on classical fuels grows with size.

Another aspect that concurs to the low regression rate commonly found for hybrids can be explained by Marxman theory. Looking at equation 1.18 it is possible to note that the regression rate is proportional to the enthalpy ratio $\Delta h/h_v$. This corresponds to physical intuition, in fact a higher enthalpy difference between the flame and the grain is related to a higher thermal gradient and consequently an increased heat flux. Moreover a lower h_v means that less energy (so heat flux) is required to vaporize the fuel. However blowing reduces the ratio $C_c f/C_{f_0}$ according to 1.16. For this reason in the final equation the blowing parameter has a much lower dependency.

The physical explanation is the following. An increase of the regression rate produces a larger blowing from the surface inhibiting the heat transfer to the wall (this behavior is beneficially exploited in the heat shield of re-entry vehicle or when using film-cooling). This phenomenon is called "blocking effect" and is responsible of the relative narrow range of regression rates encountered even considering a wide range of propellant combinations.

Equation 1.19 is valid only in a certain range of oxidizer fluxes. At low values the convective heat flux is small so the radiative term is no longer negligible compared to it.

Later Marxman introduced a correction to his model taking into account the radiative contribution. The radiative heat flux is calculated with the following equation:

$$\dot{Q}_{rad} = \sigma \epsilon_w \left(\epsilon_g T_c^4 - T_w^4 \right) \tag{1.22}$$

The radiative contribution increases the total wall heat flux. This in turn leads to higher regression rates. However again the "blocking effect" counteracts inducing a reduction of the convective heat flux and consequently limiting the actual regression rate increase. Marxman derived the following equation for the regression rate when both convective and radiative heat transfer are considered:

$$(\rho_f \dot{r})_{rad} = \frac{1}{h_v} \left[\dot{Q}_c exp \left(-0.75 \frac{\dot{Q}_{rad}}{\dot{Q}_c} \right) + \dot{Q}_{rad} \right] \tag{1.23}$$

This relation shows that for low values of the ratio $\dot{Q}_{rad}/\dot{Q}_c$ the reduction of the convective heat flux is almost equal to the radiative contribution. In fact for $\dot{Q}_{rad}/\dot{Q}_c < 0.2$ the difference is only 6%. This behavior led to consider the effect of radiation almost always negligible. An exception is the case of metallized fuels were the radiation heat transfer from the particles contributes in a significant amount to the regression rate. When the radiative flux is equal to the convective heat flux calculated without radiation the total flux is not doubled but it increases only by 47% because the convection is strongly reduced. As expected for $\dot{Q}_{rad}/\dot{Q}_c \to \infty$ the total flux becomes linearly dependent on $\dot{Q}_{rad}$. The coupling of the two heat transfers is clearly shown in figure 1.3.

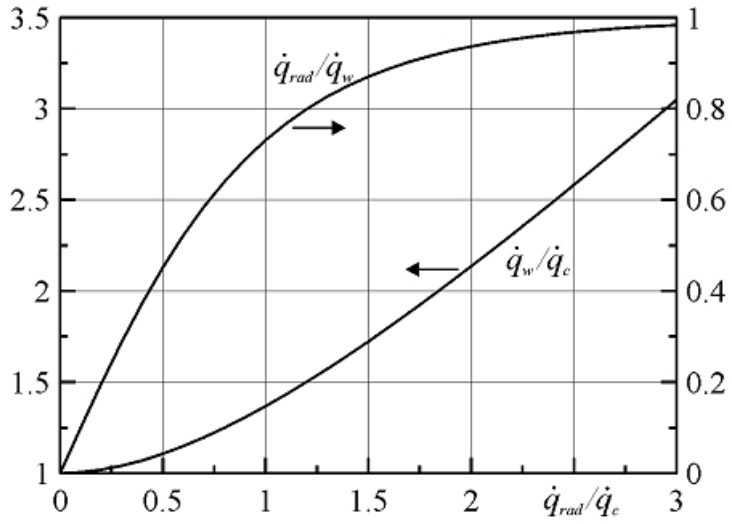

Figure 1.3: *Coupling between radiative and convective heat fluxes.*

The radiative heat flux component may originate from various sources: the gaseous products of combustion, such as H_2O and CO_2, soot made by incomplete burning of hydrocarbon, metal or other particles liberated from the pyrolysis of the solid fuel. Soot and other solid particles behaves nearly as a black body while the gaseous molecules release radiation energy only in specific emission bands related to their excited states. The emissivity of the gas phase is dependent on the number of molecules for unit volume, so it is related to pressure:

$$\epsilon_g = 1 - e^{-bpy} \tag{1.24}$$

For this reason radiation contribution increases at higher pressures. In the radiative dominated case the regression rate is not dependent on the mass flux. It is a common thought that if the regression rate does not exhibit a pressure dependency that means that radiation can be neglected. However later Chiaverini calculated that the soot contribution

is very high for HTPB burning with Oxygen, much higher than the gas emissivity. On the opposite of the gas phase, the emissivity of the soot particles is related only to the O/F ratio:

$$\epsilon_{soot} = 1 - e^{-k_s} \qquad k_s = 0.51 - 0.113 O/F \tag{1.25}$$

Unfortunately in this case there is not pressure dependency so it is not possible to asses indirectly the importance of the radiative contribution.
Chiaverini demonstrated that the total heat flux curve has nearly the same shape as the convective heat flux curve but differs in magnitude so that radiation cannot be ignored for non-metallized fuels as previously thought. However its study was related to HTPB burning with Oxygen while other propellant combinations could present a much lower soot formation.
Equation 1.19 is also not valid at very high mass fluxes. In fact in this case the residence time becomes small and it is not possible to state anymore that the ratio between the fluid dynamic timescale and the chemical reaction timescale is large. Chemical kinetics comes into play limiting the regression rate. At this point the rate at which the reagents are transported to the flame is faster than the rate of their consumption. The chemical reaction rate increases with pressure so the same should happen to the regression rate at very high mass fluxes.
Wooldridge and Marxman developed a correction to the classical regression rate equation taking into account the effect of chemical kinetics. In the kinetic limited case they found the following form:

$$\dot{r} = cp^{0.5} G^{0.4} x^{-0.1} \tag{1.26}$$

Equation 1.26 has still a qualitative meaning, however it highlights the fact that for high mass fluxes the regression rate is dependent on pressure (as expected) and less dependent on the mass flux. Actually, experimental data shows that in the limiting case mass flux dependency tends to disappears. It is useful to recap all the last considerations about hybrid regression rate in a simple graphical form such as the logarithmic plot of the regression rate as a function of the oxidizer mass flux. In fact in a logarithmic plot Marxman basic relation appears as a straight line. The slope of this curve is equal to the exponent n. For high mass flux the slope decreases because of the limit of chemical kinetic. At the same time at low G_0 the slope flattens because of the growing of the radiative term.
Moreover a family of curves appears at both extremes, showing a variation of regression rate with pressure. The highest pressures lead to the highest regression rates. The range of the

linear (in the logarithmic plot) part of the regression rate curve is enlarged by an increase of pressure at high mass fluxes, while the contrary happens at low G_0.

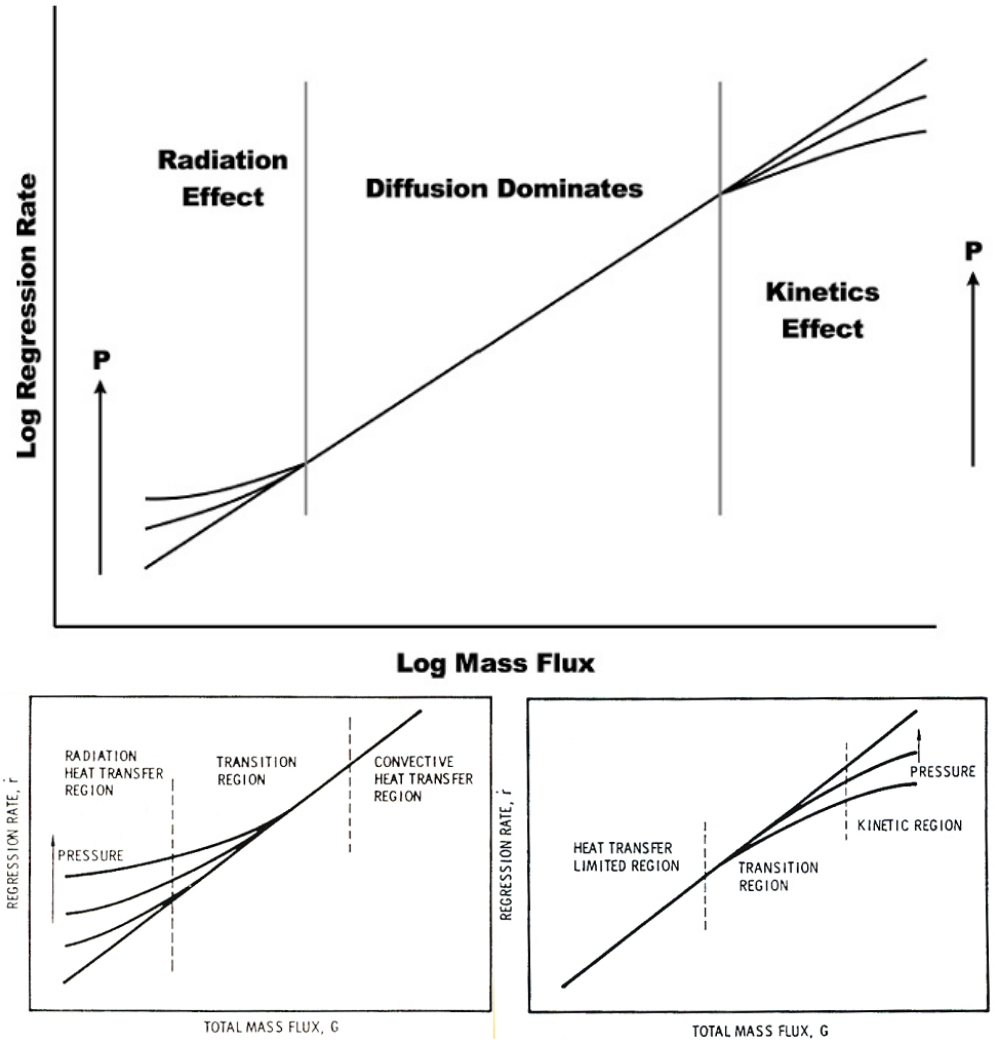

Figure 1.4: *Logarithmic plot of regression rate vs. oxidizer mass flux.*

For conventional polymeric fuels like HTPB the range of linear behavior is pretty wide. On the contrary for metalized fuels where metal particle combustion-radiation effect play a significant role the lower zone is much extended and could cover all the practical fluxes used on hybrid motors.

However Chiaverini [42] later demonstrated that sometimes also the straight line can shadow an important radiation (albeit pressure insensitive) dependency. Based on previous discussions even without a pressure dependency the importance of radiation could be inferred by a lower n exponent. Unfortunately due to the strong assumptions of Marxman theory to ascribe the finding of an exponent lower than 0.8 simply to radiation is very debatable.

Marxman theory has been a fundamental step in the understanding and description of the

basic features of hybrid regression rate. However its prediction is qualitative as it fails from a quantitative point of view. Several researchers have tried to improve the original treatment without success. No new development has found widespread diffusion as the original one, the reason for that being that they still don't eliminate the need for experimental testing in the regression rate determination. Moreover some questions were left open by Marman theory and following researches were not able to achieve some final satisfactory answers to them. Here some points that the author thinks need to be underlined.

The exponents of Marxman model are not correct. In the author opinion this aspect is a bit overlooked in hybrid literature for the following reasons. Often people are interested to find a suitable fit of experimental data in a certain flux range. Taking into account experimental errors several $a/n/m$ combinations can give a pretty good fit in a prescribed range, even if some of them show apparent unphysical trends. However the role of the exponents in relation 1.21 is much more important than for the constant a. The exponents not only determine the quantitative value of the regression rate but they influence several important trends as the uniformity of consumption along the axial direction, the scale effect, the O/F shift during the burn. So their correct evaluation has a greater impact than generally perceived. That's also why it would be useful to check the fits of the experimental regression rate data with a basic numerical simulation of pressure and thrust behavior during the burn of each test using the fits to predict the instantaneous $\dot{r}$. At least in the author knowledge very limited work has been done paying attention explicitly on the reasons of the departure of n from 0.8 (except radiation). Here some hypotheses are discussed.

The first easier explanation is the effect of radiation. However as discussed previously, it is difficult to prove that this issue is always only related to radiation.

The second easy explanation relies on the simplicity of Marxman model. Several assumptions were made in order to facilitate achieving a closed form solution. The main ones are to simplify hybrid boundary layer with the incompressible boundary layer over a flat plate and the use of Reynolds analogy with $Pr = Le = 1$.

In this context it is interesting to show the results from some CFD simulations that have been done at CISAS [10]. These simulations refer to a laboratory scale hybrid rocket motor used by Grosse [55] in its experimental investigation of diaphragm usage to improve hybrid rocket performances. The oxidizer was N_2O and fuel was paraffin wax that for simplicity in the simulation was injected from the fuel walls as gaseous C_2H_4.

The numerical results were obtained solving the Reynolds-averaged 3D compressible Navier-

Stokes equations with combustion using the eddy dissipation model. Unfortunately a complete validation of local results was impossible in the absence of detailed experimental data. However a general good agreement was found between the predicted and measured chamber pressures.

For the analysis of the validity of Marxman theory the simulation of the motor without diaphragm is of main concern. The lateral plots of the temperature and oxidizer concentration shows the typical features of hybrid combustion. A strong stratified flowfield is established in the combustion chamber with the oxidizer moving almost parallel to the flame along the port. As already explained this configuration is responsible for the generally lower performances of hybrid rocket motors. The analysis of the profiles near the grain walls can highlight other interesting aspects.

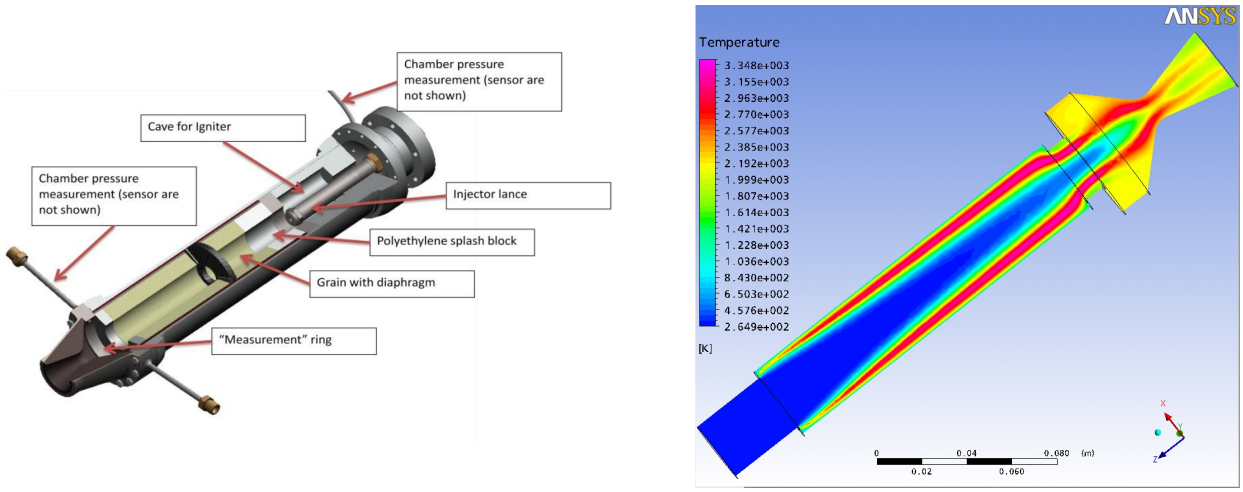

Figure 1.5: *Grosse motor (left) and CISAS simulations (right).*

First of all very large gradients of temperature, velocity, species concentration occur in a very thin region near the wall, showing an extreme variability of properties in the hybrid boundary layer. It could be intuitively affirmed that this could be one of the major point of departure of the real hybrid physic respect to Marxman mathematical model.

The flame does not form where the reactants join in stoichiometric conditions (where there is the higher minimum reactant mass fraction) because the reaction rate depends also on the turbulent eddy frequency.

The turbulent eddy frequency is higher near the walls, this accounts for a fuel-rich flame. This is confirmed by experimental results and is in contrast with the laminar flame, where the Burke-Schumann model applies.

In the turbulent case, the flame is thicker. It appears thick due to the process of time averag-

ing. In reality, the flame is thin and moves rapidly up and down due to the eddies (wrinkled laminar flame regime). Usually the flame is determined to be near 10% of the boundary layer height. The flame can also thickens when is not able to burn all the reagents sufficiently fast (generally the high fluxes region). In fact (as already stated) some experimental investigations found the presence of a non-negligible amount of oxidizer in the region below the flame.

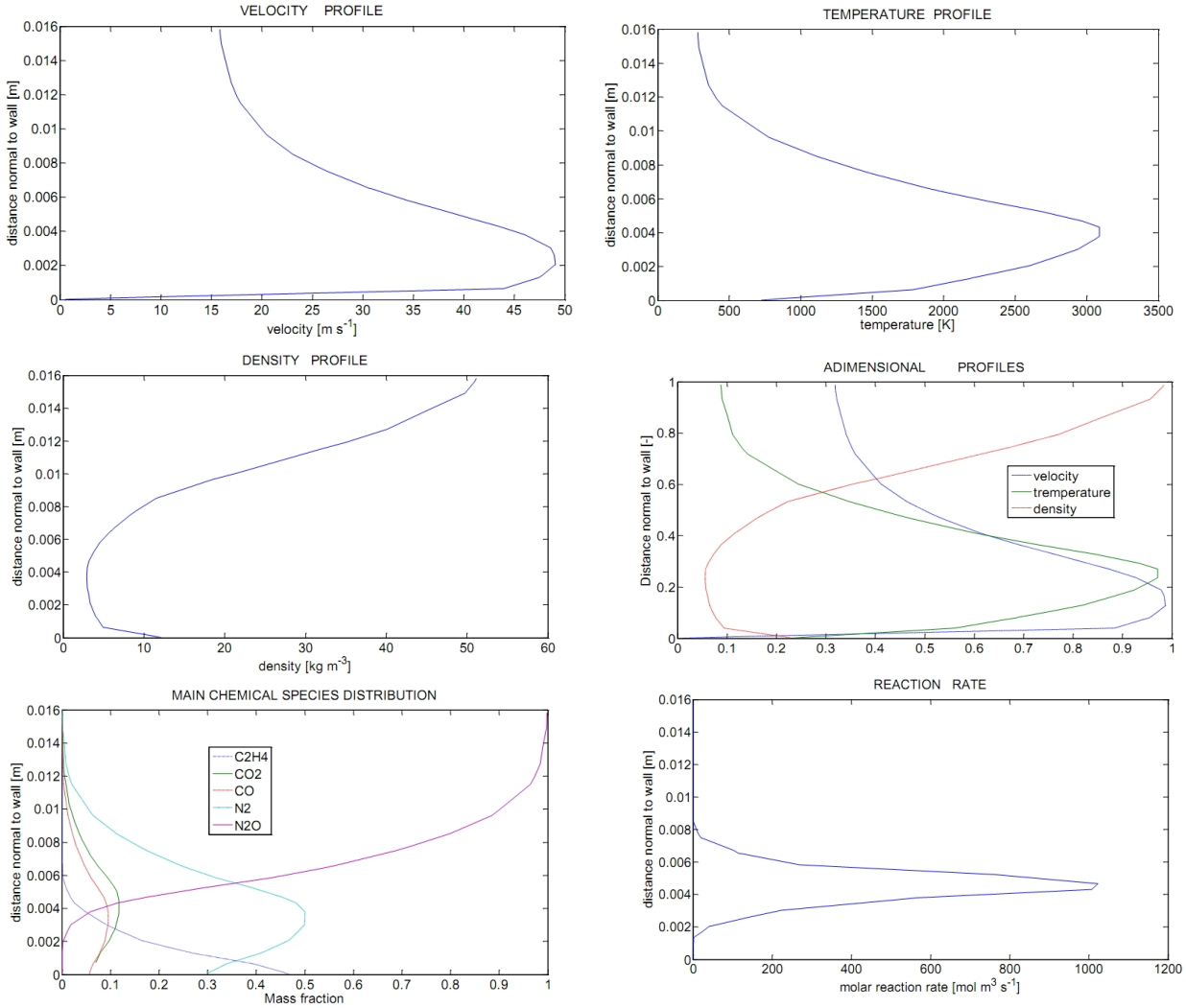

Figure 1.6: *Boundary layer profiles at half grain length, no diaphram.*

In the flame zone there is a peak of temperature and velocity while the density is minimum. The temperature peak is reached slightly above the velocity peak. The velocity inside the boundary layer is higher than in the central oxidizer core. This characteristic makes hybrid combustion to show a very uncommon behavior.

One of the classical definitions of boundary layer indicates it as the region where velocity is decreased by friction whereas in hybrid combustion the opposite occur! In fact the veloc-

ity **inside** the boundary layer is higher than in the 'external' flow! The heating from the flame determine a drop in the products density. The gas is not able to expand normally to the flame because of the inertia of the incoming horizontal oxidizer flow. Thanks to a sort of 'local Rayleigh motion' the velocity near the flame has to increase remarkably. This means that the classical regression rate theory has to be modified to take into account this unconventional behavior.

Marxman theory considers a velocity profile that is completely different from the one just described. In the case of a constant density flow the velocity reaches its maximum at the edge of the boundary layer. Several researchers (included Marxman itself) tried later to modify the original results to take into account the effects of variable fluids properties. However often the correlations and the methodology used have been developed for flows that have the same qualitative profile as the incompressible case. This is due to the fact that usually no-one of the reference cases presents a heat source (the flame) inside its boundary layer. Even in the case of very high heat fluxes and strong gradients in the fluid properties the maximum and minimum temperature are defined alternatively at the wall and at the edge of the boundary layer. In this way the velocity profile is quantitatively different from the incompressible case but resembles it qualitatively.

The inflection of the velocity profile caused by the flame location is known but often forgot or its importance overlooked. The fact that is almost never reported in typical layout of hybrid boundary layer seems to confirm that. Chiaverini reported (as previous graphs confirm) that similar inflections were also found for the sensible enthalpy and species concentration profiles, suggesting that the generalized Reynolds analogy assumption is still valid (and in a certain sense even more). However neglecting the inflection from the mathematical treatment should lead necessarily to incorrect results (e.g. the ratio u_e/u_c, flame position etc.).

Coming back to the exponents' issue, it originates first of all from the use of Reynolds analogy and then from the correlation used to determine the friction coefficient. The flux exponent 0.8 comes subtracting the Reynolds number dependency (-0.2) from the linear relation on the mass flux. Those exponents are common to almost all heat transfer correlations. Therefore almost all the efforts introduced to improve Marxman model doesn't change this basic values. Even taking account the velocity profile inflection should not apparently change this point.

One exception is a paper by Ziliac [104] where he related the n exponent to the pyrolysis Arrhenius constant based on previous numerical solution of a chemically reacting laminar

boundary layer. Unfortunately its expression is not specifically validated and it fails to explain geometrical or oxidizer dependencies. For example Lhoner [105] found very low n exponent for fuels burning with N_2O[1]. Also Stanford data for paraffin show a lower exponent for N_2O (0.5) than GOX ($0.62-0.67$) even if in this case it should be noted that the presence of the entrainment introduces further complications.

It is interesting to note that in Marxman theory the length exponent and the flux exponent are related as $n = 1 + m$. If this would hold also for $n \neq 0.8$ one could argue if it is possible to indirectly recover the length dependency from the flux exponent. Moreover this would imply that lower flux exponent mean worse scalability. However this has not been proven and it seems sometimes that the opposite occurs (as it should be if the reduction of n is due to radiation because it doesn't scale negatively as convection).

Another possible explanation to the exponent issue could be related to the variability of the parameters encapsulated in the a coefficient. In fact as showed earlier a strong variation of the gas physical properties occur in the boundary layer, mainly in the direction normal to the wall but also to a less extent in the axial direction (particularly if the boundary layers from different sides begin to merge). The values inserted in eq. 1.19 could be considered as a sort of proper averaged values. However these mean values could be different for different axial positions and mass fluxes. Following this idea the regression rate is more likely something as this:

$$\dot{r} = a'\left(G_0, x\right) G_0^{0.8} x^{-0.2} \tag{1.27}$$

Fitting the experimental data with a conventional expression should move the dependency of a directly on the flux and length exponents (not to be confused by the averaging effect described in [53]). Finally another important point is responsible to the deficit of Marxman model. Marxman theory is based on a diffusion flame formed in a turbulent boundary layer over a flat plate. However the way the oxidizer is injected can lead to a significant departure from this ideal model.

Boardman [56], Carmicino [57][58][59] and Pucci [4] have reported the effects of different types of oxidizer injectors on the fuel regression rate (as well as combustion efficiency and stability [3]). Carmicino showed that, if the oxidizer is fed into the fuel port by a conical axial nozzle, the recirculation region, established between the gaseous oxidizer jet boundary and the fuel grain's surface upstream of the impingement region, induces a convective heat

[1] However, as discussed later, perhaps such a low exponent could be related to injection effects.

flux to the fuel wall, which is higher and differently distributed when compared with the one in the turbulent flow through straight constant-cross-section pipes. Rather, the flowfield and the ensuing heat-transfer distribution in this condition are almost similar to those in a solid fuel ramjet having a sudden expansion of airflow. In fact, in both axial injector hybrid motor and solid fuel ramjet, three distinct flow regions exist (see Fig. 1.7):

1. Recirculation zone into which oxygen is transported from the jet core across the turbulent shear layer (here, fuel provided from the wall is recirculated and reacts with oxygen near the head end of the grain; the flame initiates along the shear layer).

2. Impingement or reattachment region where the oxygen attacks the grain surface.

3. The zone downstream of oxidizer impingement, where the turbulent boundary layer starts developing. Within this boundary layer a diffusion flame is, instead, formed.

This injection technique resulted in regression rates both increased (up to 2.5 times higher) and more or less unevenly distributed along the axis, depending on the ratio between the grain final diameter and the injector diameter. Furthermore, this flowfield leads to a lower dependence of regression rate on mass flux (smaller mass flux exponent, $n = 0.37$) and introduces a pure geometric effect, which is an explicit regression-rate dependence on the grain port diameter. A larger diameter moves the impingement point further downstream, extending the recirculation zone. The heat transfer (and regression rate) in the recirculation zone is high and reaches his maximum at the impingement point. The dependency of the heat transfer in the recirculation zone to the oxidizer flux is very weak, lowering the global (i.e. averaged on the entire grain length) flux exponent.
These results cannot be explained by other means than the effect induced by axial injection; in fact different results (and more aligned with Marxman theory) were obtained by Carmicino using a radial injector, confirming the strong role of oxidizer injection on hybrid flowfield and regression rate.
Boardman showed also trough CFD analyses that liquid injection (as should be used by real motors) is characterized by a more uniform inlet flow because the evaporation of the oxidizer in the pre-chamber induces a more homogeneous pattern. Undoubtedly very unconventional injection patterns like the vortex one generate a flowfield that differs completely from Marxman model even if the bases still hold (convective heat transfer, blowing, blocking effect).

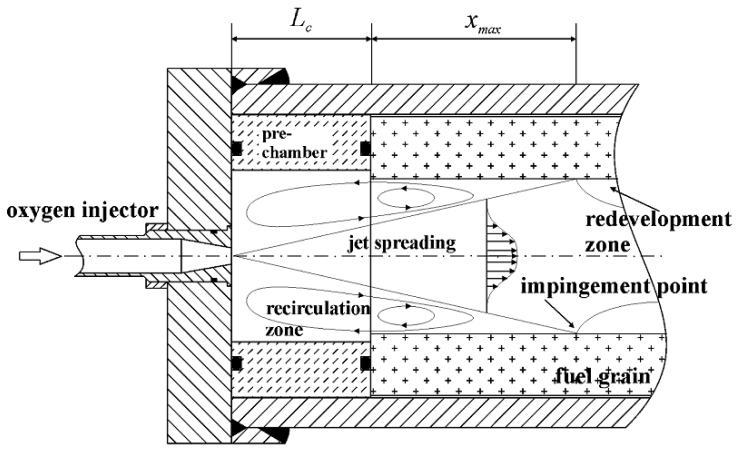

Figure 1.7: *Axial injection main flow characteristics.*

The other main point to remark about the flaws in Marxman model is related to the weak dependency of the regression rate on the propellant properties caused by the blocking effect. This is generally valid, a (unlucky) demonstration being the strong difficulties encountered to increase typical low hybrid regression rates by use of additives with lower vaporization enthalpy. On the opposite the (kinetically limited) regression rate of solid propellants can be changed easily with small amount of catalysts that allow accelerating chemical decompositions-reactions. However sometimes the regression rates of different hybrid fuels is more dissimilar than expected.

For example the data presented in for HTPB and HDPE are too similar to explain the much higher (almost doubled) regression rate of the former respect to the latter. Following Marxman theory an increase of the blowing number (for $B^{0.32}$) of ten times is necessary to double the regression rate and that seems not the case. Maybe this difference could be explained by a much higher soot production of HTPB (and radiative contribution). However as stated by some authors the difference should decrease at higher mass fluxes were the radiative contribution has less impact.

Another explanation could be related to the different molecular weight of the pyrolysis products. In fact some researchers stated that the significantly different regression rates empirically measured for polymeric fuels may be explained by the different molecular weights of their respective decomposition gases near the surface. Heavier decomposition gases reduce the blocking effect caused by mass injection into the boundary layer and therefore regress relatively faster than fuels with lower molecular weight decomposition gases that on the contrary behave as better shield of the heat flux [42].

1.1 Impact of Steady Regression Physics on Transient Behavior

A peculiar feature of hybrid combustion is that a real steady-state is never achieved. In fact the port area grows during the burn, consequently the mass flux and the regression rate change continuously with time. As a result also propellant mass flow and thrust usually vary with time. This is in contrast with liquids were a stationary condition can be met fixing the inlet propellant mass flows. Also for solids an exact steady state cannot be defined due to grain consumption; however it is possible with proper geometrical design (neutral grain) to obtain the steadiness of global parameter like burning area, chamber pressure, regression rate, propellant mass flow and thrust.

Unlike liquids, in a hybrid rocket only the oxidizer mass flow can be directly controlled. However the dependency of the regression rate to the mass flux permits to couple the fuel production to the oxidizer flow. When the oxidizer mass flow is increased/decreased the same happens to the fuel flow. Unfortunately this self-adjusting behavior is not perfect so an O/F shift occurs. Moreover even when the oxidizer mass flow is kept constant the decrease of the oxidizer flux and regression rate induces a change in the fuel production. For this reasons it is possible to state that hybrid rocket motor behavior has always a 'transient feature'.

A simple expression for the regression rate like 1.21 is sufficient to highlight the main characteristics of this specific hybrid behavior [17]. With its use the O/F ratio can be expressed as:

$$O/F = \frac{\dot{m}_{ox}}{\dot{m}_f} = \frac{m_{ox}^{1-n} D^{2n-1}}{a\pi^{1-n} 4^n \rho_f L} \tag{1.28}$$

The simplest geometrical configuration is the circular port. In fact it is the only one that preserves its shape during consumption. Any other shape will change with time becoming more round and smoothing the corners. Finally all shapes tend to convert in a circle for very long burning time. Moreover, unlike solids, hybrid regression rate is dependent on the local fluid dynamic, so being axisymmetric the circular port is the only that guarantees (nominally) a regression rate that is not dependent on the azimuthal position. However as eq. 1.21 neglects the axial variation of $\dot{r}$, at the same time as a first approximation the regression rate can be kept spatially constant (along both directions) also for different port geometries. First of all let's consider the simple case when the oxidizer mass flow is kept fixed. The opening of the circular port with time induces a decrease in the oxidizer flux and the regression

rate, but at the same time an increase of the perimeter and burning area. The fuel mass flow is proportional to both the regression rate and the burning area so the final fuel production would depend on the balance between the two. In the case examined the only parameter in eq. 1.28 that changes with time is port diameter. The exponent of the diameter dependency is $2n-1$. So if the flux exponent is 0.5 no O/F shift occurs. In this particular case all global parameter remain constant like fuel and total mass flow, chamber pressure and motor thrust. This happens because the reduction of regression rate is perfectly balanced by the increase of the burning area. For $n > 0.5$ the reduction of regression rate is larger, so the fuel mass flow, chamber pressure and motor thrust decrease with time. For $n < 0.5$ the regression rate variation is more flat so the increase of burning area prevails. Consequently the fuel mass flow, chamber pressure and motor thrust increase with time.

As already remarked a variation of the O/F with time implies a performance penalty because it is not possible to maintains the O/F ratio at the optimum value for the entire burn. However with careful design it is possible to choose the initial O/F in order to spend the major part of the burn in proximity of the optimal condition.

For non-circular ports the situation is more complex because port shape changes with time. The circle is the shape that has the lower perimeter for a given area. That implies that the rounding of non-circular port with time tends to increase the $Area/Perimeter$ ratio. This in turn induces a positive O/F shift and a regressive behavior (lower fuel mass, pressure and thrust) that however tend to diminish with time. This effect should be added to the natural growth of $Area/Perimeter$ with port size that is neutralized for $n = 0.5$. The final result is similar to the case of a circular port as if the flux exponent was replaced by an equivalent one were $n_{eq} > n$, so the neutralization requires $n < 0.5$. However n_{eq} changes with time (approaching n for $t \to \infty$) so a perfect balance is impossible. Anyway it is possible again to limit the O/F shift with careful design.

Let's consider now the variation of the O/F ratio with the oxidizer mass flow. This case highlights what happens when the motor is subjected to a throttling event. The O/F ratio is dependent on the oxidizer mass flow with the $1-n$ power. As expected for $n = 1$ no O/F shift occurs. In fact $n = 1$ represents a linear variation of the fuel flow with the oxidizer flow, that in turn produces an exact self-adjusting behavior. However the flux exponent predicted by Marxman theory is 0.8 and typical experimental values are even lower so fuel variation is sub-linear. That means that the variation is lower than desired and an O/F shift occurs when the motor is throttled. For throttling up the O/F shift is positive, the fuel production

increases less than necessary as for chamber pressure and thrust. The opposite happens in case of throttling down.

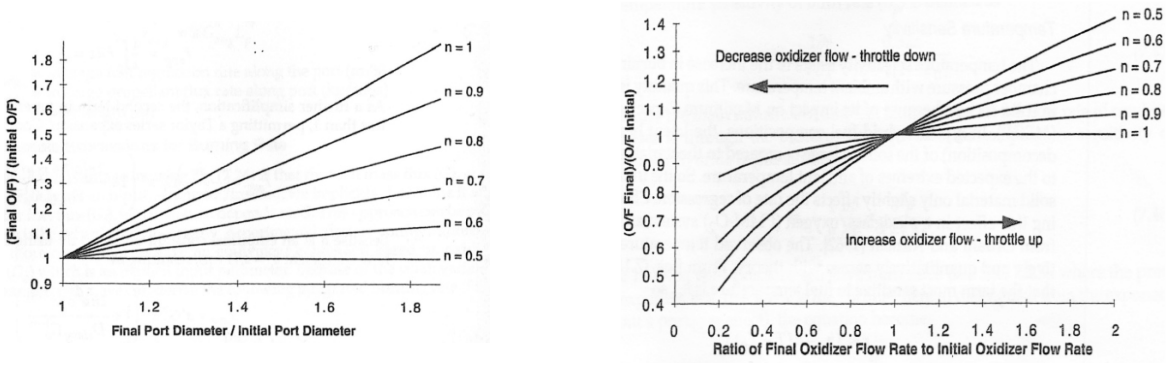

Figure 1.8: *Hybrid motors O/F shift: with diameter (left), with throttling (right).*

The fact that in case of throttling the fuel variation is lower than wanted has a twofold consequence. In fact not only as always an O/F shift translates in a performance penalty but also this effect enlarges the necessary oxidizer throttling ratio for the same total (and consequently thrust) variation. This second aspect could lead to a larger difficulty in the design of the oxidizer flow control.

To limit both issues if a motor should be throttled on a wide range a high flux exponent is preferred. However this requirement is conflicting with the need to have $n = 0.5$ to limit the O/F variation with time. A trade-off between the two is needed.

To limit the performance penalty one positive practice is to use a propellant combination that has a flat $I_{sp} - O/F$ curve, one example being the addition of metal hydrides (e.g. $LiAlH_4$ as proposed by Osmon). However this solution doesn't affect so much the problem of thrust control/variation with time. If the thrust profile is known in advance another option is to choose a propellant combination with n near 0.5 and then to design the motor to work near optimal performances, for example burning at the optimum O/F ratio at the thrust levels that contribute to the highest fraction of the total impulse. If every thrust level is kept for the same time the highest thrust levels should be favored because they consume the largest amount of propellant. Moreover fixing optimum O/F at maximum thrust help throttling because the reduction of performances with O/F shift contributes to decrease thrust during throttling down (and vice versa). However $n = 0.5$ could be no good in terms of oxidizer flow control.

Anyway another option could be used to limit this issue as all the other problems of unwanted thrust variations, that is the use of a propellant combination operating at a very high O/F

ratio. In fact in this case the oxidizer flow represents the great part of the total flow so the pressure and the thrust have a little sensitivity to any kind of O/F shift.

It's worth noting that the oxidizer mass flow can change not only by active throttling. Systems operating in blowdown or self-press mode have a natural decrease of the oxidizer flow with time. This in turn induces a negative O/F shift. In this case to limit the O/F shift with time a n slightly higher than 0.5 is recommended in order to have a partial compensation between oxidizer decline and port opening.

A slow active variation of the oxidizer flow could also be used to compensate any kind of O/F shifts due to port opening (no matter the n or the shape). However this could be not compatible with the requirements for the thrust-time profile. One drawback of hybrids is, in fact, that generally O/F ratio and thrust cannot be decoupled.

Finally let's consider the case where the regression rate has a pressure dependency [60]:

$$\dot{r} = aG_0^n p^m \tag{1.29}$$

This time the O/F ratio can be defined as:

$$O/F = \frac{\dot{m}_{ox}}{\dot{m}_f} = \frac{m_{ox}^{1-n} D^{2n-1}}{a\pi^{1-n} 4^n \rho_f L p^m} \tag{1.30}$$

Now let's relate the chamber pressure with the mass flow:

$$pA_g = \dot{m}c^* \tag{1.31}$$

And we obtain:

$$O/F = \frac{A_g^m m_{ox}^{1-n-m} D^{2n-1} (O/F)^m}{a\pi^{1-n} 4^n \rho_f L c^{*m} (1 + O/F)^m} \tag{1.32}$$

This equation is implicit respect to the O/F. Anyway it could highlight several important aspects. As in the previous case if $n = 0.5$ there is no O/F shift with port opening (for circular shape). The exponent of the term m_{ox} is now $1-m-n$, so to neutralize the effect of changes in the oxidizer flow is necessary to have $n+m = 1$. That means that for $n = m = 0.5$ the O/F ratio is independent from both throttling and port opening. Again metal addition could be an interesting option for throttleable motors because it generally reduces the flux exponent and introduces a pressure dependency. As expected, when the regression rate is dependent on pressure the O/F ratio becomes also sensitive to throat erosion (A_g^m). For high O/F ratio and/or small m it's possible to consider $(O/F)^m \approx (1 + O/F)^m$ (e.g. for

$m = 0.4$ and $O/F = 6$ we obtain 2.05 and 2.18, respectively); eq. 1.32 can be now made explicit as the following approximation:

$$O/F = \frac{A_g^m m_{ox}^{1-n-m} D^{2n-1}}{a\pi^{1-n} 4^n \rho_f L c^{*m}} \tag{1.33}$$

Although, strictly, c^* is still an implicit function of O/F.

Chapter 2

Hybrid Transient Behavior Overview

The study of transient behavior is a fundamental need for the development of high performing hybrid rocket motors, particularly when throttling is concerned. In fact hybrid motors are easy to throttle and thus they are ideal candidate for soft-landing applications and generally when propulsion energy management is required. However transient behavior is a very important aspect also for motors that have to work at a fixed nominal operating point. In fact any motor should go trough a transient phase during ignition and shut-down.
Moreover as already highlighted the fuel generation process cannot be directly controlled and it induces an inherent transient behavior that causes a shift of the operating parameters with time.
Finally the understanding of transient behavior is essential for the analysis of instabilities. The prediction and reduction of instabilities are one of the main challenges in hybrid propulsion (as it happens in general in the development of all combustion devices).
Following the previous thoughts hybrid transient behavior can be split between the quasi-steady and the full transient behavior. The first is focused only to the time-variation of operating conditions while the latter is related to the complete dynamic of the system. Concerning the last category the typical necessary or intentional transient events occurring during the operation of a hybrid rocket are classified and described in the following paragraphs[1].

[1] In contrast instabilities represent a deeply unwanted transient event.

Ignition

The ignition of an hybrid motor is composed by several steps. First of all the solid fuel is heated up to pyrolysis temperature by a (generally short duration)[2] heat source. Sometimes the heat source is pointed directly on the fuel, some others it is used to heat the oxidizer flowing afterward on the solid grain. Subsequently the hot vaporized fuel has to mix with the oxidizer and ignite, usually in a small spot near the forward end of the grain. The process is a bit different when using a hypergolic combination because the fuel can react with the oxidizer without the need of vaporization, speeding up ignition a little bit. Then there is the process of flame spreading on the entire grain length. Finally, after that the complete ignition of the grain is achieved the motor has to reach the operating condition.
In a solid rocket this last phase is determined by the pressure coupling between the filling of the motor and the fuel production. A simple analytical solution of this process can be found [40].
Unlike solids, in hybrids the motor O/F ratio during ignition is not constant but is higher (oxidizer-rich) than its steady-state value reaching it toward the end of the transient. The controlling time elements in this process are those that establish the combustion boundary layer and the thermal lag in the solid fuel [6].
In a liquid rocket motor the characteristic times are the ignition delay and the filling time of the chamber[3].
The time required to establish a steady-state in a hybrid motor is consequently higher than for both liquids or solids. However hybrid ignition is more tolerant and safer.
In fact hybrid fuel generation process and diffusion-limited combustion usually prevent small anomalies in the ignition process to produce a catastrophic failure. If an excess of propellant is present in the combustion chamber before ignition an hard start can occur. However hybrid rockets are much less prone to this issue respect to liquids because the fuel is not injected directly in the combustion chamber but it has to be vaporized and the ignition process is more gradual.
As previously explained the fuel mass flow during ignition is generally lower than the steady state value. This is in contrast with liquid rockets where (without special precautions) the initial mass flow is equal to the steady state value or even higher if isolating elements

[2]However sometimes the heat source does not cease after ignition, for example when using a catalytic decomposed oxidizer (H_2O_2, more rarely N_2O) or because of stability issues.

[3]Note that the combustion chamber of a liquid rocket motor is smaller than an equivalent solid or hybrid.

are not used and the mass flow is dependent on the injector pressure drop (i.e. higher at the beginning). Hybrid hard start are easier when using oxidizer that can self-decompose exothermically (like nitrous oxide) because in this case only the oxidizer needs to accumulate before ignition. However this issue could be managed with proper timing of the oxidizer flow and an efficient ignition source (i.e. preventing excessive accumulation).

Throttling

A hybrid motor can be throttled easily varying the oxidizer flow rate. The study of the motor response to a change in the oxidizer flow is essential to determine if the hybrid propulsion unit can fulfill mission requirements.

The quasi-steady-state analysis has been already showed but it's important also to characterize the full transient, particularly the response time and the shape of the response (e.g bounded or with overshooting). The response time is dependent on the feed system response time, the filling-emptying time of the chamber and the transient fuel production. The feed system response is common with liquid systems, the advantage being on having only one fluid to control without the need for synchronization.

The chamber filling-emptying time can be roughly estimated by the 0-Dimensional approximation:

$$\tau_{fill} = Cd_n \frac{\left(\frac{\gamma+1}{2}\right)^{\frac{\gamma+1}{2(\gamma-1)}}}{\sqrt{(\gamma RT)}} \left(\frac{V}{A^*}\right) \frac{RT}{(RT)_{av}} \tag{2.1}$$

Lately Karabeyouglu found a more accurate analytical approximation for the hybrid filling-emptying time scale [6].

The transient fuel production is dependent on the thermal lag in the solid grain and the transient relation between the heat flux and the oxidizer flow. The thermal lag in the solid grain has been discussed firstly by Marxman [15]. He showed trough analytical considerations that the thermal lag was proportional to $\kappa/\dot{r}^2$. Moreover he determined that the thermal lag increases as the value of the parameter $c\Delta T/h_v$ increases, so the transient period is somewhat more critical with fuel having a low h_v or a high vaporization temperature.

A more complete analytical and numerical analysis has been performed recently by Karabeyoglu [6]. He showed that the grain response is composed by two time scales, the largest being that found previously by Marxman. The initial grain response can be much faster

and sometimes an overshooting occurs, followed by a slow relaxation to the steady state. The ratio between the two time scales and the amount of the (eventual) overshooting is determined by the values of the activation energy and the vaporization energy.
Karabeyoglu also investigated the transient relation between the wall heat flux and the oxidizer flux [6]. He considered that in the low frequency range the heat flux could be calculated with the same approach of Marxman treatment. However in the transient case the regression rate cannot be calculated by eq. 1.3 (naturally the steady heat balance at the grain surface is no longer valid) and the blowing correction should be linked to the actual regression rate (that should determined by the complete solution of the transient thermal profile in the solid grain).
Karabeyoglu defined the blowing parameter in eq 1.8 as the aerodynamic blowing parameter B_a and the blowing parameter in eq. 1.9 (that is now unrelated with the actual fuel blowing) as the thermochemical blowing parameter B_t. The aerodynamic blowing parameter is equal to the thermochemical one only at steady state. After some manipulations he finally found the following general expression for the transient heat flux:

$$\dot{Q}_{conv} = A' x^{m/(1-k)} G^{n/(1-k)} \dot{r}^{-k/(1-k)} \tag{2.2}$$

theoretical values: $n = 0.8$ $k = 0.68$ $m = -0.2$

This equation simplify to classical Marxman heat flux at steady-state.

Thrust Termination

Generally an hybrid motor can be easily stopped terminating the oxidizer flow rate. However for solid fuels containing some oxidizer is possible that the combustion is self-sustaining even after the oxidizer flow is stopped. In fact shutting off the oxidizer flow would terminate combustion if the additive were below a critical concentration. However, this process follows the similar principle as dp/dt extinguishment in solid propellants, where a rapid pressure drops causes flame blow-off. In a given motor configuration, each oxidizing additive has a critical concentration above which sustained burning will persist. This issue is critical particularly for large motors [61].
For classical hybrid as in the case of throttling the thrust termination event is dictated by the transfer function of the feed system, the emptying time and the response of the fuel grain. The controlling factor (particularly near the end of the shutdown transient) is usually the

thermal lag of the solid [6]. Tanks to the accumulated heat in the solid the fuel production can continue even after combustion is terminated because the fuel has to cool down below its pyrolysis temperature. This further vaporization prolongs the shutdown phase and can contribute a small additional impulse in vacuum.

During the shutdown phase the regression rate drops to very low values. In this condition the fuel production could get a pulsating behavior called 'chuffing'. Another phenomenon present at very low regression rates is the increase of the thermal depth and consequently of the stay-time of the fuel at elevated temperature. In this condition some fuels can incur in cooking or charring.

Nominally an hybrid can be re-ignited almost indefinitely if a ignition source is continuously available. However sometimes the just described degradation of certain fuels during shutdown could hinder the re-ignition of the grain.

The correct determination of the thrust termination attributes (particularly duration and total impulse contribution) is important for precise control of vehicle velocity.

For the reasons just exposed hybrid rockets are not best suited for application were a very fine control of thrust and/or fast pulses operation is foreseen, as it is for liquid systems commonly used for attitude control. In fact hybrids are seldom proposed as propulsion units for attitude control[4].

[4] an exception being the paper by Ordahl and Rains [41] and the proposal of Plexiglass by Estey and Whittinghill [86].

Chapter 3

Grain Model

This chapter begins the description of the several sub-models defining hybrid rocket transient behavior. In this chapter the attention is focused on the numerical modeling of the solid grain thermal behavior.

The main object of this work is to determine the response of the solid fuel to variations of the heat flux on the surface. A 1D numerical model of transient grain thermal response has been developed with this goal. The model is based on the work performed by Karabeyoglu [6],[7],[13] and solves the temperature profile in the direction normal to the surface.

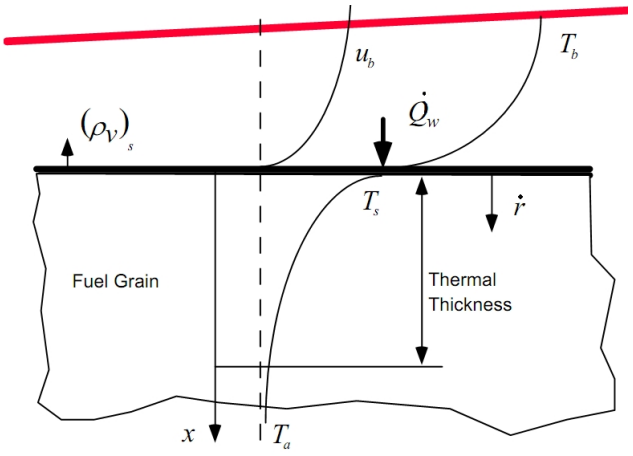

Figure 3.1: *Basic scheme of fuel grain model [11].*

In the first paragraph a model suited for classical polymeric fuels is developed. In the second paragraph the grain model is coupled with the boundary layer response in order to investigate typical hybrid low frequency instabilities. In the third paragraph a version of the original grain model suited for liquefying propellants is developed.

In fact recently a new class of fast burning fuels has been discovered at Stanford University

[6],[20],[21]. These fuels form a liquid layer on the melting surface during combustion, hence the term 'liquefying fuels'. Entrainment of droplets from the liquid-gas interface creates the desired high regression rate by increasing the rate of fuel mass transfer. Several researchers [25],[26],[27] included people at CISAS have experimental confirmed that paraffin-based fuels burn at surface regression rates 3 to 4 times that of conventional hybrid fuels. Others following studies showed with the use of visualization experiments the presences of waves on the liquid surfaces and droplets entrained by the gas flow, confirming original theoretical predictions.

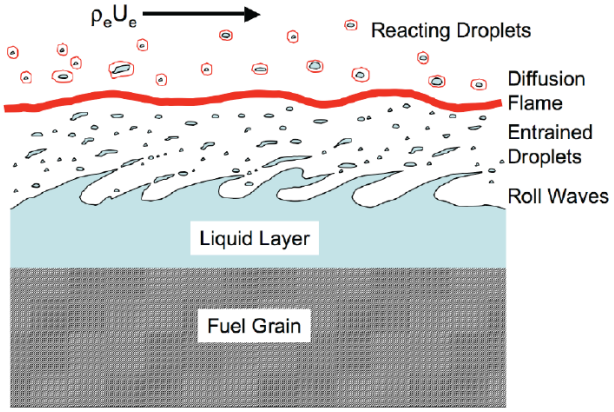

Figure 3.2: *Liquefying fuels combustion mechanism [33].*

The third paragraph is divided in three parts. In the first part the model developed to predict the regression rate and the thermal profile inside a paraffin fuel is presented. The second part deals with the phenomenology of supercritical entrainment. Finally the third part discusses the problem of the closure of the equations to take into account the space-time variability of the entrainment phenomenon.

3.1 Grain Model for a Classical Polymeric Fuel

In order to predict the transient regression rate is necessary to model the transient response of the fuel grain. A one dimensional model of the grain has been developed in the same way of Karabeyoglu[11][12][13][14]. The equation of the heat transfer inside the grain is written in a reference frame moving with the grain surface [15][1].

$$\frac{\partial T}{\partial t} = \kappa \frac{\partial^2 T}{\partial x^2} + \dot{r} \frac{\partial T}{\partial x} \qquad \kappa = \frac{\lambda}{\rho c} \tag{3.1}$$

[1] These equations are valid for both solids and hybrids, the difference stands in the heat flux determination.

The pyrolysis layer has been neglected because it is small for fuel that have high activation energies like those used in hybrid rockets. Some data [16] show that this is not completely true for HTPB, however we believe that this model can give reasonable results also for this fuel. The regression rate follow an Arrhenius law.

$$\dot{r} = Ae^{-\frac{E_a}{R_u T_s}} \qquad (T > T_p) \tag{3.2}$$

The first boundary conditions is:

$$T = T_0 \qquad \text{for } x = 10\ \delta|_{\dot{r}=\dot{r}_{op}} \tag{3.3}$$

Where $\delta = \kappa/\dot{r}$ is the thermal boundary layer thickness and $\dot{r}_{op}$ is the regression rate at the design point. The second boundary condition is the heat exchanged to the wall:

$$\dot{Q}_w = \dot{r}\rho_f L_v - \lambda \left.\frac{\partial T}{\partial x}\right|_{x=0} \tag{3.4}$$

The heat to the wall is the sum of the convective and radiative heat fluxes:

$$\dot{Q}_w = \dot{Q}_{conv} + \dot{Q}_{rad} \tag{3.5}$$

In this model the radiative heat flux is absorbed only at the surface (typical of propellant with carbon black). The unsteady convective heat transfer has been calculated with the equation [6]:

$$\dot{Q}_{conv} = a' {G_0}^{n/(1-k)} \dot{r}^{-k/(1-k)} \tag{3.6}$$

which has been obtained with the following empirical relation for blowing correction [17]

$$C_f/C_{f_0} = qB^{-k} \qquad q = 1, k = 0.68 \tag{3.7}$$

Where $B = \frac{2\rho_f \dot{r}}{G_0 C_f}$ is the blowing parameter. During throttling up the oxidizer mass flux suddenly increases while the regression rate needs some time to reach its steady state value. This means that for the first instants the blowing parameter drops to low values. At such low values eq. 3.7 produces very large errors and unphysical results (i.e. $C_f/C_{f_0} > 1$) In order to overcome this problem, for low B values the following expression is used instead:

$$C_f/C_{f_0} = \frac{1}{1 + 0.4B} \tag{3.8}$$

The two expressions differ less than 1% for $B = 6.2$. This equation satisfy the no blowing boundary condition and for low B values fits better the original Marxman analytical expression [18]. The blowing parameter is estimated as follow [17]:

$$B = \sqrt[0.32]{\frac{2\rho_f \dot{r}}{G_0 C_{f_0}}} \tag{3.9}$$

If B is less than 6.2 the convective heat flux becomes:

$$\dot{Q}_{conv} = a'' G_0^n - a''' \dot{r} \tag{3.10}$$

This equation has been obtained in the same way of eq. 3.6 but using the eq. 3.8 instead of eq. 3.7 to express C_f/C_{f_0} .

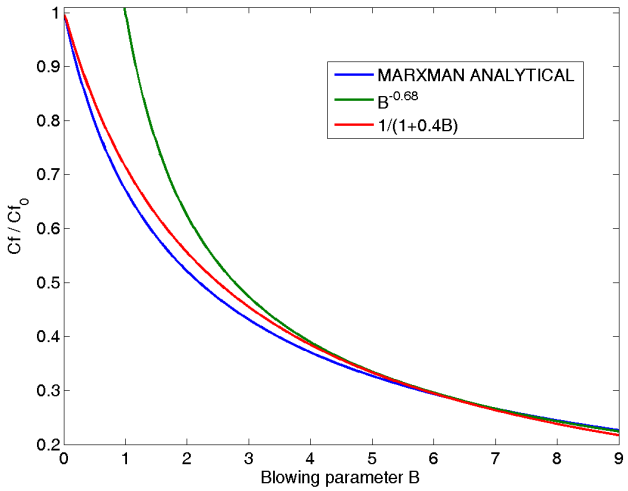

Figure 3.3: *C_f/C_{f_0} ratio as a function of blowing parameter.*

As expected for low B values the heat flux is composed by the heat flux without blowing (zero order term) minus a term proportional to the regression rate (first order correction). The parameter a'' is calculated considering the heat flux without blowing, the parameter a''' matching eq.3.6 and eq.3.10 when B=6.2. The radiative heat flux is usually expressed with the following equation [17]:

$$\dot{Q}_{rad} = \sigma \epsilon_s (\epsilon_g T_f^4 - T_s^4) \tag{3.11}$$

Due to large temperature and composition gradients between the flame and the wall some kind of averaged values need to be used inside eq.3.11. In this work a slightly different model for the radiative heat has been used. It consists of two layer of gases, the flame layer and the layer beneath the flame. Radiative heat flux is expressed as:

$$\dot{Q}_{rad} = \sigma\epsilon_s(\epsilon_f t_{bf} T_f^4 + \epsilon_{bf} T_{bf}^4 - T_s^4) \tag{3.12}$$

with $t_{bf} = 1 - \epsilon_{bf}$, $\epsilon_f = 1 - e^{-b_f p_c y_f}$, $\epsilon_{bf} = 1 - e^{-b_{bf} p_c y_{bf}}$, $y_{bf} = h_f - 1/2 y_f$.

With this model more direct physical values (e.g. flame temperature) can be used instead of averaged quantities. Input data can be directly estimated using CFD and thermo-chemical codes.

A 4th order Runge Kutta explicit scheme is used for the time derivatives and a second order central-finite- difference scheme for the spatial derivatives. The default time step is 1e-4 s. A variable timestep is applied. If the regression rate varies more than 1% the timestep is reduced. In this way the algorithm is robust, reliable and rapid variation of the regression rate are followed with a sufficient number of point and accuracy.

After the timestep has been reduced below the default value it is then slowly relaxed to its default value. With this feature a reduction in computational time was achieved respect to the case when it is suddenly increased to the default value. The accuracy of the algorithm has been tested comparing the numerical results with the steady state analytical solution:

$$T = T_0 + (T_s - T_0)e^{-x/\delta} \tag{3.13}$$

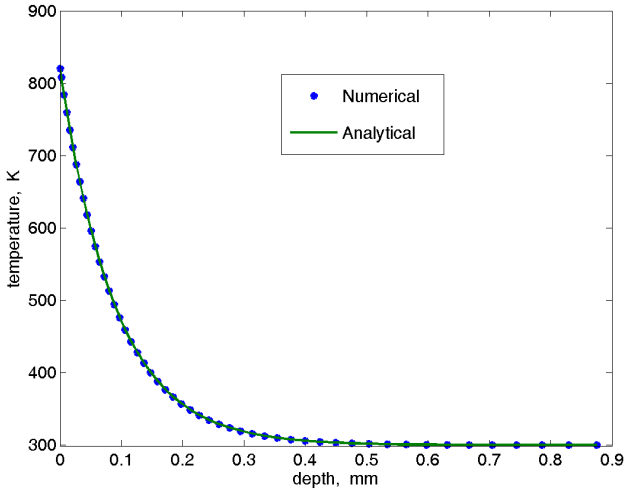

Figure 3.4: *Temperature profile within the fuel grain in the steady state solution.*

A 50 nodes mesh gives accurate results (max error less than 0.13% respect to the analytical reference). A non uniform grid has been used. The distance between one node and the following increases by 5% going in the positive x direction. In this way an increase of accuracy respect to a uniform grid has been achieved because the solution is more flat far

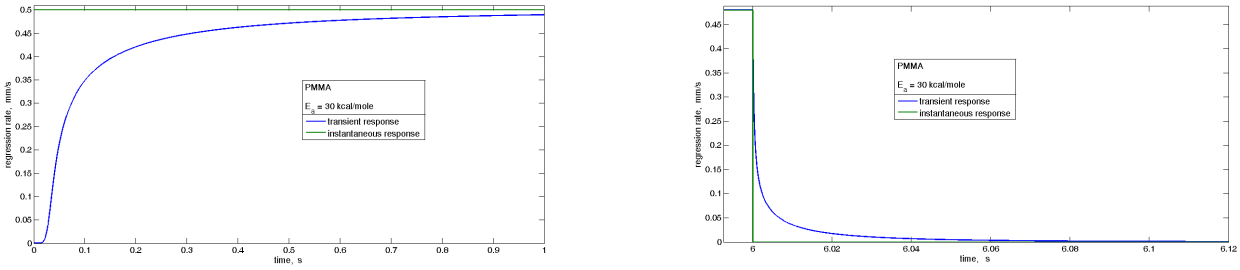

Figure 3.5: *Regression rate variation during motor ignition (left) and shut-down (right).*

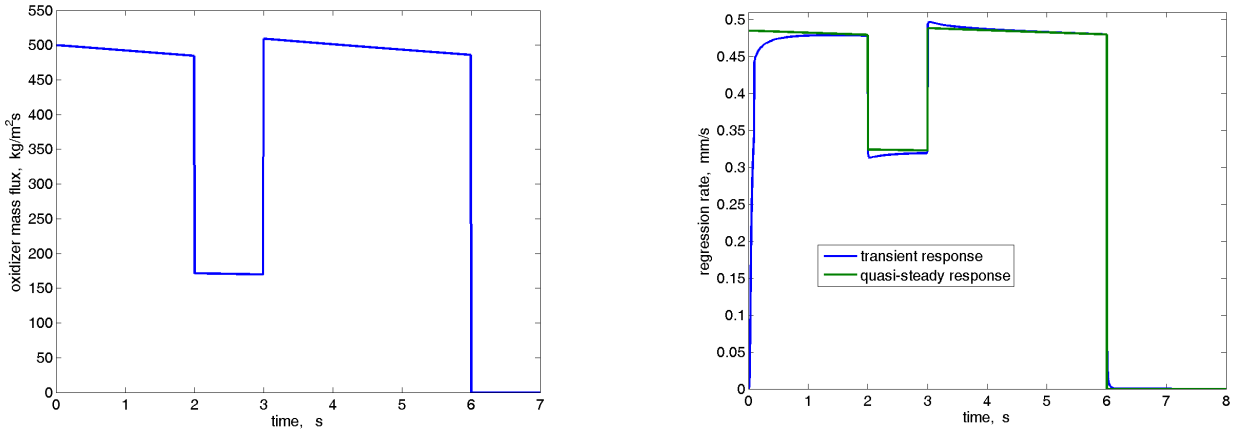

Figure 3.6: *Variable oxidizer mass flow rate (left) and regression rate profile (right).*

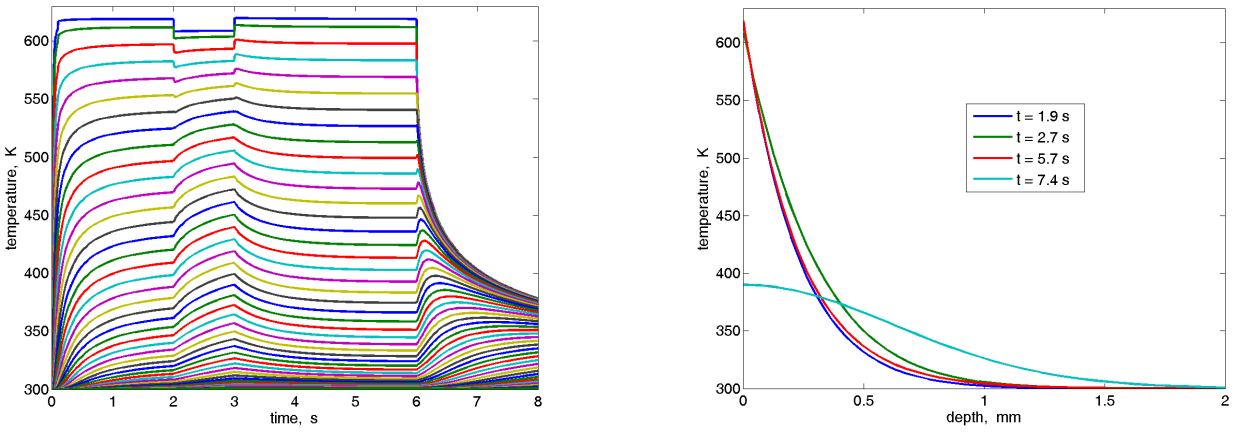

Figure 3.7: *Transient temperature profiles within the fuel grain.*

from the surface. The results of this model agree well with the original one presented in ref.[6].

The simulations predict an overshooting during throttling events. The response to a sinusoidal input leads the input at very low frequency while lags at higher frequencies. For a wide range of frequencies the response is slightly amplified. Only for large frequencies the amplitude drops under the steady state value. It is worth noting that when the regression rate decreases so does the surface temperature as expected, on the contrary the temperature

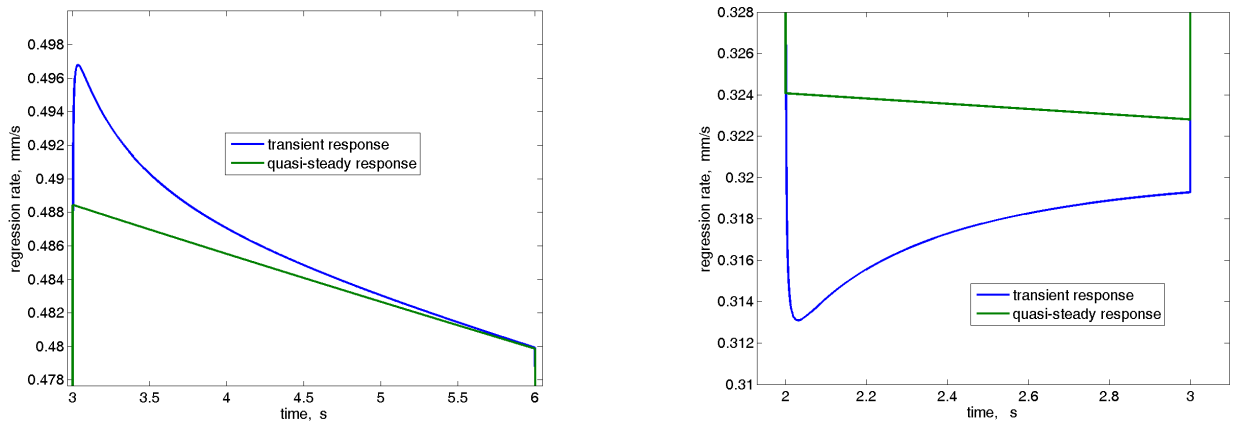

Figure 3.8: *Regression rate overshooting during throttling events: throttle up (left) and throttle down (right).*

rises in the nodes far from the surface. This is due to the fact that the thermal penetration is higher as the regression rate decreases [15]:

$$\delta = \kappa/\dot{r} \tag{3.14}$$

3.2 Boundary Layer Response and Typical Hybrid Low Frequency Instabilities

The heat flux to the grain surface is coupled with the chamber gas dynamic trough the boundary layer response. To simulate the boundary layer response we add two time lags in the heat transfer functions [6], τ_1 and τ_2:

$$\dot{Q}_{conv} = a' G_0 (t - \tau_1)^{n/(1-k)} \dot{r}(t - \tau_2)^{-k/(1-k)} \tag{3.15}$$

$$\dot{Q}_{conv} = a'' G_0 (t - \tau_1)^{n} - a''' \dot{r}(t - \tau_2) \tag{3.16}$$

τ_1 and τ_2 represent the times needed by the boundary layer to adjust to changes of the oxidizer mass flux and the regression rate, respectively. τ_1 only translate the input so the consequence is a correspondent shift of the output. On the contrary when the τ_2 lag is introduced (except for really small values) the system becomes unstable. Respect to the linear theory in this case the oscillations are bounded because the heat flux can go from zero to a maximum value in the absence of blowing. This can be an inherent advantage respect to solid rockets because the regression rate cannot diverge completely. On the contrary the

regression rate of a solid rocket is pressure dependent so it can diverge following pressure oscillations.

The difference between the maximum heat flux and the steady state one is several times higher than the difference between the minimum heat flux and the steady state one. This can be demonstrated simply using the expressions for the blowing correction considering typical values of the blowing parameter encountered in hybrid rocket steady state operation. The ratio between the heat flux and the maximum heat flux is 1 in case of no blowing, 0 for infinite blowing and usually less than 0.33 (for $B > 5$) in the steady-state case [22]. So a positive shift of the average regression rate should occur during large regression rate oscillations.

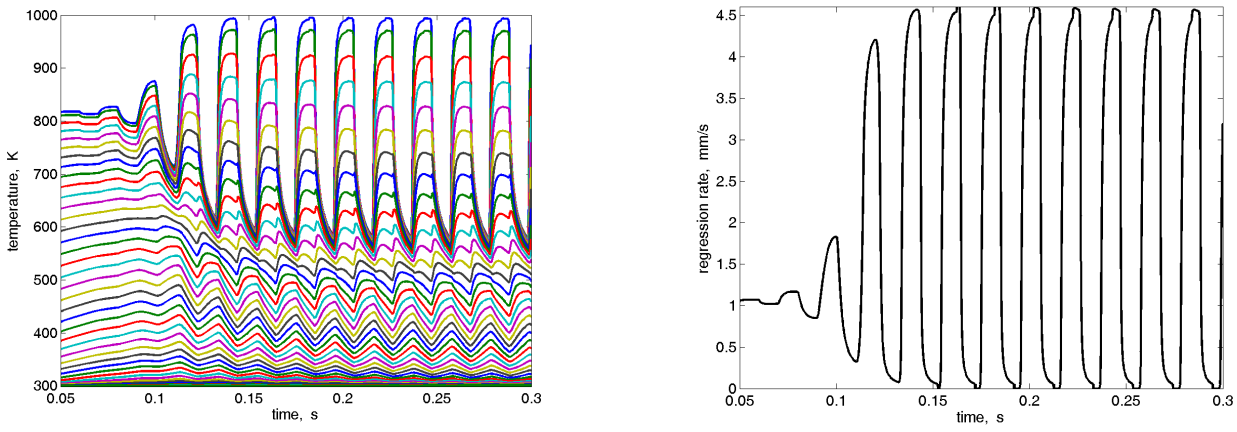

Figure 3.9: *Temperature (left) and regression rate (right) evolution of an HTPB fuel grain during unstable conditions ($\tau_2 = 10ms$).*

Due to the non sinusoidal shape of the regression rate oscillations the frequency has been estimated with the time between two following peaks. The frequency of oscillation agree well with Karabeyouglu [6] predictions: $f = 0.48/\tau_2$.

However, this model doesn't predict correctly the amplitude of the oscillations and it over-predicts them. Moreover it fails to explain while some motor are stable and other not. Even if some nonlinear dissipation mechanisms are not modeled in the present simulations they cannot solve the last question. In the author's opinion a more accurate boundary layer transfer function should be developed. Probably the new transfer function is not unstable by itself but can go into resonance if it is excited at certain frequencies by a source of disturbances (e.g. vortex shedding). The source of instabilities too can be affected by pressure oscillations. For example vortex shedding amplitude can be altered by pressure oscillations at proper frequencies. In this way the entire system becomes unstable.

A theoretical and numerical research has begun at CISAS in order to investigate transient hybrid boundary layer behavior.

3.3 Grain Model for a Liquefying Fuel

A one dimensional model of the grain of liquefying fuels has been developed. The model is suited for propellants that form a liquid layer near the surface. It should be also highlighted that the main part of the model is the same for fuel working in either subcritical or supercritical conditions; the only difference is in the relation between surface temperature and vapor regression rate.

The model is based on two heat transfer equations for the liquid and solid phases, solved together. The equations of the heat transfer inside the grain are written in a reference frame moving with the grain surface (liquid-gas interface). Again all the (eventual) radiative heat flux is assumed to be absorbed at the surface (black grain).

$$\frac{\partial T}{\partial t} = \kappa_l \frac{\partial^2 T}{\partial x^2} + \dot{r}_l \frac{\partial T}{\partial x} \qquad \kappa_l = \frac{\lambda_l}{\rho_l c_l} \tag{3.17}$$

$$\frac{\partial T}{\partial t} = \kappa_s \frac{\partial^2 T}{\partial x^2} + \dot{r}_s \frac{\partial T}{\partial x} \qquad \kappa_s = \frac{\lambda_s}{\rho_s c_s} \tag{3.18}$$

The first boundary condition is: $T = T_0$ or equivalently $\frac{\partial T}{\partial x} = 0$ for $x \to \infty$

Numerically this condition has been implemented fixing the temperature of the last node equal to T_0. After the computation the derivative of the temperature at the last node is checked. If it is not negligible, the spacing of the mesh and/or the number of nodes is increased. The process is repeated until the boundary condition is satisfied (under a certain tolerance). Usually this require no more than one iteration because the depth of the thermal boundary layer in the solid phase can be estimated as $\delta_s = \kappa_s / \dot{r}$. The boundary conditions at the solid-liquid interface are the value of the melting temperature:

$$T|_{x=h} = T_m \tag{3.19}$$

and the heat flux through the interface that is calculated as:

$$-\lambda_l \left.\frac{\partial T}{\partial x}\right|_{x=h^-} + \lambda_s \left.\frac{\partial T}{\partial x}\right|_{x=h^+} = L_m \dot{m}_m = L_m \rho_s \dot{r}_m \tag{3.20}$$

Where $\dot{r}_m$ is the regression rate of the liquid-solid interface. The boundary condition at the liquid-gas interface is:

$$\dot{Q}_w = \dot{m}_v L_v - \lambda_l \left.\frac{\partial T}{\partial x}\right|_{x=0} \tag{3.21}$$

The heat flux to the wall is the sum of the convective and radiative heat fluxes:

$$\dot{Q}_w = \dot{Q}_{conv} + \dot{Q}_{rad} \tag{3.22}$$

In this model the radiative heat flux is absorbed only at the surface (typical of propellants with carbon black). The unsteady convective heat transfer has been calculated with the equation:

$$\dot{Q}_{conv} = Fr(a'' G_0^n - a''' \dot{r}_{vap}) \tag{3.23}$$

This equation has been obtained from the equation:

$$\dot{Q}_{conv} = 1/2 Fr C_{f_0} h_v B_t C_f / C_{f_0} \tag{3.24}$$

Following the same treatment of Karabeyoglu [6].

$B_t = \frac{u_e}{u_b}\frac{\Delta h}{h_v}$ is the thermochemical blowing parameter.

The ratio C_f/C_{f_0} is expressed through the mass transfer number (or aerodynamic blowing parameter):

$$B = \frac{2\rho_f \dot{r}}{G_0 C_f} \tag{3.25}$$

For a classical fuel at steady state the thermochemical blowing parameter is equal to the mass transfer number. This doesn't hold in the transient case or when there is droplet entrainment.

It is not acceptable to adapt one of the forms that are commonly used in the hybrid literature (that is, $C_f/C_{f_0} = qB^{-k}$) in this study in which accuracy at low B values is essential. Classical expressions predict unrealistically large blocking factors (even larger than one) for B approaching zero.

In order to overcome this problem, for low B values the eq.3.8 is used instead. This equation satisfy the no blowing boundary condition and for low B values fits better the original Marxmann analytical expression [18].

As expected for low B values the transient heat flux is composed by the heat flux without

blowing (zero order term) minus a term proportional to the regression rate (first order correction). It is important to remark that the blowing is dependent only on the vaporization part of the regression rate. The constants in equation 3.23 can be determined considering the steady heat flux in the absence of entrainment:

$$\dot{r}_{cl} = aG_0^n \tag{3.26}$$

$$a'' = a\rho_s h_v(1 + 0.4B_t) \tag{3.27}$$

$$a''' = \frac{a''}{a} - \rho_s h_v = \rho_s h_v 0.4B_t \tag{3.28}$$

The parameters a and n can be estimated from the regression rate of a classical fuel with properties similar to paraffin (i.e. polyethylene) in a range where $Fr \sim 1$. For the quasi-steady behavior the convective heat flux becomes:

$$\dot{Q}_{conv} = F_r a\rho_s h_v G_0^n(1 + 0.4B_t)/(1 + 0.4B_t\dot{r}_{vap}/\dot{r}_{cl}) \tag{3.29}$$

The term Fr represents the increase of the heat flux due to the wrinkling of the surface. It was estimated by Gater and L'Ecuyer [30][31] in the following way:

$$Fr = 1 + r \tag{3.30}$$

where:

$$r = \frac{3}{X_r^{0.8}} \tag{3.31}$$

or alternatively expressed with motor operating parameters:

$$r = \frac{3\rho_g^{0.4}}{G^{0.8}} \tag{3.32}$$

In the last equations the dimensions of the roughness group X_r are $lbf^{1/2}/ft$. The fuel mass flow has two contributions, one from vaporization and another from the entrainment:

$$\dot{m} = \dot{m}_v + \dot{m}_{ent} \tag{3.33}$$

Mass flow related to entrainment is provided by[19]:

$$\dot{m}_{ent} = Kc_f\rho_l G_0^{2\alpha} h^\beta/\rho_g^\alpha \mu^\gamma \tag{3.34}$$

This equation holds far from the boundary of onset entrainment because it follows from equation [6]:

$$\dot{m}_{ent} = 1.41\ 10^{-3}(X_e - 2109)\dot{m}_l \tag{3.35}$$

where:

$$X_e = \frac{P_d^{0.5}}{\sigma}\left(\frac{T_g}{T_s}\right)^{0.25} \qquad \dot{m}_l = \frac{P_d c_f h^2}{2\mu_l} \tag{3.36}$$

Anyway the behavior near the onset of entrainment is unclear. Eq.3.35 doesn't predict a dependence of viscosity or liquid layer thickness for the onset of entrainment. In fact Gater and L'Ecuyer did not find a dependence of the surface structure on viscosity [30][31].
This is in contrast to other statements. Further investigation is needed, particularly in relation of the hybrid rocket motor conditions. The calculation of the vaporization regression rate is performed in two different ways for the subcritical and supercritical case [19].
Paraffin waxes with carbon number higher than 20 have a critical pressure less than 10 atm [19]. This means that usually the paraffin fuel in the combustion chamber is supercritical.
In the supercritical case the vaporization regression rate is determined by the pyrolysis of the fuel molecules in a small layer near the surface. The thickness of this layer has been neglected in this model because is less than 5% of the liquid layer [19] for typical values of the activation energy. In the supercritical case the mass flow of vaporization is expressed with the use of an Arrhenius law:

$$\dot{m}_v = \rho_s A e^{-E_a/R_u T_s} \qquad \text{for } T > T_p \tag{3.37}$$

For the subcritical case: $T_s = T_{vap}$ calculated at the partial pressure of the fuel $P = Y_{fs}P_c$ and the mass flow of vaporization is determined from eq.3.21. For the quasi-steady behavior we can estimate the fuel mass fraction at the surface with the use of the Reynolds analogy [19]:

$$Y_{fs} = \frac{\Delta h/h_v}{\Delta h/h_v + 1} \tag{3.38}$$

No relation is implemented at the moment for the transient case. We define the absolute liquid vertical velocity v_l:

$$v_l = \dot{r}_m(\rho_s/\rho_l - 1) \tag{3.39}$$

in order to establish a relation between the relative liquid velocity $\dot{r}_l$ (velocity of the liquid respect to the surface) and the regression rate:

$$\dot{r}_l = v_l + \dot{r} = \dot{r}_m(\rho_s/\rho_l - 1) + \dot{r} = \dot{m}/\rho_l \tag{3.40}$$

Hence the instantaneous regression rate (absolute velocity of the surface) is:

$$\dot{r} = \dot{r}_l - \dot{r}_m(\rho_s/\rho_l - 1) \tag{3.41}$$

It should be remarked that some simplifications used in the steady state analysis are not applicable to the general transient case. For example: $\dot{r} \neq \dot{r}_m$ so $\dot{m} \neq \rho_s \dot{r}$ and $\dot{r} \neq \dot{r}(\rho_s/\rho_l)$. Droplets dimension can be predicted using the following correlation for the Weber number of the volume median diameter [33]:

$$we_{d_v m} = \rho_g j_g^2 d_{vm}/\sigma = 0.028 Re_{d_h,f}^{-1/6} Re_{d_h,g}^{2/3} \left(\frac{\rho_g}{\rho_f}\right)^{-1/3} \left(\frac{\mu_g}{\mu_f}\right) \tag{3.42}$$

To solve the equations numerically a moving grid has been used. A finite number of equally spaced nodes is placed between the surface and the liquid-solid interface. Other nodes are placed in the solid part. The grid is uniform from the surface to the second node after the liquid-solid interface, then the grid distance is progressively increased as in the algorithm for classical propellants. The distance between one node and the following usually increases by 5% going in the positive x direction. In this way an increase of accuracy respect to a uniform grid has been achieved because the solution is more flat far from the surface. After every timestep the new liquid layer thickness is determined from:

$$\frac{dh}{dt} = \dot{r}_m - \dot{r} \tag{3.43}$$

A 4th order Runge-Kutta explicit scheme is used for the time derivatives and a second order central-finite-difference scheme for the spatial derivatives. The default time step is 10-4s. A variable timestep has been implemented. If the liquid layer varies more than 1/4 of the distance between the nodes around the liquid-solid interface the timestep is reduced. In this way the algorithm is robust, reliable and rapid variation of the regression rate are followed with a sufficient number of points and accuracy. After the timestep has been reduced below the default value it is then slowly relaxed to its default value. With this feature a reduction in computational time was achieved respect to the case when it is suddenly increased to the default value. Once the new liquid layer thickness is known the grid is moved

in order to have always the same discretization of the liquid layer. The initial conditions for the new timestep are calculated through interpolation of the last results. This procedure has given definitely the best results compared to the other method tested.

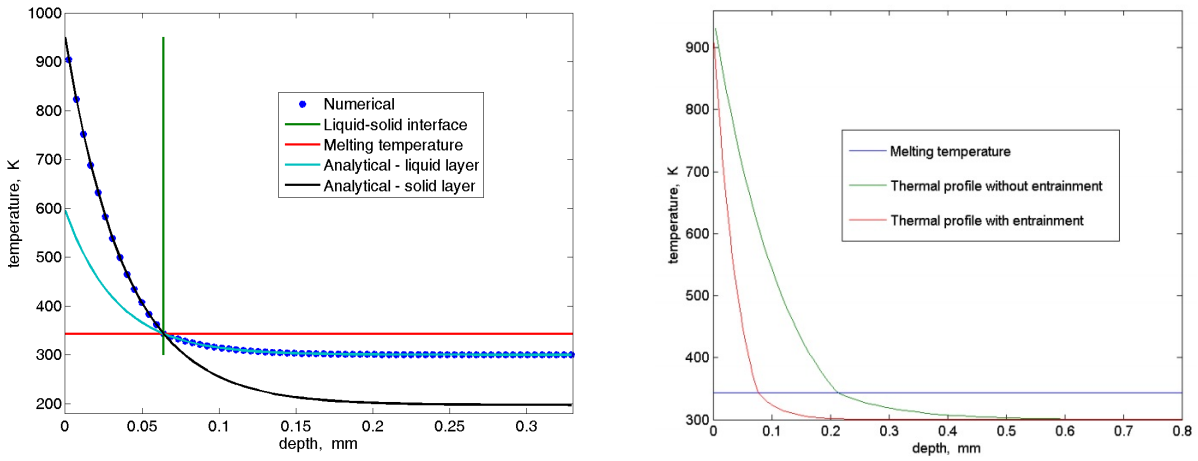

Figure 3.10: *Comparison between numerical and analytical solution (left), effect of entrainment on the temperature profile in the fuel grain (right).*

The code can be used to determine the steady-state surface temperature, the liquid layer thickness, the thermal profile inside the grain, the vapor and the entrainment mass fluxes. The results represent the exact solutions of the equations for a determined set of boundary conditions without the need for further approximations.

As expected when entrainment is present the code predicts a decrease of the surface temperature and liquid layer thickness. The drop of surface temperature and vapor regression rate is high if the same heat flux is imposed. However, when the vapor regression rate decreases the heat flux increases due to the reduction in the blocking effect so finally the surface temperature and vapor regression rate drops are more limited. The accuracy of the algorithm has been tested comparing the numerical results with the steady state analytical solution:

$$T = c_{int} + (T_s - c_{int})e^{-x/\delta_l} \tag{3.44}$$

valid for: $x < h$ with: $\delta_l = \kappa_l \dot{r}_l$ and $c_{int} = (T_m - T_s\phi)(1-\phi)$ with $\phi = e^{-h\delta_l}$ and:

$$T = T_0 + (T_m - T_0)e^{-(x-h)\delta_s} \tag{3.45}$$

valid for: $x > h$ with: $\delta_s = \kappa_s \dot{r}$

and $h = \delta_l ln(\frac{h_e}{h_m})$, $h_m = L_m + c_s(T_m - T_0)$, $h_e = h_m + c_l(T_s - T_m)$

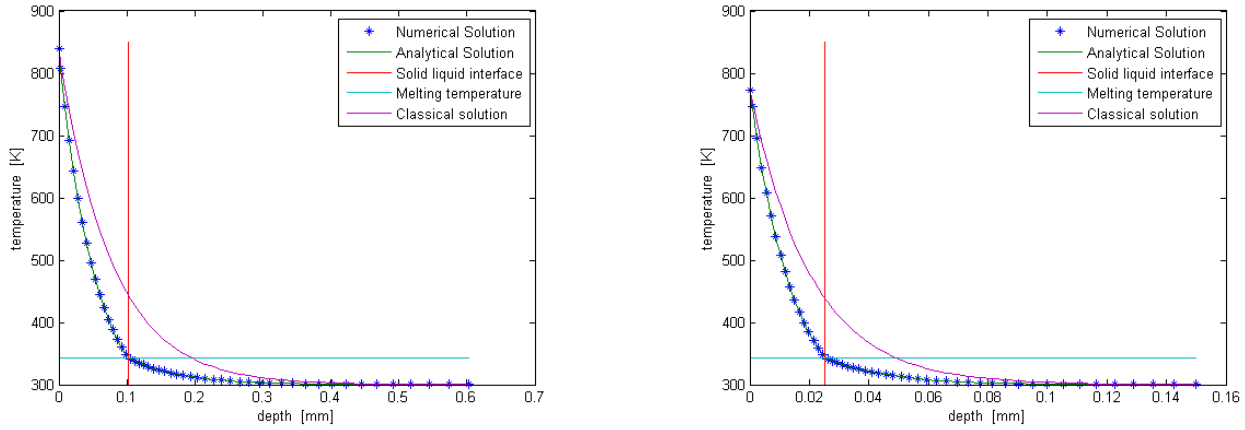

Figure 3.11: *Comparison between numerical and analytical solution,without entrainement (left), with entrainement (right).*

The algorithm is able to converge to the correct liquid layer thickness and grain temperature profile starting from a wide range of initial conditions (also incorrect ones).

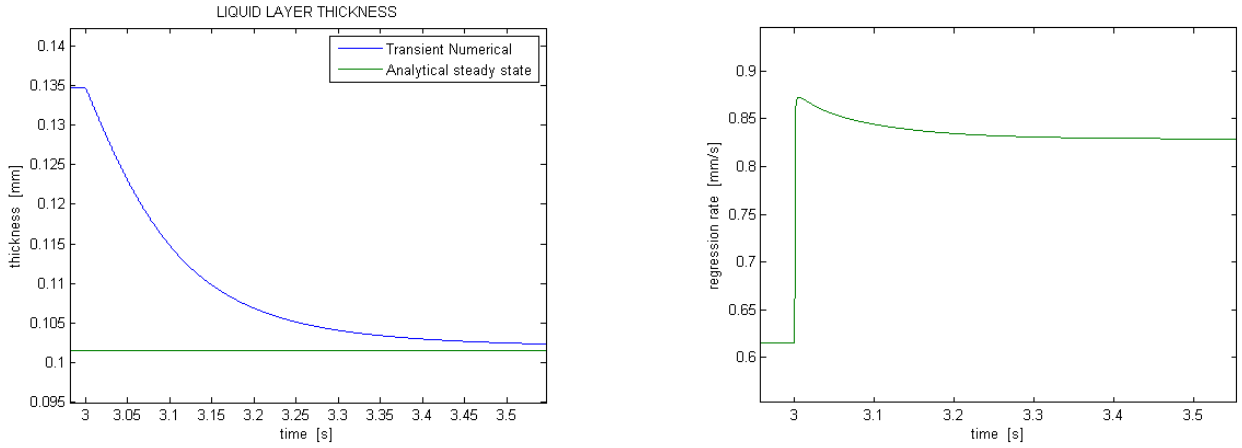

Figure 3.12: *Case without entrainment: liquid layer thickness (left) an regression rate (right) predictions.*

At the moment constant properties have been used respectively for the liquid and the solid layer. However it is straightforward to set the properties as a temperature function because the temperature is known at every node (apart from liquid density that would introduce the need for a 1D continuity equation). Moreover also the surface properties could be set temperature dependent and this can be very useful in determining the correct entrainment ratio.

However in the next paragraphs it will be shown that when entrainment is present the definition and determination of the surface temperature, droplets temperature and liquid

properties is not straightforward and the need for further modeling arises. From fig.3.11 it is possible to see that respect to the classical solution for a polymeric fuel the thermal profile is steeper in the liquid layer and more flat in the solid part. This is due to the enthalpy of melting that behaves as a heat sink. The surface time constant is much faster than the time required by the liquid layer to achieve the steady state thickness. This is consistent with previous results for the thermal lag in classical polymers and the classical analysis reported in heat transfer books [6][23]. In fact the higher is the thickness considered the higher is the thermal capacitance so the thermal response is slower and more damped.
The regression rate has an overshooting during throttling as previously demonstrated. On the contrary liquid layer behavior is monotone. The thermal lag in the solid grain is inversely proportional to the regression rate as in a classical polymer and increases with the liquid and/or solid conductivity.

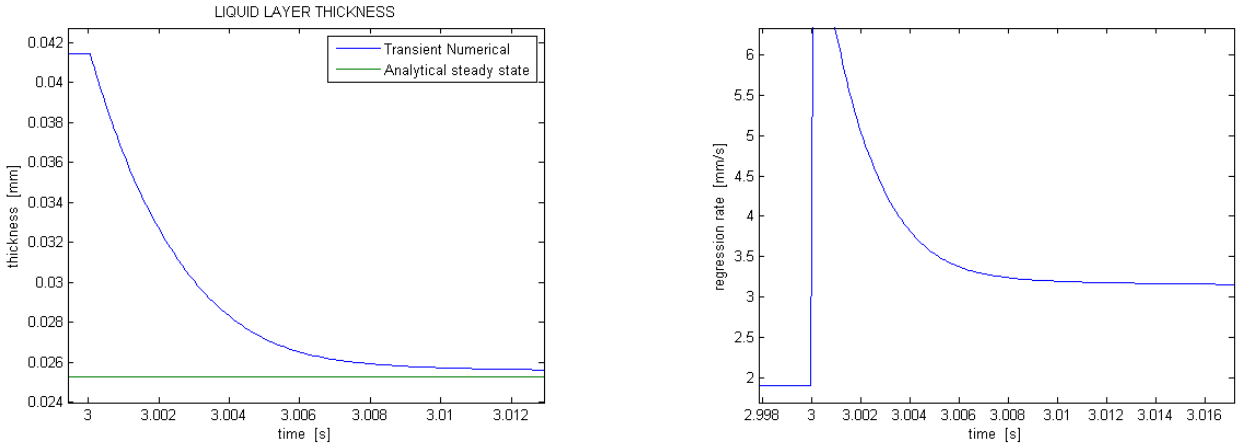

Figure 3.13: *Case with entrainment: liquid layer thickness (left) an regression rate (right) predictions*

The entrainment produce a strong self-regulating mechanism for the liquid layer thickness so the time response of paraffin based propellant during throttling events is faster than a classical polymer operating at the same mass flux. An increase of the entrainment decreases the liquid layer by mechanical consumption. Moreover now the liquid layer response time and the regression rate time are coupled by equation 3.34. A spike of the regression rate occurs during throttling events caused by the step increase in the wall shear stress. Probably in the real response these spikes are partially smoothed by the boundary layer response time (not considered in the numerical model).
The code solves the unsteady heat equation so it is able also to predict the transient behavior of the paraffin fuel. When the oxidizer mass flux is changed abruptly a spike of regression

rate occurs (see Fig.3.14).

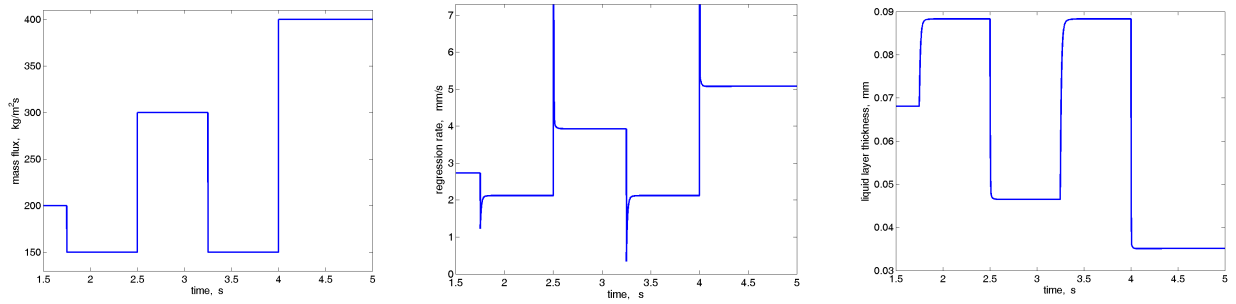

Figure 3.14: *Oxidizer mass flow rate variation versus time (left), related regression rate variation versus time (center) and liquid layer thickness variation versus time (right).*

The explanation is that the entrainment regression rate is proportional to h^2, but h reduces if the regression rate increases. This compensative effect disappears during the first instants of a step change in the oxidizer mass flux.
The entrainment mass flow equation does not take into account the correct transient dynamic of the boundary layer and of the entrainment phenomena. However the author think that at least qualitatively the behavior is correct. In fact the liquid layer thickness changes after a change in the regression rate. So when the oxidizer mass flux is suddenly increased the dynamic pressure and the shear stress would increase. No matter how this happens, at the end of this process the liquid layer thickness would be still nearly the same, so higher than its steady state value. As a consequence a peak of entrainment will occur. Afterwards the liquid layer will be consumed and finally it will reach its steady state value. The same happens, in the opposite way, for a decrease in the oxidizer mass flux. In fact the author expect that if a gas flow is suddenly passed on a small liquid layer a peak of regression rate would occur followed by an exponential decrease as the liquid layer is consumed.

Supercritical behavior

As previously mentioned most hybrid systems using paraffin based fuels are operating in the supercritical regime. In fact the predicted critical pressure of alkanes decreases with increasing carbon numbers. For carbon numbers higher than approximately 20 the critical pressure is lower than 10 atm. So its important to understand the physic of paraffin entrainment in the supercritical case.
First of all its important to review the definition of a supercritical fluid. A supercritical fluid is any substance at a temperature and pressure above its critical point, where distinct

liquid and gas phases do not exist [34]. It can effuse through solids like a gas, and dissolve materials like a liquid. In general terms, supercritical fluids have properties between those of a gas and a liquid. The density is similar to that of a liquid but the behavior resemble for certain aspects that of a gas; in fact a supercritical fluid fills completely the volume of its container and mixes completely with gases.

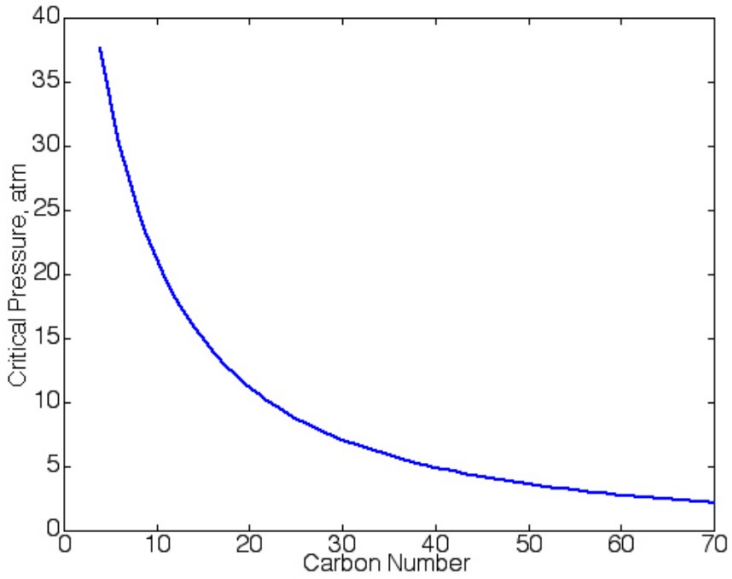

Figure 3.15: *Critical pressure as a function of the carbon number for the homologous series of n-alkanes [19].*

Below the critical pressure if a liquid is heated continuously it will reach the boiling temperature. At the boiling temperature the liquid becomes a vapor. Between a liquid and its vapor there is a discontinuity of physical properties: density, viscosity, enthalpy etc... The difference between liquid and vapor properties decreases approaching the critical point. This discontinuity between liquid and vapor is responsible for the presence of a surface tension at the interface between the two phases. Above the critical pressure a liquid that is heated will undergo a continuous change without any type of discontinuity (unlike vaporization). No interfaces exist and so the surface tension is not defined. The enthalpy of vaporization decreases to zero approaching the critical temperature. The liquid-phase solubility of gases is negligible at low pressures, but become an essential consideration at high pressures. Consequently, a single component fuel droplet would assume a multicomponent behavior, and mass transport between the two phases would become an important process [35]. In fact at the critical temperature the fluid becomes completely miscible with gases.

Almost every equation presented above and in other texts dealing with entrainment of

	Density (kg/m^3)	Viscosity (μPa·s)	Diffusivity (mm^2/s)
Gases	1	10	1–10
Supercritical Fluids	100–1000	50–100	0.01–0.1
Liquids	1000	500–1000	0.001

Figure 3.16: *Comparison of Gases, Supercritical Fluids and Liquids.*

droplets contains the explicit dependency of the surface tension [6][33]. Considering that the surface tension is not defined in the supercritical regime all the equations become singular. The predicted mass transfer approaches infinite. In fact droplets exist because surface tension tends to preserve their shape and maintain the liquid separated respect to the rest of the environment. Droplets dimensions approach zero as the surface tension vanishes.
At supercritical condition an interface is not present between liquid and its vapor and droplets cannot exist.
Running a simple simulation of two layers of gas is possible to highlight some aspects of what could be the behavior in the supercritical regime (fig.3.17). Waves at the interface are generated by Kelvin-Helmholtz instabilities followed by turbulent mixing and diffusion. At the end of the process the interface disappears because the two gases can diffuse one in each other.
The behavior of supercritical fluids has been already investigated in the propulsion community, particularly in the liquid rockets and gas-turbine combustion fields. As an example Liquid Oxygen (LOX) is a widely used oxidizer for rocket propulsion. Oxygen has a critical pressure of nearly 50 bars. Most of liquid engines run at higher chamber pressures.
For our purposes previous investigations about liquid injection in liquid rockets can be a valuable resource. The liquid jet disintegration problem presents interesting similarities with the paraffin entrainment. In the jet injection the liquid has a high velocity while the gas is at rest. In the hybrid motor the liquid is initially at rest and the gas is flowing at high velocity. Anyway considering a relative frame its possible to the two situations. In both case there is a velocity discontinuity between the gas and the liquid. This discontinuity produces very high shear stresses at the interface. Kelvin-Helmholtz instabilities develop consequently.

In the subcritical case waves are formed at the interface, they grow and break in small droplets. Looking at the pictures taken when the liquid is injected in the supercritical regime we can see that there are no more droplets. The interface still deforms due to the shear stress but the fluid mix directly with the surrounding gas. The surface seems formed by a sort of fingers. The entire phenomenology resembles that of gas injection. The process is (turbulent) diffusion controlled.
As a first sight it seems that the physics of mass transport in the supercritical regime should be substantially different respect to the subcritical case. In fact Kuo [33] underlines that the numerical method proposed to describe liquid-gas interface (i.e. level set) should not be applied in the supercritical case. This confirms implicitly that the physic is different between the two regimes.

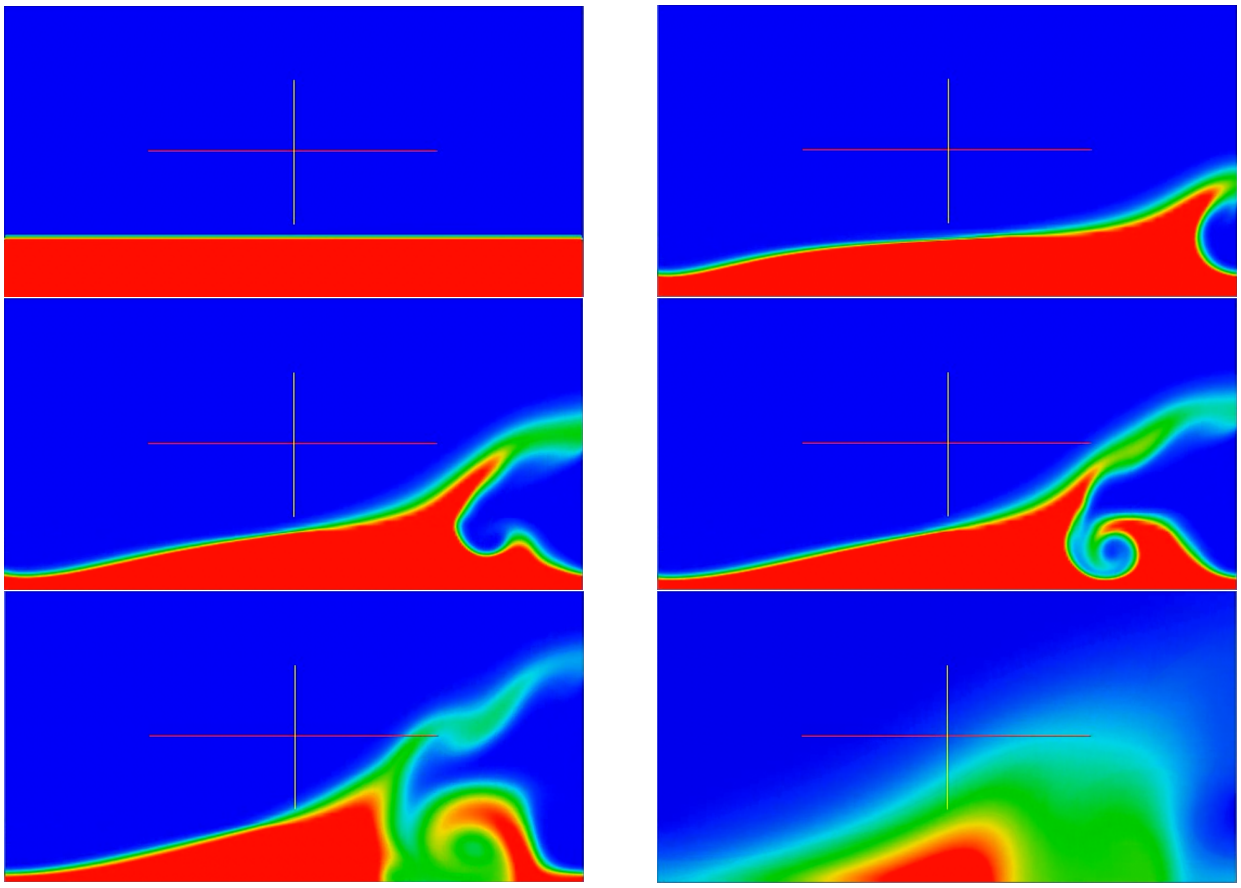

Figure 3.17: *CFD simulation of turbulent mixing between two layers of gas. The gas below (red) is at rest while the other gas (blue) is moving horizontally.*

However the classical theory of entrainment has been successful in describing the high regression rate of paraffin based fuels. The supercritical regime for paraffin was first highlighted by Karabeyoglu [19]. The theory was partially modified to take into account some

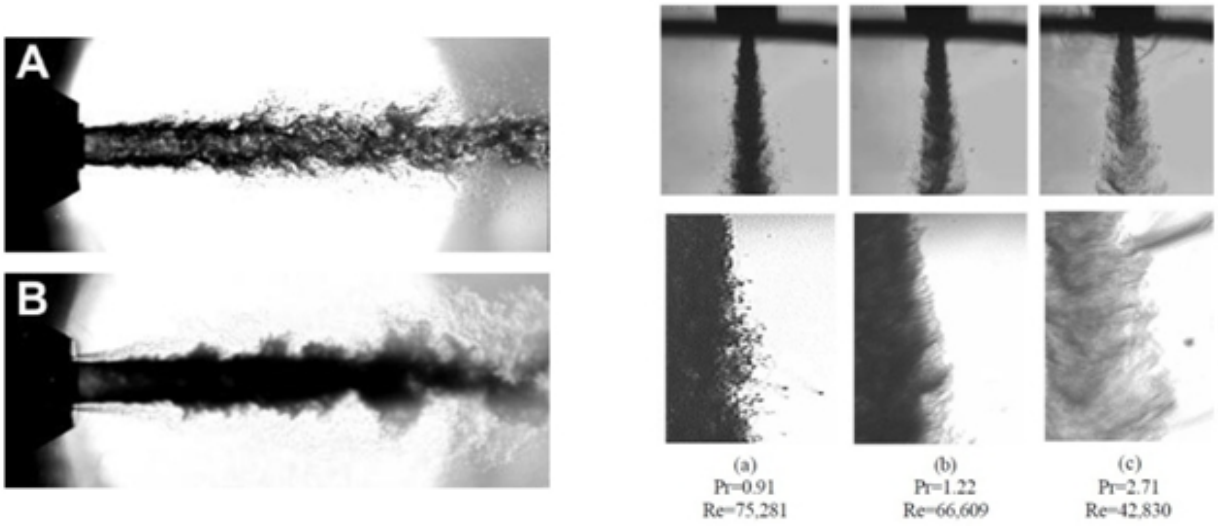

Figure 3.18: *Experimental visualization of jet disintegration: A subcritical case - B supercritical case.*

fundamental aspects (as paraffin pyrolysis) but some questions presented above remain open, particularly regarding the role of surface tension and the presence of droplets. The basic formula for liquid entrainment was used for both regimes. We have made 3 hypotheses to explain the possible use of the entrainment equation in the supercritical regime.

1st hypothesis: subcritical droplets

When paraffin is heated above the critical pressure at a certain temperature it starts decomposing. Thanks to decomposition low molecular weight products are formed. The heating breaks the long molecular chain of the paraffin. This process is called cracking. At the moment it is not well known what is the composition of the decomposed products in the case of very high heating rate typical of hybrid motors. Anyway for the purpose of this paper the exhaustive treatment of Karabeyoglu [19] is perfectly suited.

Looking at picture taken from this reference it is possible to see that the surface temperature (i.e. pyrolysis temperature) is generally below the critical temperature. That means that the paraffin does not reach the supercritical condition. Moreover the density of the liquid paraffin is much higher than the density of the decomposed products. Also other properties like viscosity diffusivity etc. are strongly different. Pyrolysis requires an enthalpy input to occur as it necessary for vaporization in the subcritical regime. The pyrolysis layer has almost negligible thickness respect to the liquid layer thickness. That means that we can define the pyrolysis layer as an interface between a liquid and a gas. So even if we are above

the critical pressure a surface separating two fluids with different properties is present as in the subcritical case. In a certain sense pyrolysis acts in the supercritical regime in an analogous way as vaporization in the subcritical one.

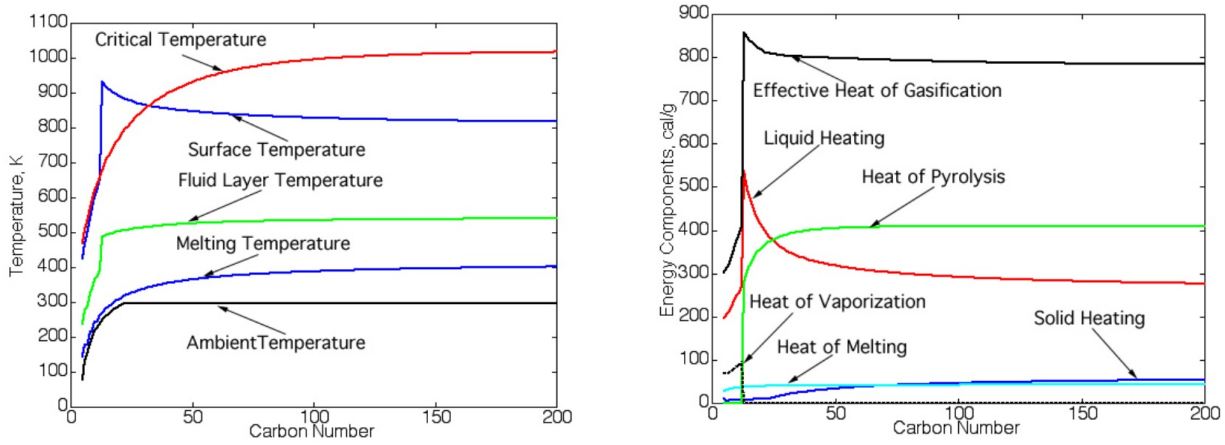

Figure 3.19: *Prediction of the temperature field in the condensed phase (left) and effective heat of gasification and its components (right) for the series n-alkanes. Both taken from Karabeyoglu et al.[19].*

It is important to remark that this behavior is strongly different respect to fluids that don't decompose (e.g. water). This phenomenon justifies an entrainment behavior analogous to the subcritical case. In fact surface tension could be still defined so droplets could exist. The surface tension of organic liquid mixtures can be determined with the following equation [37]:

$$\sigma_m = \left[(1-T_{r,m})^{0.37} T_{r,m} exp\left(0.30066/T_{r,m} + 0.86442 T_{r,m}^9\right)\left(P_{L0,m}\rho_{L,m} - P_{V0,m}\rho_{V,m}\right)\right]^4 \tag{3.46}$$

$$P_{0,ij} = (1-m_{ij})(P_{0,i}P_{0,j})^{1/2} \tag{3.47}$$

Where σ_m is the surface tension of the mixture; $T_{r,m} = T/T_{c,m}$ and $T_{c,m}$ is the pseudo-critical temperature of the liquid mixture; $\rho_{L,m}$ and $\rho_{v,m}$ are the equilibrium densities of liquid and vapor, respectively; $P_{L0,m}$ and $P_{V0,m}$ are the temperature-independent compound-dependent parameters for the liquid and vapor, respectively; $P_{c,i}$, $T_{c,i}$ and x_i are the critical pressure, critical temperature and the mole fraction for component i, respectively; $P_{0,i}$ is the temperature independent parameter for component i and m_{ij} is the unlike interaction parameter.

The first term of the equation goes to zero at the critical temperature. Below the critical temperature the surface tension has still a small but finite value. Moreover it is important to note that in the case of a simple component fluid also the last term approach zero near the critical temperature. For a fluid mixture this is not the case, in fact the density of the decomposed products is much lower (1-2 orders of magnitude) than the density of liquid paraffin. At room temperature (or more rigorously far below the critical temperature) for conventional fluids (e.g. water) there is a negligible difference between the surface tension of the liquid with its own vapor or another gas because the liquid density is much higher than the vapor/gas density so we can drop the vapor/gas density term. This is not the case approaching the critical temperature.
All supercritical fluids are completely miscible with each other so for a mixture a single phase can be guaranteed if the critical point of the mixture is exceeded [34]. The critical point of a binary mixture can be estimated as the arithmetic mean of the critical temperatures and pressures of the two components:

$$T_{c(mix)} = (\text{mole fraction A}) \times T_c(A) + (\text{mole fraction B}) \times T_c(B) \tag{3.48}$$

For greater accuracy, the critical point can be calculated using equations of state, (e.g. Peng-Robinson). The critical point of low molecular weight hydrocarbon is very different from the critical point of paraffin. Usually the critical temperature is much lower while the critical pressure is higher.

Fluid	Molecular weight	Critical temperature	Critical pressure	Critical density
	g/mol	K	MPa (atm)	g/cm^3
Methane (CH_4)	16.04	190.4	4.60 (45.4)	0.162
Ethane (C_2H_6)	30.07	305.3	4.87 (48.1)	0.203
Propane (C_3H_8)	44.09	369.8	4.25 (41.9)	0.217
Ethylene (C_2H_4)	28.05	282.4	5.04 (49.7)	0.215
Propylene (C_3H_6)	42.08	364.9	4.60 (45.4)	0.232

Figure 3.20: *Substances properties at critical point.*

The mole fraction is dependent on the local composition. Fortunately the change in the composition happens in a very small thickness near the surface so that as a first approximation is possible to consider the paraffin mole fraction equal to 1 up to the surface. That means that the critical point of the paraffin remains unchanged.

2nd hypothesis: transcritical droplets

It is possible to see that in a region of carbon number the surface temperature exceeds the critical temperature. The width of this region depends on the motor operating pressure. So in this case the n-alkane becomes a supercritical fluid before decomposing. Anyway the layer of melted paraffin is composed mainly by liquid and only in a small thickness near the surface the fluid is completely supercritical. Only for very low carbon number at high pressures the supercritical part of the layer become substantial.

It is possible again to consider liquid injection to try to figure out the expected behavior. When a liquid is injected in the chamber above the critical pressure but far below the critical temperature droplets are formed by the disintegration of the liquid jet. When heated these droplets cannot vaporize because the pressure is above the critical one. Instead they reach the critical mixing temperature (or pseudo-critical temperature). Above this temperature the fluid can diffuse completely in the environment.

The surface at the critical mixing temperature is (arbitrary) defined has the boundary of the droplet. This kind of droplets is called transcritical [38].

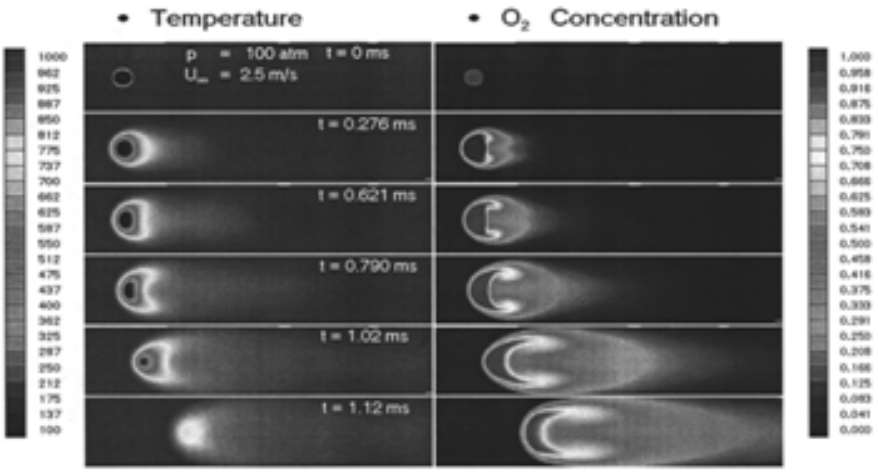

Figure 3.21: *Transcritical droplet evolution.*

Here it is postulated that the interaction of the high speed low density gas with the double layer of liquid and supercritical fluid produces transcritical droplets. The supercritical part can diffuse in the gas phase while the droplet core should be composed by liquid paraffin. These liquid droplets are then heated and consumed as the surface at the critical mixing temperature approaches the center of the droplet. Respect to the previous case the gas can diffuse downward in the supercritical layer, so the paraffin mass fraction cannot be considered one up to the pyrolysis layer. The critical conditions of the mixture should evolve

consequently. However it is postulated that the convective flux upward is stronger than the diffusive flux downward. As a consequence the paraffin mole fraction remains near to one up to the pyrolysis layer (remember that the solution of a convective-diffusion problem is an exponential profile).

3rd hypothesis: no droplets entrainment

The third hypothesis states that droplet entrainment doesnt occur above the critical pressure. Instead a different transport mechanism is foreseen. All the equations about droplets size and onset of entrainment are not valid anymore. However even in this case the mass transport originates from a Kelvin-Helmholtz type instability. A layer of a high density fluid is present underneath the low density high velocity gases. So it is possible that the following general equation (or a similar one):

$$\dot{m}_{ent} = K c_f \rho_l G_0^{2\alpha} h^{\beta} / \rho_g^{\alpha} \mu^{\gamma} \tag{3.49}$$

still holds in the supercritical regime. The exponent of the scaling law and the coefficient K would be probably different respect to the subcritical case but the general form of the mass transfer could continue to be valid. Its important to remark that turbulent structures are related to the Reynolds number that is dependent on G_0 and the properties of the fluids. It is worth noting that the three hypotheses are not mutually exclusive. It would be much important in the understanding of paraffin behavior to perform investigations similar to what has been done in the liquid field. In particular visualization experiments would be much useful in the determination of supercritical entrainment physic.
Some of these experiments have been already performed or at least they are being set-up [25][27][39]. The preliminary pictures show droplets entrainment. Unfortunately at the moment the pressure used in these experiments are not clearly reported or usually it is low (a few bars), so its not possible to determine if the regime is supercritical or not. It would be important to establish a coherent test matrix in order to visualize paraffin entrainment in a wide (and representative) range of pressures.

Closure problem

It is possible to state that the output of the numerical code presented above represents the exact solution of the heat equation in the solid fuel when the liquid is not moving in the hor-

izontal direction. On the contrary the pure 1D approach could not describe the entrainment of liquid droplets. In fact for low viscosity liquids waves are formed and droplets detach from the surface with periodicity. The wavelength on the surface is comparable with the liquid layer thickness. The real entrainment phenomenon is spatial and time dependent. The pure 1D code could only describe average quantities of surface temperature and liquid layer thickness because the local instantaneous values are not described by the simple equations. This problem resembles the description of turbulence by means of numerical codes. In fact turbulence is a spatial and time varying phenomenon. Its not possible to apply the classical Navier-Stokes equations to the average values of the fluid dynamic unknowns because the equations are not linear. To use the RANS (Reynolds Averaged Navier-Stokes) is necessary to model these non-linear effects (i.e. the effect of turbulence on the mean flow). This is called the *closure problem*. A *closure problem* arises also in the case of droplets entrainment. As a simple example we consider an (arbitrary) sinusoidal variation of the surface temperature.

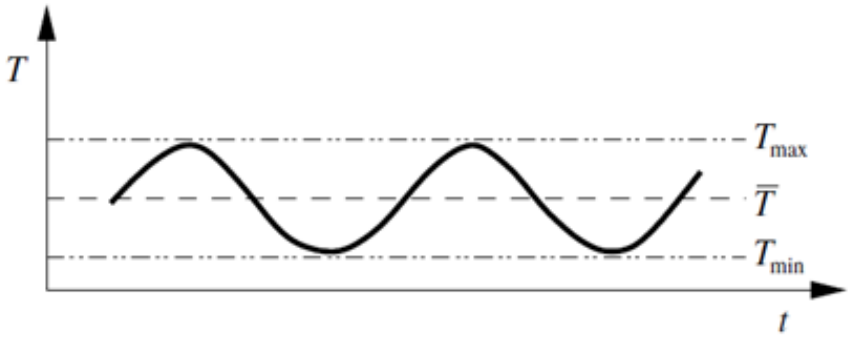

Figure 3.22: *Sinusoidal temperature variation.*

The regression rate could be calculated with an Arrhenius law. These are the computation results:

- $2E_a$= 45 kcal/mole
- Max T = 900 K
- Average T = 800 K
- Minimum T = 700 K
- Arrhenius constant= 600

- Average regression rate = 0.73 mm/s
- Regression rate at average temperature = 0.425 mm/s

As expected the regression rate calculated with the average temperature is different from the average regression rate. To match the two regression rates a higher than the average surface temperature should be used. Its worth noting that an increase of the temperature is equivalent to a decrease in the activation energy. So one of the apparent effects of the entrainment is a reduction of the fuel activation energy.
Using the code as it is implemented now means to consider the temperature of the droplets equal to the surface temperature and consider negligible the fluctuations of the surface temperature respect to the average.

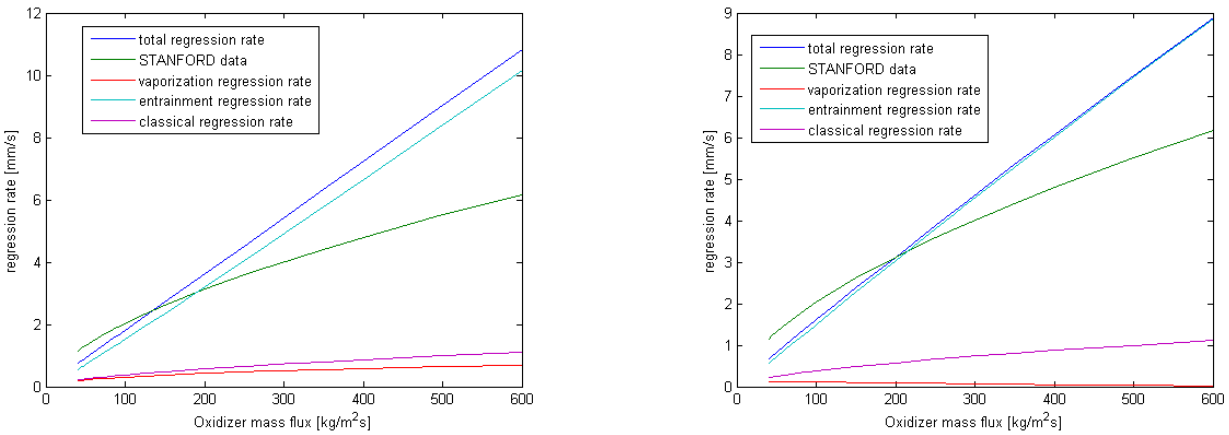

Figure 3.23: *Regression rate predictions:* $\alpha = 1.5$, $\beta = 2$ *(left),* $\alpha = 1$, $\beta = 1$ *(right).*

The code has been used to determine the regression rate of paraffin fuels as a function of the oxidizer mass flux. The coefficient K in the entrainment law has been selected in order to match the experimental and numerical results at one point of the curve. Some numerical results are presented hereafter.
The entrainment regression rate is a strong function of the oxidizer mass flux (2α). The liquid layer thickness decreases with increasing regression rate and increases with higher heat flux. Increasing the oxidizer flux increases both the heat flux and the regression rate. The final result is a slower decrease of the liquid layer thickness. The entrainment is also dependent on the liquid layer thickness (β) so finally there is a sort of compensation and the final dependency of $\dot{r}_{ent}$ from G_0 is less than 2α. The value of α and β in the literature varies from 1.5-2 to 1-1 [6][19][33].
Both cases have been simulated. The final slope of the entrainment regression rate is near one.

In fact, neglecting the vaporization regression rate ($\dot{r}_{ent} \approx \dot{r}$) it is possible to demonstrate the following:

$$\dot{r}_{ent} \propto G_0^{2\alpha} h^{\beta} \qquad h = a_t/\dot{r}^{\beta} \qquad \rightarrow \qquad \dot{r}_{ent} \propto G_0^{\frac{2\alpha}{1+\beta}} \tag{3.50}$$

For both couples of value of α and β a linear dependency of $\dot{r}$ on the oxidizer flux is predicted. The slope of the total regression rate is somewhere between the entrainment one and the classical one. The numerical model predicts a negligible vaporization regression rate so the final slope is similar to the slope of the entrainment part.

The model overestimates the slope of the regression rate curve respect to Stanford experimental data [21]. This means that the exponents of the entrainment law are not correct or a different treatment of the closure problem should be addressed.

As an attempt the exponents α and β of the entrainment law have been set equal to 1 and 2, respectively. As expected in this case the slope is slower ($n \approx 2/3$) and more in agreement with the experimental results.

This highlights the importance of dedicated experiment in order to determine properly the scaling law of entrainment. In particular these experiments should be more linked the conditions of the hybrid rocket environment. In fact classical experiments consider a film of decreasing thickness because the entrainment is not compensated by transversal injection. New experiments should be considered where the films are continuously fed by new liquid as in transpiration cooling.

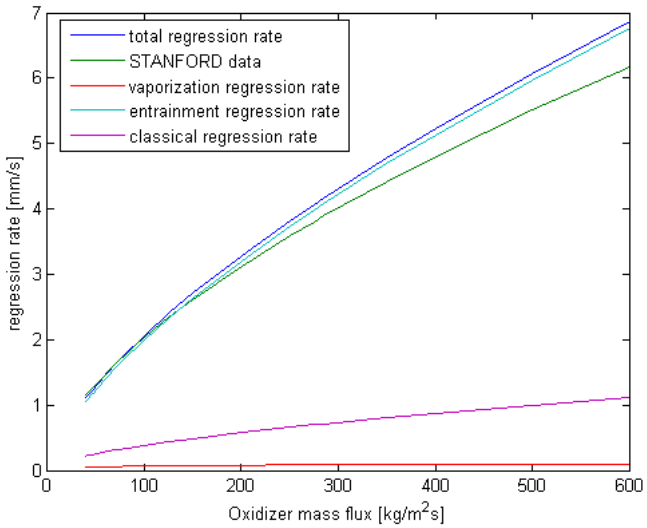

Figure 3.24: *Regression rate predictions:* $\alpha = 1$, $\beta = 2$.

To explain the very low vaporization rate predicted by the code we make use of the energy

balance from Karabeyoglu [19]:

$$\Phi = \Phi_v + \Phi_{ent} \tag{3.51}$$

$$\Phi_v + (R_{he} + R_{hv}\frac{\Phi_v}{\Phi})\Phi_{ent} = \frac{Fr}{C_{B1} + C_{B2}\Phi_v} \tag{3.52}$$

$$\Phi_{ent} = \frac{R_{ent}}{\Phi^\beta} \tag{3.53}$$

If we solve the set of equations above we obtain a vaporization rate much higher than showed before. However if we drop the term Φ_v/Φ from the enthalpy of the droplets the results are more in agreement with the presented numerical model.

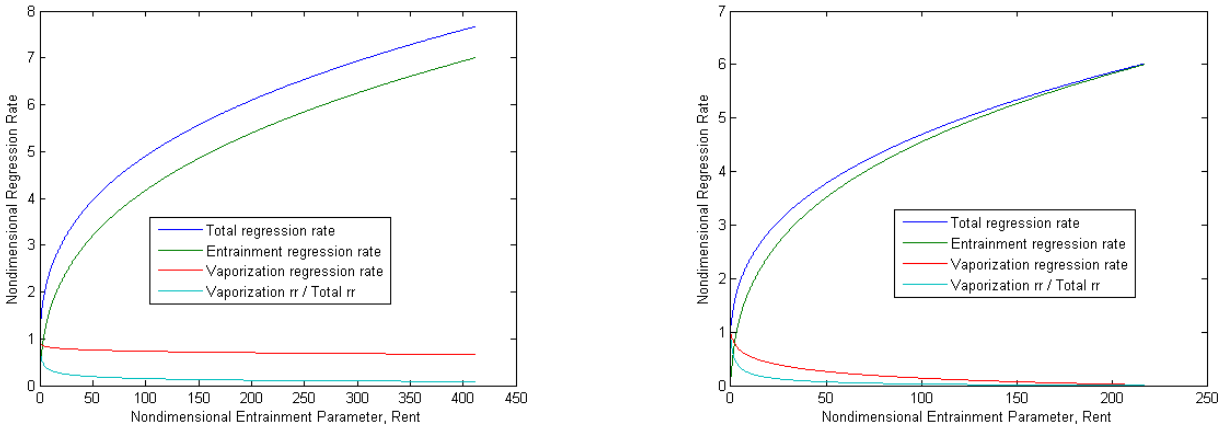

Figure 3.25: *Regression rate predictions: with decrease of droplets temperature (left), without decrease of droplets temperature (right)*

Looking at figure 3.19 it is possible to notice that the total enthalpy of vaporization is only nearly half reduced for the droplets respect to the gas phase. Whit the same heat flux its not possible to have a total regression rate more than twice the classical case. The six-fold increase of regression rate should be explained also by other aspects. In fact the reduction of the vaporization regression rate reduces the blocking effect increasing the wall heat flux. The maximum wall heat flux could be nearly three times the classical value (for B = 4.7). The numerical code presented in this paper determines that the paraffin regression rate is nearly six times that of polyethylene because vaporization almost doesnt occur so the heat flux is 3 times higher and the enthalpy of the droplets is halved. This is due to the fact that the activation energy of the fuel is high so small changes in the surface temperature produce a strong decline in the vapor regression rate. In the extreme case of infinite activation

energy the surface temperature remains constant until there is vaporization. The effect of the entrainment in this case is to reduce the vaporization rate without affecting the surface temperature.

The results are exactly the same obtained solving the set of equations previously without the term Φ_v/Φ. Only when vaporization disappears completely the surface temperature begins to decrease as the entrainment grows further. On the contrary in Karabeyoglu model [19] a strong reduction of the droplets enthalpy is modeled from the beginning as the entrainment grows. In this way it is possible to increase the total regression rate 6 times with a decrease of the vapor regression rate of nearly 30% that corresponds to an increase of the heat flux by only 25%.

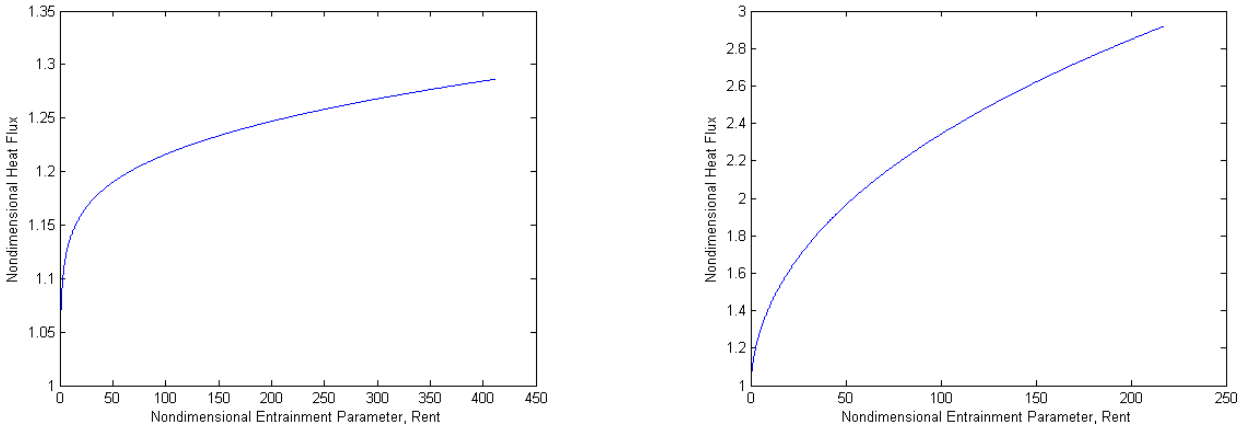

Figure 3.26: *Heat flux predictions:: with decrease of droplets temperature (left), without decrease of droplets temperature (right).*

It is important to remark that the maximum value of the regression rate is the same for both models. In eq. 3.52 the reduction of droplets enthalpy is achieved at the same time that the reduction of Φ_v. On the contrary in the code of this thesis firstly a strong decrease of Φ_v happens and only after R_{hv} decreases to zero.

A simulation has been run reducing droplets temperature by Φ_v/Φ. Its important to note that in this case surface temperature and vaporization temperature remain equal while droplets temperature is decoupled. The results are the following:

As expected now the vaporization regression rate is not negligible and it is a bit lower than the classical regression rate. However the ratio between the vaporization regression rate and the total regression rate is between 0.2 and 0.1 so the slope of the total regression rate is not changed substantially respect to the previous case.

Finally a last attempt has been done. The vaporization regression rate has been decoupled

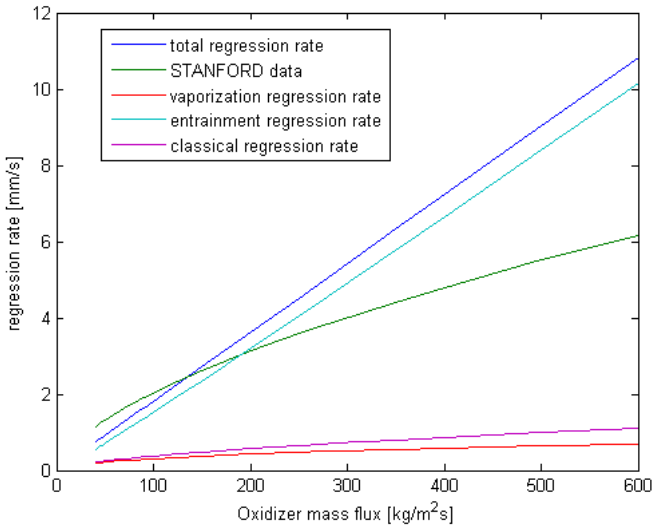

Figure 3.27: *Regression rate predictions: with decrease of droplets temperature,* $\alpha = 1.5$, $\beta = 2$.

from the surface temperature and set equal to 0.7 times the classical one. The surface temperature and the droplets temperature have been set as equal. This is the opposite of the previous case.

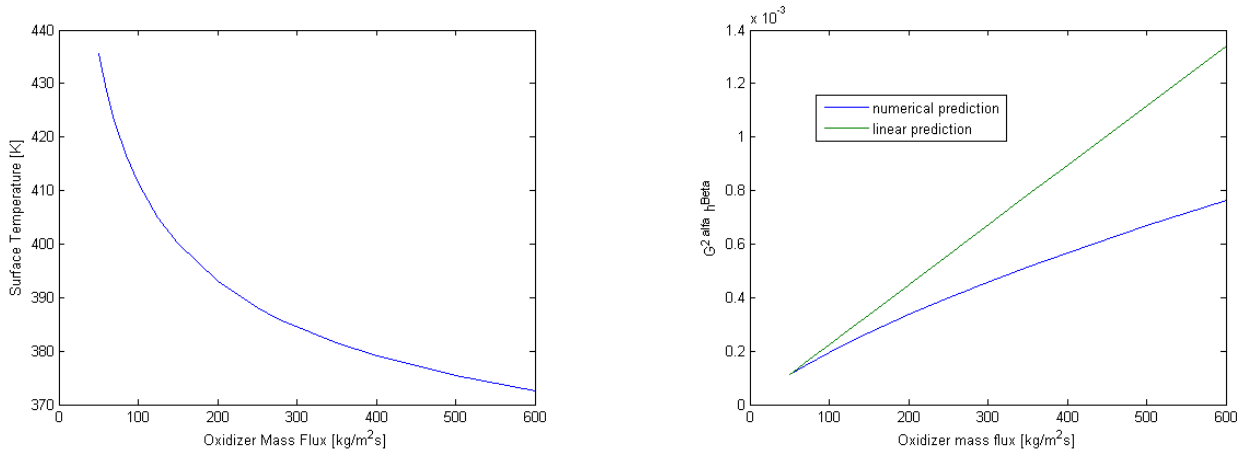

Figure 3.28: *Surface temperature (left) and product* $G_0^{2\alpha}h^{\beta}$. *Case with temperature decoupled from vaporization,*$\alpha = 1.5$, $\beta = 2$.

The results of this case are presented in figure 3.27. The slope of the regression rate curve is now more similar to the experimental results. The reason for this behavior is due to the fact that a strong reduction of the surface temperature predicted in this case produces a significant reduction in the liquid layer thickness. That means that a_t cannot be considered constant even if the liquid layer thickness has a logarithmic dependency on the energy terms. In fact for Φ_v/Φ between 0.2 and 0.1 the liquid layer reduction can be between 2 and 4 times.

Thanks to this $\dot{r}_{ent} \neq G_0^{\frac{2\alpha}{1+\beta}}$ as illustrated in Fig. 3.28.

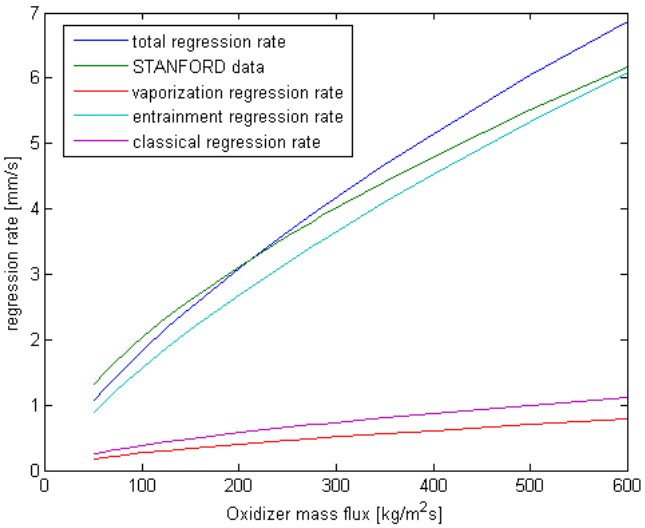

Figure 3.29: *Regression rate predictions: surface temperature decoupled from vaporization,* $\alpha = 1.5$, $\beta = 2$.

Concluding it is possible to say that the exponents of the entrainment law and the closure of the equations for surface-droplets-vaporization temperatures are the most influencing aspects that determine the correct slope of the regression rate curve for a paraffin based propellant.

It would be important also to get an estimate of the value of K because different models need different order of magnitude of value of K, so an estimate of K could be used to help the selection between different models.

Possible steps to solve the 'closure problem' are:

- decouple droplets average temperature, Arrhenius temperature and surface average temperature;
- find physical based relations between the previous three temperatures.

Due to the difficulties to determine these quantities by experiments it is possible that dedicated CFD simulations of the droplet entrainment process could be the only valuable mean to get more insight of paraffin regression rate mechanism.

3.4 Conclusions for Grain Model

In this chapter a numerical model able to solve the one dimensional unsteady heat equation inside the thermal grain has been implemented. The model is able to determine the transient temperature profile and regression rate. Numerical results showed that during throttling an overshooting of the regression rate can occur for high activation energies typical of hybrid fuels.

Afterwards the heat flux to the grain surface has been coupled with the chamber gas dynamic trough the boundary layer response.

To simulate the boundary layer response two time lags have been added in the heat transfer functions representing, respectively, the times needed by the boundary layer to adjust to changes of the oxidizer mass flux and the regression rate. It was shown that the second time lag was responsible for the typical hybrid low frequency instabilities. Moreover it was demonstrated that a positive shift of the average regression rate should occur during large regression rate oscillations.

Due to the importance of paraffin wax as a fuel for hybrid rockets, a version of the model suited for propellants that form a liquid layer has been developed. The model takes also into account the possibility of liquid entrainment. The code determines transient paraffin thermal profile and regression rate.

Paraffin based fuels usually operates above their critical pressure. For this reason the importance of an analysis of the supercritical regime was highlighted. For this purpose it was shown that jet disintegration morphology in liquid engines changes passing from subcritical to supercritical conditions. Three hypotheses have been made in order to figure out the behavior of supercritical entrainment in hybrid rocket motors.

Finally the numerical results have been compared with experimental data reported in the literature. It has been demonstrated that the predicted slope of the regression rate is almost linear. It was suggested that the reason for this mismatching is to be related to the uncertainty in the exponent of the entrainment law and to the fact that droplet entrainment is a non-linear, spatially and time-varying phenomenon.

This last aspect in turn induces the need to define suitable relations between droplet average temperature, surface average temperature and vaporization temperature as it is done in the problem of turbulence closure.

Chapter 4

Combustion Chamber Models

In this chapter the attention is focused on the gas dynamic inside the hybrid combustion chamber[1]. For this purpose two time-varying numerical models are developed in the following sections.

The aim of these unsteady codes is to determine the transient behavior of the main parameters of the hybrid rocket motor. The combustion chamber model represents the core of the hybrid rocket motor simulation. In fact the combustion chamber model gives directly the main parameter of a propulsion system, that is, motor thrust.

The sub-models presented in the previous and the next chapters define the input parameters for the combustion chamber model. In fact the grain model of chapter 3 determine the fuel mass flow while the tank and feed lines model of chapter 5 gives the oxidizer mass flow.

In the first part of this chapter a global 0D time-varying numerical model of the combustion chamber is developed. The code is then coupled with the grain model described in the previous chapter to account for the transient fuel production. It follows a brief discussion about the main hybrid rocket motor characteristic times and their relative values.

In the second part a 1D time-varying numerical model of the combustion chamber is developed. The unsteady 1D code is able to simulate all the features of the 0D code. It should add the acoustic response of the system and the spatial variation of the fluid-dynamic unknowns along the flow direction, increasing the accuracy of the results at the expense of an higher computational effort.

[1] In this chapter the term combustion chamber is used with an extended meaning, including the strictly speaking combustion chamber and the nozzle. Some authors call the combination of the combustion chamber with the nozzle as 'thrust chamber', but this term is not used here because it usually includes also the injector plate and liquid manifold.

4.1 0D Chamber Model

A zero dimensional model of the hybrid rocket combustion chamber has been implemented based on the mass conservation equation and energy conservation equation, as it is described in the following. Mass continuity equation:

$$\frac{d\rho}{dt} = \left(\dot{m}_{ox} + \dot{m}_f - \dot{m}_{pr}\right)/V_c - 4\dot{r}\rho/D_p \tag{4.1}$$

The volume of the combustion chamber is the sum of the port volume and the fixed volumes (pre/post chambers, convergent nozzle part). The diameter of the combustion chamber varies with the regression rate:

$$\frac{dD_p}{dt} = 2\dot{r} \tag{4.2}$$

The fuel mass flow rate is:

$$\dot{m}_f = \dot{r}\rho_f \pi D_p L_p \tag{4.3}$$

The mass exhausted by the nozzle is provided by:

$$\dot{m}_{pr} = p_c \Gamma_{pr} A_t / \eta \sqrt{R_{pr} T_{pr}} \tag{4.4}$$

The products properties are calculated with the instantaneous values of temperature, O/F ratio and pressure. The instantaneous O/F ratio is calculated using the following set of equations:

$$\frac{d\rho_{ox}}{dt} = \left(\dot{m}_{ox} - f\dot{m}_{pr}\right)/V_c - 4\dot{r}\rho_{ox}/D_p \tag{4.5}$$

$$f = \rho_{ox}/\rho \qquad OF = f/\left(1-f\right) \tag{4.6}$$

An ideal gas behavior is assumed:

$$p_c = \rho R_c T_c \tag{4.7}$$

The energy equation is the following:

$$\rho V_c \frac{de_c}{dt} = \dot{m}_{ox} h_{ox} + \dot{m}_f h_f - \dot{m}_{pr} h_{pr} - p_c \dot{r} L \pi D_p - \left(\dot{m}_{ox} + \dot{m}_f - \dot{m}_{pr}\right) e_c + \left(m_f + m_{ox}\right) Q_{comb} \tag{4.8}$$

Heat of combustion is calculated using CEA code [9] based on instantaneous O/F ratio and pressure in the combustion chamber:

$$Q_{comb} = Q_{comb}\left(O/F, p_c\right) \tag{4.9}$$

The temperature of the combustion products needs to be linked with the temperature in the combustion chamber that is determined through the energy equation. The following equation states that the temperature of combustion products is a-time the average temperature inside the combustion chamber where a is considered fixed in this code.

$$T_{pr} = aT_c \tag{4.10}$$

It's easy to see from eq. 4.8 that at steady state T_{pr} tends to the adiabatic flame temperature (neglecting the chamber volume variation term). Enthalpy and energy are defined as follows:

$$e = e_{op} + c_v\left(T - T_{op}\right) e_{op} = \int_{T_ref}^{T_op} c_v dT \tag{4.11}$$

$$h = h_{op} + c_p\left(T - T_{op}\right) h_{op} = \int_{T_ref}^{T_op} c_p dT \tag{4.12}$$

For simplicity, the energy and enthalpy have been linearized around the operating temperature T_{op}. The operating temperature has not to be confused with the reference temperature, to which the reference enthalpy and energy values are referred.
The operating temperature is a 'suitable' temperature chosen to linearize the equations from it to the actual temperature. For greater accuracy the operating temperature should be selected near the actual temperature during nominal operations. Different operating temperatures can be chosen for different species.
It is possible in the future to introduce more complicated expressions like those used in the CEA code.
It is worth to remark that the terms related to the time variation of port dimensions in eq.4.1 4.5 4.8 provide a minor contribution respect to the others, especially increasing the thrusters scale.
Finally the thrust is: $T = \dot{m}c^*C_f$
The model is solved using a 4th order Runge Kutta time marching scheme. The 0-D model

is able to catch the basic filling-emptying dynamic of the combustion chamber as it is shown in the following pictures.

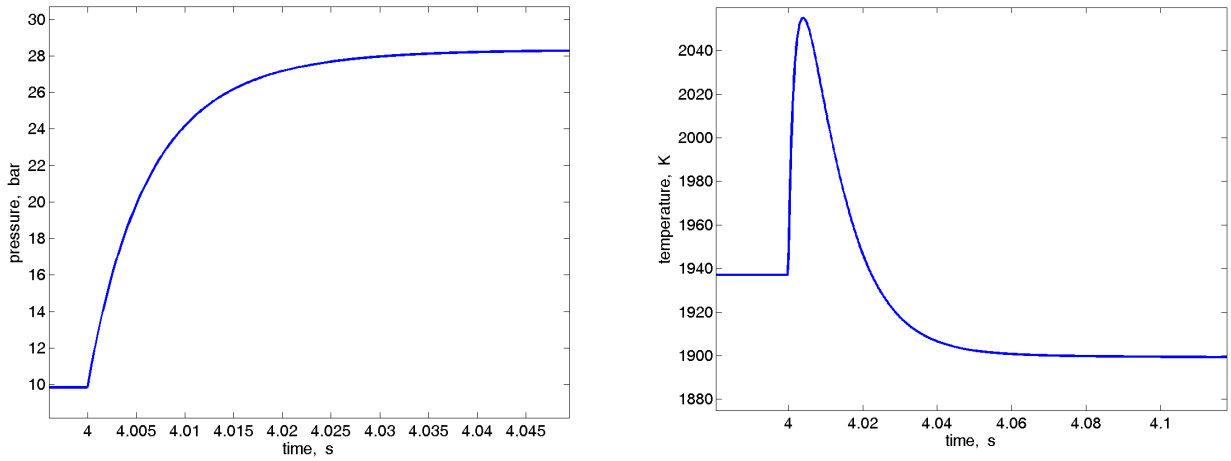

Figure 4.1: *Simulation of pressure (left) and temperature (right) responses to a positive step change of oxidizer mass flow rate.*

During a step change in the oxidizer mass flow the chamber temperature suddenly increases due to compression and then relaxes to its steady state value related to the combustion energy balance (O/F ratio). The same, in a reverse behavior happens for a sudden decrease in mass flow. This means that is not possible in general to replace the energy equation with a polytropic relation. However in an analysis where the input has a determined frequency this can be possible as a first approximation. For high frequency the polytropic exponent would be near the ratio of specific heats (adiabatic transformation) while for low frequencies it would depend on combustion (isotherm in the extreme case of a the combustion not sensitive to O/F shift).

However it is worth noting that the fundamental variables are far from being uniform inside the hybrid combustion chamber [10]. Moreover a 0D model cannot determine the acoustic response of the hybrid motor. So if a higher degree of accuracy in the prediction of hybrid transient behavior is needed it is suggested to shift to a one dimensional port model.

Some samples of the code outputs are presented in the following pictures. The results have been compared with the experimental data given by NAMMO Raufoss [71]. They are referred to a lab-scale H_2O_2-HTPB hybrid rocket motor developed in the frame of the SPARTAN project [72].

The efficiency cannot be determined directly by a lumped parameter code because it is dependent on the complex three-dimensional mixing inside the combustion chamber. However it could be defined as an empirical function of several parameters like O/F ratio, chamber

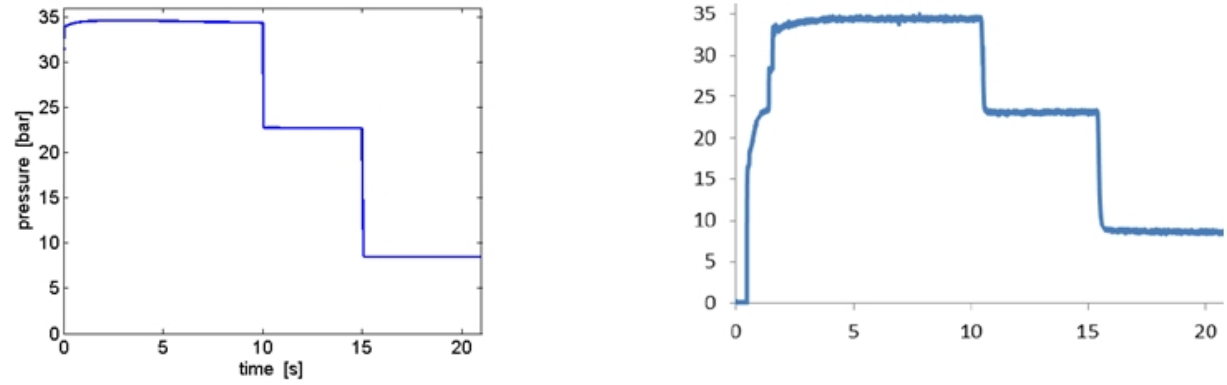

Figure 4.2: *Numerical pressure profile (left), experimental pressure profile provided by NAMMO (right).*

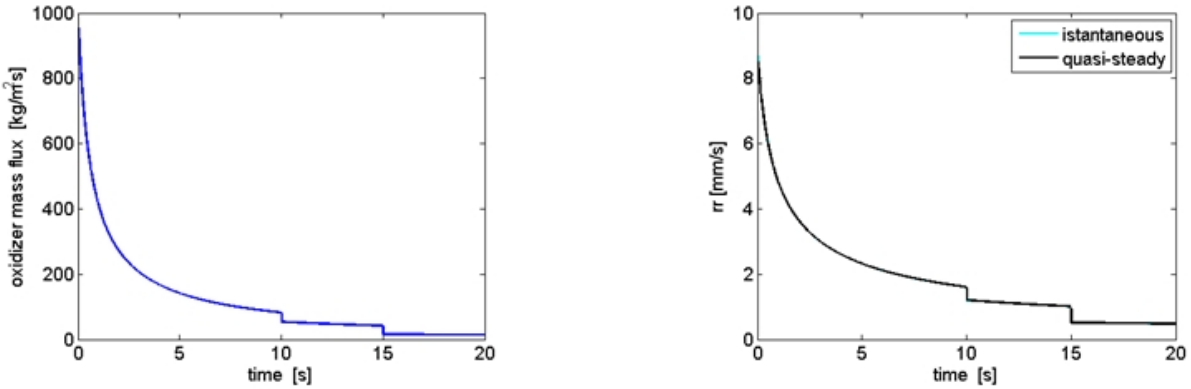

Figure 4.3: *Predicted oxidizer mass flux (left), predicted regression rate (right).*

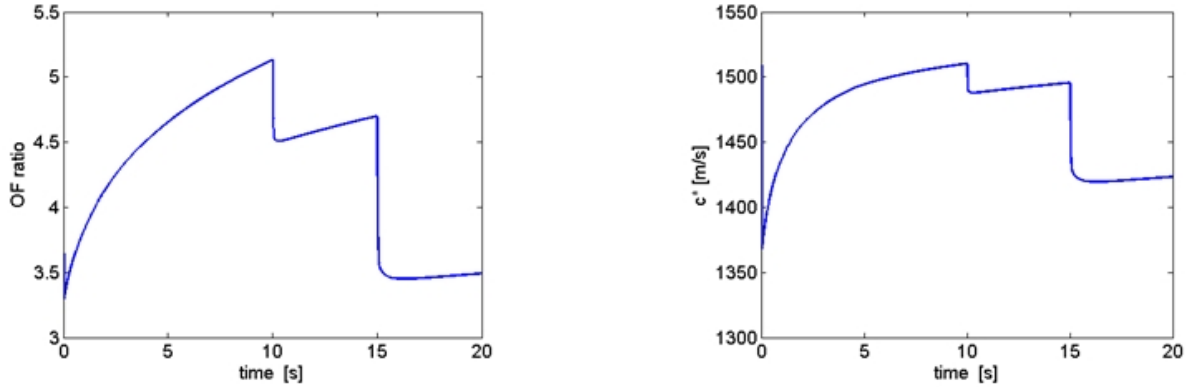

Figure 4.4: *Predicted oxidizer to fuel ratio (left), predicted characteristic velocity (right).*

L/D, scale, propellant combination, oxidizer flux etc.

For the particular motor presented in the previous and following pictures a simple function of the oxidizer flux has been defined. The equation has been chosen to match the experimental results. The physical basis has been demonstrated by complete Navier-Stokes simulations.

In fact a 3% decrease in the efficiency is predicted at maximum oxidizer fluxes by the 3D CFD simulations. The chamber model just shown can be coupled with the 1D grain model presented in chapter 3. In this way it is possible to determine the influence of the grain response on the fuel production and consequently on the motor transient behavior.
As previously highlighted in chapter 2, when studying hybrid transient behavior one of the main important parameter to determine is the response time of the hybrid motor. Neglecting in the present analysis the feed system response time, the limiting times for typical hybrid operations are the chamber filling-emptying time, the boundary layer response times and the thermal lag in the solid grain. The filling-emptying time of the combustion chamber scales with the formula:

$$\tau_{fill} \propto L^*/c^* \tag{4.13}$$

as it is shown by eq.2.1. It is important to note that in a hybrid rocket the flow tends to be highly stratified due to the peculiar separation between the fuel and oxidizer injection regions. Moreover the combustion is distributed in the axial direction because the fuel is continuously added along the grain, so eq. 2.1 should considered as a rule of thumb. However it's possible to state that the chamber response time increases with the scale of the propulsion system. The boundary layer response times scale with the following expression:

$$\tau_{bl} \propto L/u_e \tag{4.14}$$

Also these times increase with motor size. The final characteristic time is the thermal lag in the grain. This has been predicted by Marxman [15] with the following expression:

$$\tau_{tl} \propto \kappa/\dot{r}^2 \tag{4.15}$$

where κ is the grain thermal diffusivity. The regression rate at denominator indicates that the response is slower at lower mass fluxes. Consequently, grain response slows during the burn as port diameter increases. For a throttleable hybrid propulsion system the grain response is also more critical when the motor is operating at its lowest thrust levels. A variable time response is not a good attribute when a very precise and repeatable control is needed.
Eq. 4.15 suggests that hybrid configurations producing high regression rates (like vortex type) are inherently faster responding than a conventional motor. The thermal lag is not

directly related to the scale of the system because the thermal penetration is very small compared to port diameter. However usually larger motors have lower regression rates so their thermal lag is larger. Anyway if the regression rate scales according to Marxman law ($\dot{r} \propto L^{-0.2}$) the final thermal lag scales with $L^{0.4}$.

The comparison between the several hybrid time scales shows that for large motors the filling-emptying and the boundary layer times should be larger than the thermal lag[2]. The opposite should happen for small motors. For this reason experimental testing about transient response and instabilities at lab-scale level could be misleading if the results are used directly to infer large scale behavior. Moreover for small motors at low pressures also chemical kinetics could play an important role.

When studying hybrid transient behavior and particularly instabilities the author recommend the choice of a minimum appropriate scale according to the previous time scale analysis (not necessary the scale of the final system, but also not too small). Pressures and oxidizer fluxes should also be in the range of the expected application.

The thermal lag still remains predominant at every scale during thrust termination because of the mass flux (i.e regression rate) decay. The thermal lag could also limit the use of small hybrids for pulsed operations or fine thrust control[3].

Karabeyoglu [6] later demonstrated that at least two thermal lag time scales exist. For typical activation energy encountered with common fuels the surface time scale is much faster than the time required by the complete thermal thickness to reach the steady state. In fact the surface responds almost instantaneously to the heat input and then slowly relaxes to its steady state value. This is due to the fact that at the beginning of the transient event the surface is exposed to a strong heat flux but at the same time the thermal gradient in the grain is lower (for a positive throttling) than its steady-state value so the surface is not able to transfer all the the heat to the inferior layers.

This is confirmed by the thermal profile resulting from the simulations. As shown in the previous chapter during step changes of the oxidizer mass flow an overshooting of the regression rate occurs. This can be easily explained taking the limit for infinite activation

[2]This sentence should not be considered as allowing to neglect the grain response for large motors, particularly in the analysis of instabilities, because as already said in chapter 3 the grain transfer function is responsible for a slight amplification at low frequencies.

[3]It is important to remark also that for this kind of applications the use of hybrids is difficult because in a conventional hybrid design the web thickness required for a long total duration burn is not compatible with the small port diameter required by the low thrust levels.

energy. In this case the surface temperature is constant and the excess heat at the beginning of the transient event should determine an excess of the regression rate. For low activation energies the excess heat is instead used to rise the surface temperature and the grain response becomes more similar to the classical bounded non-regressive wall heating problem. This behavior is affected also by the fact that during rapid transients the blocking effect is different from its steady state value.

From a system point of view the main parameter of interest is motor thrust. The motor thrust is dependent on the propellant mass flow and so (obviously) it is related with fuel production. This in turn is dependent on the instantaneous regression rate. The regression rate follows the grain surface dynamic.

The peculiar transient regression rate behavior just highlighted by the 1D grain model implies both positive and negative aspects. From one side if the fuel overshooting stays under the acceptable tolerance the behavior just shown could be seen as an advantage because the fuel response time is much faster than predicted by eq. 4.15. On the other side the response is not bounded between the initial and final steady-state and this could be considered not acceptable for certain applications. The effect of the overshooting on thrust can be accurately calculated for any specific case by mean of the code.

However some rough estimates can be done in order to make some general comments. The regression rate overshooting is usually less than 10% of its nominal value. The influence of the fuel mass flow on the total propellant flow is dependent on the O/F ratio.

The pressure and thrust overshooting can be roughly estimated as the product of the relative regression rate overshooting by the fuel mass fraction. For oxidizers like N_2O or H_2O_2 the oxidizer flow is more than 70% (nominally more than 85%) of the total flow so fortunately the effect of the fuel flow fluctuations on pressure/thrust are smoothed (often less than 1%). Oxygen has a nominal oxidizer fraction near 72% but thanks to O/F shift during throttling down this value can drop significantly. Again the low thrust levels are more critical because according to eq. 1.28 the O/F ratio is lower.

When a wide, efficient and effective throttling capability is required the use of Hydrogen Peroxide is suggested (considering also the quasi steady analysis of the last section of the introduction).

4.2 1D Chamber Model

As previously stated the properties of the flow in a hybrid rocket evolve slowly along the axial direction. For this reason the development of a 1D description of the combustion chamber is highly recommended in order to increase the accuracy of the numerical results. For this purpose the conservation equations have been written respect to the axial direction.
Mass continuity equation:

$$\frac{\partial \rho}{\partial t} = -\frac{\partial G}{\partial x} + \frac{4\rho_f \dot{r}}{D_p} \tag{4.16}$$

The momentum equation is the following:

$$\frac{\partial G}{\partial t} = -\frac{\partial G^2/\rho}{\partial x} - \frac{\partial p}{\partial x} - \frac{2c_f G^2}{D_p \rho} \tag{4.17}$$

The molecular mass is a linear interpolation between the value at the injection and in the post-chamber:

$$M(x) = M_{in}(1-x) + M_{out}x \tag{4.18}$$

The products properties are calculated with the instantaneous value of the post-chamber temperature, pressure and global O/F ratio. Again an ideal gas behavior is assumed at every cell:

$$p = \rho R T \tag{4.19}$$

The energy equation is the following:

$$\frac{\partial e^0}{\partial t} = \frac{4\rho_f \dot{r} h_f}{D_p} - \frac{\partial G h^0}{\partial x} + q \tag{4.20}$$

The heat source is uniformly distributed along the x direction:
$q = (\dot{m}_f + \dot{m}_{ox}) Q_{comb} / (n A_p dx)$ where n is the number of nodes.
The mass exhausted by the nozzle is provided again by:

$$\dot{m}_{pr} = p_c \Gamma_{pr} A_t / \eta \sqrt{R_{pr} T_{pr}} \tag{4.21}$$

The global heat source Q_{comb} and the global O/F ratio have been calculated as in the 0D code. The regression rate can be calculated with classical expressions like $\dot{r} = a G_0^n x^m$.

However for an accurate description of hybrid transient behavior the 1D chamber gas dynamics should be coupled with the unsteady grain equations as it has been shown before with the 0D chamber model. Currently for simplicity and to limit computational resources the regression rate is considered uniform along the axial direction and the heat equations are solved only in the direction normal to the surface.

To solve the unsteady one dimensional equations presented above several numerical schemes have been attempted. The spatial derivatives have been approximated with a 1st order upwind scheme or a 2nd order central difference scheme. Some algorithms solve the equations on a staggered grid. All the unknowns are evaluated at the center of the cells while the velocity is evaluated at the cell faces.

Other implemented codes use a collocated arrangement, where all the variables are calculated at the same nodes. The resulting equations have been solved respect to time with a 4th order Runge-Kutta scheme as in the 0D model.

Every numerical scheme has its own advantages and drawbacks [73]. First order methods are known to be less accurate and to require a higher discretization. Moreover the upwind scheme introduces a numerical diffusion that smooths the gradient in the flowfield. Second order method are more accurate on the same grid but in contrast to 1st order ones they are not bounded, so the numerical results can present oscillations exceeding the exact values near steep gradients.

For the time integration the 4th order Runge-Kutta scheme has been chosen because it is accurate, explicit and easy to implement and upgrade when further equations have to be included or modified.

For the spatial discretization in the present case it is possible to display the following arguments. No diffusive terms are present in the equations, so the steady state solution doesn't show the classical convective-diffusive exponential behavior. In fact the steady state solution is smooth without steep gradients. With the number of nodes used (>50) the error is less than 1% with every method respect to analytical reference cases.

During transient events steep gradients are produced by acoustic oscillations. The frequency of oscillations is correctly determined compared with analytical cases. On the contrary the amplitude and the damping of the oscillations is different between different numerical schemes.

As expected the damping of the 1st order upwind scheme is stronger than predicted by higher order methods. However some complex three-dimensional phenomena and damping

mechanisms that are not considered directly in the one dimensional mathematical treatment are present in a real motor. Higher order methods are more accurate with regard to the exact solutions of the 1D mathematical model, this does not guarantee the necessary accuracy in respect with the real motor physical behavior.

The author advise to use the upwind scheme when the interest is not focused on the acoustic response of the motor because this method is robust and produces a 'cleaner' signal. When the acoustic response is of main interest a more complex analysis would be necessary[4]. However with the spatial 2nd order code it was possible to simulate the typical ringing decay of AMROC motors[5] [6].

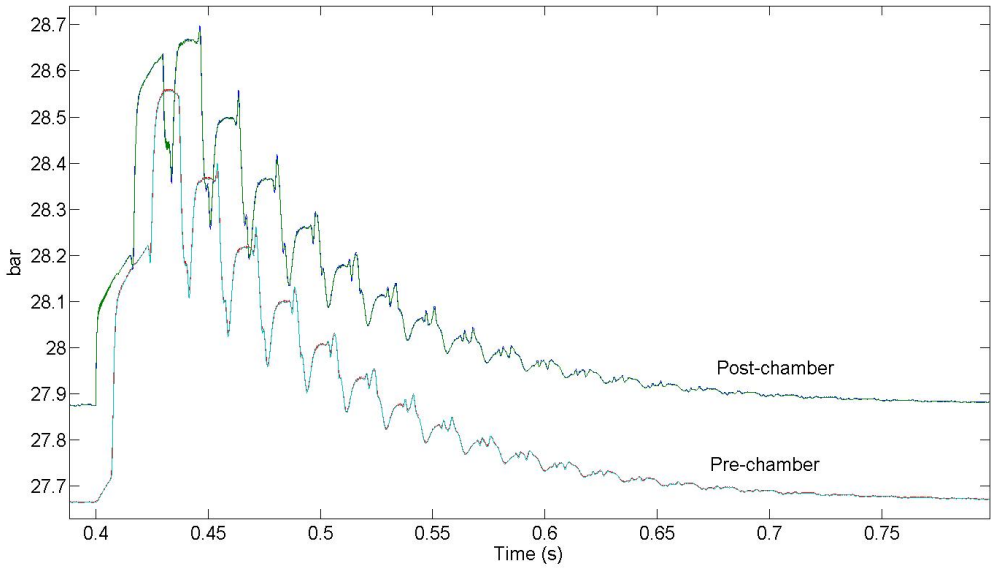

Figure 4.5: *Response of chamber pressure to a disturbance of the oxidizer mass flow rate for a simulated AMROC test.*

The 1D code is able to predict the variation of the fluid unknowns in the axial direction. As expected the temperature rises along the port while the pressure decreases. The effect of friction is negligible and the axial pressure drop is mainly due to mass addition and Rayleigh-pipe heat addition. In fact its numerical value corresponds nearly to:

$$\Delta p = \left.\frac{G^2}{\rho}\right|_{out} - \left.\frac{G^2}{\rho}\right|_{in} \tag{4.22}$$

[4]Moreover a better description of nozzle impedance should be introduced

[5]To obtain this picture the oxidizer mass flow input is suddenly increased to 10% above its operating value and held at this level for 0.03 seconds before it is suddenly reduced to its original value.

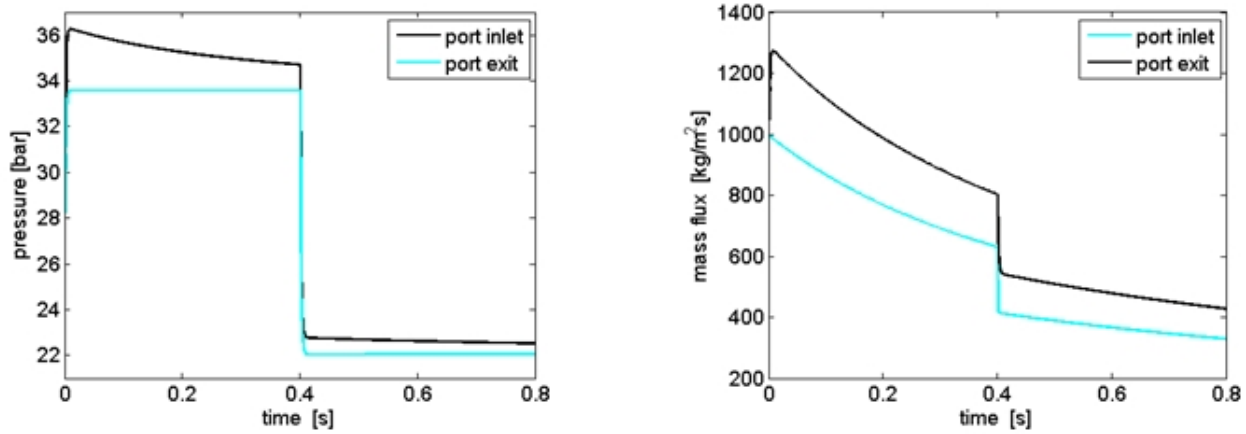

Figure 4.6: *Pressure vs. time (left) and mass flux vs. time (right) during a throttling event.*

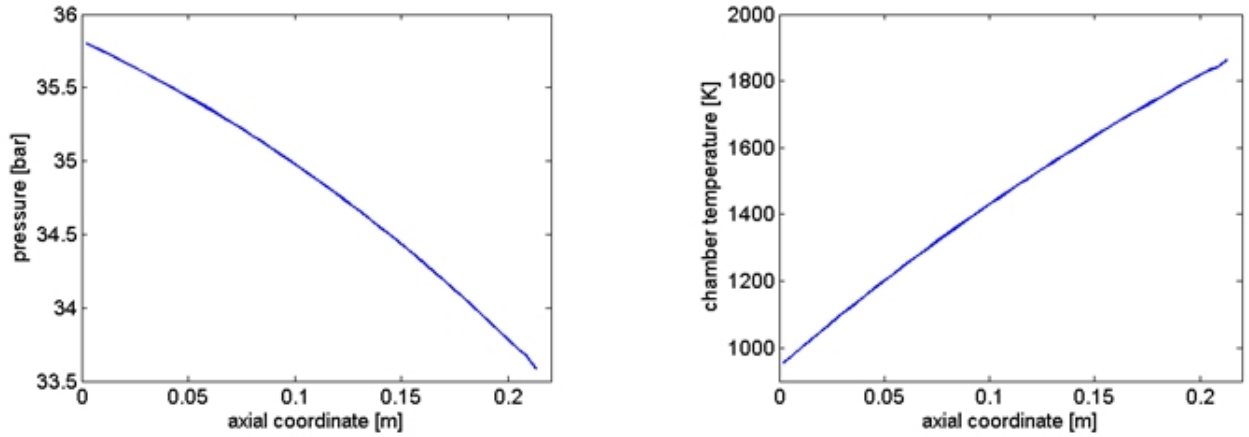

Figure 4.7: *Axial pressure drop (left), chamber temperature axial profile (right).*

The results are confirmed by 3D CFD simulations. The pressure drop is higher at the beginning of motor operation when the oxidizer flux is maximum and consequently also the Mach number at port exit.

4.3 Conclusions for the Combustion Chamber Models

In this chapter a 0D and a 1D unsteady combustion chamber model have been developed using the proper conservation equations. These codes are able to simulate hybrid rocket motor transient behavior and global performances.

The code can be coupled with the unsteady 1D model of the fuel grain in order to take into account transient fuel production. It has been shown that a regression rate overshooting occurs during a throttling events. The regression rate overshooting is usually less than 10% of its nominal value. For high optimum O/F ratio oxidizers like N_2O or H_2O_2 the oxidizer

flow is more than 70% (nominally more than 85%) of the total flow so fortunately the effect of the fuel flow fluctuations on pressure/thrust are smoothed (often less than 1%).
It has been determined that the thermal lag in the solid grain is the limiting time for small motors and during thrust termination events while for large motors the longest times are the boundary layer diffusion times and the filling-emptying times.
Thanks to these code it is possible to predict the global O/F ratio, pressure, mass fluxes, characteristic velocity and thrust during the burn. The codes could be inserted in a more complex simulation of the entire flight system. In this way they can be used to optimize the rocket motor to achieve the maximum performances. Moreover, thanks to their transient nature it is possible to assess the effect of the motor response to the complete flight dynamic in order to establish a satisfactory control law.

Chapter 5

Tank, Feed Lines and Injection

This chapter end the description of the several sub-models of the hybrid rocket propulsion system. Together with chapter 3 and 4 it composes the code describing hybrid rocket transient behavior. In this chapter the attention is focused on the the numerical modeling of the oxidizer path. This includes the sub-systems ahead of the combustion chamber like the pressurization system, the main tank and the feed lines. Moreover it considers also the injector elements and some aspects of droplets vaporization and atomization in the combustion chamber.

This work is complementary to the one described in chapter 3, defining the input parameters for the core of the code, that is the chamber gas-dynamic model shown in chapter 4. In fact the grain model of chapter 3 gives the fuel mass flow while the tank and feed lines model of this chapter determines the oxidizer mass flow.

The main object of this work is to determine how the feed system affects the performance parameters of the hybrid motor with time. For this purpose the prediction of several unknowns like the oxidizer mass flow, tank pressure and the amount of residual gases is obtained through the modeling of the principal subsystem behavior. Moreover the full transient coupling between the feed system and the combustion chamber is also investigated.

This chapter is divided in three parts. The topic of the first paragraph regards the main tank and the pressurization system. After a brief description of the main alternatives the discussion goes on with the numerical modeling of the typical solutions adopted for hybrid rockets (i.e. pressure-regulated, blowdown and self-press). First of all a numerical model of a pressure fed tank is developed. The code is able to predict several parameters like masses, densities, temperatures and pressures of the gas in the ullage volume and in the pressurant tank, the pressurant mass flow and the filling level of the tank. The model takes into account

several aspects like heat losses, liquid oxidizer evaporation, eventual gas phase combustion of the pressurant gas, the use of by-pass and digital valves.
Later a numerical model of a self pressurized tank is developed. The code is able to determine the oxidizer mass, temperature, pressure, density and the vapor/liquid volume/mass fractions during the discharge. The numerical results are compared with experimental hot tests performed at CISAS.
The second paragraph takes into account the the full transient coupling between the feed system and the combustion chamber. The main challenge is to determine the instantaneous liquid mass flow and the relation between the liquid oxidizer and the gaseous oxidizer that takes part in the hybrid motor combustion processes (i.e. droplets vaporization). In this way it is possible to simulate feed system coupled instabilities.
The third paragraph deals with the prediction of the mass flow through the injector elements. In particular the behavior of self-pressurized systems is investigated. In this case the chamber pressure is below the vapor pressure of the liquid inside the tank. Consequently cavitation and flashing occur inside the injector elements. This kind of two-phase flow with vaporization involves several important modeling issues. Different models are compared with cold-flow tests performed at CISAS in order to check the accuracy of their predictions.

5.1 Tank and Pressurization System Model

In a hybrid rocket as in its liquid counterpart the liquid oxidizer is stored in a tank and subsequently injected in the combustion chamber during operation trough the feed system. For this scope the pressure of the liquid oxidizer should be raised above the value in the combustion chamber. Consequently a pressurization system is needed.
Two main types of pressurization system can be defined: tank-pressure fed and pump pressure fed.
In the pump fed case the liquid oxidizer is stored at a chosen pressure below the motor chamber operating pressure and the pressure of the liquid is increased through a pump system. This allow the tank to be lightweight because approximately the wall thickness is proportional to internal pressure meanwhile reaching very high chamber pressures.
For this reason there is a long history of pump fed usage in the liquid propulsion community, particularly for large launchers. Usually a turbopump is used with the pump being of centrifugal type and the turbine driven by moderately (turbine blade limited) hot gas. The

hot gas is produced by monopropellant decomposition (H_2O_2 for Soyuz launcher), by propellant evaporation after cooling the combustion chamber or by a propellant feed fuel-rich or oxidizer-rich gas generator. For small systems positive displacement pump could be used (Xcorr [95], Lawrence Livermore National Laboratory [96]).

Small pumps have long been proposed also for satellites but nothing has reached operational status, mainly because of reliability worries. Pump-fed system are generally considered very expensive and complex to develop and produce, mainly because of the number of components, tight tolerances and a reputation for being extremely hard to design to get optimum performance.

The use of pump-fed in hybrid propulsion is much less common, mainly because only few large hybrid systems have been developed while the great part of work has focused on medium to small systems. Moreover the will for simplicity characteristic of the hybrid concept favors the choice of the much simple pressure fed solution. However is worth noting that both AMROC and Lockheed Martin began large scale development considering pressure fed rockets while shifting to pump fed in the following [64].

The same trend has been seen in the liquid field where the *Big dump booster* concept has been proposed several times to decrease cost/complexity but it has never been successful (up to now).

The use of a pump fed system in a hybrid rocket could share much of the technology with the liquid field. However some peculiarities need to be underlined. First of all only one liquid has to be pumped and this is fairly claimed has a significant advantage of hybrid propulsion. However as the typical design of an hybrid rocket does not consider the use of regenerative cooling (even if it is possible but not attractive) the choice is limited mainly to the use of a gas generator (GG). H_2O_2 gas generators have been used by AMROC and are very attractive for systems using H_2O_2 also as oxidizer. An alternative is the use of small hybrids as gas generators [64]. The use of hybrids is favored respect to small liquid GG because is preferable not to use liquid fuels in Hybrid systems to preserve their 0 TNT features.

In a tank pressure fed system the pressure in the oxidizer tank is above chamber pressure. As previously mentioned this solution implies a much higher tank weight but no complex moving parts so its generally considered much simpler, cheaper and reliable. This is confirmed by the historical monopoly of this solution for spacecraft propulsion units. Without any counteraction the pressure in the tank decreases during the liquid discharge because of the expansion of the ullage gas. This is called the *blowdown* mode.

On the contrary in the pressure-regulated mode a gas is pushed in the tank in order to preserve the initial pressure. Usually this gas is a low molecular weight gas like He fed from a pressurant tank, but it could be also the hot gas produced by a gas generator.
An intermediate option is the use of *Trydine*. *Trydine* is a mixture of He with a very small quantity of H_2 and O_2. The gas could be considered inert but trough the use of a catalyst the reaction between hydrogen and oxygen heats up the He reducing significantly the required amount of pressurant gas.
Several other techniques have been proposed/tested/patented (e.g. hypergolic injection in the tank) but with little usage so they would not be investigated in this thesis.
Another very common type of pressure-fed technique for hybrid propulsion is self pressurization. In this case the liquid is stored and used as in the blowdown mode. However if the pressure in the tank is near the vapor pressure of the liquid oxidizer during the discharge a portion of liquid begins to boil behaving as a pressurant gas. In the isothermal case the pressure in the tank remains constant. For a real discharge the heat of the environment is small compared to the latent heat of vaporization so the liquid cools and the pressure decreases by $20 - 50\%$ depending on conditions.
The advantage of this technique is related to the fact that it share the simplicity of a blowdown system with a much more limited pressure drop in the tank during the discharge for the same ullage volume. For the *same pressure drop* usually the volume required for an oxidizer operating in blowdown mode is higher than the volume required for the same oxidizer in self-press mode (e.g. subcooled N_2O vs self-press N_2O). However the density of the oxidizer gas remaining in the tank is much higher than the density of a common pressurant like He so the burning of the residual gas is highly recommended.
Self pressurization has been considered for long for liquids but rarely used. Self-pressurization is more attractive for hybrids than for liquids. First of all self-press fuels have much lower densities than hybrid fuels. Than hybrid combustion is much more tolerant than liquid combustion so gas phase combustion and self press operation are easy to obtain.
The self-compensating characteristics of hybrid regression rate helps a lot. In a liquid system the pressure in the oxidizer and fuel tanks could follows different path leading to O/F shifts that are much more tedious on a liquid motor. The shift from liquid to gas phase can happen at different instants for the two liquid propellants. Even if self-press liquids have been developed and tested [97] the use of this technique has been much more successful in hybrid propulsion.

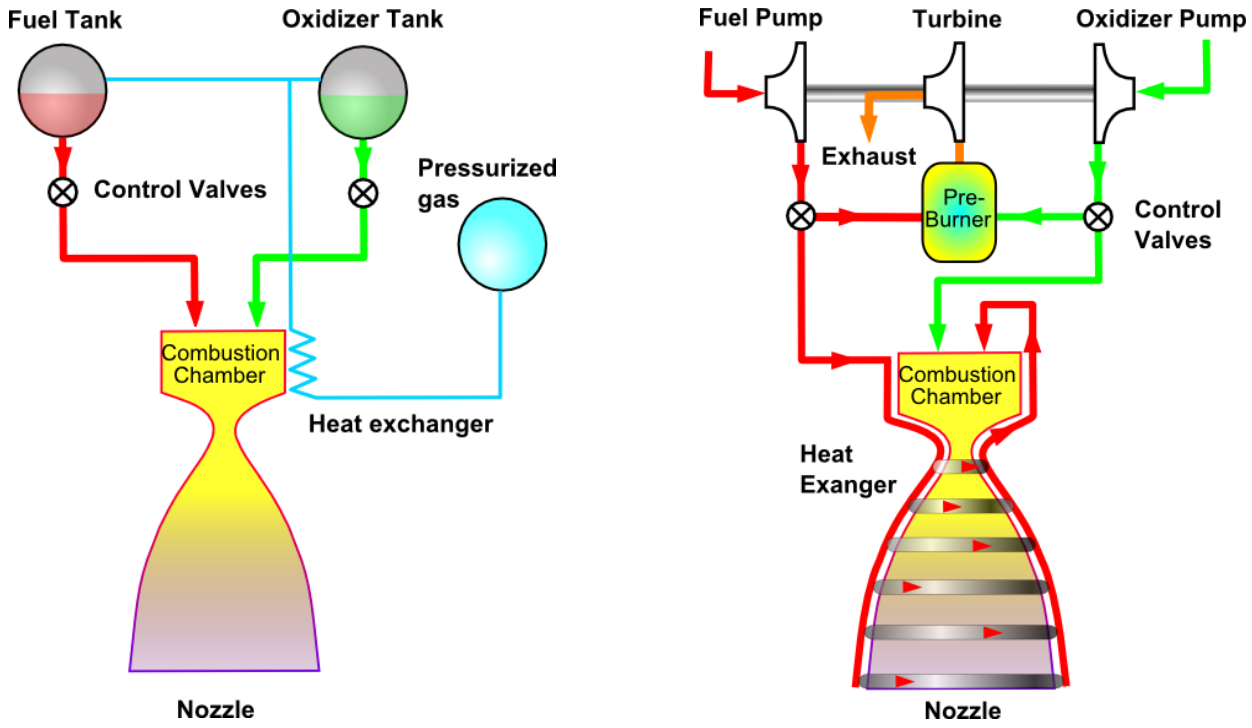

Figure 5.1: *Examples of tank pressure fed (left) and pump pressure fed (right) schematics.*

In this thesis the attention is focused on pressure fed systems. The general simulation of a pump fed system could be performed adding a pressure rise between the tank and the injector plate. The detailed analysis of a pump fed system is out of the scope of this work but could be performed using the extensive liquid literature.

Pressure fed systems are more interesting in this context because of CISAS activities in the past and the near future. CISAS has been testing hybrid rocket motors since 2007 in pressure regulated and self-press mode mainly using N_2O as oxidizer.

In this section several aspects of pressure-regulated and self-press hybrid behavior have been investigated. The governing equations for the combustion chamber have been solved for the quasi-steady solution for the sake of simplicity and to reduce computational time. We begin with the mathematical model for a conventional pressure fed (pressure-regulated or blowdown) system. For an incompressible liquid the oxidizer mass flow is calculated with Bernoulli equation:

$$\dot{m}_{ox} = Cd_{inj} A_{inj} \sqrt{2\rho_l \left(P_0 - p_c\right)} \tag{5.1}$$

However for an incompressible liquid is usually advised to use a cavitating venturi in order to decouple the oxidizer mass flow from the combustion chamber pressure. This has a twofold advantage: it increases the stiffness of the injection system and it allows an easier

control of the oxidizer mass flow. In this case the mass flow is dependent only on the upstream pressure:

$$\dot{m}_{ox} = Cd_{cv} A_{cv} \sqrt{2\rho_l \left(P_0 - p_{vap}\right)} \tag{5.2}$$

With equation 5.1 is possible to determine the actual pressure drop trough the injector plate. If the pressure upstream the injector is higher than a certain fraction (nearly 85%) of the venturi upstream pressure the venturi does not work properly (i.e. choked).
The following equations are used to compute the fundamental parameter in the oxidizer tank.

Energy equation for the ullage:

$$\frac{dE}{dt} = -P\dot{V} + \dot{m}_{press} h_{press} + \dot{m}_{ev} h_{ev} - \dot{Q}_w - \dot{Q}_i \tag{5.3}$$

Volume for the ullage:

$$\frac{dV}{dt} = \frac{\dot{m}_{ox} + \dot{m}_{ev}}{\rho_l} \tag{5.4}$$

Continuity equation:

$$\frac{dM}{dt} = \dot{m}_{ev} + \dot{m}_{press} \tag{5.5}$$

Heat losses (gain) trough tank wall (w) and between oxidizer-gas interface (i):

$$\dot{Q} = \alpha A \Delta T \tag{5.6}$$

Continuity equation for the pressurant tank:

$$\frac{dM}{dt} = -\dot{m}_{press} \tag{5.7}$$

Energy equation for the pressurant:

$$\frac{dE}{dt} = -\dot{m}_{press} h_{press} - \dot{Q}_w \tag{5.8}$$

The pressurant mass flow can be calculated using a model for the pressure regulator based on empirical data given by the manufacturer. Its important to note that a pressure regulator for a pressure fed system is much heavier than for a pump fed one because it has to handle a much higher mass flow. Pressure regulators used in space have to handle very low mass flows compared to propulsion systems used for boosters or launchers. The behavior of a pressure regulator at high fluxes could be very different from ideal. For the ideal case the mass flow is adjusted iteratively in order to maintain the pressure in the tank fixed to the design value.

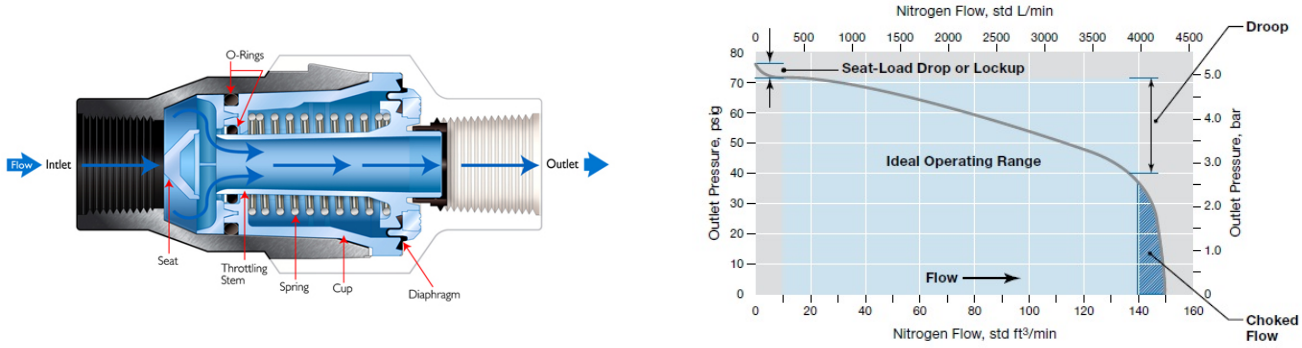

Figure 5.2: *Typical pressure regulator (left) and its flow curve (right).*

Some results of the ideal case simulation are shown in the following figures.

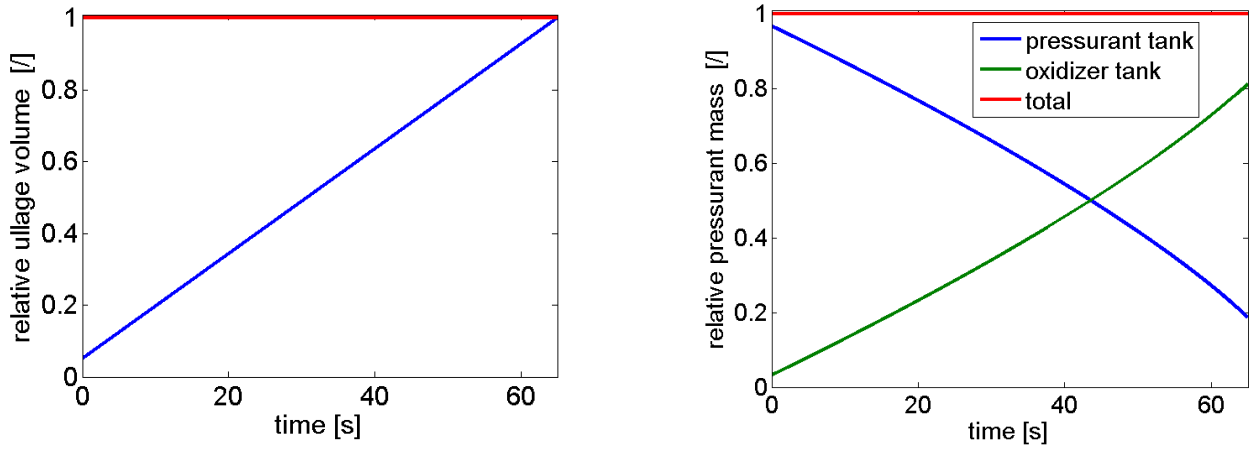

Figure 5.3: *Relative ullage volume (left) and relative pressurant mass (right).*

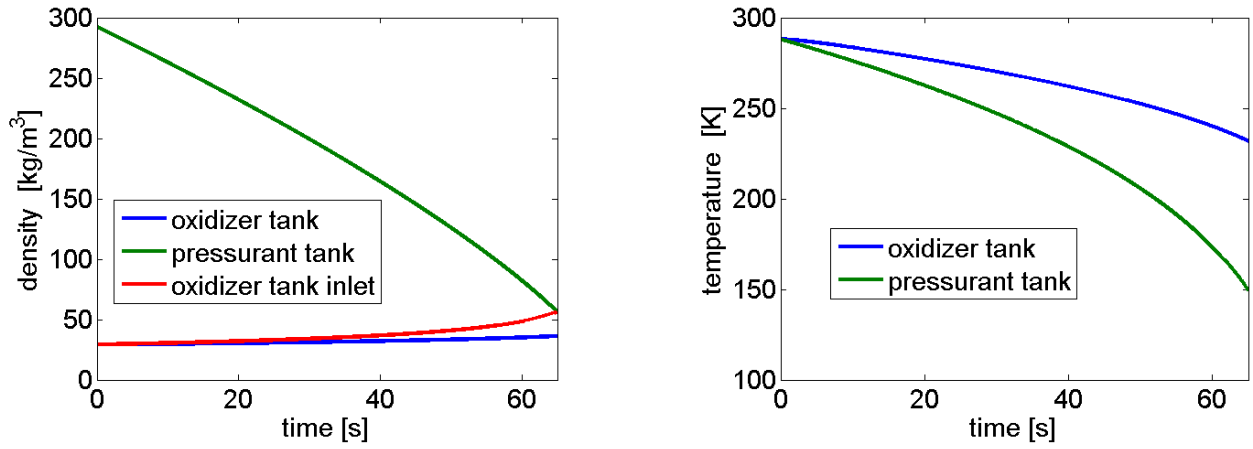

Figure 5.4: *Gas density (left) and temperature (right).*

With the help of this code is possible to determine the actual amount of required pressurant at every instant. The code has been validated with classical adiabatic relations for

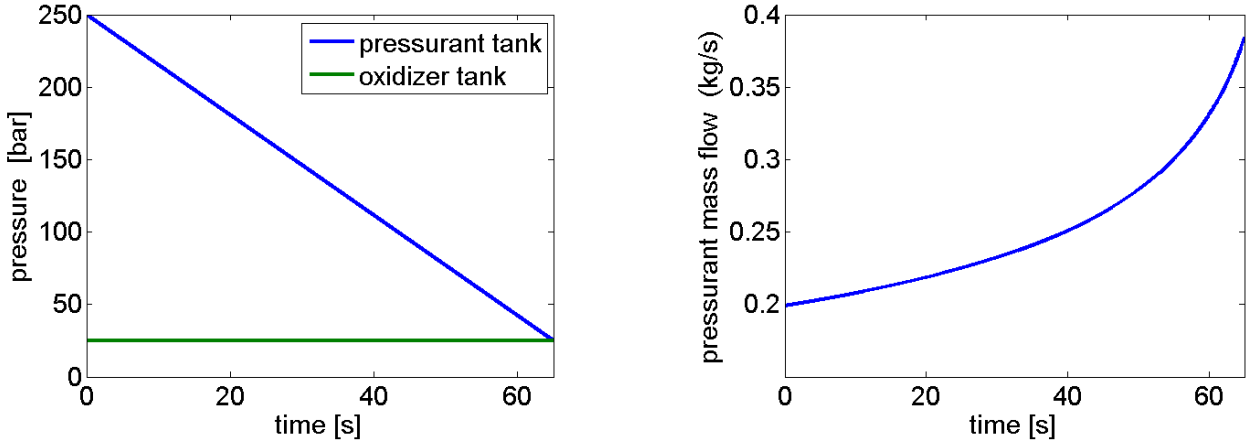

Figure 5.5: *Pressure (left) and pressurant mass flow (right) evolution.*

the ideal case:

$$m_{press} = \frac{\gamma_{press} P_t V_t}{R_{press} T_0 \left(1 - \frac{P_f}{P_0}\right)} \tag{5.9}$$

Heat losses increase this amount while a positive heat flux helps the pressurization system. Heat losses are important for cryogenic liquids (LOX) where the wall and the liquid are very cool. The cooling of the pressurant increases its density reducing its capabilities. This reduction is considered with the collapse factor [98]. The most important effect in the collapse factor is the stratification of the temperature in the gas phase. However this is a lumped parameter code so stratification is simply simulated with a proper ullage temperature different from the liquid temperature. However a more detailed analysis necessitates more complex models [98].

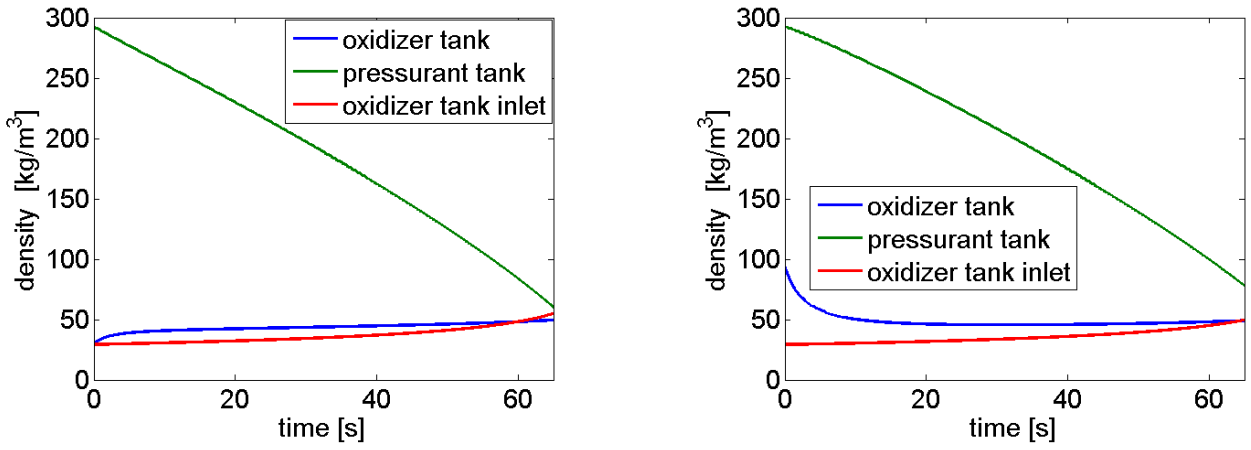

Figure 5.6: *Gas density, cases with heat losses. Initial ullage temperature equal to pressurant temperature(left) and liquid oxidizer temperature (right).*

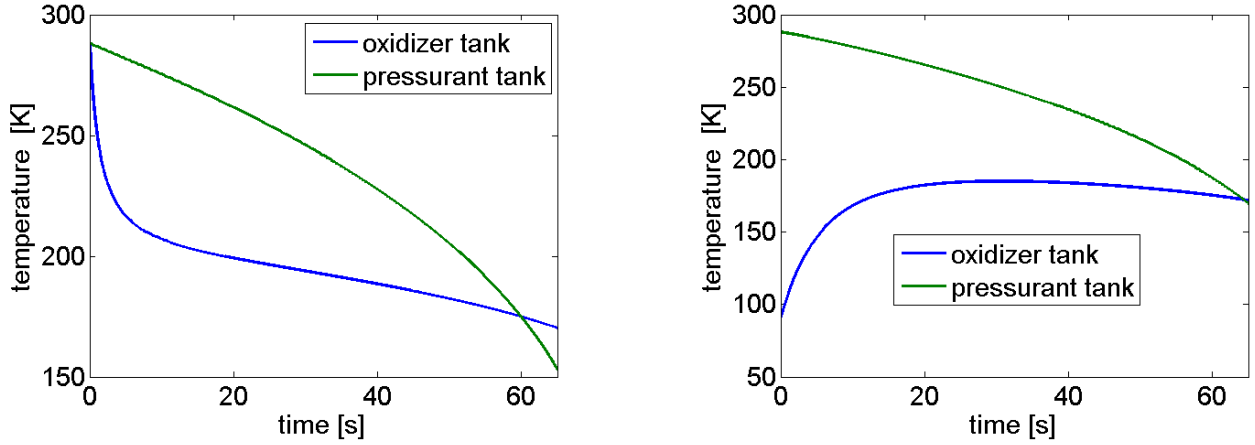

Figure 5.7: *Gas temperature, cases with heat losses. Initial ullage temperature equal to pressurant temperature(left) and liquid oxidizer temperature (right).*

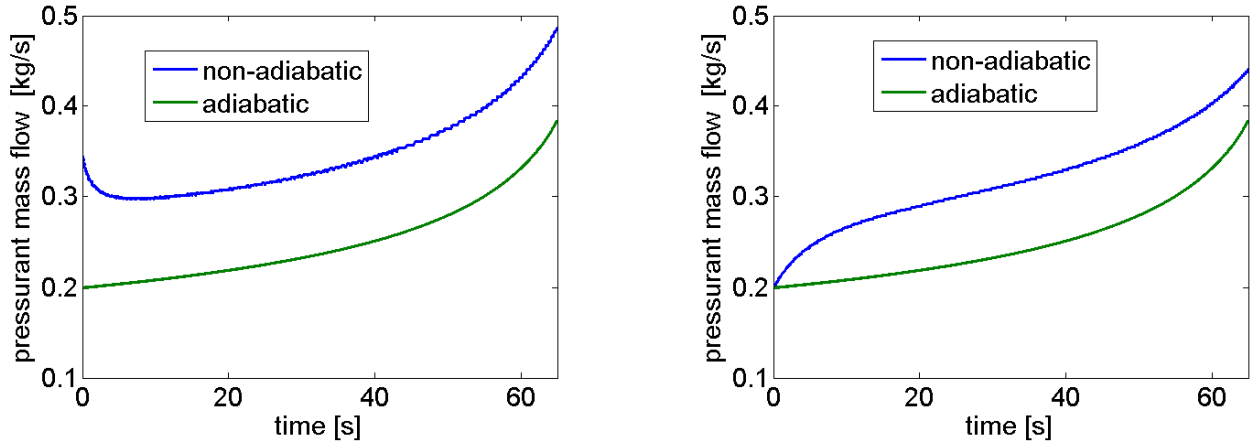

Figure 5.8: *Pressurant mass flow, cases with heat losses. Initial ullage temperature equal to pressurant temperature(left) and liquid oxidizer temperature (right).*

The heat losses are proportional to the $Area/Volume$ ratio so they are more important for smaller systems. The same happens for the venting of LOX during wait at the launch pad, making this oxidizer less attractive for small systems. However stratification is more important for larger systems.

The heat between the gas-liquid interface is much smaller[98] than the heat exchanged with tank walls. The evaporation of the liquid due to the heat flux between the gas-liquid interface is calculated in this way:

$$\dot{m}_{ev} = \dot{Q}_i / h_v \tag{5.10}$$

where h_v is the effective heat of evaporation.

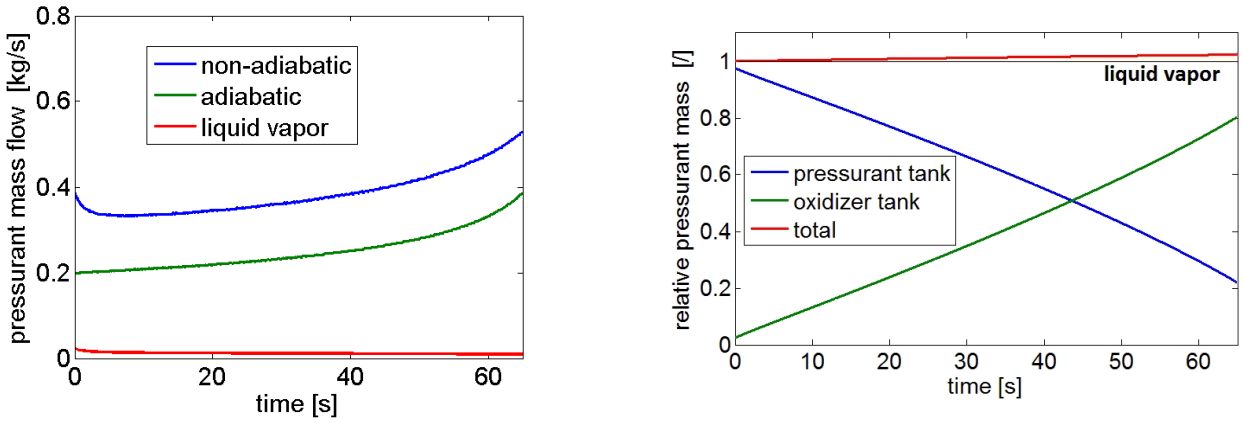

Figure 5.9: *Case with heat losses and liquid oxidizer evaporation. Pressurant mass flow (left) and relative pressurant mass (right).*

Heat losses have to be considered also for storable propellants when using an hot pressurant gas.

Thermal exchange is important for storable propellant in space. For very high mass flows the discharge is isentropic while for very small mass flows (long times) the discharge is isotherm. Moreover when the time between two following discharges is relevant the final pressure decay corresponds to the isotherm case (even if during the discharge the behavior can be isentropic).

The difference is very relevant; in fact a tank filled at 75% operated in blowdown mode (typical case for spacecrafts) has a pressure ratio between initial and final pressure of 4 in the isotherm case and 6-11 for the isentropic one (depending on the ratio of specific heats). This highlight the fact that pressure fed systems have higher penalties for launchers than spacecraft.

If the pressurant is an oxidizer it is possible to simulate the gas phase combustion of the pressurant and determine the final amount of pressurant that remains in the tank at the end of the burn.

It is important to notice that the gas phase combustion produces a non-negligible thrust tail. Moreover an O/F shift occurs during final gas-phase combustion because of the strong reduction of the oxidizer mass flow due to the much lower density of the gas phase. This in turn decreases the motor I_{sp}.

To compensate for the O/F shift it is possible to use a layer of low-regressing material if the main fuel is high regressing. Moreover the pressure reduction during the gas phase combustion produces a decrease of the C^*. The reduction of I_{sp} could be much stronger if

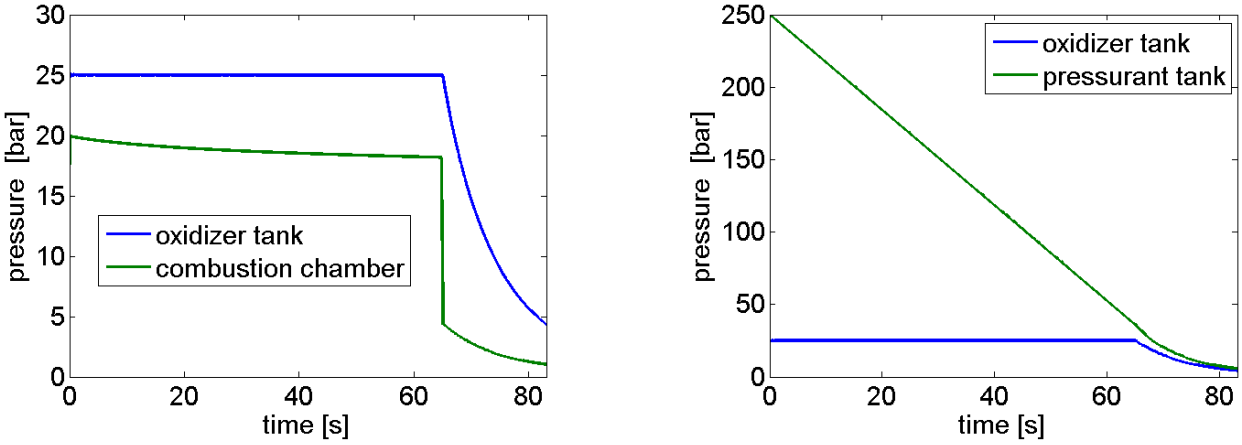

Figure 5.10: *Case with gas phase combustion. Pressures evolution.*

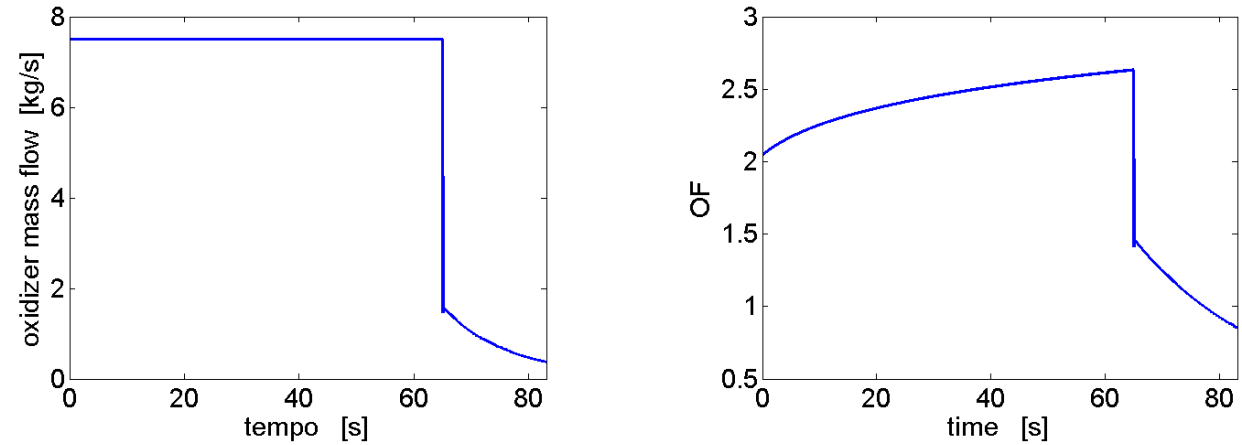

Figure 5.11: *Case with gas phase combustion. Oxidizer mass flow (left) and O/F ratio (right).*

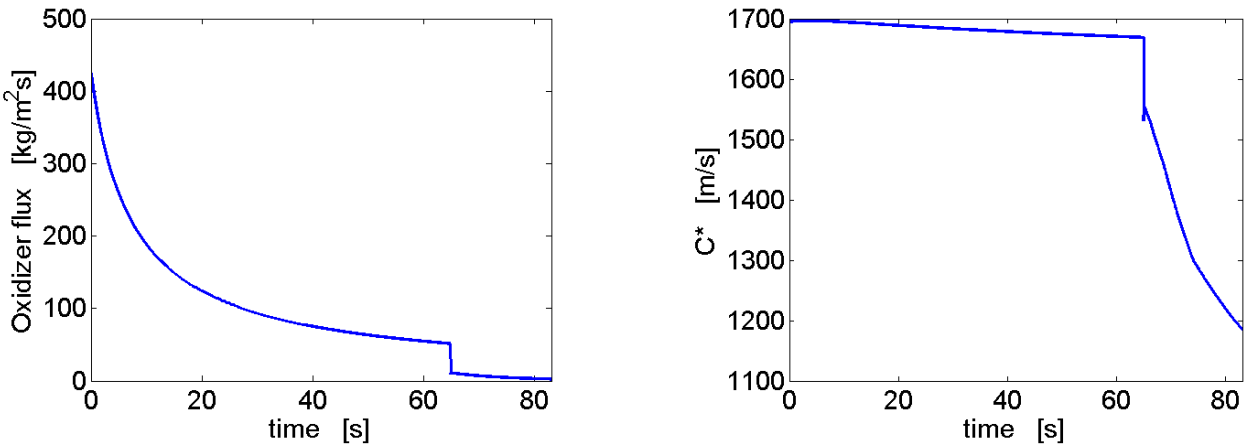

Figure 5.12: *Case with gas phase combustion. Oxidizer mass flux (left) and chamber characteristic velocity (right).*

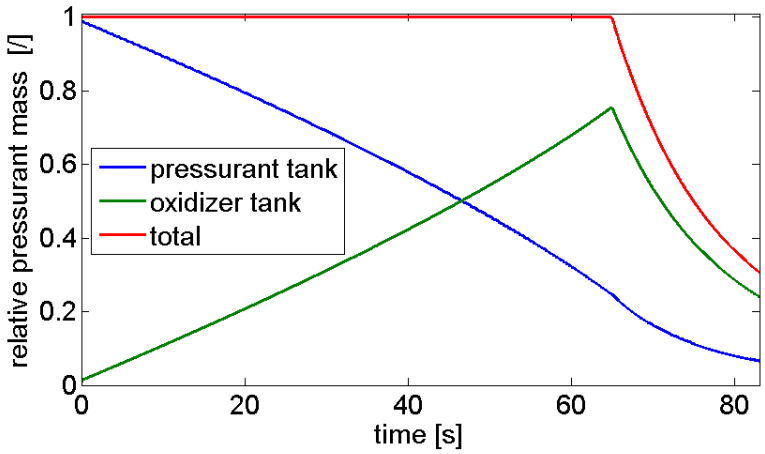

Figure 5.13: *Case with gas phase combustion. Relative pressurant mass.*

the motor is operating at sea level.

To reduce the thrust tail time and increase the average pressure it is possible to put a by-pass on the injector plate in order to increase the mass flow at the end of the burn.

From the following figures it is possible to see that the drawbacks of gas phase combustion are reduced by this technique at the expense of added complexity of the injection system. However the thrust tail could produce gravity losses and other penalties so its total impulse contribution could be not exploited completely.

The thrust tail should be avoided for soft lander and other applications where a specific value of the thrust is required. On the opposite for launcher's stages and sounding rockets it could add an important contribute to the total impulse.

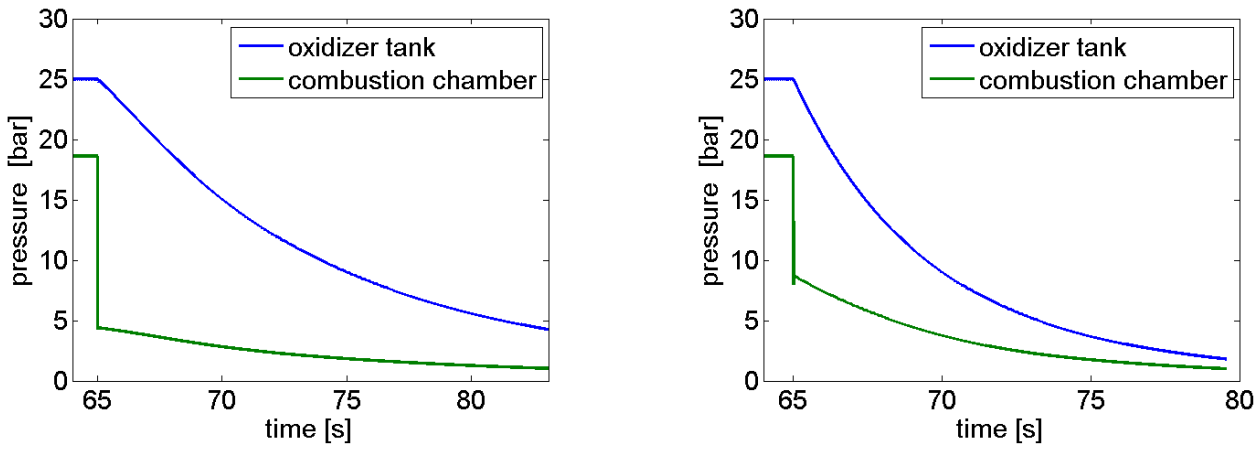

Figure 5.14: *Gas phase combustion, pressure evolution. No by-pass (left) and with by-pass (right).*

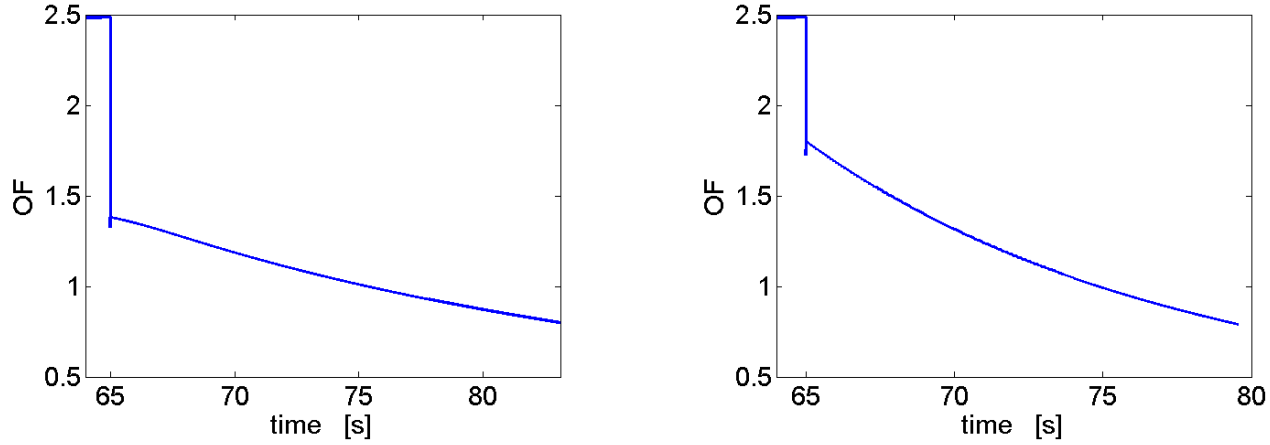

Figure 5.15: *Gas phase combustion, O/F ratio. No by-pass (left) and with by-pass (right).*

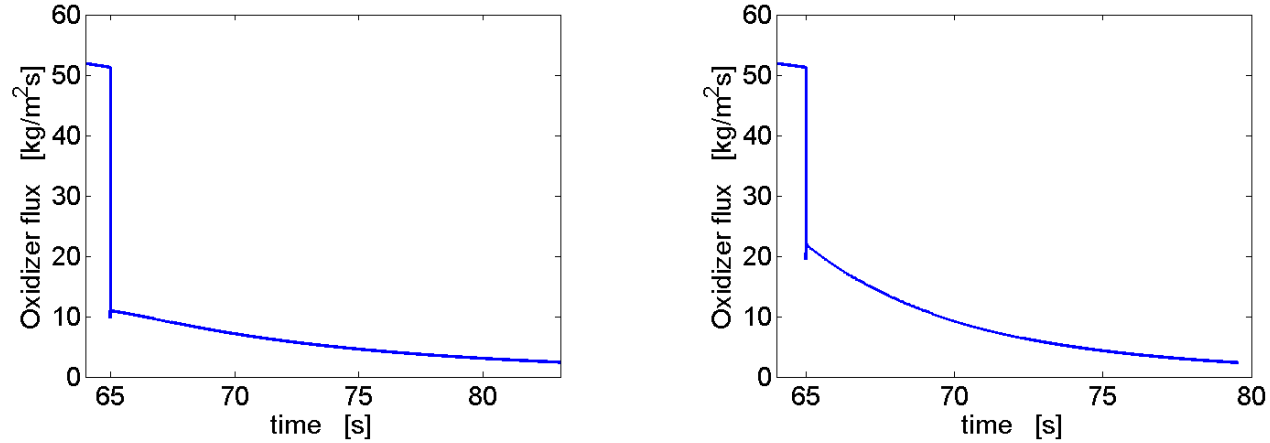

Figure 5.16: *Gas phase combustion, oxidizer mass flux. No by-pass (left) and with by-pass (right).*

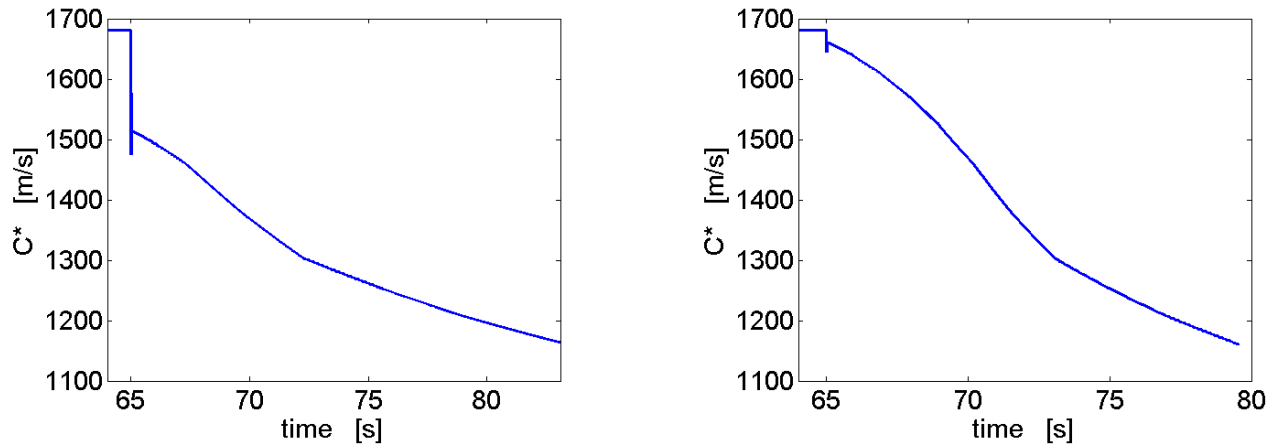

Figure 5.17: *Gas phase combustion, oxidizer mass flux. No by-pass (left) and with by-pass (right).*

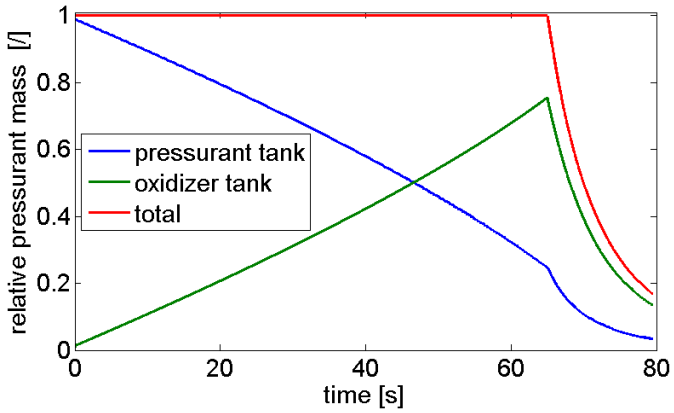

Figure 5.18: *Gas phase combustion, relative pressurant mass with by-pass.*

However it is important to note that Oxygen is much heavier than He as a pressurant so a complete analysis of the total impulse contribute with the added weight is necessary. This could be done coupling this code with a trajectory simulation.

In the case of mechanical pressure regulators a minimum pressure drop is often required to allow a pressurant mass flow. To use more efficiently the gas in the pressurant tank a by-pass is needed to increase the mass flow at the end of burn. Also in this case this is counterbalanced by an added complexity.

To save the weight and limitations of a pressure regulator other solutions can be conceived. AMROC designed a pressure control system consisting of a normally open pressurant control orifice and one or more normally closed orifices which will maintain the tank pressure within the desired control band [99].

Another option is to consider a digital valve operating between the pressurant tank and the oxidizer tank. The valve is controlled by a feedback on the main tank pressure. This solution could be considered to reduce weight even if it is not a passive system and it requires an active control. However electronic miniaturization is producing a shift from mechanical to electric systems.

In this case the mass flow is calculated with the classical isentropic relation when the valve is open: $\dot{m} = CdA_v P_{press}/c^*_{press}$, and is zero when closed.

The valve is activated when the pressure in the tank is below the design value. The valve has a digital input composed by two signals: ON and OF. This choice is related to the simulation of digital valves. Analog valves are too slow and heavy for this scope and in this case a pressure regulator is preferred.

The valve is modeled to open linearly with a defined time constant. In this way the mass

flow is $\dot{m}_{press} = V_a C d A_v P_{press}/c^*_{press}$ with $\frac{dV_a}{dt} = +/- \frac{1}{\tau}$ and $0 \leq V_a \leq 1$.
The signal is sampled at a certain frequency. Even if it is a simplified model some interesting aspects could be highlighted. The input signal is a PWM style signal. The amplitude of the open signal increases with time because of the increased required mass flow. If the valve is too small the blowdown mode begins before the liquid oxidizer has been depleted because the pressurant is no more able to maintain the correct pressure. Bigger valves are heavier (and probably slower) and they produce an high mass flow at the beginning of the discharge.

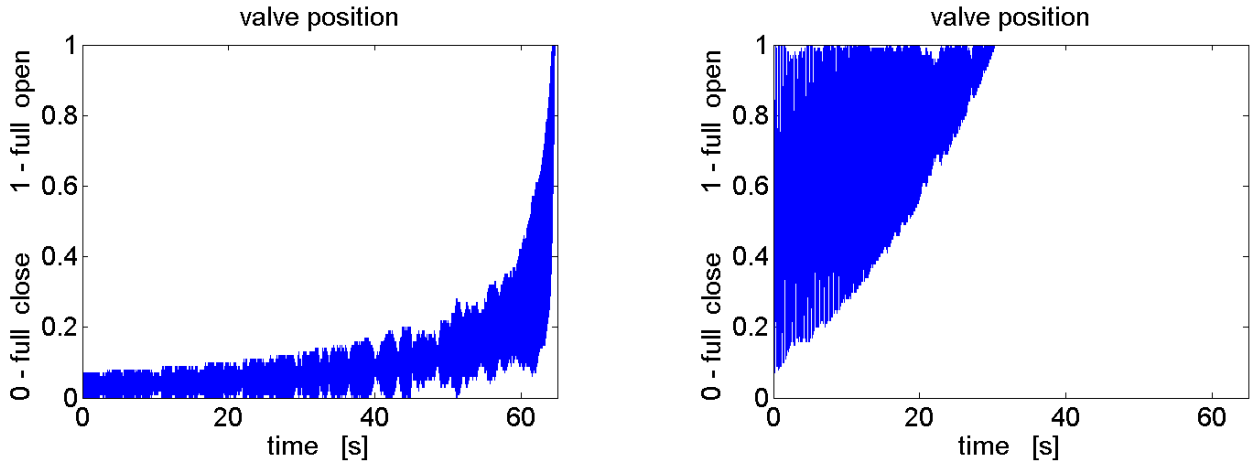

Figure 5.19: *Valve position: correct valve (left) and undersized valve (right).*

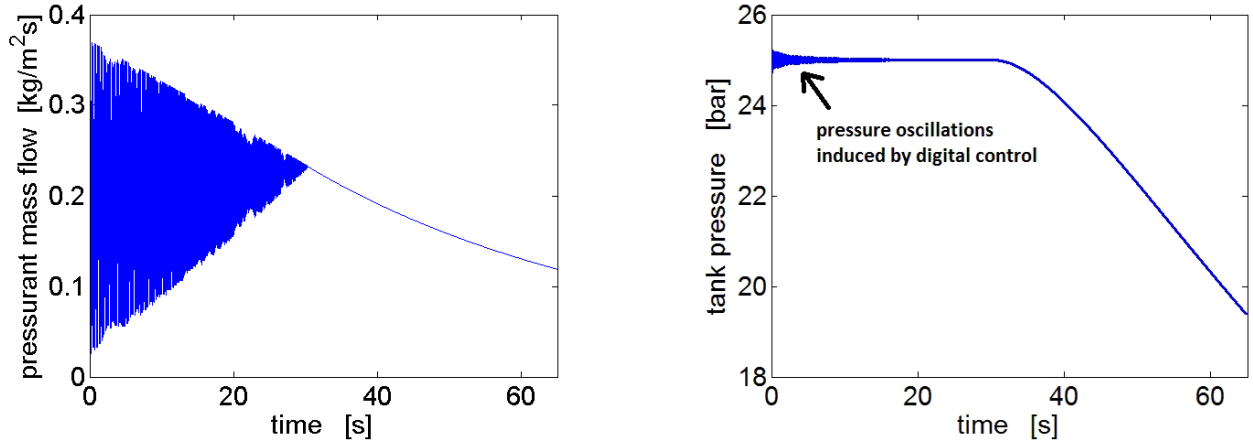

Figure 5.20: *Case with undersized valve: pressurant mass flow (left) and tank presure (right).*

The on-off control produces a pulsation of the pressure in the oxidizer tank, particularly at the beginning when the pressure drop and consequently the mass flow is higher. The pulsation amplitude increases with increased valve size. For this reason an optimum dimension exists, the minimum size that guarantee the necessary pressurant flow at the end of the liquid phase discharge. This pulsation could have negative aspects like vibrations and fluctuations

in the mass flow. Considering also the velocity of the valve and the sampling frequency the situation becomes more complex. Higher sampling frequencies are better because they reduce pressure fluctuations. The valve response time however has not a monotonic effect because a bit slower valve can act as a sort of continuous regulation (even if it has a digital input). Obviously too slow valves produce large pressure variations.

All the previous examples show how pressure regulated systems present some aspects often overlooked by hybrid designer. In light of these arguments the simplicity of a self-press system is very attractive. To model self-pressurization a homogeneous equilibrium model has been chosen. The liquid and the vapor phase are considered in saturated conditions at every instant. The equation for the liquid and gas in the tank are:

$$\frac{1}{\rho} = \frac{1-x}{\rho_l} + \frac{x}{\rho_v} \qquad \frac{dM}{dt} = -\dot{m}_{ox} \tag{5.11}$$

$$E = M_l e_l + M_v e_v = M\left(1-x\right) e_l + M x e_v \qquad \frac{dE}{dt} = -\dot{m}_{ox} h_l \tag{5.12}$$

These equations are solved with an iterative scheme at every time step. Heat flux is neglected because the temperature drop respect to tank walls is limited. For very long discharge time an isotherm model (that means also constant pressure) can be used instead of an isentropic one. For moderately long discharge this simple model gives good results. For short burning time the predictions are worse.

More complex models have been proposed but they require some empirical fittings like the heat transfer coefficient between the gas and the liquid phase [100] or the equation of state for metastable conditions (spinodal line) [101]. However in the author opinion hybrid systems could not be competitive for short burning time with solids unless performances are considered secondary. For this reason it has not been given a priority to the development of more complex models.

Anyway real-time measurement of the vapor and liquid temperature would be useful to the development of a more accurate model. To check the validity of the model an alternative has been implemented substituting energy equation with entropy conservation: ($\frac{dS}{dt} = -\dot{m}_{ox} s_l$)

As expected the two alternatives give the same results at 4 digits.

The model has been compared with experimental results from previous CISAS activities. Data for N_2O properties have been taken by interpolation from NIST database. The first case represents the operation of a 20 kN peak thrust hybrid motor. The discharge time is very small (4s) so it can be considered an extreme case for the present homogeneous equilibrium

model. Strong stratification and non-equilibrium effects are present. However the model is able to give satisfactory results for preliminary considerations.

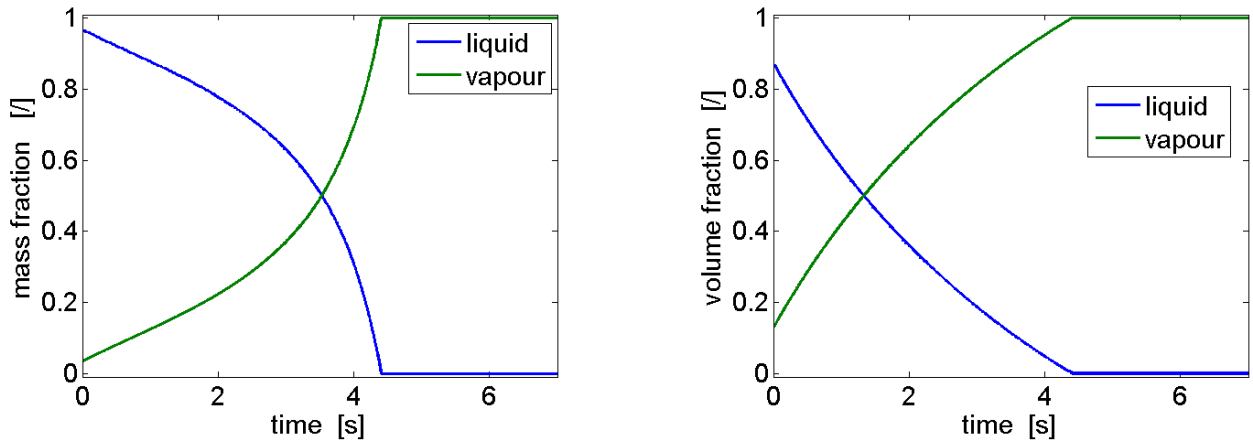

Figure 5.21: *20 kN motor test: prediction of mass (left) and volume (right) fractions.*

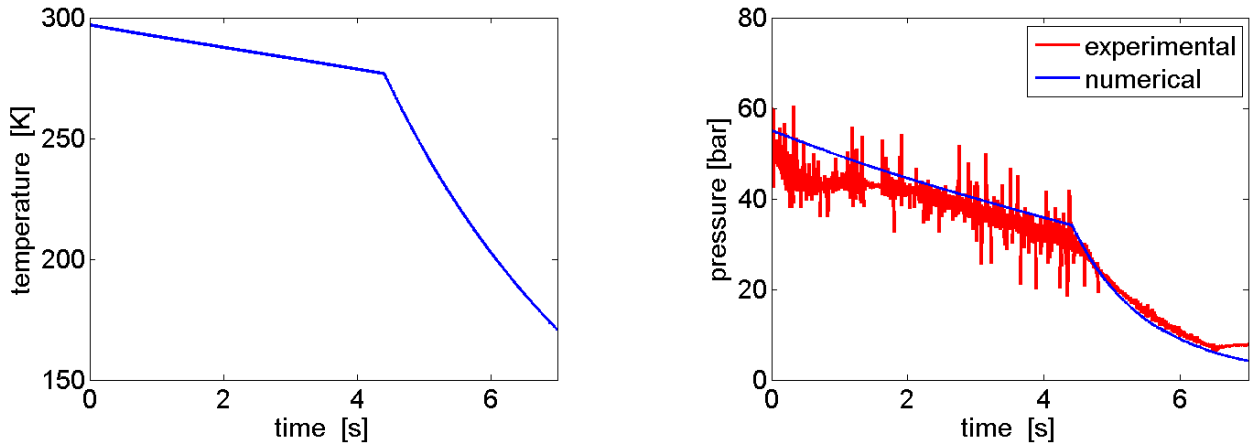

Figure 5.22: *20 kN motor test: prediction of temperature (left) and pressure (right).*

It is possible to denote four phases of the pressure plot: a sudden pressure drop, a partially blowdown phase with pressure recover, the self-press mode and the final gas discharge. The reference oxidizer mass flow has been calculated considering the total oxidizer mass consumed divided by the discharge time. Then the instantaneous mass flow has been calculated as $\dot{m} = a\dot{m}_{ref}P/P_i$. The coefficient a has been selected in order to match the total consumed mass. This pressure correction was applied because its use for the oxidizer flow gave a good agreement of the chamber pressure profile. A correction to the final gas discharge was implemented for two reasons. First of all the discharge has been modeled with the isentropic relation for an ideal gas while the compressibility factor at the end of the liquid phase consumption is 0.7. Than the motor was equipped with a passive normally closed valve that

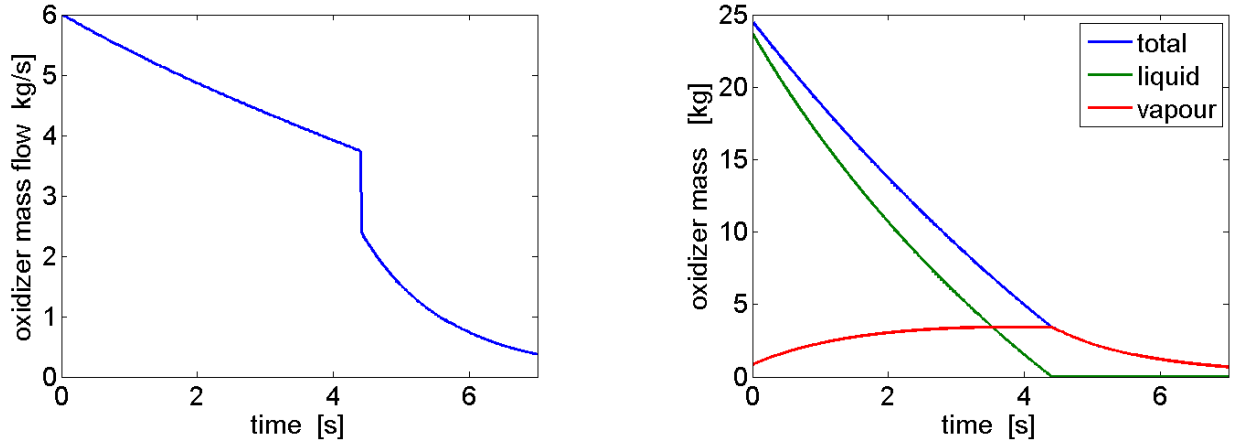

Figure 5.23: *20 kN motor test: prediction of oxidizer mass flow (left) and oxidizer mass contributions (right).*

reduced the flow passages at low pressures.

The initial blowdown phase is related to the time need for self-pressurization to develop. Afterward there is a pressure recover near the ideal value. The initial non-ideal phase should be much less important for well mixed systems operating for longer discharge times.

The second plots relate to the test of a 3kN motor. In this case the discharge is interrupted closing an active valve at the end of the burn before the tank was empty of liquid. The burning time is higher than in the previous case. Moreover the tank was not fully loaded of liquid at the beginning of the test. The tank was shaken before the burn in order to limit oxidizer stratification. All these aspects should get close the experiment to the numerical model. The results confirm this prediction.

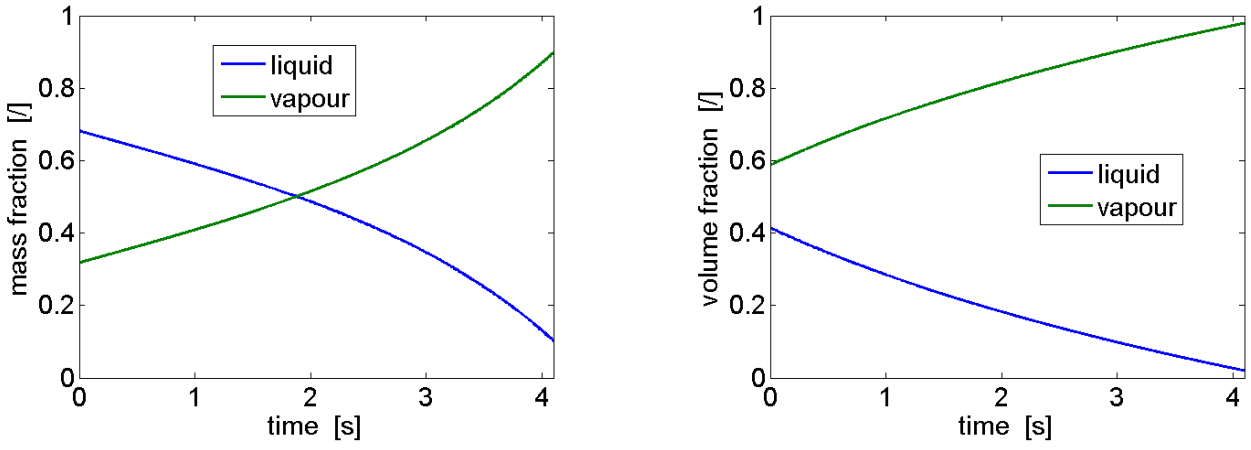

Figure 5.24: *3 kN motor test: prediction of mass (left) and volume (right) fractions.*

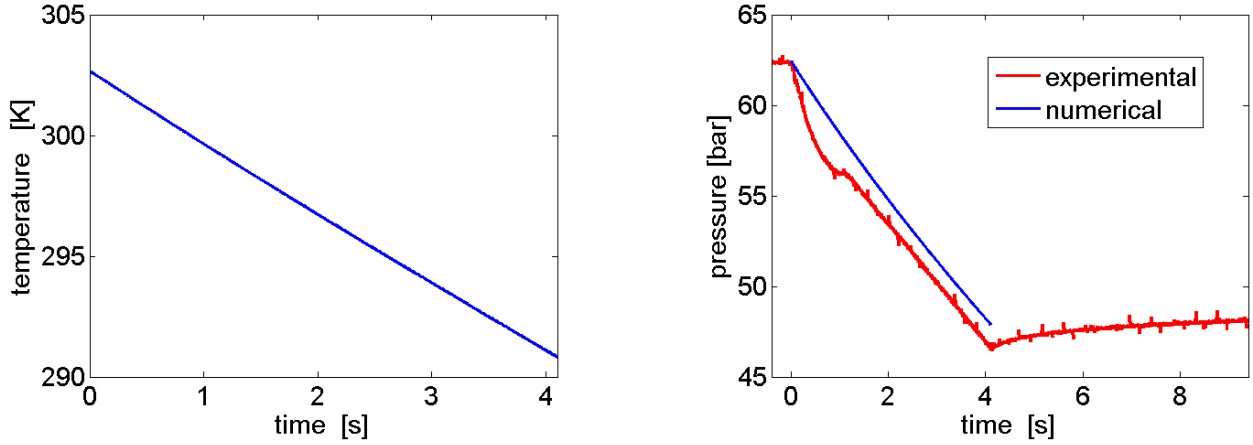

Figure 5.25: *3 kN motor test: prediction of temperature (left) and pressure (right).*

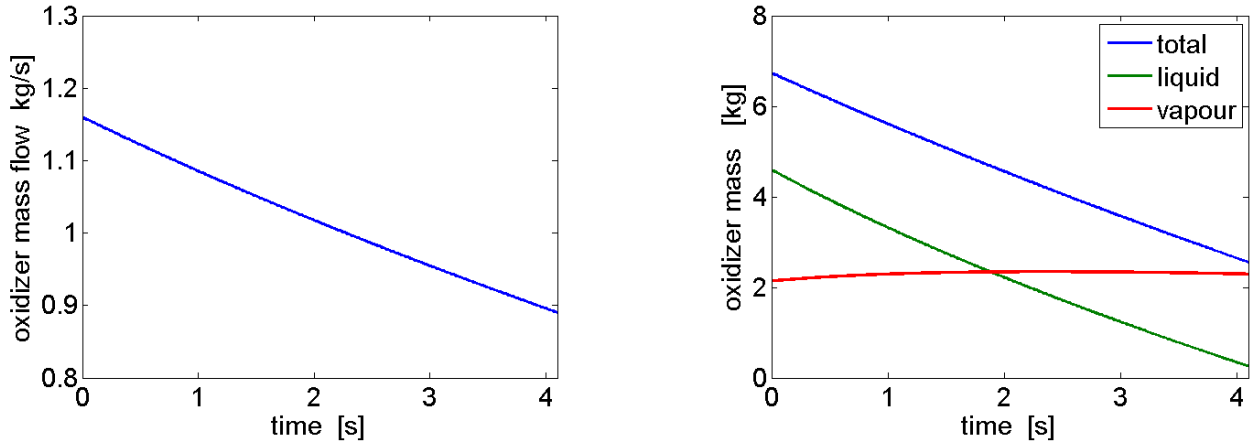

Figure 5.26: *3 kN motor test: prediction of oxidizer mass flow (left) and oxidizer mass contributions (right).*

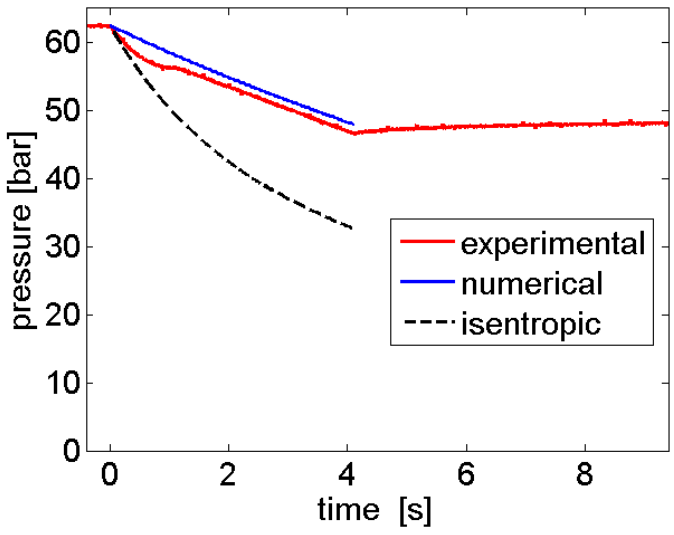

Figure 5.27: *3 kN motor test: pressure prediction.*

The error is nearly 1 bar that corresponds to less than 5% for this case. The error could be related to non-equilibrium effects and/or stratification. It is important to avoid stratification before motor operation in order to achieve the maximum performances from self-pressurization. When performances are critical a good thermal control should foreseen. In a certain sense in case of a poor matching between experimental and numerical results the disagreement highlights more the need for a better thermal control than the need for better model unless the actual operating conditions cannot be changed.

The model can be used to highlight the following aspects. The isentropic expansion of a saturated vapor produces condensation. In the process the vapor mass fraction is reduced. The isentropic expansion of a saturated liquid produces vapor. In this case the vapor mass fraction is increased. For the expansion of a mixture of vapor and liquid the vapor mass fraction could increase or decrease depending to its initial value. In the case of the oxidizer discharge from its tank condensation and boiling tend to occur simultaneously.
The instantaneous vapor mass is dependent on the predominant between the two. When the tank is fully loaded boiling prevails for almost the entire discharge. Near the end the vapor mass fraction is very high so condensation prevails, reducing the vapor mass. This condensation prolongs the liquid discharge phase. However the vapor mass fraction continues to increase because the liquid is drained from the tank. The liquid mass flow that is drained is much higher than the evaporated mass because the vapor has a much lower density.
For this reason the liquid volume fraction, oxidizer mass in the tank and the vapor volume fraction change almost linearly with time for a constant expelled oxidizer mass flow. Vapor mass increases almost linearly at the beginning than the counteracting effect of condensation become relevant. The vapor mass fraction has a slow increase at the beginning and a sudden increase near the end.

The pressure ratio between the initial and final tank pressure is higher at increased pressures. Moreover the liquid density is higher at reduced temperatures. The gaseous oxidizer density at saturation is lower at reduced temperatures. For this reason the ratio between liquid and gas density is higher at lower pressures, consequently the amount of residual gas is lower.
This is very important in the absence of gas phase combustion but also in this case because, as previously seen, gas phase combustion is less effective, particularly at sea level. Moreover lower tank pressures (temperatures) means less weight and also increased oxidizer density, with a volume reduction and a weight saving. However a reduction in the oxidizer tank

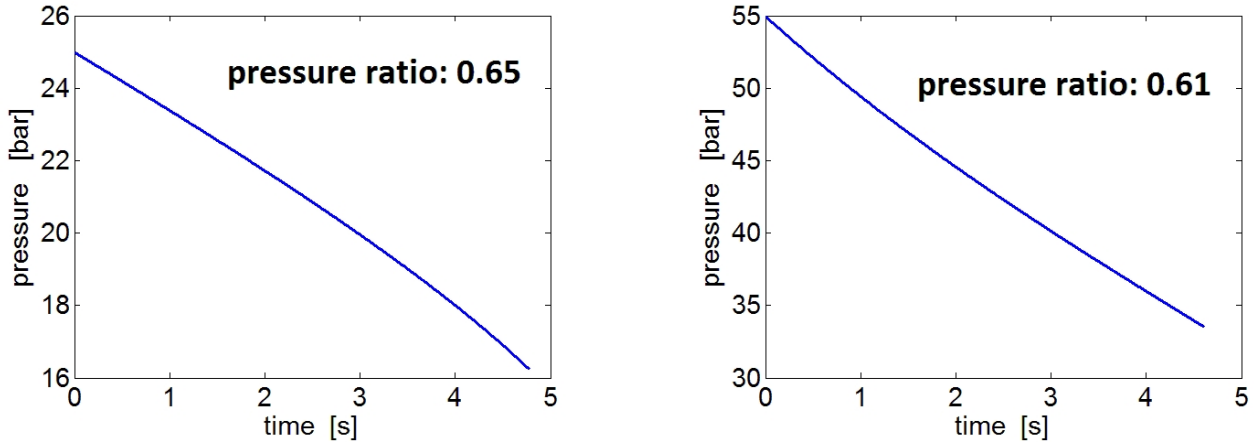

Figure 5.28: *Self press simulations. Initial pressure: 25 bar (left) and 55 bar (right).*

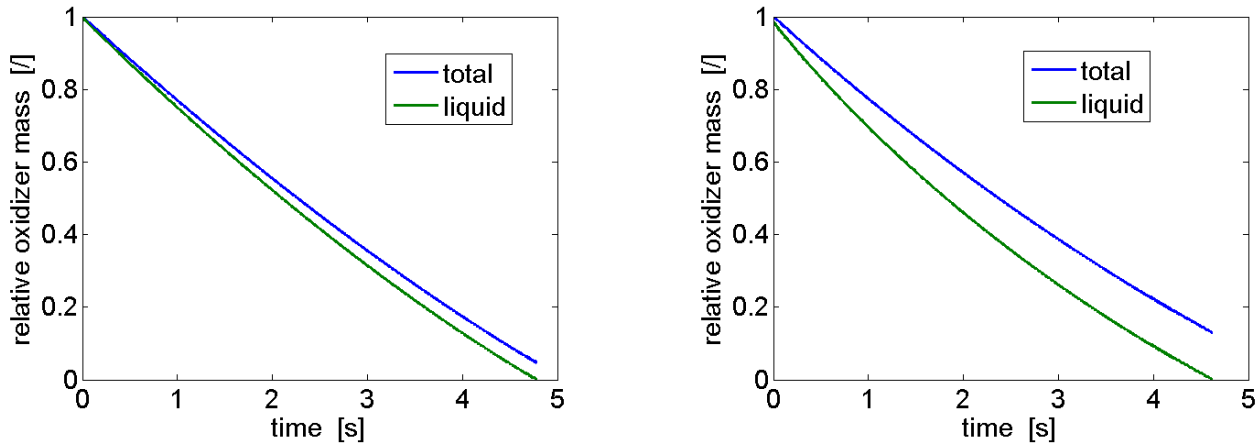

Figure 5.29: *Self press simulations. Initial pressure: 25 bar (left) and 55 bar (right).*

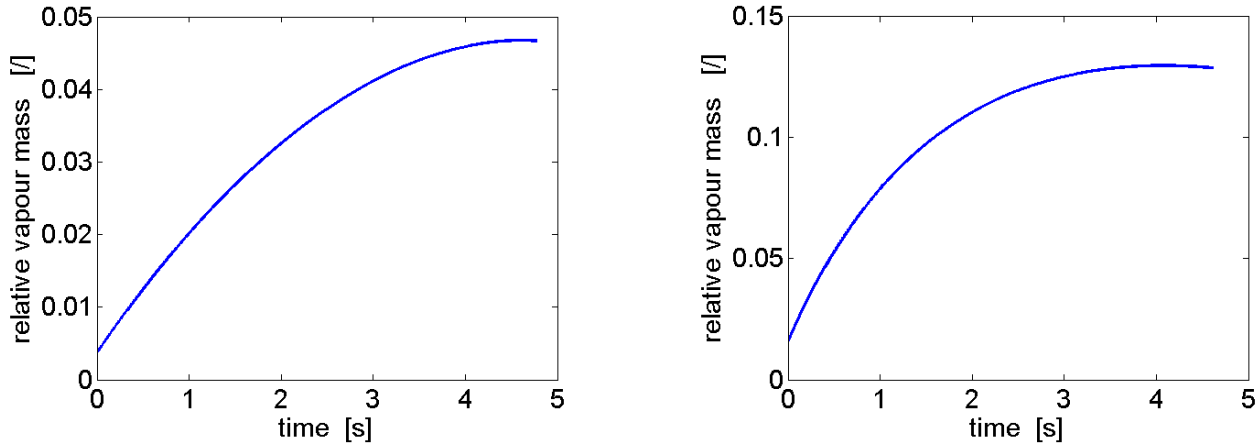

Figure 5.30: *Self press simulations. Initial pressure: 25 bar (left) and 55 bar (right).*

pressure is coupled in turn with a decrease of chamber pressure, affecting I_{sp} at sea level. A trade off can be selected with the help of the presented code. Results show that N_2O should be generally cooled below 10° C. For example lets consider two systems: one with a

tank pressure of 60 bar (27°C) and the other at 40 bar (10°C), with initial chamber pressure being respectively 45 and 30 bar. The average specific impulse during a burn at sea level is nearly 5% higher for the system at 60 bar. However the volume of its tank is nearly 20% larger, the pressure is 50% higher so the tank weight is almost (approximately) 80% heavier. Anyway is it possible to state that self pressurization is particularly effective at high altitude (or vacuum) where the nozzle C_F is not dependent on chamber pressure. In this case the lowest possible tank pressure should be selected that guarantees a chamber pressure compatible with a sufficient C^*. In fact C^* has an asymptotic behavior with pressure. This chamber pressure is usually between 10 and 20 bars.

Self pressurization usually provokes a decrease of the mass flow with time. This in turn induces an O/F shift trough a fuel rich condition. For motors/propellant combinations with n higher than 0.5 this can partially compensate the natural O/F shift towards oxidizer rich conditions due to port opening.

The final O/F shift can be positive or negative depending how much the two effects compensate each other. For n near 0.5 the decrease in mass flow prevails (negative O/F shift), for high n values the opposite occurs. A small O/F shift coupled with a decreasing thrust with time could be a very interesting feature for hybrid sounding rockets or boosters (beside simplicity).

The highest is the initial filling level the highest is the pressure drop. This is expected as in the case of a blowdown system. In fact the higher is the ratio between the initial and final volumes the lowest is the ullage expansion. However a strong difference occurs. The ratio between the initial and final pressure achieves an asymptote in the self press mode for filling ratios approaching 100%. On the opposite the pressure ratio for a blowdown system is : $\frac{P_f}{P_i} = \left(\frac{V_i}{V_f}\right)^{\gamma}$.

The pressure ratio goes to infinite for ullage initial volume $\rightarrow 0$. This happens because in the self press mode the new gas volume is composed also (mainly) by the vapor evaporated from the liquid phase. The self press mode is advantageous when small pressure decays are required because of the higher filling level.

For example considering N_2O at 25 bar (self-press) $\rho = 800\ kg/m^3$ while N_2O at -80°C (blowdown) has $\rho = 1200\ kg/m^3$ but for the same pressure drop with N_2 ($\gamma = 1.4$) a filling level of only 40% is necessary so $\rho_e = 500\ kg/m^3$. However the weight of the residual gas is higher for N_2O so gas phase combustion is recommended to avoid this penalty. If this is not possible and/or large pressure drops (and strong sub-cooling) are tolerable or the

initial pressure in self press mode is incompatible with requirements the blowdown mode is preferable.

5.2 Injection and Feed System Model

To predict the transient behavior of an hybrid rocket motor it is necessary to consider also the response of the injection and feed system. In fact they drive the amount of oxidizer that enters in the combustion chamber at every instant. Gaseous injection does not represent a particular challenge, neither from the motor design point of view nor for the numerical simulation.

However liquid injection, particularly for systems that don't use isolating elements in the feed lines (e.g. cavitating venturi) is more difficult to design and can lead to feed coupled instabilities. An extensive description of feed coupled instabilities in hybrid rocket is provided by Karabeyoglu [8].

Also the modeling of liquid injection is more difficult. The main challenge is to determine the instantaneous liquid mass flow and the relation between the liquid oxidizer and the gaseous oxidizer that take part in the hybrid motor combustion processes (i.e. droplets vaporization).

In the present model the following equations are used to describe injection behavior. If $p_0 > p_p > p_c$:

The continuity equation in the pipe is:

$$\frac{d\rho_p}{dt} = \left(\dot{m}_p - \dot{m}_l\right)/V_p \tag{5.13}$$

The mass flow rate through the injector plate is:

$$\dot{m}_l = Cd_{inj}A_{inj}\sqrt{2\rho_p\left(p_p - p_c\right)} \tag{5.14}$$

The mass flow rate from the tank is:

$$\dot{m}_p = Cd_pA_p\sqrt{2\rho_0\left(P_0 - p_p\right)} \tag{5.15}$$

If $p_0 < p_p$:

$$\dot{m}_l = 0 \qquad p_p = p_c \tag{5.16}$$

The volume between the tank and the injector plate has been modeled as a single node. The pressure inside the tank has been considered a fixed boundary condition. Based on experimental results the pressure in the pipes has been considered to change almost in phase with the combustion chamber. If the pressure inside the chamber is lower that the pressure inside the pipes the liquid flows into the chamber. On the opposite when the pressure inside the chamber is higher some gas will enter the injector. This mass flow is small and has been neglected. In this case the pressure in the pipes has been fixed equal to the chamber pressure.

A general equation of state has been used to describe the behavior of the liquid inside the pipes:

$$p_p = p_{ref} Z \left[\left(\frac{\rho_p}{\rho_{ref}} \right)^{\gamma} - 1 \right] + p_{ref} \tag{5.17}$$

This equation can represent liquids, gas and two-phase mixtures depending on the choice of the empirical coefficients Z and γ.

The final step in setting up the model is the description of droplet vaporization. Droplet vaporization is often modeled as a finite time lag between the liquid mass flow through the injector and the gas mass flow that is used as an input for the combustion chamber. The time lag model is useful to explain the main mechanism of feed coupled instabilities but it fails to determine the amplitude of the oscillations. Moreover an analysis of droplets behavior shows that the process of vaporization is continuous and not instantaneous as in the time lag model. For this reason the following approach has been selected.

First of all the classical model of droplet evaporation called the 'D^2 law' has been considered [23]. This theory predicts that the squared of the droplet diameter varies linearly with time:

$$D^2 = D_0^2 - Kt \tag{5.18}$$

$$t_{vap} = \frac{D_0^2}{K} \tag{5.19}$$

With a one dimensional energy balance is possible to show that the vapor mass flow released by the droplets is proportional to the instantaneous droplet diameter:

$$h_{vap} \dot{m}_d \propto \pi D^2 \frac{\partial T}{\partial n} \Rightarrow \dot{m}_d \propto D \tag{5.20}$$

For the complete treatment the reader is referred to ref. [23]. What is of interest here is that the droplet vapor mass flow can be described by the following relation:

$$\dot{m}_d \propto \sqrt{1 - t/t_{vap}} \tag{5.21}$$

Considering a droplet as an impulse of liquid mass flow it is possible to establish the transfer function between the liquid and the vapor mass flow:

$$\dot{m}_{ox}(t) = \frac{\sum \dot{m}_l \left(t - t_{vap} + t_i\right) \sqrt{1 - t/t_{vap}}}{dt \sum \sqrt{1 - t/t_{vap}}} \tag{5.22}$$

$0 < t_i < t_{vap}$ and $t_{i+1} = t_i + dt$

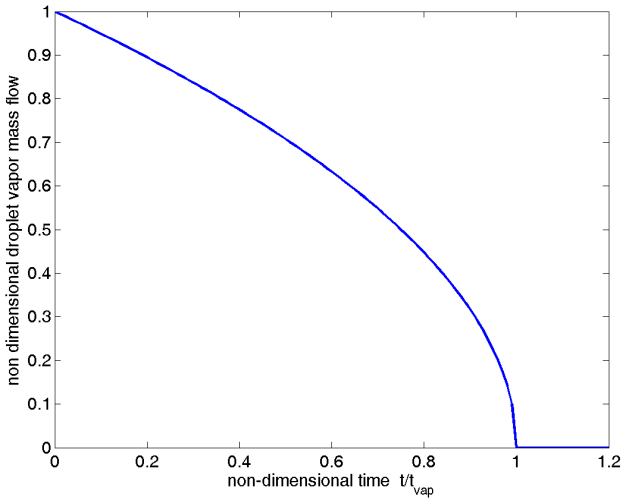

Figure 5.31: *Impulse response function of droplets evaporation model.*

The response of a system without the droplet evaporation model is monotone. On the contrary the response of a system with the evaporation model is stable but (except in the case of really small vaporization times) damped oscillations occur around the steady state value.

However, this model is not yet satisfactory in simulating feed coupled instabilities. Thus, a constant time lag that represents droplets breakup and heating to the vaporization temperature has been added.

The physical meaning of the vaporization lag is to account for the time for braking up and heating particles during which no evaporation takes place. The complete model is a **two-times-model** composed by an initial time lag followed by droplets evaporation equations.

To check the validity of the model a comparison has been made with experimental results presented in ref. [8]. The delay times selected in order to achieve a good match of the

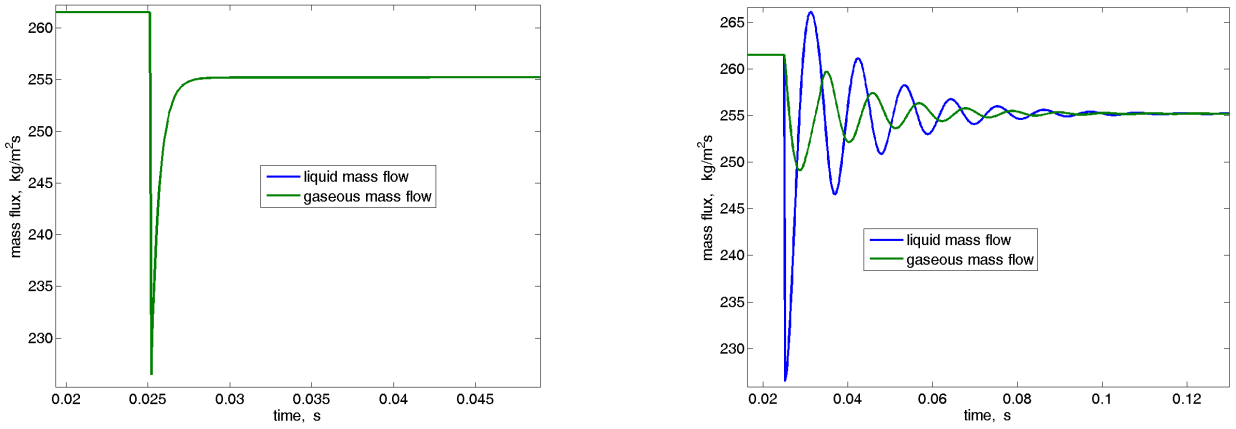

Figure 5.32: *System response without droplets evaporation (left) and with droplets evaporation (right).*

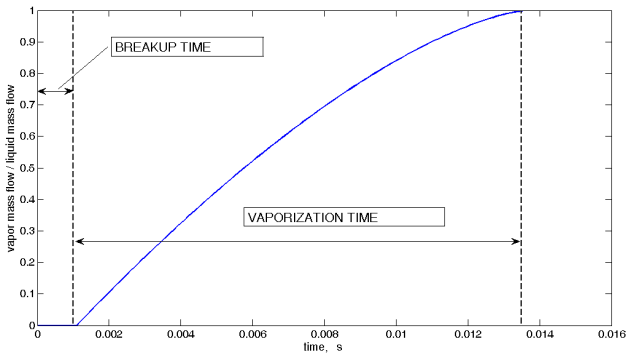

Figure 5.33: *Response of two-times droplet vaporization model to a step mass flow input.*

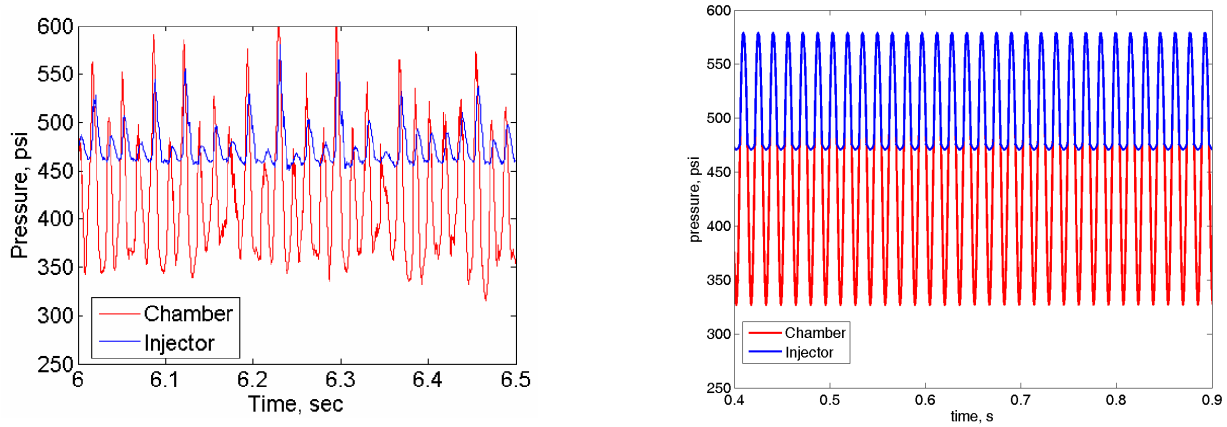

Figure 5.34: *Comparison between experimental data from ref.[8] (left) and numerical simulations (right).*

numerical simulation with the experimental results are 1 ms for breakup and 12.5 ms for evaporation. These time are of the same order of magnitude of the (single) value predicted by Karabeyoglu [8]. Moreover they are compatible with droplets evaporation rates found in literature [23].

The vaporization time is higher than predicted by CISAS CFD simulations [24], the difference is due to different injector design and higher pressure drops that produce smaller droplets.

The simulations show a good agreement especially considering the uncertainties in the inputs and the level of approximation of the model. The code is able to simulate the oscillations in the chamber and in the injector.

In the experimental data there was also a 30 Hz activity related to typical hybrid low frequency instabilities that is not modeled in the simulation. The waves form of injector oscillations are clipped at the lower end. This is due to the mass flow equation. When chamber pressure is minimum the mass flow is maximum and so it is also the difference between injector and chamber pressure. On the other end when pressure in the chamber is higher than in the injector there is a negligible gaseous counter flow and the two pressures tend to equalize. The predicted frequency is 65 Hz against 60 Hz of the experiments. The amplitude are slightly overpredicted, possibly because the model does not take into account all the complex nonlinear dissipation mechanisms that are present in the real three dimensional flow field.This phenomena are generally amplitude dependent and tend to limit the growth of large oscillations.

For a constant breakup time lag we varied the vaporization time. The frequency of the oscillations always decreases with an increase in the vaporization time. The amplitude of the oscillations reaches a maximum near $t_{vap}/t_{break} = 5$ and then decreases with increased vaporization time. For large value of the ratio the system becomes again stable.

This behavior has the following explanation. The response of the vaporization model is oscillating while the original response is monotone. This means that the vaporization model is slightly de-stabilizing. This explains the increase of amplitude of the two-times-model with an increase of the vaporization time. For large ratio the first time lag becomes negligible respect to the vaporization time so the response tends to the stable oscillating response of the vaporization model alone.

5.3 Injector Mass Flow Model

In the previous paragraphs the mass flow through the injector elements has been calculated with the use of Bernoulli equation or semi-empirical fits. Here more attention is focused on this issue.

Bernoulli equation is valid for incompressible liquids, as the major part of oxidizer can be considered. The main aspect is the characterization of the injector Cd. A large literature is available on this subject for liquid propulsion and other applications so we avoid further considerations.

What is peculiar of hybrid motor is the frequent use of self-press system. In this case the liquid is saturated or partially above saturation. The last case is called overcharging, a practice used to avoid cavitation in the feed lines and sometimes to reduce N_2O decomposition hazard [102] (using He or O_2 for diluting N_2O gas phase). In both cases the chamber pressure is below saturation pressure so flashing and large cavitation occurs in the injector.

Cavitation is the evaporation of liquid in a region where the local pressure is below the saturation pressure. This happens also for liquid far from saturation (considering inlet and outlet reference pressures) near zones of high velocity (and consequently low local pressure, below saturation), particularly in proximity of sharp edges. This is a 2 (or 3) dimensional effect and is dependent on the streamlines pattern.

Usually cavitation is avoided in conventional liquid injection because it reduces the mass flow (requiring larger injector plates) and can produce unsteady behavior and poor atomization (e.g. flipping).

Flashing is the evaporation of liquid in the bulk because the average pressure in the section falls below saturation. For this to happen in a plain orifice the discharge pressure should be under saturation. In this case the pressure behavior could be predicted (at least in theory) by 1D models. Obviously cavitation could be present without flashing but the opposite is not. For this reason the separation of the two effects in the injector elements of a self-press system is very difficult. The prediction of the mass flow for a two phase evaporating fluid is very difficult.

As in the case of nozzle flow two basic cases can be considered: *frozen* and *shifting equilibrium*.

In the first case the liquid parameters are considered fixed and the mass flow is computed as for an incompressible liquid: $\dot{m} = CdA\sqrt{2\rho_l \Delta P}$. This condition represents the limiting case when the ratio between the residence time τ_r and the time required for the phase change τ_b go to zero.

On the opposite when τ_b is much smaller than τ_r it is possible to think to a process proceeding always in equilibrium with the local values of temperature and pressure. The ratio $k = \tau_b/\tau_r$ can be considered as analogous to the Damkohler number for chemical kinetics.

The latter kind of process is reversible and dependent only on the initial and final state. A reversible flow without work and heat exchange is isentropic conserving also the total enthalpy. The conservation of total enthalpy combined with the mass flow equation gives the following result:

$$\dot{m}/A = G = \rho_2 \sqrt{2\,(h_1 - h_2)} \tag{5.23}$$

The vapor mass fraction can be obtained through the conservation of entropy:

$$x = \frac{s_0 - s_l}{s_v - s_l} \tag{5.24}$$

In this way it is possible to determine h_2.

In any compressible fluid it is possible to define a critical velocity $c^2 = \frac{\partial p}{\partial \rho}$. Increasing the pressure drop of the injector the mass flow and the exit velocity increase. When the local velocity reaches the critical speed the flow is choked and the mass flow cannot increase further for a decrease in the downstream pressure. The mass flow becomes dependent only on the inlet conditions.

Equation 5.23 is still valid replacing outlet pressure with critical conditions.

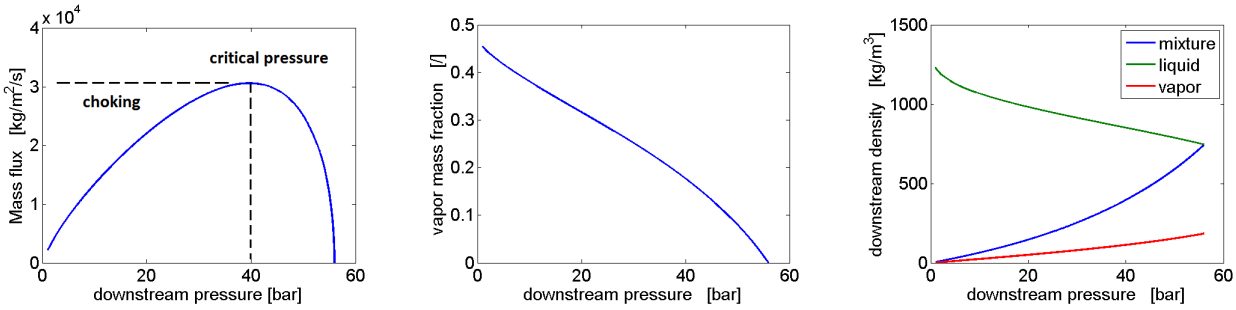

Figure 5.35: *Mass flux (left), vapor mass fraction (center), and density (right) vs. downstream pressure predicted by the HEM model.*

This model is also called homogeneous because it considers the flow as 1 dimensional with a common velocity for both phases. The validity of this hypothesis has obtained no agreement between different researchers.

Usually in accelerating flows there is a well mixing of the different phases, particularly in bubbly flow. For other type of flow (e.g. annular) the slip between the gas and the liquid could be significant. Moreover 2D effects are important for rapid or sharp change of geometry. Experimental results show that the mass flow is poorly predicted by both models [79]. The incompressible equation gives too high mass flow while the homogeneous equilibrium model

(HEM) underestimates it. However the previous extreme cases can be used to define an upper and lower bound to the predicted mass flow. Unfortunately in certain circumstances the upper bound can be several time higher than the lower bound.

The two models differ not only quantitatively but also they show opposite trends. In fact for the same pressure drop the frozen model predicts a decrease of the mass flow with higher pressures, the opposite for the HEM. This is due to the fact that lower temperatures are related to higher liquid densities. At the same time the vapor density decreases and the vapor mass fraction variation is higher at lower initial pressures explaining the mass flow reduction predicted by the HEM.

Dyer et al. [78] at Stanford suggested a way to determine the mass flow blending the results from both model trough the use of the parameter k.

The residence time is approximated with: $\tau_r = L/u = \frac{L}{\sqrt{2\Delta P \rho_l}} = L\sqrt{\frac{\rho_l}{2\Delta P}}$ while the bubble growing time with $\tau_b = 1/\frac{dr}{dt} = \sqrt{\frac{3}{2}\frac{\rho_l}{P_v - P_2}}$.

k is defined approximately as the ratio between the two:

$$k = \frac{\tau_b}{\tau_r} = \sqrt{\frac{P_1 - P_2}{P_v - P_2}} \tag{5.25}$$

The final function is the following:

$$G = Cd\left(\frac{1}{1+k}G_{HEM} + \left(1 - \frac{1}{1+k}\right)G_{frozen}\right) \tag{5.26}$$

For $k \to \infty$ we get the incompressible model while for a saturated liquid $k = 1$ the mass flow is defined arbitrarily as the arithmetic mean between the two. In this model the dependency of the residence time on the length of the injector has been withdrawn in the final equation. However experimental results confirm that long injectors tends to approach the equilibrium condition tanks to higher residence time [79].

Equation 5.26 has been used to compute the mass flow of nitrous oxide of some experiments made at CISAS laboratory. The work was done as a preliminary step to a more complete activity concerning the study of nitrous oxide behavior in terms of self-press tank discharge, injection mass flow and jet atomization. Two 1.4 mm diameter plain orifices with sharp entrance were tested. One orifice has a length of 3.8 mm, the other 12 mm. Slightly different results have been obtained for the two different lengths. As expected mass flows for the long injector are generally lower than with the short injector.

One important issue is the determination of the discharge coefficient. Several empirical

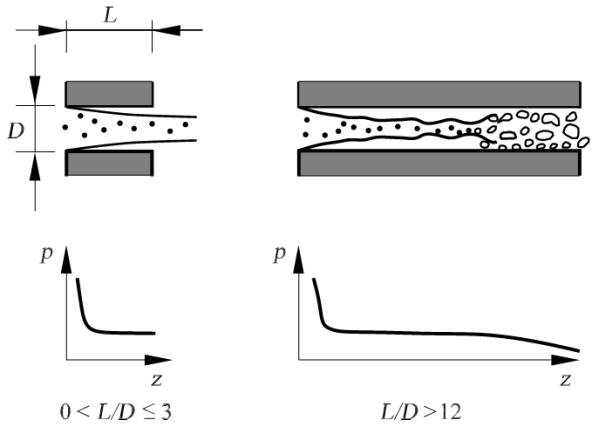

Figure 5.36: *Outflow of a two-phase mixture through short (left) and long (right) injectors [79].*

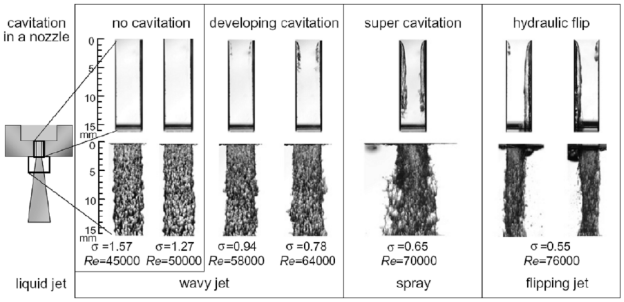

Figure 5.37: *Images of cavitation in a 2D nozzle and liquid jet [103].*

relations have been developed to determine the discharge coefficient of a nozzle [80].

First of all it is necessary to determine the condition of the nozzle. The plain orifice may operate in three different regimes: single-phase, cavitating and flipped.

In a *single-phase nozzle flow* the liquid completely fills the orifice.

In a *cavitating nozzle flow* vapor pockets form just after the inlet corners.

Finally in a *flipped nozzle flow* downstream gas surrounds the liquid jet inside the nozzle.

The condition of the nozzle is determined by the K parameter (not to be confused with Dyer k parameter):

$$K = \frac{P_1 - P_v}{P_1 - P_2} \tag{5.27}$$

Flipping of the nozzle occurs if $K < K_{crt}$ with

$$K_{crt} = 1 + \frac{1}{\left(1 + \dfrac{L}{4d}\right)\left(1 + \dfrac{2000}{Re_h}\right) e^{70r/d}} \tag{5.28}$$

For a flipped nozzle $Cd = 0.611$.

Cavitation occurs if $K_{crt} < K < K_{inc}$ with:

$$K_{inc} = 1.9\left(1 - \frac{r}{d}\right)^2 - \frac{1000}{Re_h} \tag{5.29}$$

where Re_h is the Reynolds number:

$$Re_h = \frac{d\rho_l}{\mu}v = \frac{d\rho_l}{\mu}\sqrt{\frac{2\left(P_1 - P_2\right)}{\rho_l}} \tag{5.30}$$

In this case:

$$Cd = 0.611\sqrt{K} \tag{5.31}$$

Single phase flow occurs if $K > K_{inc} > K_{crt}$

$$Cd = \frac{1}{\frac{1}{Cdu} + 20\frac{(1 + 2.25L/d)}{Re_h}} \tag{5.32}$$

where Cdu is the ultimate discharge coefficient:

$$Cdu = 0.827 - 0.0085\frac{L}{d} \tag{5.33}$$

The decision tree is shown in the following picture [80].

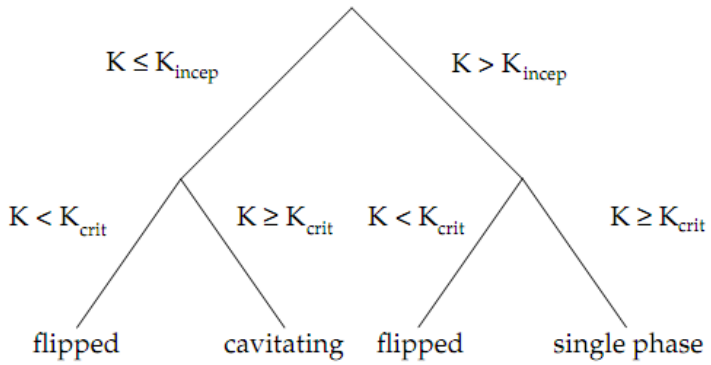

Figure 5.38: *Decision tree for the state of a cavitating nozzle [80].*

Unfortunately these relations are not strictly valid for $K < 1$. For the computations two different Cd have been used.

The first is 0.61, the value of a flipped injector as expected by the decision tree ($K < K_{crt}$, $K < K_{inc}$). Unfortunately in this case the experimental results for low ΔP are outside the boundaries given by the two basic models (incompressible and HEM). This could be related to the inapplicability of previous relations when $K < 1$ or a problem in the measurements.

The other Cd has been set arbitrary equal to 1 as a reference comparison.
Equation 5.26 is not able to give accurate results for all the condition tested. It is possible to guess that Stanford model is better suited for high value of k and low ΔP were the difference between the two models is lower. For low ΔP both models predict an increase of the mass flow with a decrease of the discharge pressure. After a certain pressure drop the equilibrium model predict the choking of the injector while classical eq.5.1 never predicts a choking. For this reason equation 5.26 (being the average between the two) is not able to determine when the injector is choked.
This is an important information because in this case the feed line is decoupled from the combustion chamber and the mass flow cannot increase anymore.
The preliminary experimental results seem to show that the mass flow tends to shift more toward equilibrium for high ΔP. Moreover at high ΔP the mass flow is constant (choked). The trend predicted by the HEM appears as the more similar to the experimental results, even if the absolute values are generally lower, particularly in the flat (choked) region.
For $Cd = 1$ the HEM predictions fall in the experimental bandwith.

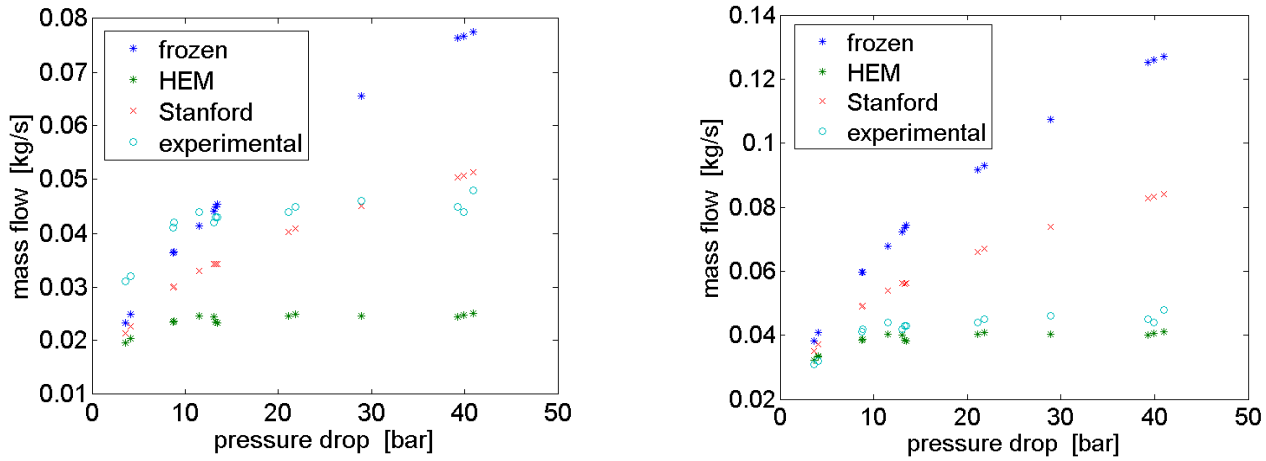

Figure 5.39: *Comparison between numerical predictions and experimental data. 12 mm injector.* $Cd = 0.61$ *(left) and* $Cd = 1$ *(right).*

However a strong uncertainty arises in the definition of the discharge coefficient. The discharge coefficient for a saturated liquid is strongly different from the value measured for a conventional liquid. The presence of large cavitation regions could affect the amount of vena contracta, particularly for sharp entrances.
Similitude is not preserved between the two cases. It is possible that the discharge coefficient is different for different boundary conditions (as it happens for $K > 1$). However in a certain

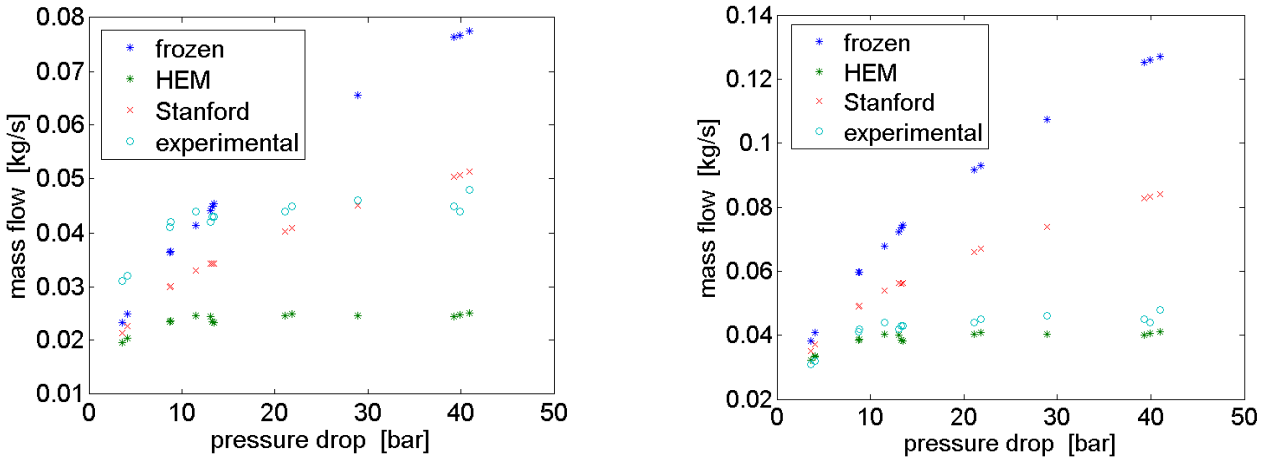

Figure 5.40: *Comparison between numerical predictions and experimental data. 3.8 mm injector.* $Cd = 0.61$ *(left) and* $Cd = 1$ *(right).*

sense the meaning of the discharge coefficient tends to be more questionable when is not strictly related to the incompressible model. In fact its original meaning was to account for area contraction, friction and other losses respect to the ideal incompressible case.

When other types of complex (and strongly coupled) phenomena occur together and a specific model to predict the mass flow is developed, the effect of all the losses, contraction, slip etc. on the value of the mass flow should be part of the solution itself (so no Cd should be added).

New models have not been developed in the frame of this doctorate because the original experimental activity about injection has been postponed. To develop more detailed models a wide rigorous experimental campaign is necessary in order to analyze several upstream and downstream conditions together with different injector geometries.

With the increase in computational means two-phase CFD simulations are becoming more attractive to understand and predict two-phase injection. As for other aspect of hybrid propulsion much work could be borrowed from other more developed fields.

5.4 Conclusions for Tank, Feed Lines and Injection

In this chapter the behavior of the hybrid rocket feed system has been investigated. The attention has been focused on the pressure fed mode because, thanks to its simplicity, it is often preferred in hybrid rocket applications, particularly for small/medium scales. First of all a numerical model of a pressure fed tank has been developed using the proper conservation

equations for the main tank and the pressurant tank. The code is able to predict several parameters like masses, densities, temperatures and pressures of the gas in the ullage volume and in the pressurant tank, the pressurant mass flow and the filling level of the tank. The model takes into account several aspects like heat losses and liquid oxidizer evaporation. If the pressurant is an oxidizer it is possible to simulate the gas phase combustion of the pressurant and determine the final pressurant residuals. It was noticed that the gas phase combustion produces a non-negligible thrust tail. Moreover, together with the pressure decay, an O/F shift occurs during final gas-phase combustion with a consequent I_{sp} penalty, particularly at sea level. It was shown that the penalty can be reduced using a by-pass at the expense of added complexity of the injection system. The thrust tail should be avoided for soft lander and other applications where a specific value of the thrust is required. On the opposite for launcher's stages and sounding rockets it could add an important contribute to the total impulse. However this total impulse contribution should be weighted with the increased gravity losses and other penalties. The use of a digital valve instead of a pressure regulator has been simulated. It was shown that the width of the PWM signal increases with time because of the increased required mass flow as inlet pressure decay. If the valve is too small the blowdown mode begins before the liquid oxidizer has been depleted because the pressurant is no more able to maintain the correct pressure. Moreover the on-off control produces a pulsation of the pressure in the oxidizer tank, particularly at the beginning when the pressure drop and consequently the mass flow is higher. To further improve the simplicity of a hybrid rocket a self-pressurization system is very attractive. To model the self-press mode a homogeneous equilibrium model has been chosen. The liquid and the vapor phase are considered in saturated conditions at every instant. The model has been compared with experimental results from previous CISAS activities. The agreement is generally good but it worsen for very short burning times The error could be related to non-equilibrium effects and/or stratification. It is important to avoid stratification before motor operation in order to achieve the maximum performances from self-pressurization. When performances are critical a good thermal control should foreseen. An analysis has been made about the influence of the initial temperature on performance. Results showed that N_2O should be generally cooled below 10° C. In fact a reduction of the temperature implies an increase in oxidizer density, a decrease of pressure, a small I_{sp} penalty, a decrease of the pressure decay during the discharge, large savings in tank weight and vapor residuals. The mass flow decay induced by self-pressurization partially compensates the O/F shift with time

for propellants with $n > 0.5$. It was shown also that generally the self-press mode offers higher performances than the blowdown mode. Later the full transient coupling between the feed system and the combustion chamber has been investigated. The main challenge was to determine the instantaneous liquid mass flow and the relation between the liquid oxidizer and the gaseous oxidizer that takes part in the hybrid motor combustion processes (i.e. droplets vaporization). This has been done with a two-times model. The first time is a constant time lag that represents droplets breakup and heating to the vaporization temperature. The second time is based on the classical model of droplet evaporation called the 'D^2 law'. In this phase the squared of the droplet diameter varies linearly with time. In this way it was possible to simulate feed system coupled instabilities. The simulations showed a good agreement with experimental results especially considering the uncertainties in the inputs and the level of approximation of the model. The code is able to simulate the oscillations in the chamber and in the injector with good accuracy, showing in particular the typical clipped waves form of injector oscillations. Finally a study has been done about the prediction of the mass flow through the injector elements for a self-press oxidizer. Three models have been compared with CISAS cold flow tests: the incompressible model, the homogeneous equilibrium model (HEM) and one model developed at Stanford. The latter is a weighted-average of the other two models based on a estimate of the ratio between the residence time and the bubble growth time. The trend predicted by the HEM appears as the more similar to the experimental results, even if the absolute values are generally lower, particularly in the flat (choked) region. For $Cd = 1$ the HEM predictions fall in the experimental bandwith. However it has been shown that a strong uncertainty arises in the definition of the discharge coefficient. The usual empirical correlations are not valid when the downstream pressure is below oxidizer saturation level.

Chapter 6

Advanced Techniques

In this chapter some advanced techniques developed to increase the regression rate and combustion efficiency of hybrid rockets are investigated with a particular focus on their influence on the transient behavior of the motor, particularly regarding combustion instabilities.
The two methods studied in this thesis are the use of a diaphragm in the midst of the grain and the use of a swirling oxidizer injection. The reason for this choice is related to the fact that both solutions have been tested (among others) at CISAS [28][76][77] and look very promising with respect to the overcoming of historical hybrid weaknesses.
Even if working in very different ways both methods induce a strong increase of the turbulence level and mixing of the reactants in the combustion chamber, promoting a more complete combustion and an higher heat flux on the grain surface. Beside improving significantly hybrid performances this two techniques can affect the stability behavior of an hybrid motor directly (i.e. modifying the flowfield in the chamber) and indirectly (e.g. reducing the chamber length due to increased regression rate).

6.1 Diaphragm

In this paragraph the use of a diaphragm placed in the midst of the grain is investigated. Respect to past researches the attention is focused particularly in the capability of the diaphragm to modify the acoustic response of the combustion chamber in terms of frequency and amplitude of the acoustic waves.
The use of a diaphragm was first proposed and investigated by the governmental French research institution ONERA, which was the European leader of hybrid rocket development and research in the 1960's [82]. Such efforts resulted in one of the few example of a successful

flying hybrid motor, the M27 that propelled the LEX sounding rocket [83].

Recently, Grosse [55] investigated the use of the diaphragm in a lab-scale motor using the propellant combination nitrous oxide-paraffin wax. He tested two types of diaphragm placed at various positions of the grain length. The two configurations presented respectively 1 (circular) hole and 4 holes (cross). Grosse finally discovered that the positions between 24 to 33% of the grain length achieved very high combustion efficiencies and very high and smooth regression rates in the second grain section.

Subsequently a CFD investigation [10] of Grosse experiments has been performed at CISAS. These simulations highlighted the effect of the diaphragm on the hybrid motor flow-field. The diaphragm acts in two ways. First of all it has a local effect just after it. The diaphragm forces the mixing of the oxidizer with the fuel generated before it, enhancing the local completeness of the combustion (particularly for the 4-holes case).

The second effect is distributed along the second part of the motor. In fact the diaphragm induces an increase in turbulence level that improves mixing and heat transfer at downstream grain section (particularly for the 1-hole case). The 1-hole configuration forces flow to pass at center of the section while in the 4-holes the flow is pushed and accelerated near the grain. The 4-holes diaphragm drives the oxidizer towards flame while the 1 hole drives flame to the central core and then it comes back again near the grain.

The simulations explained also why the pressure drop of a diaphragm placed at 24-33% is lower respect to the same device positioned at the end of the grain. The mach number increases with mass and heat addition so if the diaphragm is placed ahead the initial mach number just before it is lower and this reduce the pressure drop. Moreover there is also enough space for a pressure recover. On the contrary with the diaphragm at the end of the grain there is not enough space for a pressure recovery, the flow goes directly from the hole of the diaphragm to the throat.

Later an experimental campaign followed with numerical simulations has been performed at CISAS [28]. The experimental tests were divided in two parts. In the first part several circular 1-hole diaphragm have been tested in a small scale motor (70 mm OD) at CISAS facility in Rossano. The choice of the 1 hole configuration has been done because of ease of manufacturing. Moreover the 1-hole diaphragm has less issues of thermo-mechanical loads during operation. The motor were characterized by a compact design. In fact the pre and post chambers were absent.

That study focused on the influence of the hole diameter to the performances. As expected

the results of both tests and CFD revealed that the smallest is the hole the highest are the flow acceleration, the pressure drop, the mixing of the reactants and the efficiency.
Finally a 1-hole diaphragm has been tested in a larger hybrid motor (110 mm OD) at CISAS facility in Soverzene in order to assess scalability of the diaphragm behavior. The results confirmed that diaphragms are effective also in larger motors. The diaphragm showed to be an helpful tool in increasing the regression rate and the combustion efficiency of hybrid motors. Considering pressure oscillations in the chamber, motor with diaphragm had a more stable combustion, even if its measure was not objective of that study. The use of a diaphragm certainly affects also the stability behavior of the motor. Here it is claimed that the diaphragm could give a positive contribution to motor stability.
The diaphragm acts as a flame-holder, inducing a better mixing of the propellants. The increased turbulence level should reduce the boundary layer diffusion times, thus improving the stability of the motor respect to typical hybrid intrinsic low frequency instabilities (ILFI).

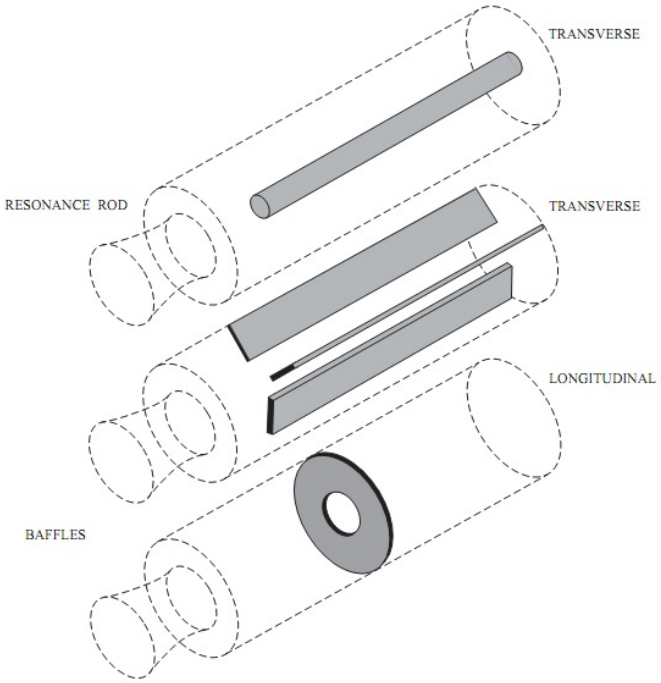

Figure 6.1: *Simple forms of baffles for solid propellant rockets [1].*

The diaphragm affects also the acoustic response of the combustion chamber. First of all the diaphragm behaves as an acoustic baffle, probably reflecting part of the acoustic wave and partially leaving part of it to pass through. This phenomenon should contribute to the dispersion of the acoustic waves. The diaphragm should modify the wavelength of the longitudinal modes (partially breaking the longest wavelength in two other shorter

wavelength), thus changing the natural frequency of the system.
Moreover it is believed also to damp the amplitude of the oscillations because it increases the energy dissipation in the combustion chamber. A sort of partial decoupling of the flow-field between the sections before and after the diaphragm is also expected.
A second indirect effect of the diaphragm is related to the regression rate increase that it produces. In fact, this means that for the same motor design O/F ratio a motor with a diaphragm is shorter, thus it has higher natural frequencies (both for ILFI and acoustics).
The use of a diaphragm introduces also additional degrees of freedom to the design engineer. In fact if some instabilities occur it is possible to move the diaphragm back and forth in order to change the natural frequency of the system and reduce the coupling with the disturbances. Also the shape of the diaphragm could be changed in order to modify the acoustic response of the chamber and fix possible motor instabilities.
It can be argued if the diaphragm could excite some kind of vortex shedding in a similar way as it happens for inert rings used to separate different propellant segments in solid rockets [1][84]. Anyway if this should happen, again the diaphragm shape and/or position could be adjusted to influence the vortex shedding characteristics (frequency, intensity...), the chamber response and the coupling between the two.

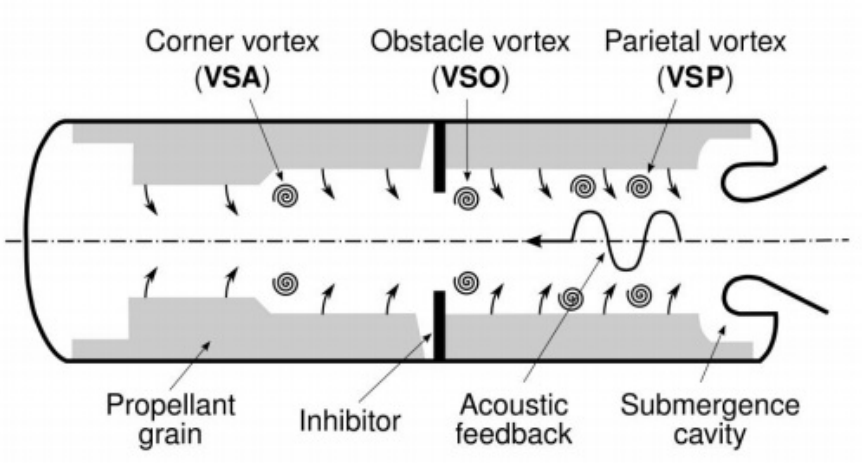

Figure 6.2: *Vortex shedding in solid rocket motors [84].*

Coming back to CISAS experimental campaign it is possible to state that, as expected, all the fires with the small scale motor were stable. This is due to axial showerhead injection, large injection pressure drop and high natural frequency of the chamber. Experimental tests with the increased scale motor showed a reduction of pressure oscillations in the case of the diaphragm respect to the baseline motor. However no several stability issues were

encountered in the whole test campaign. In fact, even if a little bit larger the increased scale motor was still small respect to the size of a typical application.
Usually stability issues increase with motor scales. So it will be desirable to test the diaphragm with larger scale motors (e.g. the Peregrine sounding rocket [65][66][67]) to asses if it would be a valuable mean to suppress or reduce hybrid motors instabilities.

6.2 Swirl Injection

In this paragraph the use of oxidizer swirl injection is investigated.
First of all it is important to clarify one point. The terms swirl injection and vortex injection are often used interchangeably. Both refer to the practice of producing a rotational pattern of the incoming oxidizer flow. However this could be done in different ways for different reasons with consequently strong different effects. There is no general agreement on when using one term or the other. The focus of the following discussion is related to injection systems that produce **a significant rotational flow inside the combustion chamber**. On the contrary small swirl injectors have been designed to provide a strong rotational motion (prior the combustion chamber) for atomization purposes. These injectors are largely used in a wide range of industrial application.
Considering combustion-related usage, swirl atomizers are very widely applied for liquid-fuel combustion in gas turbines, oil furnaces, and direct-injection spark-ignited automobile engines.
Particularly in the aerospace fields they have been successfully used in several russian liquid engines[1]. The rotational motion in the injector elements produces a very thin (unstable) liquid sheet at the injector exit that is broken into very small droplets by shear stresses. The strong centrifugal forces are responsible for an higher injection angle and very good atomization properties compared to classical plain orifice. However the ratio between the combustion chamber diameter and the exit injector diameter is very high. For this reason droplets depart straightly impacting the chamber walls almost normally.

The swirl number calculated respect to the combustion chamber diameter is negligible. No swirling flow is produced inside the combustion chamber. The use of this type of injec-

[1] Among them the nitric acid/kerosene sustainer motor of the SA-2 'Guideline' (S-75 Dvina) surface to air missile and several famous LOX/kerosene engines like the RD-120 (Zenit launcher), RD-170 (Energia), RD-171 (again Zenit), RD-180 (Atlas V) and RD-191 (Angara).

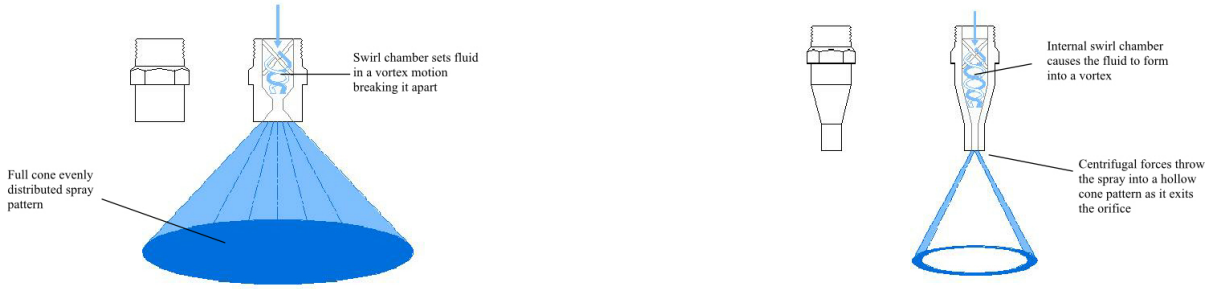

Figure 6.3: *Typical swirl atomizers.*

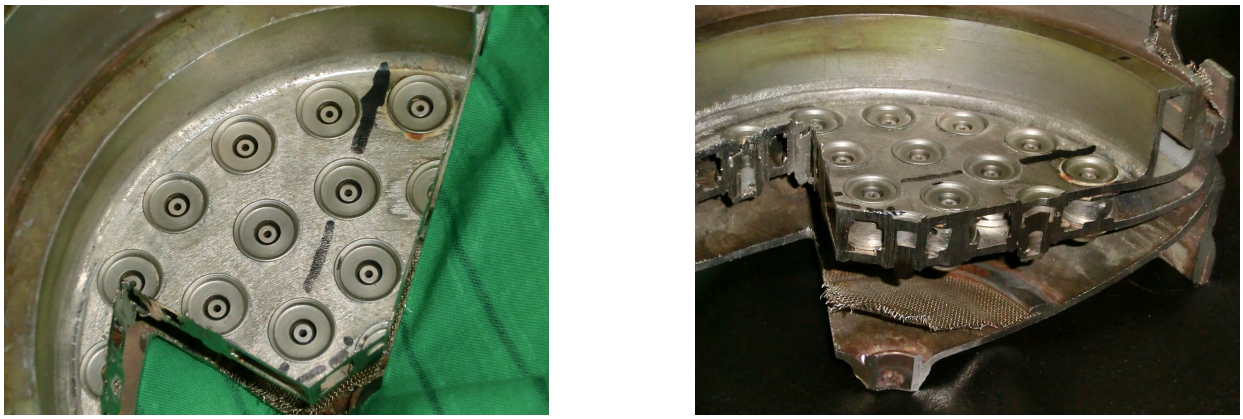

Figure 6.4: *Pictures of the multiple swirl injector plate of the liquid motor of the russian S-75 missile.*

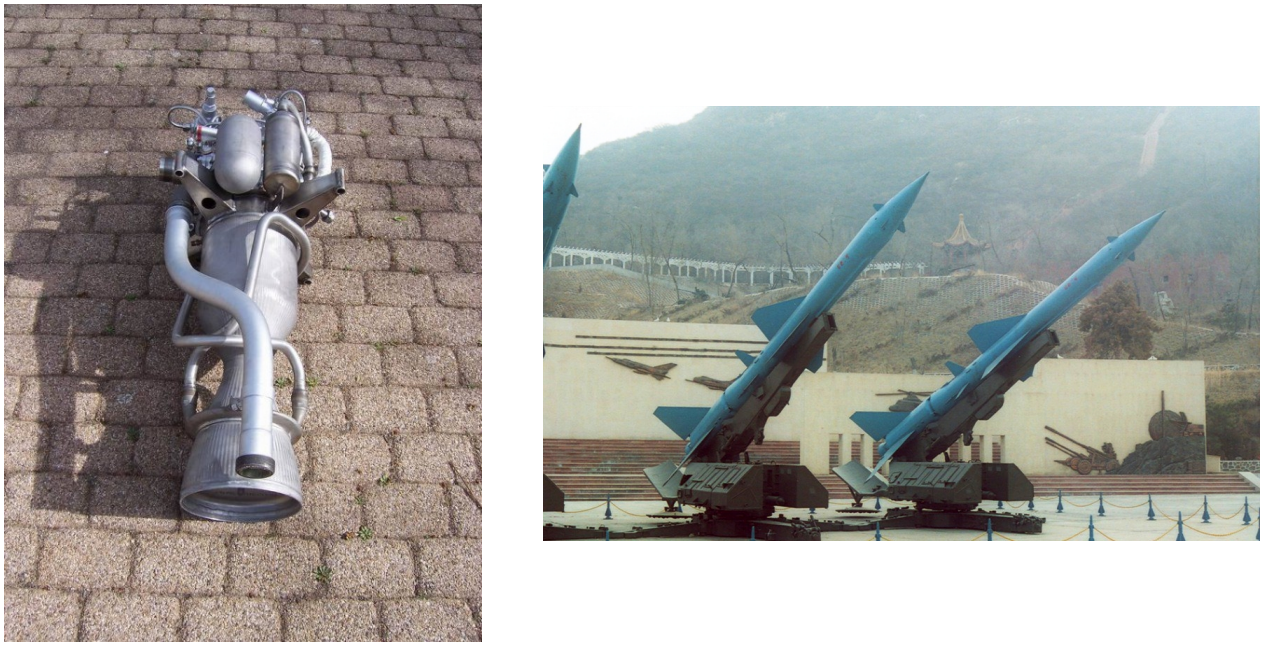

Figure 6.5: *Liquid sustainer motor (left) of the russian S-75 missile (right).*

tors for hybrids could have interesting features (fine atomization, different injection angle, different jet's interactions for multiple elements), but it is important not to make confusion

between the results obtained with these elements with those (profoundly different) of the vortex injection described in the following.

In the latter case the oxidizer is injected tangentially to the combustion chamber walls inducing, as already said, a rotational fluid pattern inside the engine. The swirl injection can be located at the head end of the grain case, producing an helical flow path moving from the port entrance to the exit nozzle. This configuration has been tested by several researchers [29][50][87][88].

Alternatively the swirl injection can be located at the aft end of the fuel grain just upstream of the converging part of the exit nozzle. This latter configuration has been tested by Knuth et al. at ORBITEC [46]. With the help of visualization experiments and numerical simulations they discovered that this arrangement generate a pair of coaxial, bidirectional vortices in the combustion port. The outer vortex spiraled toward the head end of the motor across the fuel surface, mixing and burning with the pyrolized fuels. At the head end, the vortex flows inward toward the motor axis and forms an inner vortex that spirals downward and out the nozzle. Thanks to this peculiar behavior of the flow the mixing and residence time of the reactants are strongly enhanced.

This fluid pattern was also confirmed by the analytical treatment made by Majdalani [89]. He demonstrated that the flow is dominated by a free vortex motion dictated by the inviscid solution of the momentum equation in the tangential direction. He also developed viscous corrections of the main inviscid solution for the regions where viscous forces dominate, that is, near the centerline (where a singularity of the free vortex occurs and a forced vortex behavior is established) and near the sidewalls (where a thin boundary layer develops as a result of the no-slip condition in the wall-tangential direction).

Regarding the head end swirl injection numerical, analytical and experimental activity has been performed at CISAS [76][77]. Several CFD simulations with a finite-volume commercial code have been done in order to investigate the effect of different aspects on the swirl flow characteristics. With the aim of partially decouple (at least qualitatively) the influence of many different phenomena affecting the flowfield an additive approach has been pursued, increasing step by step the amount of physical aspects inserted in the simulations.

First of all cold flow simulations without gas addition from the sidewalls have been performed, then cold flow simulations with blowing and finally hot flow simulations with combustion.

For the cold case without lateral mass addition some important analytical considerations can be done from the compressible Navier-Stokes equations, neglecting the gravity term

and normal viscous terms. Some simplifications can be introduced based on the following hypothesis:

- steady state flow;
- axis-symmetry null derivative over the tangential direction;
- variation of tangential velocity in the longitudinal direction can be neglected;
- radial velocity is negligible respect to axial and tangential.

The last two assumptions have been validated through the CFD simulations. In cylindrical coordinates, the momentum balance in the tangential direction is the following:

$$\begin{aligned}\rho\left(\frac{\partial u_\theta}{\partial t}+u_r\frac{\partial u_\theta}{\partial r}+\frac{u_\theta}{r}\frac{\partial u_\theta}{\partial \theta}+u_z\frac{\partial u_\theta}{\partial z}+\frac{u_r u_\theta}{r}\right)&=-\frac{1}{r}\frac{\partial p}{\partial \theta}\\ +\mu\left[\frac{1}{r}\frac{\partial}{\partial r}\left(r\frac{\partial u_\theta}{\partial r}\right)+\frac{1}{r^2}\frac{\partial^2 u_\theta}{\partial \theta^2}+\frac{\partial^2 u_\theta}{\partial z^2}-\frac{u_\theta}{r^2}+\frac{2}{r^2}\frac{\partial u_r}{\partial \theta}\right]&\end{aligned} \tag{6.1}$$

from the previous hypothesis eq. 6.1 becomes:

$$\frac{1}{r}\frac{\partial}{\partial r}\left(r\frac{\partial u_\theta}{\partial r}\right)-\frac{u_\theta}{r^2}=0 \tag{6.2}$$

the only possible solution is the forced vortex:

$$\omega r = u_\theta \tag{6.3}$$

The CFD simulations confirm the forced-vortex behavior of the head-end injected vortex flow. This fact represents a strong difference respect to Majdalani solution where a free-vortex prevails.

The reason for this discrepancy is the following. In the aft-injected vortex (or double vortex) configuration the fluid begins to go along the 'wrong direction' so it has to turn and pass from the outer vortex to the inner vortex to get out the nozzle. For this reason a significant radial velocity is present even when there is no blowing from the sidewalls. This is in contrast with the case of the head-end swirl flow where the fluid proceeds always in the 'right' direction so no significant radial velocity is present[2].

[2]This is not exactly through because, as showed in the following, a suction effect exist near the head-end that entrains part of the flow, forcing it to turn and move backward. However this effect doesn't change the basic forced-vortex motion, as it is confirmed by the CFD simulations.

When the radial velocity is non-zero eq.6.1 could be simplified to give an inviscid (free-vortex type) solution.

On the contrary when the radial velocity is negligible it is necessary to retain the viscous terms in eq.6.1 otherwise the equation would vanish completely. This fact explain why the two vortex injection configurations have different leading order solutions (free and forced-vortex, respectively).

Going on with the analytical work some other aspects could be highlighted. In a cylindrical reference frame, the balance in the radial direction gives:

$$\begin{aligned}\rho\left(\frac{\partial u_r}{\partial t}+u_r\frac{\partial u_r}{\partial r}+\frac{u_\theta}{r}\frac{\partial u_r}{\partial \theta}+u_z\frac{\partial u_r}{\partial z}-\frac{u_\theta^2}{r}\right)&=-\frac{\partial p}{\partial r}\\ +\mu\left[\frac{1}{r}\frac{\partial u_r}{\partial r}+\frac{1}{r^2}\frac{\partial^2 u_r}{\partial \theta^2}+\frac{\partial^2 u_r}{\partial z^2}-\frac{u_r}{r^2}-\frac{2}{r^2}\frac{\partial u_\theta}{\partial \theta}\right]&\end{aligned} \tag{6.4}$$

Applying the same simplifications as in the previous case we get:

$$\rho\frac{u_\theta^2}{r}=\frac{\partial p}{\partial r} \tag{6.5}$$

Considering an ideal gas and a forced vortex we obtain:

$$\rho\frac{u_\theta^2}{r}=\frac{\partial p}{\partial r}=\frac{\omega^2 r M_m p}{R_u T} \tag{6.6}$$

For constant M_m and T along the radial direction the previous equation can be integrated between the center ($r=0$ and $p=p_i$) and a radial position r:

$$\frac{\omega^2 r^2 M_m}{2R_u T}=ln\left(\frac{p}{p_i}\right)=ln\left(\frac{\rho}{\rho_i}\right) \tag{6.7}$$

$$p\left(r\right)=p_i e^{\frac{\omega^2 r^2 M_m}{2R_u T}} \qquad\qquad \rho\left(r\right)=\rho_i e^{\frac{\omega^2 r^2 M_m}{2R_u T}} \tag{6.8}$$

These equations describe the centrifugal effect due to the rotation of the flow, pushing the fluid towards the sidewalls of the combustion chamber. This behavior has been confirmed by visualization experiments performed by other researchers comparing classical and swirling hybrid rockets [87]. The swirling flames were found to develop closer to the grain surface than those without swirl.

The predictions of eq.6.8 match accurately CISAS CFD results for the cold case without blowing.

Moreover even when blowing and combustion are considered (producing chemical and temperature gradients in the radial direction) the same qualitative behavior is recognized and a good approximation can be found with eq. 6.8 introducing proper averaged values on the section. To better investigate the behavior of the vortex scheme and explain its performance gain a CFD comparison with a classical axial configuration has been performed.

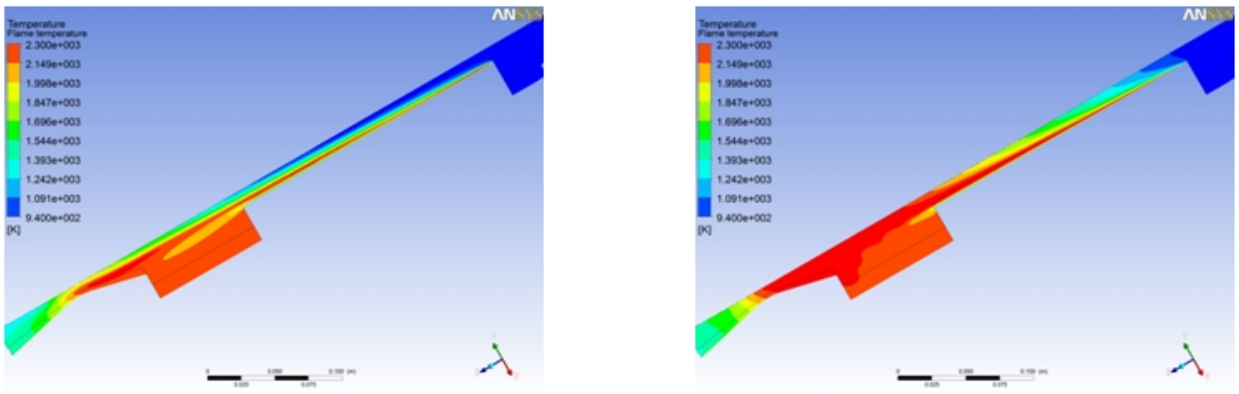

Figure 6.6: *Temperature profile for axial injection (left) and vortex injection (rigth).*

The axial injection produces the typical strong stratified flowfield with the fuel and the oxidizer moving almost parallel to the flame along the port. This produces the typical low performances normally encountered in hybrid rockets.

On the contrary the helical flow produced by vortex injection strongly enhances the turbulence level and mixing in the combustion chamber. The hot products are mixed with the central cold core and this allows for fresh oxidizer to reach the flame. Moreover, as already said, centrifugal forces push the flame near the wall enhancing the heat flux and thus the regression rate.

As shown in the analytical part these centrifugal forces produce a pressure gradient in the radial direction that is absent in the axial case. Moreover there is a sort of suction at the head of the motor; in fact the axial pressure drop at the centerline of the combustion chamber is lower than in the axial case. This suction is explained by the slow decay of the swirl velocity along the axial direction. The slow reduction of the rotational velocity implies a decrease of the radial pressure gradient. When the swirl motion has vanished the pressure on a section normal to the longitudinal axis is almost uniform. Going backward up to the head end of the motor in order to respect the increasing radial pressure gradient the pressure on the centerline has to increase slower than on the sidewalls (or even decrease).

Thanks to the improved turbulent mixing higher values of combustion efficiency are reached by the vortex hybrid. This is confirmed by both CFD simulations and experimental data.

An important parameter in the study of swirling flows is the swirl number. The swirl number is calculated as the ratio between the axial flux of the swirl momentum and the axial flux of the axial momentum:

$$SN = \frac{\int \rho v_z v_\theta r dA}{R_{max} \int \rho v_z^2 dA} \tag{6.9}$$

It is possible to define the reference swirl number at injection by the following geometrical formula:

$$SN_g = \frac{(r_{inj} - r_{holes})\, r_{inj}}{N_{holes} r_{holes}^2} \tag{6.10}$$

This parameter is useful to compare different situations without the need for specific measurements of fluid unknowns. This swirl number can give information about the relative intensity of the rotational flow and how it varies along the motor because of heating, friction, mass addiction and section changes.

The CFD simulations demonstrate that friction has a minor effect in reducing the swirling component while heat and mass addition along the grain cause a larger drop of the swirl number, mainly because they force an increase of the axial velocity component. In fact the continuity equation states that the axial velocity has to increase when the axial mass flux increase (through blowing[3]) or the density decrease (because of heating).

In particular combustion is the major source of swirl decay (through Rayleigh-style axial acceleration) along the grain length; this in turn can affect the uniformity of grain consumption.

Every time there is a change in the cross section the swirl number is strongly affected. In fact the axial velocity component changes following the continuity equation while the tangential component follows the conservation of angular momentum. Considering an incompressible flow without blowing (for simplicity) that means:

$$v_a A = cost_1 \qquad v_a \propto 1/r^2 \tag{6.11}$$

$$v_t r = cost_2 \qquad v_t \propto 1/r \tag{6.12}$$

So $SN \sim v_t/v_a \rightarrow SN \propto r$

[3]In this respect motor operating at high O/F ratio should suffer less losses for fuel mass addition.

For a determined injector pressure ratio (i.e. injection velocity) the swirl number is higher for motors designed to work at lower (longitudinal) mass fluxes and higher pressures (i.e. lower axial velocity).

Following the previous considerations it is possible to show that the swirl number is proportional to the product of the local radius and the injection radius ($cost_2 = v_{t_{inj}} r_{inj}$). So the swirl number is nearly proportional to the square of the injection radius when the port radius scale accordingly (from eq. 6.10, $SN_g \sim r_{inj}^2$).

On the contrary if the port radius is taken constant the swirl number is linearly proportional to the injection radius ($SN \sim SN_g r / r_{inj} \rightarrow SN \propto r_{inj}$). This is caused by the reduction of SN from SN_g due to the contraction from r_{inj} to r.

Several simulations of a motor similar to the one designed by NAMMO Raufoss for the SPARTAN project[72] have been performed. The set of simulations is listed in table of fig. 6.7.

N° Case	Purpose
C1	Reference case
C2	Evaluate the effect of doubling the swirl number
C3	Evaluate the effect of an axial-tangential injection
C4	Evaluate the effect of removing the post-cc
C5	Evaluate the effect of removing the pre-cc
C6	Evaluate the effect of removing the pre-cc and the post-cc
C7	Evaluate the engine behavior varying the grain port
C8	Evaluate the engine behavior at 10% of the nominal m_{ox}
C9	Evaluate the engine behavior at 50% of the nominal m_{ox}

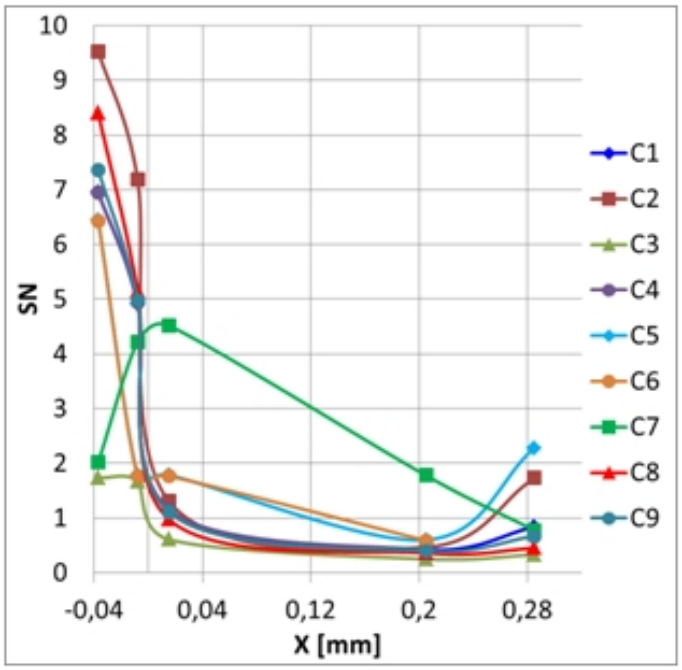

Figure 6.7: *Simulated cases (left) and swirl number axial profiles (right).*

The CFD results show a strong drop of the SN when a contraction occurs (like from the pre-chamber to the port) and a recover when there is an enlargement (i.e. from the port to

the post-chamber), confirming the predicted general trend. However this is only a qualitative statement because of the complex flowfield inside the combustion chamber, affected by strong temperature, density and velocity gradients and three-dimensional recirculations.
Generally all these phenomena contribute to a decrease of the swirl number trough dissipative mechanisms. Moreover this explains while the computed swirl number slightly changes also if the reference geometrical swirl number remains constant (like in the case of constant geometry and different mass flows). In fact at reduced mass flows the dissipation is reduced so the swirl number results higher.
It's worth nothing that dissipative phenomena act in different ways in the axial and tangential directions. In the axial direction they cause a pressure drop (because the velocity is constrained by the continuity equation) while in the tangential direction they induce a decrease of the rotational velocity (because of a loss in the angular momentum). The final result is a decrease in the swirl number.
A partial-axial injection as expected shows a significant reduction of the swirling flow and consequently of performances respect to the basic case. Doubling the swirl number on the contrary shows the opposite effect. In general higher swirl numbers force higher mixing and consequently lead to higher efficiencies.
The elimination of the enlargement in the pre-chamber reduces the dissipation caused by recirculations.
The use of a post-chamber helps the final mix of the reactants. Even if this effect is less important in the case of the vortex motor it is still present because the high regression rate allows for shorter grain ports. Moreover it helps the flow to enter the nozzle without a strong swirling component.
Simulations of throttling down respect to the nominal case have been performed together with a simulation of the same motor geometry but with a larger port area (describing a later instant during combustion). At lower mass fluxes the efficiency is higher because of the increased residence time. Moreover in the case of the large port area the swirl number is preserved because no strong contraction occurs.
Ultimately the swirl number and its distribution along the axis has a crucial influence on motor performances and regression uniformity. Considering the latter point experimental results are contrasting. Some researchers found a pretty uniform burn along the grain while some others noted a strong consumption near the injection end.
This fact is dependent on the complex flowfield that establishes in the region between the

injector and the initial part of the grain which can vary considerably from case to case. In particular a critical aspect is the eventual direct impingement of the oxidizer flow on the grain surface that usually induces a strong local increase of the heat flux in the corresponding region.

Finally the resulting behavior is related to the geometry of the pre-chamber, the injection angle, the ratio between port diameter and injection diameter, and the possibility of burning for the grain frontal face (or its inhibition).

It is worth noting that the previous discussions don't hold for ORBITEC vortex hybrid. In fact in this case the axial velocity has a inherently two-dimensional variation (changing direction passing from the inner to the outer vortex) so it's not possible to apply the same 1-dimensional approach as above. Considering a cylindrical control volume corresponding to a slice of the outer vortex (a 3D ring) it is possible to show that the axial velocity should not necessary increase because of heating and/or mass addition because some mass continuously escapes from the internal face separating the outer vortex to the inner one (the mantel location).

On the contrary Majdalani solution [89] predicts indeed a decrease of the axial velocity in the outer core (as it is expected from the boundary condition of inert head end which imposes that the longitudinal velocity should vanish approaching the head end of the chamber).

Numerical simulations performed with and without the nozzle show that the nozzle has a very limited effect on the flow in the combustion chamber. As predicted by the previous equations the streamlines straighten passing though the nozzle because of the strong longitudinal acceleration. The flow exits with a little swirl component and this could determine a roll reaction on the propulsion unit. However this effect is often negligible.

Another concern with swirling flow through nozzles is the blocking effect on the mass flow caused by the centrifugal forces opposing the fluid approaching the throat. Several authors have investigated this subject developing some analytical solutions [90][91][92][93]. The use of a mixer that disrupts the swirling flow before the nozzle entrance could prevent the previous issues.

The great part of experiments with vortex injection up to now have been performed using gaseous injection, usually with GOX. However in a real motor the oxidizer should be stored in the liquid phase. Unfortunately liquid injection necessarily reduces the performance of swirl injection.

First of all the liquid flow is pushed directly by centrifugal forces on the grain surfaces. This

in turn can result in difficult ignition caused by flooding if the heating from the flame is not able to vaporize the necessary liquid flow. Moreover issues concerning droplets atomization arise. This is also common with conventional axial injection but some peculiar aspects are present in the vortex case.

In fact the droplets flight time from injection to wall impingement is lower, with the effect already cited. Moreover droplet atomization requires preserving small holes dimensions. In this way as the motor scales up the holes size cannot change accordingly. For typical axial injection this is faced increasing the number of holes. Retaining similar geometry ratios both the injector plate area scales with mass flow and the number of holes could be increased proportionally.

On the contrary for vortex injections the holes are placed on the perimeter of the injection plate so their number scale with the diameter and not with the square of the diameter as happen for mass flow. One solution could be to place several raw of holes in order to maintain the foreseen total holes number. No multi-raw liquid vortex injector has been tested up to now, but double raw gaseous injectors have been successfully tested by NAMMO[4].

No final assessment could be done at the moment about multi-raw elements.

Other concerns could be related to the (larger?) weight of the injector plate/pre-chamber assembly (respect to the axial case) but this is out of the scope of this thesis.

Finally the most important thing is the decrease of the swirl number caused by liquid evaporation. In fact the phase change of a liquid oxidizer produces a swirl decay in a similar way as combustion. The tangential velocity remains nearly constant while the axial component should accelerate (as density decreases) to respect the continuity equation. Ultimately the axial velocity after complete evaporation should be the same as for gaseous injection (for the same general motor design condition) while the injection velocity is lower. In fact injection velocity for a gas is on the order of hundreds of m/s while it is hardly above 50 m/s for liquids. Velocities intermediate between the two can be obtained in the case of two phase flows as it is expected with self-press oxidizers (like N_2O). As a first approximation the swirl reduction for liquid evaporation can be estimated in this way:

$$SN_l = SN_g \rho_g / \rho_l \tag{6.13}$$

However this simplified treatment considers a uniform fluid mixture changing is density along the axial direction. While this should be a fairly good assumption for combustion

[4]But in this case there is no relation with the size of the system because the holes can be scaled accordingly.

heating this is more debatable for the last considerations about phase-change because it doesn't take into account the complex effect of droplets liquid evaporation (two-phase flow). Liquid vortex injection experiments have been performed with bad results with LOX [75] and fairly good results for N_2O [76][77] (this because of two-phase flow injection and help by self-decomposition). However for the reasons previously discussed the outstanding results obtained by gaseous injection cannot be replied. So it is desirable to use gaseous injection even for liquid oxidizers. This in turn arise the need for a gasification system. This could be a regenerative system used for nozzle or pre-chamber cooling or a heat exchanger fed by gases spilled from the combustion chamber.
An alternative is to burn a small part of the oxidizer with a liquid fuel in a pre-burner, vaporizing the rest of the incoming oxidizer flows. A kerosene fed pre-burner has been successfully used by Orbitec to gasify LOX for their double vortex hybrid rocket [74]. Unfortunately these solutions could add complexity and the need for liquid fuels, compromising the inherent characteristic of simplicity of hybrid propulsion.
Probably the most promising solution is the use of catalytic decomposed Hydrogen Peroxide. H_2O_2 catalyst decomposition is well developed[5] and it could allow a simple, cold, multiple self-starting motor ignition system together with high performing gaseous injection.

As last topic of this paragraph the swirl injection is investigated by the instability point of view. The attention should focus particularly on understanding how the swirl flow affects the hydrodynamic stability and the generation of sources of local (pressure, velocity, equivalence ratio) fluctuations. swirl.
Useful informations can be drawn by other combustion fields. For example flames in gas turbine (GT) combustors are most often stabilized by inducing a swirling ow of the reactants [94]. In fact due to stringent emission requirements, modern combustors work under lean conditions, which lead to lower ame temperatures and therefore reduced NO_x emissions. Lean flames are more sensitive to equivalence ratio fluctuations and thus they are more prone to instability. Vortex breakdown of the swirling ow and cross-section extension at the nozzle exit lead to the formation of inner and outer recirculation zones. These zones transport hot combustion products back to the nozzle, which enhances the ignition of unburned gas and thereby stabilizes the ame.
Combustion instabilities are commonly encountered in the development of lean-premixed

[5]Moreover nowadays there is a renewed interest for hydrogen peroxide as a GREEN monopropellant and liquid oxidizer for bipropellant systems.

(LPM) gas-turbine engines. The spontaneous generation of unsteady ow oscillations in the combustion chamber may cause structural vibration and excessive heat transfer to the chamber, and consequently lead to failure of the system. As already said, most LPM gas-turbine engines utilize swirling ows to stabilize the ame for efficient and clean combustion.

One of the most important ow features produced by a swirl injector is a central toroidal recirculation zone (CTRZ), which serves as a ame stabilization mechanism. Flows in this region are, in general, associated with high shear rates and strong turbulence intensities resulting from vortex breakdown. Although this type of ows has been extensively studied, there remain many unresolved issues, such as swirl generation, vortex breakdown, axisymmetry breaking, and azimuthal instability. In particular, the effect of ow swirl on combustion dynamics has not been well studied, at least in a quantitative sense.

Swirling ows may affect ame dynamics in two aspects. First, large-scale unsteady motions arising from shear-layer instability and vortex breakdown, as well as precession of vortex core (PVC), may couple resonantly with acoustic waves in the combustor, and subsequently cause combustion instabilities.

Second, ow swirl may alter the ame structure and combustion intensity, and as a consequence inuence the heat-release behavior in a combustion chamber. The ensuing effects on the stability characteristics could be substantial.

The situation for hybrid rocket motors presents some analogies and some significant differences respect to the case of GT combustors. Hybrids work with a diffusion flame while GT combustors often use a partially or complete premixed flame. Even in the case of a diffusion flame, in a GT combustor the energy is released near the head-end of the chamber (as in liquid rockets) while in the hybrid it is distributed along the entire grain length. As previously said, hybrid flame is less sensitive to (pressure, O/F ratio...) fluctuations because the heat release (and consequently fuel production) is diffusion limited and the fuel entrance (the grain surface) is separated from the oxidizer inlet.

It is important to note that in a GT combustor the injection diameter is lower than the chamber diameter. This fact is responsible for the flow characteristics described above. The sudden expansion of the swirl flow favors the formation of the recirculation zones and vortex breakdown.

The same condition could arise in a hybrid rocket when the injection radius is lower than the port radius, particularly as the burn progresses and the port enlarges. Regarding the activity about swirl injection in hybrid rockets Pucci [4] found that weak swirl produced unstable

combustion, whereas strongly swirling injection produced a stable combustion. The work of Knuth [46] on vortex injection hybrids, Haag [48] for vortex pancake and NAMMO [70] for the head-end vortex confirmed that a strong swirl is usually followed by a very smooth combustion.

Majdalani [81] in its discussion about biglobal instability of the bidirectional vortex stated that high speed swirling velocity brings about two physical attributes: a shear layer near the centerline and strong centrifugal forces. While the new centerline shear layer introduces vorticity near $r = 0$, the centrifugal forces will act to negate vortex generation along the sidewall. As the swirl intensity increases, and the overall oweld becomes more swirl dominated. Through its mathematical analysis he found that (as suggested by intuition) intensication of swirl would stabilize the ow through increased centrifugal action that serves to inhibit vortex generation and promote a crisper denition of the mean ow.

It's possible to state as a general conclusion that a swirling motion should generally improve the stability of combustion but it does not guarantee the absence of instabilities in every situation.

As in the case of diaphragm it will desirable to test vortex injection at larger scales. In the author knowledge the only tests done at increased scale have been done by Orbitec [74]. Apparently the results were good but unfortunately not much information has been provided.

6.3 Conclusions for Advanced Techniques

In this chapter two advanced techniques developed to improve hybrid rocket performances have been investigated.

The first is the positioning of a diaphragm in the midst of the grain while the second one is the use of a swirling injection of the oxidizer. Both solutions have been tested (among others) at CISAS and look very promising with respect to the overcoming of historical hybrid weaknesses, in particular low regression rate and combustion efficiency.

The presence of a diaphragm between 1/4 and 1/3 of the grain length introduce a strong increase of the turbulence level and mixing of the reactants in the second part of the combustion chamber, promoting a more complete combustion and an higher heat flux on the grain surface, thus improving the efficiency and the regression rate. Concerning the effect of the diaphragm on motor stability it is claimed that the diaphragm could act as a flame-holder,

anchoring the flame and at the same time it should work as a baffle, affecting the acoustic response of the motor, the energy dissipation, the generation and damping of disturbances, and the coupling between them.

Moreover the diaphragm adds a further degree of freedom in the design of an hybrid rocket motor. In fact the shape and the position of the diaphragm can be adjusted in order to modify the response of the system and suppress or reduce possible instabilities.

The second advanced option that has been considered here for improving hybrid rocket performances is swirl injection. In this case the oxidizer is injected tangentially to the combustion chamber walls in order to induce a rotational fluid pattern inside the engine.

The influence of many different phenomena on the swirl flow characteristics has been investigated with the help of CFD simulations and mathematical analysis. A step-by-step additive approach has been pursued in order to partially decouple (at least qualitatively) the different physical aspects affecting the swirling flowfield. In contrast with the free-vortex dominated aft-end swirl injection, it has been demonstrated that the leading solution in the case of head-end swirl injection is a forced vortex because the absence of a radial velocity impose to retain the viscous terms in the tangential momentum equation also for the zero order solution.

A comparison has been made between the classical axial injection and the vortex configuration. The axial injection produces the typical strong stratified flowfield with the fuel and the oxidizer moving almost parallel to the flame along the port. This produces the typical low performances normally encountered in hybrid rockets. On the contrary the helical flow produced by vortex injection strongly enhances the turbulence level and mixing in the combustion chamber. The hot products are mixed with the central cold core and this allows for fresh oxidizer to reach the flame. Moreover, as already said, centrifugal forces push the flame near the wall enhancing the heat flux and thus the regression rate.

As expected, it has been shown that the swirl number has a fundamental role in the description of swirling flows. In a head-end vortex hybrid rocket the swirl number decreases along the port for several reasons. In particular combustion is the major source of swirl decay (through Rayleigh-style axial acceleration) along the grain length; this in turn can affect the uniformity of grain consumption. Every time there is a change in the cross section the swirl number is strongly affected, increasing as the cross section area grows and decreasing where there is a geometrical contraction. Ultimately the swirl number and its distribution along the axis has a crucial influence on motor performances and regression uniformity.

Very different consumption behaviors can be found, especially near the injection end. This fact is dependent on the complex flowfield that establishes in the region between the injector and the initial part of the grain which can vary considerably from case to case. In particular a critical aspect is the eventual direct impingement of the oxidizer flow on the grain surface that usually induces a strong local increase of the heat flux in the corresponding region.
Ultimately the resulting behavior is related to the geometry of the pre-chamber, the injection angle, the ratio between port diameter and injection diameter, and the possibility of burning for the grain frontal face (or its inhibition).
Two peculiar aspects of swirling flows through nozzles are the bloking effect on the mass flow caused by the centrifugal forces opposing the fluid approaching the throat and the roll reaction on the motor caused by the residual swirl component at nozzle exit. The use of a mixer that disrupts the swirling flow before the nozzle entrance could prevent these issues.
It has been shown that liquid injection cannot achieve the outstanding results obtained by gaseous injection. In fact the atomization/evaporation of the liquid oxidizer produces a swirl decay and a loss of performance.
For this reason the most promising solution related to vortex injection is the use of catalytic decomposed Hydrogen Peroxide because it allows a simple, cold, multiple self-starting motor ignition capability together with high performing gaseous injection.
Finally the effect of the swirl flow on the stability of the motor has been discussed using data from studies about gas turbine combustors and hybrid rocket motors. It is possible to state that intensification of the swirl motion should generally improve the stability of the flow through increased centrifugal action that serves to inhibit vortex generation and promote a stronger denition of the mean ow, but this does not guarantee the absence of instabilities in every situation.
For both advanced techniques examined, particularly in relation of instability behavior, further testing at larger scales is recommended.

Chapter 7

Summary and Conclusions

The study of transient behavior is a fundamental need for the development of high performing hybrid rocket motors, particularly when throttling is concerned.
In fact hybrid motors are easy to throttle and thus they are ideal candidate for soft-landing applications and generally when propulsion energy management is required. However transient behavior is a very important aspect also for motors that have to work at a fixed nominal operating point. In fact any motor should go trough a transient phase during ignition and shut-down.
Moreover the fuel generation process cannot be directly controlled and it induces an inherent transient behavior that causes a shift of the operating parameters with time.
Finally the understanding of transient behavior is essential for the analysis of instabilities. The prediction and reduction of instabilities are one of the main challenges in hybrid propulsion (as it happens in general in the development of all combustion devices).
Hybrid transient behavior can be split between the quasi-steady and the full transient behavior. The first is focused only on the time-variation of operating conditions while the latter is related to the complete dynamic of the system. Both have been investigated in the frame of this doctoral thesis.

In the first chapter hybrid boundary layer steady combustion is introduced together with a discussion about the effect of steady hybrid regression physics on the shift of motor operating parameters with time.

In the second chapter typical necessary or intentional transient events occurring during the operation of a hybrid rocket (ignition, throttling and shutdown) are classified and described. It has been shown that the controlling time elements in these processes are those that establish the combustion boundary layer, the filling-emptying time and the thermal lag

in the solid fuel.

In the third chapter a numerical model able to solve the one dimensional unsteady heat equation inside the thermal grain has been implemented. The model is able to determine the transient temperature profile and regression rate. Numerical results showed that during throttling an overshooting of the regression rate can occur for high activation energies typical of hybrid fuels. Afterwards the heat flux to the grain surface has been coupled with the chamber gas dynamic trough the boundary layer response.
To simulate the boundary layer response two time lags have been added in the heat transfer functions representing, respectively, the times needed by the boundary layer to adjust to changes of the oxidizer mass flux and the regression rate. It was shown that the second time lag was responsible for the typical hybrid low frequency instabilities.
Moreover it was demonstrated that a positive shift of the average regression rate should occur during large regression rate oscillations.
Due to the importance of paraffin wax as a fuel for hybrid rockets, a version of the model suited for propellants that form a liquid layer has been developed. The model takes also into account the possibility of liquid entrainment. The code determines transient paraffin thermal profile and regression rate.
Paraffin based fuels usually operates above their critical pressure. For this reason the importance of an analysis of the supercritical regime was highlighted. For this purpose it was shown that jet disintegration morphology in liquid engines changes passing from subcritical to supercritical conditions. Three hypotheses have been made in order to figure out the behavior of supercritical entrainment in hybrid rocket motors.
Finally the numerical results have been compared with experimental data reported in the literature. It has been demonstrated that the predicted slope of the regression rate is almost linear. It was suggested that the reason for this mismatching is to be related to the uncertainty in the exponent of the entrainment law and to the fact that droplet entrainment is a non-linear, spatially and time-varying phenomenon. This last aspect in turn induces the need to define suitable relations between droplet average temperature, surface average temperature and vaporization temperature as it is done in the problem of turbulence closure.

In the fourth chapter a 0D and a 1D unsteady combustion chamber model have been developed using proper conservation equations. These codes are able to simulate hybrid rocket motor transient behavior and global performances. The codes can be coupled with the unsteady 1D model of the fuel grain in order to take into account transient fuel production.

It has been shown that a regression rate overshooting occurs during a throttling events. The regression rate overshooting is usually less than 10% of its nominal value. For high optimum O/F ratio oxidizers like N_2O or H_2O_2 the oxidizer flow is more than 70% (nominally more than 85%) of the total flow so fortunately the effect of the fuel flow fluctuations on pressure/thrust are smoothed (often less than 1%).
It has been determined that the thermal lag in the solid grain is the limiting time for small motors and during thrust termination events while for large motors the longest times are the boundary layer diffusion times and the filling-emptying times.
Thanks to these codes it is possible to predict the global O/F ratio, pressure, mass fluxes, characteristic velocity and thrust during the burn.
The codes could be inserted in a more complex simulation of the entire flight system. In this way they can be used to optimize the rocket motor to achieve the maximum performances. Moreover, thanks to their transient nature it is possible to assess the effect of the motor response to the complete flight dynamic in order to establish a satisfactory control law.

In the fifth chapter the behavior of the hybrid rocket feed system has been investigated. The attention has been focused on the pressure fed mode because, thanks to its simplicity, it is often preferred in hybrid rocket applications, particularly for small/medium scales.
First of all a numerical model of a pressure fed tank has been developed using the proper conservation equations for the main tank and the pressurant tank. The code is able to predict several parameters like masses, densities, temperatures and pressures of the gas in the ullage volume and in the pressurant tank, the pressurant mass flow and the filling level of the tank. The model takes into account several aspects like heat losses and liquid oxidizer evaporation.
If the pressurant is an oxidizer it is possible to simulate the gas phase combustion of the pressurant and determine the final pressurant residuals. It was noticed that the gas phase combustion produces a non-negligible thrust tail. Moreover, together with the pressure decay, an O/F shift occurs during final gas-phase combustion with a consequent I_{sp} penalty, particularly at sea level. It was shown that the penalty can be reduced using a by-pass at the expense of added complexity of the injection system.
The thrust tail should be avoided for soft lander and other applications where a specific value of the thrust is required. On the opposite for launcher's stages and sounding rockets it could add an important contribute to the total impulse. However this total impulse contribution should be weighted with the increased gravity losses and other penalties.

The use of a digital valve instead of a pressure regulator has been simulated. It was shown that the width of the PWM signal increases with time because of the increased required mass flow as inlet pressure decay. If the valve is too small the blowdown mode begins before the liquid oxidizer has been depleted because the pressurant is no more able to maintain the correct pressure. Moreover the on-off control produces a pulsation of the pressure in the oxidizer tank, particularly at the beginning when the pressure drop and consequently the mass flow is higher.

To further improve the simplicity of a hybrid rocket a self-pressurization system is very attractive. To model the self-press mode a homogeneous equilibrium model has been chosen. The liquid and the vapor phase are considered in saturated conditions at every instant. The model has been compared with experimental results from previous CISAS activities. The agreement is generally good but it worsen for very short burning times The error could be related to non-equilibrium effects and/or stratification. It is important to avoid stratification before motor operation in order to achieve the maximum performances from self-pressurization. When performances are critical a good thermal control should foreseen.

An analysis has been made about the influence of the initial temperature on performance. Results showed that N_2O should be generally cooled below 10° C. In fact a reduction of the temperature implies an increase in oxidizer density, a decrease of pressure, a small I_{sp} penalty, a decrease of the pressure decay during the discharge, large savings in tank weight and vapor residuals. The mass flow decay induced by self-pressurization partially compensates the O/F shift with time for propellants with $n > 0.5$. It was shown also that generally the self-press mode offers higher performances than the blowdown mode.

Later the full transient coupling between the feed system and the combustion chamber has been investigated. The main challenge was to determine the instantaneous liquid mass flow and the relation between the liquid oxidizer and the gaseous oxidizer that takes part in the hybrid motor combustion processes (i.e. droplets vaporization).

This has been done with a two-times model. The first time is a constant time lag that represents droplets breakup and heating to the vaporization temperature. The second time is based on the classical model of droplet evaporation called the 'D^2 law'. In this phase the squared of the droplet diameter varies linearly with time. In this way it was possible to simulate feed system coupled instabilities.

The simulations showed a good agreement with experimental results especially considering the uncertainties in the inputs and the level of approximation of the model. The code is able

to simulate the oscillations in the chamber and in the injector with good accuracy, showing in particular the typical clipped waves form of injector oscillations.
Finally a study has been done about the prediction of the mass flow through the injector elements for a self-press oxidizer.
Three models have been compared with CISAS cold flow tests: the incompressible model, the homogeneous equilibrium model (HEM) and one model developed at Stanford. The latter is a weighted-average of the other two models based on a estimate of the ratio between the residence time and the bubble growth time. The trend predicted by the HEM appears as the more similar to the experimental results, even if the absolute values are generally lower, particularly in the flat (choked) region. For $Cd = 1$ the HEM predictions fall in the experimental bandwith.
However it has been shown that a strong uncertainty arises in the definition of the discharge coefficient. The usual empirical correlations are not valid when the downstream pressure is below oxidizer saturation level.

In the sixth chapter two advanced techniques developed to improve hybrid rocket performances have been investigated. The first is the positioning of a diaphragm in the midst of the grain while the second one is the use of a swirling injection of the oxidizer. Both solutions have been tested (among others) at CISAS and look very promising with respect to the overcoming of historical hybrid weaknesses, in particular low regression rate and combustion efficiency.
The presence of a diaphragm between 1/4 and 1/3 of the grain length introduce a strong increase of the turbulence level and mixing of the reactants in the second part of the combustion chamber, promoting a more complete combustion and an higher heat flux on the grain surface, thus improving the efficiency and the regression rate.
Concerning the effect of the diaphragm on motor stability it is claimed that the diaphragm could act as a flame-holder, anchoring the flame and At the same time it should work as a baffle, affecting the acoustic response of the motor, the energy dissipation, the generation and damping of disturbances, and the coupling between them.
Moreover the diaphragm adds a further degree of freedom in the design of an hybrid rocket motor. In fact the shape and the position of the diaphragm can be adjusted in order to modify the response of the system and suppress or reduce possible instabilities.
The second advanced option that has been considered here for improving hybrid rocket performances is swirl injection. In this case the oxidizer is injected tangentially to the com-

bustion chamber walls in order to induce a rotational fluid pattern inside the engine. The influence of many different phenomena on the swirl flow characteristics has been investigated with the help of CFD simulations and mathematical analysis.

A step-by-step additive approach has been pursued in order to partially decouple (at least qualitatively) the different physical aspects affecting the swirling flowfield. In contrast with the free-vortex dominated aft-end swirl injection, it has been demonstrated that the leading solution in the case of head-end swirl injection is a forced vortex because the absence of a radial velocity impose to retain the viscous terms in the tangential momentum equation also for the zero order solution.

A comparison has been made between the classical axial injection and the vortex configuration. The axial injection produces the typical strong stratified flowfield with the fuel and the oxidizer moving almost parallel to the flame along the port. This produces the typical low performances normally encountered in hybrid rockets. On the contrary the helical flow produced by vortex injection strongly enhances the turbulence level and mixing in the combustion chamber. The hot products are mixed with the central cold core and this allows for fresh oxidizer to reach the flame. Moreover, as already said, centrifugal forces push the flame near the wall enhancing the heat flux and thus the regression rate.

As expected, it has been shown that the swirl number has a fundamental role in the description of swirling flows. In a head-end vortex hybrid rocket the swirl number decreases along the port for several reasons. In particular combustion is the major source of swirl decay (through Rayleigh-style axial acceleration) along the grain length; this in turn can affect the uniformity of grain consumption.

Every time there is a change in the cross section the swirl number is strongly affected, increasing as the cross section area grows and decreasing where there is a geometrical contraction. Ultimately the swirl number and its distribution along the axis has a crucial influence on motor performances and regression uniformity.

Very different consumption behaviors can be found, especially near the injection end. This fact is dependent on the complex flowfield that establishes in the region between the injector and the initial part of the grain which can vary considerably from case to case. In particular a critical aspect is the eventual direct impingement of the oxidizer flow on the grain surface that usually induces a strong local increase of the heat flux in the corresponding region.

Ultimately the resulting behavior is related to the geometry of the pre-chamber, the injection angle, the ratio between port diameter and injection diameter, and the possibility of burning

for the grain frontal face (or its inhibition).
Two peculiar aspects of swirling flows through nozzles are the blocking effect on the mass flow caused by the centrifugal forces opposing the fluid approaching the throat and the roll reaction on the motor caused by the residual swirl component at nozzle exit. The use of a mixer that disrupts the swirling flow before the nozzle entrance could prevent these issues.
It has been shown that liquid injection cannot achieve the outstanding results obtained by gaseous injection. In fact the atomization/evaporation of the liquid oxidizer produces a swirl decay and a loss of performance.
For this reason the most promising solution related to vortex injection is the use of catalytic decomposed Hydrogen Peroxide because it allows a simple, cold, multiple self-starting motor ignition capability together with high performing gaseous injection.
Finally the effect of the swirl flow on the stability of the motor has been discussed using data from studies about gas turbine combustors and hybrid rocket motors. It is possible to state that intensication of the swirl motion should generally improve the stability of the flow through increased centrifugal action that serves to inhibit vortex generation and promote a stronger denition of the mean ow, but this does not guarantee the absence of instabilities in every situation.
For both advanced techniques examined, particularly in relation of instability behavior, further testing at larger scales is recommended.

Thanks to the work done for this thesis the author has gained much insight on hybrid rocket transient behavior. Moreover the codes developed in this frame can be used to describe several aspects of hybrid transient operations. However much further work is needed to establish a comprehensive reliable predicting capability. This work should be associated by (preferably dedicated) experimental activities. These tests are fundamental for a more detailed validation of the numerical models and to improve the physical understanding of the complex phenomena involved. Testing should be done not only at lab-scale level but also at larger scales. In the author's opinion scaling-up is crucial, particularly in the analysis of instabilities.

Bibliography

[1] Culick, F. E. C., *Unsteady Motions in Combustion Chambers for Propulsion Systems*, Research and Technology Organization AGARDograph, AG-AVT-039, Dec. 2006

[2] Wooldridge, C., Marxman, G. A., and Kier, R., *Investigation of Combustion instability in hybrid rockets*, NASA CR-66812 Final Rept., 1969

[3] Carmicino C., *Acoustics, Vortex Shedding, and Low-Frequency Dynamics Interaction in an Unstable Hybrid Rocket*, Journal Of Propulsion And Power, Vol. 25, No. 6, November-December 2009

[4] Pucci, J. M., *The Effects of Swirl Injector Design on Hybrid Flame-Holding Combustion Instability*, AIAA Paper 2002-3578, July 2002.

[5] G. Story, T. Zoladz, J. Arves, D. Kearney, T. Abel, 0. Park, *Hybrid Propulsion Demonstration Program 250K Hybrid Motor*, 39th AIAA/ASME/SAE/ASEE Joint Propulsion Conference and Exhibit 20-23 July 2003, Huntsville, Alabama

[6] Karabeyoglu, M. A.,*Transient combustion in hybrid rockets*, PhD dissertation, Stanford Univ., Dept. of aeronautics and Astronautics, Stanford, CA, Aug. 1998,

[7] Karabeyoglu, A., *Combustion Instability and Transient Behavior in Hybrid Rocket Motors*, Fundamentals of Hybrid Rocket Combustion and Propulsion, edited by M. J. Chiaverini, and K. K. Kuo, Vol. 218, Progress in Astronautics and Aeronautics, AIAA, Reston, VA, 2007

[8] Karabeyoglu, M. A., Stevens, J., Cantwell, B., *Investigation of Feed System Coupled Low Frequency Combustion Instabilities in Hybrid Rockets*, 43rd AIAA/ASME/SAE/ASEE Joint Propulsion Conference and Exhibit, 8-11 July 2007, Cincinnati, OH

[9] Gordon, S., McBride, J., *Computer program for calculation of complex chemical equilibrium compositions and Applications*, NASA reference Publication 1311, October 1994

[10] Bellomo, N., Lazzarin, M., Barato, F., Grosse, M., *Numerical Investigation of the Effect of a Diaphragm on the Performance of a Hybrid Rocket Motor*, AIAA 2010-7033, 46th AIAA/ASME/SAE/ASEE Joint Propulsion Conference and Exhibit, 25-28 July 2010, Nashville, Tennesse

[11] Karabeyoglu, M. A., De Zilwa, S., Cantwell, B. J., Zilliac, G., *Transient modeling of hybrid of hybrid rocket low frequency instabilities*, 39th AIAA/ASME/SAE/ASEE Joint Propulsion Conference and Exhibit 20-23 July 2003, Huntsville, Alabama

[12] Karabeyoglu, M. A., De Zilwa, S., Cantwell, B., and Zilliac, G., *Modeling of Hybrid Rocket Low Frequency Instabilities*, Journal of Propulsion and Power, Vol. 21, No. 6, 2005

[13] Karabeyoglu, M. A., and Altman, D., *Dynamic Modeling of Hybrid Rocket Combustion*, Journal of Propulsion and Power, Vol. 15,No. 4, 1999, pp. 562-571.

[14] Karabeyoglu, M. A., *Thermal Transients in Hybrid Rocket Fuel Grains - Nonlinear Effects*, 43rd AIAA/ASME/SAE/ASEE Joint Propulsion Conference and Exhibit, 8-11 July 2007, Cincinnati, OH

[15] G. A. Marxman, C. E. Wooldridge and R.J. Muzzy, *Fundamentals of Hybrid Boundary Layer Combustion*, Progress in Astronautics and Aeronautics, Vol.15, 1964 p. 485-522.

[16] Chiaverini, M. J., Harting, G. C., Lu, Y. C., Kuo, K. K., Peretz, A., Jones, S.,Wygle, B., and Arves, J. P., *Pyrolysis Behavior of Hybrid Rocket Solid Fuels Under Rapid Heating Conditions*, Journal of Propulsion and Power, Vol. 15, No. 6, 1999, pp. 888-895.

[17] Altman, D. and Humble, R.*Hybrid Rocket Propulsion Systems* in Space Propulsion Analysis and Design, edited by Humble, R. W., Henry G. N., Larson, W. J., McGraw Hill, Space Technology Series, 1995

[18] Marxman, G. A., *Combustion in the Turbulent Boundary Layer on a Vaporizing Surface*, 10th (International) Symposium on Combustion, The Combustion Institute, Pittsburgh, PA, 1965, pp. 1337-1349.

[19] Karabeyoglu, M. A., Cantwell, B. J., Stevens, J., *Evaluation of Homologous Series of Normal Alkanes as Hybrid Rocket Fuels*, 41st AIAA/ASME/SAE/ASEE Joint Propulsion Conference and Exhibit, July 2005, Tucson, AZ

[20] Karabeyoglu, M. A., Altman, D., Cantwell, B. J., *Combustion of Liquefying Hybrid Propellants: Part 1, General Theory* , Journal Of Propulsion And Power, 2002, Vol.18; No. 3, pages 610-630

[21] M. A. Karabeyoglu, Greg Zilliac, Brian J. Cantwell, Shane DeZilwa and Paul Castellucci, *Scale-up Tests of High Regression Rate Liquefying Hybrid Rocket Fuels*, AIAA-2003-1162, 41st Aerospace Sciences Meeting and Exhibit, Reno Nevada, January 2003.

[22] Marxman, G. A., and Gilbert,M., *Turbulent Boundary Layer Combustion in the Hybrid Rocket*, Ninth International Symposium on Combustion, Academic, New York, 1963, pp. 371-383.

[23] Turns, S. R., *An Introduction to Combustion, Concepts and Applications*, Second edition, 2000, McGraw-Hill Higher Education

[24] Lazzarin, M., Faenza, M., Barato, F., Bellomo, N., Bettella, A., Pavarin, D., Grosse, M., *CFD Simulation of a Hybrid Rocket Motor with Liquid Injection*, AIAA 2011-5537, 47th AIAA/ASME/SAE/ASEE Joint Propulsion Conference and Exhibit, 31 July-3 August 2011, San Diego, California

[25] Hikone, S., Maruyama S., Isiguro T., Nakagawa I., *Regression Rate Characteristics and Burning Mechanism of Some Hybrid Rocket Fuels*, 46th JPC 2010, Nashville, Tennessee.

[26] Weinstein, A., Gany, A., *Testing and modeling liquefying fuel combustion in hybrid propulsion*, 4th European Conference for Aerospace Sciences (EUCASS), St. Petersburg, Russia, July 2011.

[27] Jerome, A., Prvost, M., *Hybrid propulsion: an overview of the Onera activities*, 4th European Conference for Aerospace Sciences (EUCASS), St. Petersburg, Russia, July 2011.

[28] Bettella, A., Lazzarin, M., Bellomo, N., Barato, F., Pavarin, D., Grosse, M., *Testing and CFD Simulation of Diaphragm Hybrid Rocket Motors*, AIAA 2011-6023, 47th

AIAA/ASME/SAE/ASEE Joint Propulsion Conference and Exhibit, 31 July-3 August 2011, San Diego, California

[29] Yuasa, S., Shimada, O., Imamura, T., Tamura, T., Yamamoto, K., *A technique for Improving the Performance of Hybrid Rocket Engines*, AIAA 99-2322, 35th AIAA/ASME/SAE/ASEE Joint Propulsion Conference and Exhibit, Los Angeles, California, USA, 20-24 June 1999

[30] Gater, R. A., L'Ecuyer, M. R., Warner C. F., *Liquid-film Cooling Its Physical Nature and Theoretical Analysis*, JET PROPULSION CENTER, PURDUE UNIVERSITY, October, 1965.

[31] Gater, R. A., L'Ecuyer, M. R., *A Fundamental Investigation of The Phenomena That Characterize Liquid-Film Cooling*, JET PROPULSION CENTER, PURDUE UNIVERSITY, January, 1969.

[32] Nigmatulin, R., Nigmatulin, B., Khodzaev, Y. A., and Kroshilin, V., *Entrainment and Deposition Rates in a Dispersed-Film Flow*, International 5Journal of Multiphase Flow, Vol. 22, No. 1, 1996, pp. 19-30.

[33] Kuo K. K., Houim R. W., *Theoretical Modeling and Numerical Simulation Challenges of Combustion Processes of Hybrid Rockets*, 47th AIAA/ASME/SAE/ASEE Joint Propulsion Conference and Exhibit, AIAA-2011-5675, 31 July - 03 August 2011, San Diego, California, USA.

[34] Wikipedia *http://en.wikipedia.org/wiki/Supercritical_fluid*

[35] Zhu G. S., Aggarwal S. K., *Fuel Droplet Evaporation in a Supercritical Environment*, ASME, Vol. 124, pp. 762-770, October 2002.

[36] M. Oschwald, J.J. Smith, R. Branam, J. Hussong, A. Schik, B. Chehroudi, D. Talley, *Injection of Fluids into Supercritical Environments Report*, 2 September 2004.

[37] Joel Escobedo and G. Ali Mansoori., *Surface Tension Prediction for Liquid Mixtures*, AIChE Journal, Vol. 44, No. 10, pp. 2324-2332, 1998

[38] Yang, V., *Modeling of Supercritical Vaporization, Mixing, and Combustion Processes in Liquid-Fueled Propulsion Systems*, Proceedings of the Combustion Institute, Vol. 28, Pt. 1, pp, 925-942, 2007

[39] Kim S., Lee J., Moon H., Sung H., Kim J., Cho J., *Effect of Paraffin-LDPE Blended Fuel in Hybrid Rocket Motor*, 46th JPC 2010, Nashville, Tennessee.

[40] Brian J. Cantwell, *Course material for Aircraft and Rocket Propulsion*, Chapter 10, Stanford University, 05 Jan 2012

[41] D. D. Ordahl and W. A. Rains, *Hybrid Propulsion for advanced missions, recent developments current status and future outlook*, AIIA 64-226, Sunnyvale, California, USA, 11 Jan 1967

[42] Chiaverini, M., *Review of Solid Fuel Regression Rate Behavior in Classical and Nonclassical Hybrid Rocket Motors*, Fundamentals of Hybrid Rocket Combustion and Propulsion, edited by M. J. Chiaverini, and K. K. Kuo, Vol. 218, Progress in Astronautics and Aeronautics, AIAA, Reston, VA, 2007

[43] Grosse, M., *Design Challenges for a Cost Competitive Hybrid Rocket Booster*, EUCASS, 2nd EUROPEAN CONFERENCE FOR AEROSPACE SCIENCES, Brussels, Belgium, July 1-6, 2007

[44] R. J. Kniffen, *Development Status of the 200,000 lb_f Thrust Hybrid Rocket Booster*, AIAA 92-1657, Huntsville, Alabama, USA, 24-27 March 1992

[45] K. R. Wagner, R. H. Schmucker, *Hybrid Rockets for Space transportation - A Critical Assessment*, AIAA 92-3305, 28th Joint Propulsion Conference and Exhibit, Nashville, TN, USA, 24-27 July 6-8, 1992

[46] W. H. Knuth, M. J. Chiaverini, J. A. Sauer, D. J. Gramer, *Solid-Fuel Regression Rate Behavior of Vortex Hybrid Rocket Engines*, JOURNAL OF PROPULSION AND POWER, Vol 18, No. 3, May-June 2002

[47] J. Arves, M. Gnau, K. Joiner, D. Kearney, C. McNeal, M. Murbach, *Overview of The Hybrid Sounding Rocket (HYSR) Project*, AIAA 2003-5199

[48] D. Gibbon, G. S. Haag, *Investigation of an Alternative Geometry Hybrid Rocket for Small Spacecraft Orbit Transfer*, 27 July 2001

[49] G. Williams, F. Macklin, M. sarigul-Klijn, N. Sarigul-Klijn, J.Benson, *Almost There: Responsive Space*, 2nd Responsive Space Conference, Los Angeles, CA, USA April 19-22, 2004

[50] S. Yuasa, K. Yamamoto, H. Hachiya, K. Kitagawa, Y. Oowada, *Development of a Small Sounding Hybrid Rocket with a Swirling-Oxidizer-Type Engine*, AIAA 2001-3537, 37th Joint Propulsion Conference and Exhibit, Salt Lake City, Utah, USA, 8-11 July, 2001

[51] M. Smiley, M. Veno, R. Bell, *Commercial Crew development - Round One, Milestone 3: Overview of Sierra Nevada Corporation's Hybrid Motor Ground Test*, AIAA 2011-5717, 47th Joint Propulsion Conference and Exhibit, San Diego, CA, USA, 31 July-03 August, 2011

[52] Greg Zilliac, *Hybrid Rocket Propulsion: Past, Present, and Future*, Presentation, 04 November, 2010

[53] M. A. Karabeyoglu, B. J. Cantwell, G. Zilliac, *Development of Scalable Space-Time Averaged Regression Rate Expressions for Hybrid Rockets*, AIAA 2005-3544, 41th Joint Propulsion Conference and Exhibit, Tucson, AZ, USA, 10-13 July, 2005

[54] M. A. Karabeyoglu, J. Stevens, D. Geyzel, B. Cantwell, D. Micheletti, *High Performance Hybrid Upper Stage Motor*, AIAA 2011-6025, 47th Joint Propulsion Conference and Exhibit, San Diego, CA, USA, 31 July - 03 August, 2011

[55] M. Grosse, *Effect of a Diaphragm on Performance and Fuel Regression of a Laboratory Scale Hybrid Rocket Motor Using Nitrous Oxide and Paraffin*, AIAA 2009-5113, 45th Joint Propulsion Conference and Exhibit, Denver, Colorado, USA, 2-5 August, 2009

[56] T. A. Boardman, R. L. Carpenter, S. E. Claflin, *A Comparative Study of the Effects of Liquid -Versus Gaseous - Oxygen Injection on Combustion Stability in 11-inch-Diameter Hybrid Motors*, AIAA 97-2936, 33rd Joint Propulsion Conference and Exhibit, Seattle, Washington, USA, 6-9 July, 1997

[57] C. Carmicino, A. Russo Sorge, *Influence of a Conical Axial Injector on Hybrid Rocket Performance*, JOURNAL OF PROPULSION AND POWER, Vol 22, No. 5, September-October 2006

[58] C. Carmicino, A. Russo Sorge, *Role of Injection in Hybrid Rockets Regression Rate Behavior*, JOURNAL OF PROPULSION AND POWER, Vol 21, No. 4, July-August 2005

[59] C. Carmicino, A. Russo Sorge, *The Effect of Oxidizer Injector Design on Hybrid Rockets Combustion Stability*, AIAA 2006-4677, 42nd Joint Propulsion Conference and Exhibit, Sacramento, CA, USA, 9-12 July, 2006

[60] D. D. Ordahl and W. A. Rains, *Recent Developments and Current Status of Hybrid Rocket Propulsion*, JOURNAL OF SPACECRAFT AND ROCKETS, Vol 2, No. 6, November-December 1965

[61] Altman, D., A. Holzman, *Overview and History of Hybrid Rocket Propulsion*, Fundamentals of Hybrid Rocket Combustion and Propulsion, edited by M. J. Chiaverini, and K. K. Kuo, Vol. 218, Progress in Astronautics and Aeronautics, AIAA, Reston, VA, 2007

[62] G., Story, *Large-Scale Hybrid Motor Testing*, Fundamentals of Hybrid Rocket Combustion and Propulsion, edited by M. J. Chiaverini, and K. K. Kuo, Vol. 218, Progress in Astronautics and Aeronautics, AIAA, Reston, VA, 2007

[63] G., Story, J. Arves, *Flight testing of Hybrid-Powered Vehicles*, Fundamentals of Hybrid Rocket Combustion and Propulsion, edited by M. J. Chiaverini, and K. K. Kuo, Vol. 218, Progress in Astronautics and Aeronautics, AIAA, Reston, VA, 2007

[64] D. A. Kearney, K. F. Joiner, M. P. Gnau, M. A. Casemore, *Improvement to the Marketability of Hybrid Propulsion Technologies*, in Proceedings of the AIAA Space Conference, pp. 1674-1688, September 2007, AIAA Paper 2007-6144.

[65] Jonny Dyer, Eric Doran, Zach Dunn, Kevin Lohner, Cedric Bayard and Andy Sadhwani, Greg Zilliac, Brian Cantwell and Arif Karabeyoglu, *Design and Development of a 100 km NitrousOxide/Paraffin Hybrid Rocket Vehicle*, AIAA 2007-5362, 43rd AIAA/ASME/SAE/ASEE Joint Propulsion Conference and Exhibit; Cincinnati, Ohio, USA, 8-11 July 2007.

[66] Jonny Dyer, Greg Zilliac, Eric Doran, Mark Marzona, Kevin Lohner, Evan Karlik, Brian Cantwell and Arif Karabeyoglu, *Status Update Report for the Peregrine 100km Sounding Rocket Project*, AIAA 2008-4829, 44th AIAA/ASME/SAE/ASEE Joint Propulsion Conference and Exhibit; Hartford, CT, USA, 21-23 July 2008.

[67] Eric Doran, Jonny Dyer, Mark Marzona, Arif Karabeyoglu, Greg Zilliac, Robert Mosher, Brian Cantwell, *Status Update Report for the Peregrine Sounding Rocket*

Project: Part III, AIAA 2009-4840, 45th AIAA/ASME/SAE/ASEE Joint Propulsion Conference and Exhibit; Denver, Colorado, USA, 2-5 August 2008.

[68] J. R. Wertz, R. C. Conger, M. Rufer, N. Sarzi-Amad, R. E. Van Allen, *Methods for Achieving Dramatic Reductions in Space Mission Cost*, RS-2011-5002, Reinventing Space Conference; Los Angeles, CA, USA, 2-5 March 2011.

[69] J. E. Ronningen, J. Husdal, *Test Results from Small-Scale Hybrid Rocket Testing*, SP2012-2364847, Space Propulsion 2012; Bordeaux, France, 7-10 May 2012.

[70] J. E. Ronningen, J. Husdal, M. Berger, R. Vesteras, G. Raudsandmoen, *Nammo Hybrid Rocket Propulsion TRL Improvement Program*, AIAA 2012-4311, 48th Joint Propulsion Conference and Exhibit, Atlanta, Georgia, USA, 29 July - 1 August, 2012

[71] *personal communications between CISAS researchers and Jan-Erik Ronningen from NAMMO Raufoss.*

[72] G. Parissenti et al., *Throttleable Hybrid Engine for Planetary Soft Landing*, 4th EUROPEAN CONFERENCE FOR AEROSPACE SCIENCES (EUCASS), St. Petersburg, Russia, July 2011

[73] J. H. Ferziger, M. Peric, *Computational Methods for Fluid Dynamics*, 3rd edition, Springer, 2002

[74] *http://www.orbitec.com/documents/hybrid_rocket_motor.html*

[75] Kitagawa, K., Mitsutani T., Ro, T., Yuasa, S., *Effects of Swirling Liquid Oxygen Flow on Combustion of a Hybrid Rocket Engine*, AIAA 2004-3479, 40th Joint Propulsion Conference and Exhibit, Fort Lauderdale, Florida, USA, 11-14 July, 2004

[76] Bellomo, N., Barato, F., Faenza M., Lazzarin, M., Bettella, A., Pavarin, D., *Numerical and Experimental Investigation on Vortex Injection in Hybrid Rocket Motors*, AIAA 2011-5675, 47th AIAA/ASME/SAE/ASEE Joint Propulsion Conference and Exhibit, 31 July-3 August 2011, San Diego, California

[77] Bellomo, N., Faenza M., Barato, F., Bettella, A., Pavarin, D., Selmo, A., *The "Vortex Reloaded" project: experimental investigation on fully tangential vortex injection in N2O-paraffin hybrid motors*, 48th Joint Propulsion Conference and Exhibit, Atlanta, Georgia, USA, 29 July - 1 August, 2012

[78] Dyer, J., Doran, E., Dunn, Z., Lohner, K., Zilliac G., B., Cantwell, *Modeling Feed System Flow Physics for Self-Pressurizing Propellants*, AIAA 2007-5702, 43rd AIAA/ASME/SAE/ASEE Joint Propulsion Conference and Exhibit, Cincinnati, OH, USA, 8-11 July, 2007

[79] Herbert Oertel, *Prandtl's essentials of Fluid Mechanics*, Second Edition, Applied Mathematical sciences, Volume 158, Springer, 2004

[80] *Fluent 6.2 User's Guide*, Fluent Inc., January 2005

[81] Batterson J., Majdalani, J., *Biglobal Instability of the Bidirectional Vortex. Part 2: Complex Lamellar and Beltramian Motions*, AIAA 2011-5649, 47th AIAA/ASME/SAE/ASEE Joint Propulsion Conference and Exhibit, 31 July-3 August 2011, San Diego, California

[82] Calabro, M., *Overview on Hybrid Propulsion*, Progress in Propulsion Physics 2, pp. 353-374, 2011

[83] C. Delisle, *Caractristiques principales des fusees-sondes O.N.E.R.A.*, note Technique N° 118, 1967

[84] Cavallini, E., Di Giaginto, M., Favini, B., *Solid Rocket Motors Internal Ballistics over the IT: Driving Phenomena*, Modelling & Applications, Course material for Modellistica per la Propulsione a Solido, Sapienza University of Rome 2011-2012

[85] Boardman, Terry A., Hybrid Propellant Rockets, *Rocket Propulsion Elements*, Seventh Edition, edited by Sutton, G. P., Biblarz O., Jhon Wiley & Sons, Inc., 2001

[86] Estey, P. N., Whittinghill, G. R., *Hybrid Rocket Motor Propellant Selection Alternatives*, AIAA 92-3592, 28th AIAA/ASME/SAE/ASEE Joint Propulsion Conference and Exhibit, 6-8 July 1992, Nashville, TN, USA

[87] Masugi, M., Ide, T., Yuasa, S., Sakurai, T., Shiraishi, N., Shimada. T., *Visualization of Flames in Combustion Chamber of Swirling-Oxidizer-Flow-Type Hybrid Rocket Engines*, 46th AIAA/ASME/SAE/ASEE Joint Propulsion Conference and Exhibit, 25-28 July 2010, Nashville, Tennessee, USA

[88] Myre, D. D., Canton P., Cowart J. S., Jones C. C., *Exhaust Gas Analysis of a Vortex Oxidizer Injection Hybrid Rocket Motor*, 46th AIAA/ASME/SAE/ASEE Joint Propulsion Conference and Exhibit, 25-28 July 2010, Nashville, Tennessee, USA

[89] J., Majdalani, *Vortex injection Hybrid Rockets*, Fundamentals of Hybrid Rocket Combustion and Propulsion, edited by M. J. Chiaverini, and K. K. Kuo, Vol. 218, Progress in Astronautics and Aeronautics, AIAA, Reston, VA, 2007

[90] Andrew D. Cutler, Richard W. Barnwell, *Vortex Flow in a Convergent-Divergent Nozzle*, AIAA JOURNAL, VOL. 37, NO. 10: TECHNICAL NOTES, pp. 1329-1331, 1999

[91] A. Abdelhafez, A. K. Gupta, *Propagation of Swirl in Transonic Airflow*, 45th AIAA/ASME/SAE/ASEE Joint Propulsion Conference and Exhibit, 2-5 August 2009, Denver, Colorado, USA

[92] Mager, A., *Approximate Solution of Isentropic Swirling Flow Through a Nozzle*, American Rocket Society Journal, Vol. 31, No. 8, 1961, pp. 1140-1148.

[93] A. Gany, M. Mor, C. Goldman, *Analysis and Characteristics of Choked Swirling Nozzle Flows*, AIAA JOURNAL Vol. 43, No. 10, October 2005, pp. 2177-2181

[94] Y. Huang, V. Yang, *Effect of swirl on combustion dynamics in a lean-premixed swirl-stabilized combustor*, Proceedings of the Combustion Institute, 30, pp. 1775-1782, 2005

[95] *http://www.xcor.com/products/pumps/*

[96] A. G. Ledebuhr, D. R. Antelman, D. W. Dobie, T. S. Gorman, M. S. Jones, J. F. Kordas, D. H. McMahon, L. C. Ng, D. P. Nielsen, A. E. Ormsby, L. C. Pittenger, J. A Robinson, K. M. Skulina, W. G. Taylor, D. A. Urone, B. A. Wilson. *Recent Development in Hydrogen Peroxide Pumped Propulsion*, 2nd Missile Defense Conference and Exhibit, Washington, DC, United States 22-26 March, 2004

[97] Debra Facktor Lepore, Ralph Ewig, *Results of QuickReach^{TM} Small Launch Vehicle Propulsion Testing and Next Steps to Demonstration Flights*, SSC08-IX-5, 22nd Annual AIAA/USU Conference on Small Satellites, Logan, Utah, USA, 2008

[98] Laurence de Quay, B. Keith Hodge, *A History of Collapse Factor Modeling and Empirical Data for Cryogenic Propellant Tanks*, AIAA 2010-6559, 46th AIAA/AS-

ME/SAE/ASEE Joint Propulsion Conference and Exhibit, 25-28 July 2010, Nashville, Tennessee, USA

[99] K. J. Flittie, S. Jones, Chuck Shaeffer, *HyFlyer: A Hybrid Propulsion Suborbital Launch Vehicle*, AIAA94-3149, 30th AIAA/ASME/SAE/ASEE Joint Propulsion Conference, Indianapolis, IN, USA, 27-29 June, 1994

[100] G. Zilliac, M. A. Karabeyoglu, *Modeling of Propellant Tank Pressurization*, AIAA2005-3549, 41st AIAA/ASME/SAE/ASEE Joint Propulsion Conference, Tucson, AZ, USA, 10-13 July, 2005

[101] L. Casalino, D. Pastrone, *Optimal Design of Hybrid Rockets with Self-Pressurizing Oxidizer*, AIAA2006-4501, 42nd AIAA/ASME/SAE/ASEE Joint Propulsion Conference, Sacramento, CA, USA, 9-12 July, 2006

[102] A. Karabeyoglu, J. Dyer, J. Stevens, B. Cantwell, *Modeling of N_2O Decomposition Events*, AIAA2008-4933, 44th AIAA/ASME/SAE/ASEE Joint Propulsion Conference, Hartford, CT, USA, 21-23 July, 2008

[103] Akira Sou, Shigeo Hosokawa, Akio Tomiyama, *Effects of cavitation in a nozzle on liquid jet atomization*, International Journal of Heat and Mass Transfer, Volume 50, Issues 17-18, August 2007, Pages 3575-3582

[104] G. Zilliac, M. A. Karabeyoglu, *Hybrid Rocket Fuel Regression Rate Data and Modeling*, AIAA2006-4504, 42nd AIAA/ASME/SAE/ASEE Joint Propulsion Conference, Sacramento, CA, USA, 9-12 July, 2006

[105] K. Lohner, J. Dyer, E. Doran, Z. Dunn, G. Zilliac, *Fuel Regression Rate Characterization Using a Laboratory Scale Nitrous Oxide Hybrid Propulsion System*, AIAA2006-4671, 42nd AIAA/ASME/SAE/ASEE Joint Propulsion Conference, Sacramento, CA, USA, 9-12 July, 2006

At the end of this challenging period of work, I would like to express sincere thanks to the staff of the space propulsion group at CISAS, my colleagues, my friends:

Daniele, Alberto, Marco,
Enrico, Nicolas, Federico, Marta, Martina, Marco,
Davide, Andrea, Fabio, Francesco, Alberto